UNIVERSITÀ DEGLI STUDI DI PAVIA

Department of Molecular Medicine

Unit of Cardiology

PhD course in Translational Medicine

XXXIV cycle

Stem cells for translational research in cardiology

Tutor:

Prof. Massimiliano Gnecchi

PhD thesis by:

Francesca Bastaroli

Academic Year 2020/2021

Contents

1 INTRODUCTION

The term “Translational research” refers to the branch of scientific research aimed at transferring discoveries obtained in basic research investigations (“bench”) to the clinical practice (“bedside”), to improve the management and treatment of human diseases.

Medicine in general, and cardiology, are very interested by the translational concept.

The reason behind the interest for translational research in the cardiovascular field is obvious. Although great advances in the treatment of cardiovascular diseases have been made during the last decades, the morbidity and mortality associated with heart diseases are still too high.

Progress in translational cardiovascular research has been significantly hindered by the lack of appropriate research models. In vitro and in vivo models currently available are often inadequate for studies at cellular levels, and patient-specific cardiomyocytes cannot be easily obtained. The paradigm-shift that followed the development of induced pluripotent stem cells (iPSCs) has changed both our perspective and research potential. Now, by simply collecting somatic cells from a patient, we can obtain cardiomyocytes (CM) derived from the iPSCs (iPSC-CMs) of the same subject in just a few weeks. iPSC-CMs express cardiac-specific ion channels and regulators of intracellular Ca^{2+} dynamics like native CMs. Most importantly, patient-specific iPSC-CMs recapitulate the abnormal cardiac phenotype of several hereditary cardiac diseases and can be used to test antiarrhythmic drugs.

iPSC-CMs faithfully summarize ‘clinical trial on a plate’ (population level) and even ‘patient on a plate’ (individual level) conditions, thus representing a good model for the implementation of Precision Medicine, which is an innovative translational approach for disease treatment and prevention that considers individual genetic and phenotypic variability, allowing doctors to develop tailored therapies.

During my PhD, a lot of my work was dedicated to the expansion of a biobank of iPSC derived from patients affected by inherited cardiovascular diseases, and the iPSC technology was used to model two different types of life-threatening cardiac diseases: long QT syndrome (LQTS) and the cardiovascular complications of coronavirus disease-19 (COVID-19).

LQTS was chosen since it is the best characterized arrhythmogenic disorder of genetic origin and a leading cause of sudden death below age 20 and because the Fondazione IRCCS San Matteo is a referral center for this inherited disease. One critically important and still unexplained feature of LQTS, which hampers risk stratification and correct management, is the unpredictable variability in the severity of clinical manifestation among carriers of the same mutation. Here, hiPSC-CMs were used as an *in vitro* model to study sex hormones as disease modifiers of LQTS in a patient affected by polycystic ovary syndrome (PCOS), a disease associated with high levels of testosterone and low levels of estrogen. The first manifestation of LQT2 in this patient occurred during puberty, after starting an estro-progestin therapy, which was never regularly taken by the patient, especially when cardiac events occurred. Therefore, the impact of estrogen spikes on action potential duration and arrhythmogenesis were investigated to help in the clinical decision to resume or not resume hormone replacement therapy, and, more broadly, to gain new insights into the role of sex hormones in the modulation of QT interval and ventricular arrhythmia susceptibility.

At the beginning of the second PhD year, when I returned to work after the lockdown due to COVID-19 emergency, I mostly worked on new projects aiming at clarifying important aspects related with the pandemic. At first, it was investigated if the etiological agent of COVID-19, the Severe Acute Respiratory Syndrome-Coronavirus-2 (SARS-CoV-2) can directly infect hiPSC-CMs, and if some widely used anti-hypertensive drugs such as angiotensin II type 1 receptor blockers (ARBs) and angiotensin-converting enzyme inhibitors (ACEIs) may modulate the risk of infection. Indeed, it was reported in animal models that some of these drugs at high dosages might increase the expression of ACE2, the host receptor used by SARS-CoV-2 to enter the cells.

Then, it was investigated if mesenchymal stromal cells (MSCs), currently under investigation for the treatment of COVID-19, are “safe”; namely, for the first time was tested if they express ACE2, the main host cell factor for SARS-CoV-2 entry, and if they can be infected by SARS-CoV-2.

1.1 Induced Pluripotent Stem Cells

1.1.1 Definition and history

Induced pluripotent stem cells described by Takahashi and Yamanaka in 2006[1], are de-differentiated somatic cells, which recover the ability to generate many other cell types of different lineages (pluripotency). They are self-renewing and can replicate and differentiate into all kind of somatic cell types of an organism[2]. The "epigenetic landscape" model postulated by Waddington in 1957 describes the differentiation potential of a pluripotent cell during embryonic development. The model, graphically represented in figure 1.1, is constituted by a "mountain" with numerous "valleys". A totipotent cell, which is completely undifferentiated, is represented as a ball rolling down to different valleys, proceeding from the top of the landscape to the bottom. The cell switches from undifferentiated (totipotent and pluripotent), to partially differentiated (progenitor) to terminally differentiated status. At each bifurcation point the potential of the cell to choose different cell fates diminishes irreversibly[3]. This model has been modified by John Gurdon in 1962 demonstrating that a somatic cell can de-differentiate, recovering the ability of generating different other cell types (i.e. pluripotency)[4].

Figure 1.1. Waddington's epigenetic landscape.

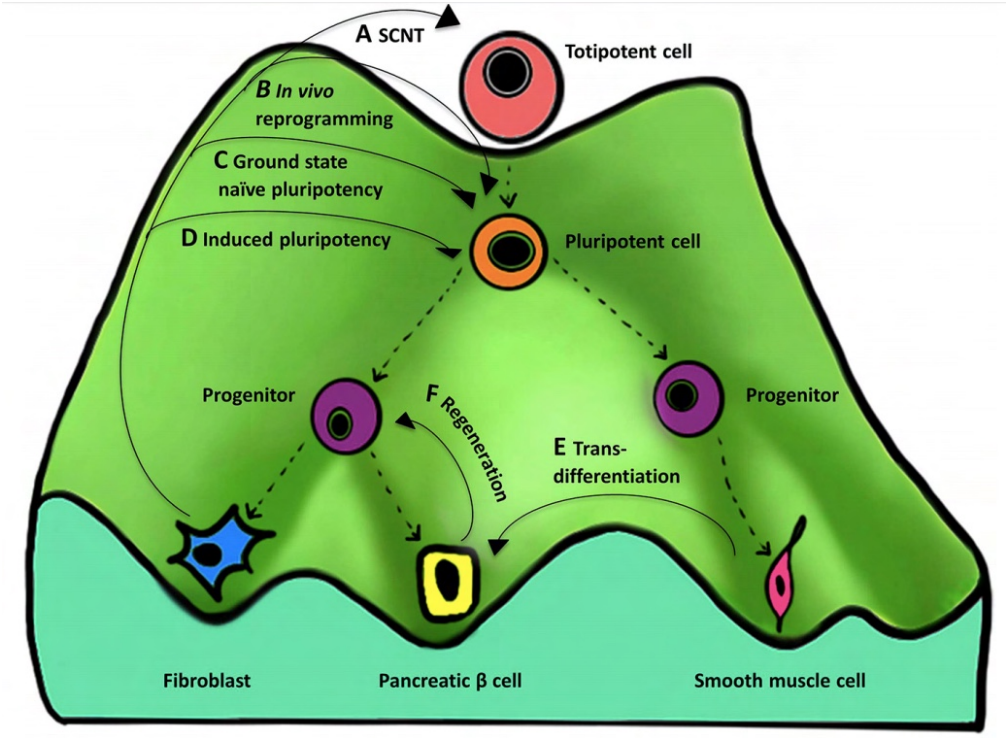

An epigenetic landscape is a graphical rendering of cell populations originated after hierarchically determined developmental restrictions during development. On the top of the mountain there is a totipotent stem cell whereas at the bottom of the mountain there are terminally differentiated cells. Valleys represent the different cell fates. ***(A–F)*** *represent the different methods to reverse the cell fate to a more primitive state. There are four types of methods that are currently known for reprogramming to* ***(A)*** *totipotency,* ***(B,C)*** *near totipotency, and* ***(D)*** *pluripotency.* ***(E)*** *trans-differentiation—one differentiated cell type (smooth muscle cell) is converted to another (pancreatic beta cell) and* ***(F)*** *regeneration—derivation of a progenitor-like cell from a differentiated cell during wound healing. Reproduced from Kanherkar et al*[3].

Most stem cells are of embryonic origin (ESC), which form the inner cell mass of the blastocyst, or derive from adult tissues (e.g., bone marrow). Pluripotent cells that could be grown *in vitro* are embryonic carcinoma (EC) cells isolated from gonadal teratocarcinomas, and embryonic germ (EG) cells, isolated from primordial gonads of post-implantation embryos.

In 2012, Gurdon and Yamanaka won the Nobel Prize in physiology and medicine "for the discovery that mature cells can be reprogrammed to become pluripotent". Yamanaka's group, starting from a set of 24 pluripotency genes, identified the 4 reprogramming factors (c-MYC, OCT3/4, SOX2 and KLF-4) able to reprogram mouse embryonic fibroblasts (MEFs) into a pluripotent state[1]. After obtaining iPSCs from mouse cells, Yamanaka and colleagues tried to

generate human iPSCs (hiPSCs) from dermal fibroblasts. In 2007 Thompson's group succeeded in generating hiPSCs using a different combination of human factors: NANOG, OCT3/4, SOX2 and LIN28A[5]. Importantly, iPSCs bypass the ethical concerns related to embryonic stem cells (ESCs).

PSCs were traditionally cultured on feeder layers of mouse or human fibroblast[6]. Most iPSCs are now cultured in feeder-free condition using cell-free matrices, maintaining pluripotency and the ability to differentiate into cells of the three germ layers (ectoderm, mesoderm and endoderm) without causing chromosomal aberrations.

1.1.2 Development of reprogramming methods

The fundamental principle of iPSC generation is to express the Yamanaka's reprogramming factors (c-MYC, OCT3/4, SOX2 and KLF-4) in somatic cells to trigger the expression of pluripotent genes. Fibroblasts derived from skin biopsy have been widely used to generate iPSCs (figure1.2A/B), even if collection is invasive and painful; thus, other alternatives are now available, including peripheral blood mononuclear cells (PBMC) from a blood sample (figure 1.2A/B) and renal epithelial cells from urine[7]. Different methods to deliver the factors into the somatic cells have been developed. The first one is based on retroviral or lentiviral vectors to transduce fibroblasts, but viral integration into the host genome makes this method unsuitable for clinical application. Lentiviral vectors result in a higher efficacy of reprogramming than retroviruses with fewer viral integrations. As integration-free systems recombinant reprogramming proteins, small molecules and episomal DNA plasmids have been adopted. However, these methods result in low efficiency.

Nowadays, Sendai virus (SeV) based vector, a single chain RNA virus vector, is the method used to generate most human iPSCs. The viral RNA remains in the host cell cytoplasm, and it is diluted out of the host cell ~5 passages after virus infection. Engineered mRNA or microRNA are also used to generate iPSCs, avoiding the risk of insertional mutagenesis and reduced clonal variations.

1.1.3 Main feature of human iPSCs

Human iPSCs are self-renewing, clonogenic and maintain chromosomal stability through passages. They form sharp-edged, flat, tightly packed colonies, constituted by round-shaped cells, with large nucleoli and scant cytoplasm[8] (figure 1.2C). hiPSCs express hESC-specific markers such as OCT3/4, NANOG, REX1, NODAL, SOX2, and hESC surface antigens like TRA-1-60, SSEA-3 and SSEA-4. The DNA methylation profile of hiPSCs is similar to hESCs. DNA methylation is the transfer of a methyl group to a cytosine molecule in a CpG island. Methylation of a gene prevents its transcription. In hiPSCs the main pluripotency genes are demethylated. Finally, they can form embryoid bodies (EBs) *in vitro*, which can differentiate into cells of the three germ layers, and they can spontaneously form teratomas when injected into adult immune-compromised animals.

Figure 1.2. Generation and applications of hiPSCs.

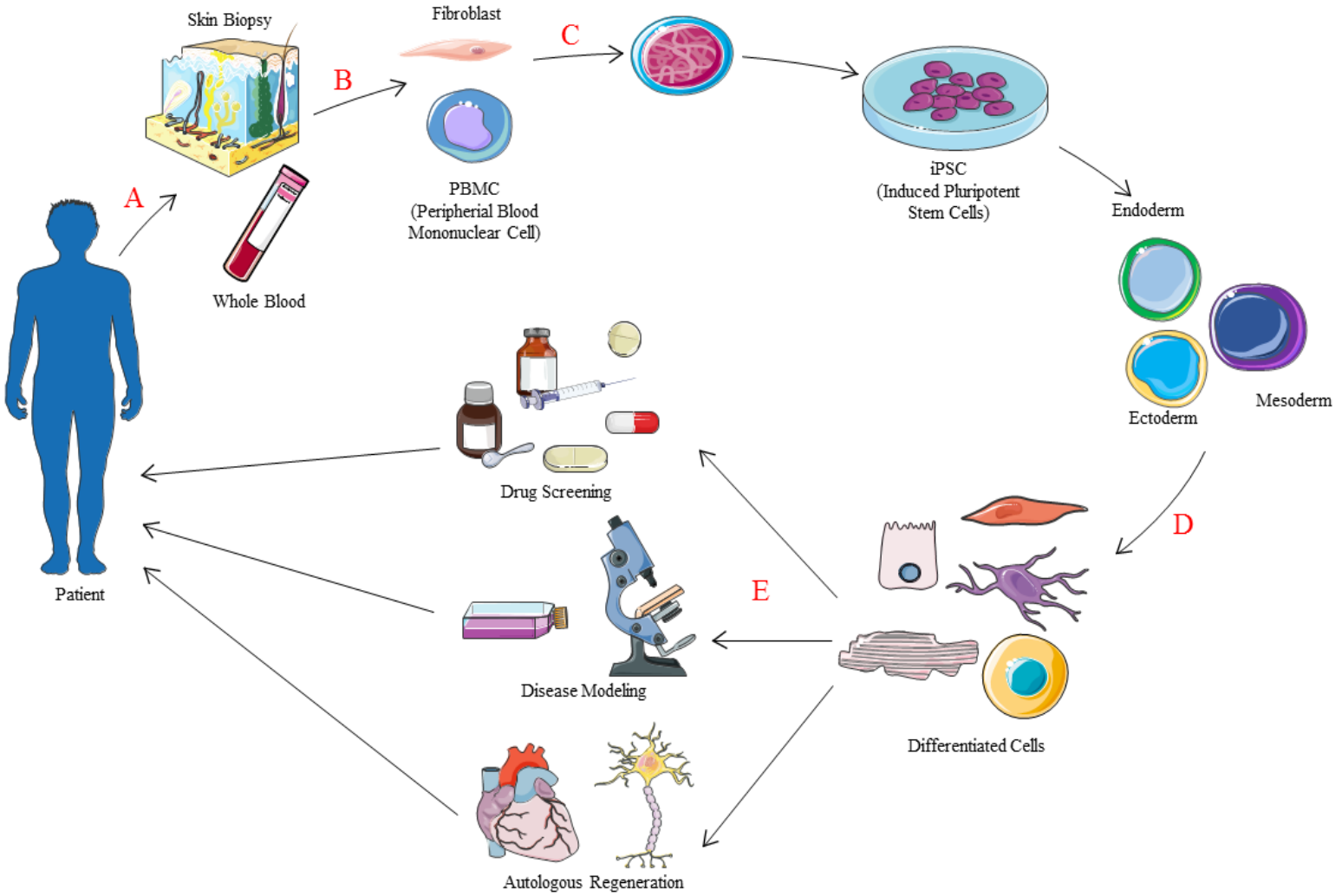

*Skin biopsy or blood samples are harvested from patients **(A)**, somatic cells are isolated **(B)** and reprogrammed into patient-specific hiPSCs **(C)**. Then, hiPSCs can be differentiated into different cell types **(D)**, such as cardiomyocytes, smooth muscle cells, endothelial cells and neurons, each of them suitable for different applications **(E)**. Figure generated with Servier Medical ART (SMART), licensed under a Creative Commons Attribution 3.0 Unported License.*

1.1.4 Applications of iPSCs technology

iPSC discovery has opened several gateways for disease modeling, drug discovery/screening, regenerative medicine and tissue engineering (figure 1.2E). An iPSC-based model has different advantages than the traditional cell line cultivations[7]. For instance, iPSCs can be derived from a readily accessible somatic cell source of diseased or healthy individuals, retaining both the same donor's genotype and phenotype. This feature makes them an ideal *in vitro* model to study genetic syndromes. The development of the CRISPR-Cas9 system has enabled to genetically manipulate the iPSC line to either correct or introduce genetic mutations[9]. The differentiation potential of hiPSCs allows the study of different diseases such as diabetes or heart, neurological, and liver diseases, just to name some[2] (figure 1.2D). Most relevant is the utility of iPSC technology in modelling rare and genetic diseases. Importantly, patient-derived hiPSCs can be exploited for precision medicine approaches to establishing novel treatment strategies based on disease-specific phenotypes. Moreover, the high proliferation rate and the self-renewal property allow for generation of libraries used for drug screening of known or predicted disease-modulators[10].

Finally, allogenic iPSCs display no immunogenicity after transplantation in mouse models[11], therefore they are under study for stem cell-based regenerative therapies.

1.1.5 hiPSCs biobank

Biorepositories of iPSCs are large collections of iPSC lines obtained from both healthy and diseased donors of different gender and age, that make it easier for researchers to access and share clinically relevant disease models affecting any tissues of an organism. Indeed, hiPSCs are pluripotent and may differentiate also into terminally differentiated cells of once-inaccessible tissues such as heart or brain. Collection of hundreds to thousands of cell lines allow creating a compendium of cell systems, ideal for "population on a dish" mechanistic studies[12]. Indeed, for drug discovery and development, the possibility to test new

compounds on high numbers of differentiated hiPSCs, enable recapitulating the human phenotype variability more closely than other previously used engineered cell systems.

A fundamental feature of pluripotent stem cell banking is the implementation of a management system that allows the prompt availability of hiPSC collections to the research community. This can be achieved through national and international repositories that accept, expand, qualify, and distribute the stem cell lines on a large scale. Distribution requires a series of documents with information regarding the stem cell provenance (acquired through the informed consent) and raw primary data (genomic and functional characterization); quality controls (QCs) and consistency of protocols used in manufacturing. All information should be stored and easily traced[13].

hiPSC lines collected into a biobank should meet high quality and safety standards. For clinical applications, it is fundamental that hiPSCs never comes in contact with animal-derived products nor xenogeneic reagents, unless they have been tested as clinical-grade (Good Manufacturing Practice-grade); whereas for research grade, it is sufficient to operate under Good Laboratory Practice conditions. However, regardless of the end use, it is important that every step in the whole process, starting from the original cells throughout expansion and manipulation, must be performed and recorded rigorously[13].

For the storage and distribution of high-quality and stable research-grade hiPSCs the biobanking set up should include the following steps[13]:

- Verification of the hiPSC line's identity, by short tandem repeat (STR) profiling. STR profiling is an easy, sensitive and reliable technology based on polymerase chain reaction (PCR)–based genotyping that is routinely used to prove hiPSC actually belong to human species and derive from its donor. For disease-specific line, it is also required to demonstrate that the disease-causing mutation is present in the iPSC line, whereas for genetically modified line, it should be proved that genetic modification was successful, and it is strongly encouraged to test number of insertions into the genome and off-target analysis.

- Data anonymization of donor, with the possibility to retrieve its clinical information, its genetic sequence and its appropriate consent. About this aspect, in May 2018 the new General Data Protection Regulation (GDPR) has released with the scope to "pseudonymized data"; the sample donor is de-identified but a key that allow a connection to the original donor is maintained[14].
- Provide all the information regarding the reprogramming method (vector system used, reprogramming factors used, demonstration that reprogramming vectors are no longer expressed in derivative stem cell lines).
- Verification of the absence of mycoplasma bacteria, and fungus contamination, and/or viral pathogens (HIV1, HIV2, HBV, HCV, HTLV1&2).
- Verification of genetic stability under culture by at least karyotyping (minimum resolution 5-10MB) and Fluorescent in Situ Hybridization (FISH) to detect or localize chromosomal abnormalities.
- Verification of the expression of pluripotent markers such as OCT4, SOX2 NANOG, NODAL, REX1 by RT-qPCR and/or immunocytochemistry and/or FACS, alkaline phosphatase staining.
- Verification of the ability to differentiate into three gem layers by EB formation assay.

1.1.6 Differentiation of iPSCs into CMs

During vertebrate embryonic development, the heart is the first organ to form and work. It forms soon after gastrulation, cells coming from the primordial anterior ectoderm undergo epithelial to mesoderm transition and settle between ectoderm and endoderm in the primitive streak[15]. The main steps needed to generate cardiomyocytes (CMs) from iPSCs are: (1) epithelial to mesenchymal transition, (2) formation of mesoderm, (3) patterning of mesoderm toward anterior mesoderm or cardiogenic mesoderm, (4) formation of cardiac mesoderm, (5) emerging of beating cardiomyocytes and (6) cardiomyocyte

maturation. Cardiac development is a dynamic process that is tightly regulated by the sequential expression of signal transduction proteins and transcription factors. A core set of evolutionary conserved transcription factors (Nkx2.5, Tbx5, Isl1, GATA4 and MEF2C) controls the expression of genes encoding contractile proteins, the morphogenesis of cardiac structures and consequently cardiac cell fates (figure 1.3).

Over the years, differentiation protocols that mimic the signaling pathways involved in embryonic cardiovascular development have been generated to obtain functionally mature hiPSC-CMs. Initially, protocols to differentiate iPSC into cardiomyocytes were highly inefficient (8-22% efficiency)[16]; current methods allow achieving a high yield of cardiac troponin-T positive cells[17]. The first differentiation protocol was based on suspension cultures of iPSCs that spontaneously aggregate forming EBs. After EB formation, cells differentiated into the three germ layers, and a few of them eventually acquired a cardiac phenotype. This first protocol was highly inefficient and not reproducible across cell lines. Currently, several commercially available optimized differentiation kits containing defined media enable more robust and reproducible results.

With these protocols/kits, iPSCs are grown in monolayer until confluence. Mesoderm induction is prompted by addition of specific growth factors such as fibroblasts grow factors (FGFs), bone morphogenic proteins (BMPs), and transcription factor inhibitor such as Wnt and glycogen synthase kinase 3 (GSK3). Several studies have shown that combinations of BMP4, Wnt3a and Activin A induce gastrulation-like events and meso-/endoderm development in pluripotent stem cells. At least a part of the cardio-inductive activity of anterior endoderm is mediated by growth factors belonging to the TGFβ-superfamily.

Figure 1.3. Schematic of cardiac lineage differentiation from human iPSCs.

		Cardiomyocytes Differentiation			
Stage	hiPSCs (day 0)	Mesoderm (day 2)	Cardiac Mesoderm (day 3-4)	Cardiac Progenitor (day 5-6)	Cardiomyocyte (day 7-10)
		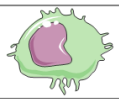			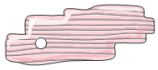
Markers	Nanog Oct4 Sox2 SSEA-3 SSEA-4 TRA1-60	T MixL I NCAM SSEA-1	MespI KDR PDGFRα KIT	Nkx2.5 Tbx5 Isl 1 GATA4 MEF2C	cTnT cTnI α-actin α-MCH β-MHC MCL2a MCL2v

The four primary stages of in vitro *CM differentiation from hiPSCs. Transcription factors and cell surface markers expressed by each cell type are indicated. Figure generated with Servier Medical ART (SMART), licensed under a Creative Commons Attribution 3.0 Unported License.*

The CMs differentiated from iPSCs are a mixed population of atrial, ventricular and nodal-like cells, but recent studies have demonstrated that it is possible to obtain subtype-specific hiPSC-derived cardiomyocytes with the addition of specific molecules[18–20].

1.1.7 Characterization of hiPSC-CMs

Cardiomyocytes derived from hiPSCs are recognized from undifferentiated cells by their ability to spontaneously beat in culture after 10-12 days from the induction of differentiation. They express structural proteins well organized in sarcomeres: α-MHC, β-MHC, MLC2a, MLC2v, cardiac troponin I and T and α-actinin. Isolation of hiPSC-CMs from non-cardiac cells can be achieved using a glucose-depleted culture medium containing lactate, since other cell types are not capable of using it for energy production[21]. To determine the yield of a cardiac differentiation protocol, fluorescent-activated cell sorting (FACS) or immunostaining for specific cardiac proteins should be carried out.

Electrophysiological analysis must be conducted to complete the functional characterization of hiPSC-CMs[22]. Patch clamp analysis is used routinely for quantitative recordings, at single cell level, of action potential (AP) and ion currents of cardiomyocytes[23]. Electrophysiology characterization evidenced immature characteristics in morphology of cytoskeletal proteins and ion channel expression and organization. Human iPSC-CMs are closer to fetal and embryonic-derived CMs than to mature adult CMs[24]. Isolated hiPSC-CMs showed an intrinsically reduced inward rectifier potassium current (I_{K1}) magnitude that can be compensated by dynamic patch clamp technique, which injects an artificial I_{K1} in real-time[25]. This technique changes the AP of hiPSC-CMs into one with more mature features such as greater upstroke velocity and the presence of the AP notch, allowing voltage-gated ion channels to properly work as they were in more physiological conditions.

Since the heart is a functional syncytium, also the measurements on multicellular networks provide a great amount of information in hiPSC-CMs characterization. The multi-electrode array (MEA) technology enables the investigation of the conduction system[26]. By culturing a functional beating mono- or multi- layered sheets of iPSC-derived cardiomyocytes on the MEA plate, voltage changes due to depolarization and repolarization across the surface can be simultaneously recorded to reveal the action potential conduction velocity.

The main ion involved in the excitation-contraction (EC) coupling pathway is the Ca^{2+}, which is a critical regulator of myocardial function. During AP, in response to depolarization caused by a large influx of sodium ions, Ca^{2+} crosses the sarcolemma and transverse-tubules (T-tubular) membrane entering the cell through the voltage gated L-type Ca^{2+} channels. Ca^{2+} influx triggers the release of a larger quantity of Ca^{2+} into the cell, called Ca^{2+} sparks, binding to and activating a type 2 ryanodine receptor (RyR2) located on the membrane of sarcoplasmic reticulum (SR). Therefore, the initial flow of Ca^{2+} into the cell, caused a larger release of Ca^{2+} within the cell, causing a process called calcium induced calcium release (CICR). The binding of cytosolic Ca^{2+} to the myofilaments initiates cardiomyocyte contraction[27]. Therefore, another method widely used to characterize hiPSC-CMs involved the use of calcium-sensing

fluorochromes to trace the intracellular calcium transient. Upon electrical stimulation, the release of intracellular calcium is indicated by the fluorescent emission that is recorded with an ultra-fast and sensitive camera[28].

1.1.8 Applications of iPSC-CMs for cardiovascular research

The advantages to reproduce in a dish the genetic, molecular, and electrophysiological characteristics of selected subjects makes iPSC-CMs candidate experimental models to study cardiac diseases of genetic origin and non-genetic origin, to develop personalized therapies, to test both existing drugs and new therapeutic compounds and for precision medicine, such as gender and population-specific differences in drug responses. It comes as no surprise that they have been the object of very active research.

One of the earliest reported iPSC-based disease models of a cardiac disease is the genetic form of Long QT Syndrome (LQTS)[29]. Inherited channelopathies refer to diseases caused by mutations in genes encoding ion channels, transporters, and accessory subunits that lead to cardiac electrophysiology impairment and result in life-threatening ventricular arrhythmia[30].

Recent studies demonstrate that hiPSC-CMs express angiotensin-converting enzyme 2 (ACE2) and are susceptible to severe acute respiratory syndrome coronavirus 2 (SARS-CoV-2) infection[31–33]. Therefore, hiPSC-CMs are a very good model to study the effect of SARS-CoV-2 infection at cardiac level and possible therapeutic compounds.

1.2 Long QT Syndrome

1.2.1 Cardiomyocyte action potential and electrocardiogram

Ventricular cardiac action potential is generated by a sequence of ion fluxes through specialized ion channels localized in the cardiomyocyte membrane. It matches with cardiac contraction/relaxation. The cardiac action potential is divided in 5 phases: phase 0 (depolarization), phase 1 (early repolarization), phase 2 (the plateau phase), phase 3 (repolarization) and phase 4 (the resting phase); figure 1.4.

Figure 1.4. Temporal correlation between action potential duration and the QT interval on the surface ECG.

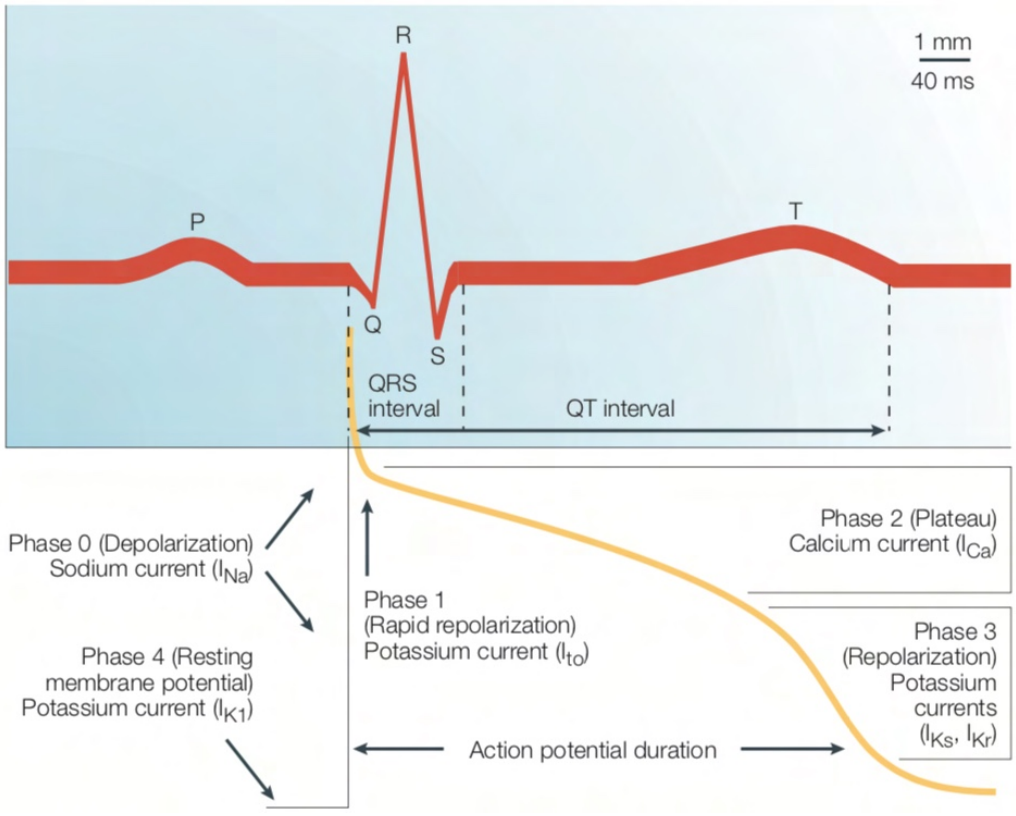

The P wave reflects atrial depolarization, the QRS complex reflects ventricular depolarization, and the T wave is indicative of ventricular repolarization. The QRS complex is produced by the upstroke (phase 0) of the action potential. The isoelectric S–T segment corresponds to the plateau (phase 2), whereas the T wave is indicative of ventricular repolarization (phase 3). The resting membrane potential corresponds to phase 4. The duration of the QT interval on the ECG is defined as the duration between the beginning of the QRS complex and the end of the T wave. Reproduced from Fermini et al[34].

During phase 0 sodium ions enter the cell through voltage-gated sodium channels (I_{Na}). The large amount of sodium ions creates a current that depolarizes the transmembrane potential and leads to a fast sodium channel closure. Also, L-type ("long-opening") calcium channels open and a small but steady influx of calcium occurs following its concentration gradient. Phase 1, also known as early repolarization phase, is mainly caused by activation of the transient outward potassium currents (I_{to}) together with a corresponding rapid decay of the sodium current. The following phase, phase 2, or plateau phase, involves L-type late calcium current (I_{CaL}) and a small amplitude late sodium current which allows calcium and sodium ions to enter the cell balancing the effect of outward potassium currents. The decay of the calcium current and the increase in delayed rectifier potassium current (I_{Ks}), in the rapid activation component of the delayed rectifier potassium current (I_{Kr}), and particularly in the late activation of the inward rectifier potassium current (I_{K1}), is responsible for the repolarization (phase 3) and finally to the resting potential (phase 4).

The electrocardiogram (ECG) is a record of voltage versus time of the electrical activity of the heart, due to the summation of all action potentials elicited by the cardiomyocytes forming the cardiac tissue. Its morphology consists of a P-wave, a QRS-complex and a T-wave. The QT-interval on the ECG is measured from the beginning of the QRS-complex to the end of the T-wave. The QT interval represents the depolarization and the repolarization phases of the cardiac ventricular action potentials (AP). The QT-interval is most affected by alterations in channels involved in plateau and repolarization phases of the action potential[35]. QT-interval can be shorten downregulating the I_{CaL}, and upregulating I_{Ks}, I_{Kr}, and I_{K1} channel currents, whereas upregulation of the I_{CaL}, and downregulation of potassium channels prolong the QT-interval[36].

In the normal heart, the QT-interval shortens with an increase in heart rate, so the Bazett correction formula is exploited to correct the QT-interval for the heart rate (QTc-interval).

1.2.2 Long QT Syndrome (LQTS)

Normal QT interval at the surface ECG is above 430 ms in male and above 450 ms in female. When the QT interval is longer than 450 and 470 ms respectively there is a pathogenic condition, called Long QT Syndrome (LQTS).

LQTS is a life-threatening cardiac arrhythmogenic syndrome characterized by abnormally prolonged ventricular repolarization which predisposes to syncope, "Torsade de Pointes" (TdP) type of ventricular tachycardia, or sudden cardiac death (SCD), mainly precipitated by emotional or physical stresses.

The prolongation of the QT interval, the phenotypic hallmark of LQTS, is caused either by genetic alterations (congenital LQTS), or by exogenous factors such as drugs (acquired or drug induced LQTS)[37,38].

Congenital LQTS is caused by mutations in genes encoding ion channels, or proteins involved in ion channels regulation, both responsible for the timely execution of the cardiac action potential. So far, 16 genes have been discovered [table 1.1; figure 1.5]; *KCNQ1*, *KCNH2* and *SCN5A* are the most common LQTS genes, accounting for ~75% of all genotype-positive cases[39]. *KCNQ1* and *KCNH2* encode for ion channels involved in the transport of potassium into the cell, while the transcription of *SCN5A* produces a subunit of a sodium channel[40].

Table 1.1. LQTS genes.

Type	Gene	Frequency	Locus	Protein
LQT1	*KCNQ1*	30-35%	11p15.5	K_v7.1 (↓)
LQT2	*KCNH2*	25-30%	7q35-36	K_v11.1 (↓)
LQT3	*SCN5A*	5-10%	3p21-p24	Na_V1.5 (↑)
LQT4	*ANKB*	<1%	4q25-q27	Ankyrin B (↓)
LQT5	*KCNE1*	<1%	21q22.1	MinK (↓)
LQT6	*KCNE2*	<1%	21q22.1	MiRP1 (↓)
LQT7	*KCNJ2*	<1%	17q23	K_{ir}2.1 (↓)
LQT8	*CACNA1C*	<1%	12p13.3	L-type calcium channel (↑)
LQT9	*CAV3*	<1%	3p25	Caveolin 3 (↑)
LQT10	*SCN4B*	<1%	11q23.3	Sodium channel β4 (↑)
LQT11	*AKAP9*	<1%	7q21-q22	Yotiao (↓)
LQT12	*SNTA1*	<1%	20q11.2	Syntrophin α1 (↑)
LQT13	*KCNJ5*	<1%	11q24	K_{ir}3.4 (↓)
LQT14	*CALM1*	<1%	14q32.11	Calmodulin 1 (↓)
LQT15	*CALM2*	<1%	2p21	Calmodulin 2 (↓)
LQT16	*CALM3*	<1%	19q13.32	Calmodulin 3 (↓)

KCNQ1, potassium voltage-gated channel; KCNH2, potassium voltage-gated channel, subfamily H, member 2; SCN5A, sodium voltage-gated channel, type V, α subunit; ANKB, ankyrin B; KCNE1, potassium voltage-gated channel, ISK-related subfamily, member 1; MinK, minimal K+ ion channel; KCNE2, potassium voltage-gated channel, ISK-related subfamily, member 2; MiRP, MinK-related peptide 1; KCNJ2, potassium channel, inwardly rectifying, subfamily J, member 2; AS, Andersen syndrome; CACNA1C, calcium voltage-dependent channel, L type, α-1C subunit; CAV3, caveolin 3; SCN4B, sodium voltage-gated channel, type IV, β subunit; AKAP9, A-kinase anchor protein 9; SNTA1, syntrophin α1; KCNJ5, potassium channel, inwardly rectifying, subfamily J, member 5; CALM1, calmodulin1; CALM2, calmodulin2; CALM3, calmodulin3. Functional effect: (↓) loss-of-function or (↑) gain-of-function at the cellular in vitro level.

Figure 1.5. Classification of LQTS susceptibility genes.

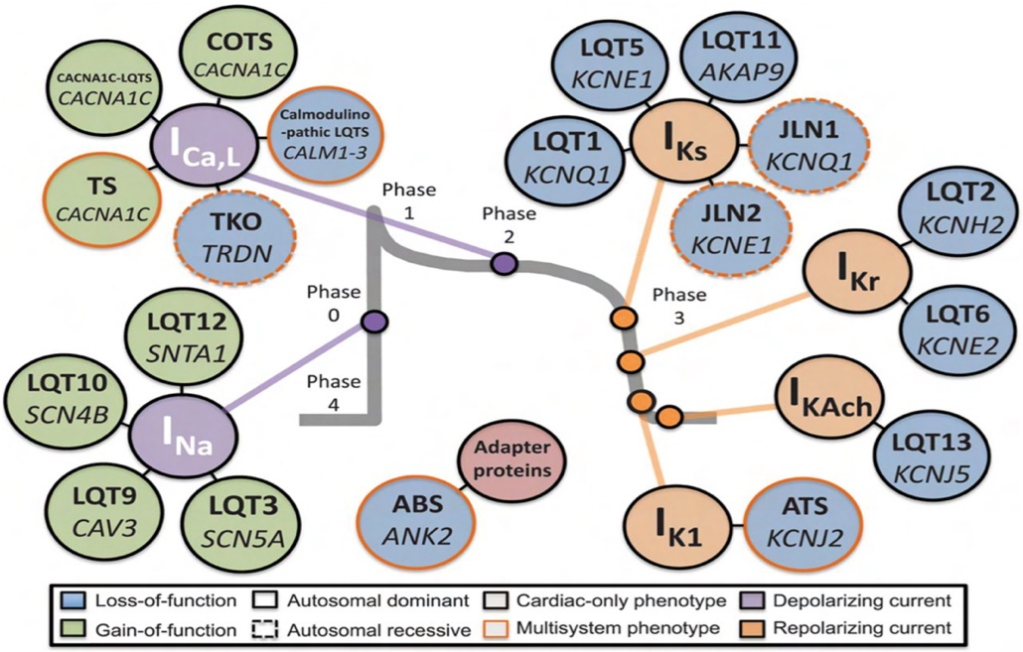

Perturbation of ventricular cardiac action potential (CAP) depolarization (purple), repolarization (orange), or adaptor/signaling proteins that influence CAP (maroon) by mutations in LQTS genes. Blue circles represent loss-of-function, green circles represent gain-of-function, solid lines indicate autosomal dominant and dashed lines indicate autosomal recessive. COTS, Cardiac Only Timothy Syndrome; TS, Timothy Syndrome; TKO, Triadin Knockout Syndrome; JLN, Jervell and Lange-Nielsen Syndrome; ABS, Ankyrin-B Syndrome; ATS, Arterial Tortuosity Syndrome. Adapted from Giudicessi et al[41].

1.2.2.1 LQTS type 2 (LQT2)

The *KCNH2* gene encodes for the α-subunit $K_v11.1$ of the voltage-gated potassium (K^+) channel hERG (human ether-a-go-go-related gene). Four $K_v11.1$ α-subunits co-assemble into a tetrameric ion channel which mediates rapid delayed rectifier K^+ current (I_{Kr}), that plays a fundamental role in the repolarization phase of the cardiac action potential, effectively regulating the action potential duration (APD) and QT interval observed in ECG[42,43].

hERG is expressed in multiple tissues and cell types, including neural[44,45], smooth muscle[46] and tumor cells[47]. However, hERG is mostly expressed in the heart, and this is where its function and dysfunction are best studied.

LQTS type 2 is caused by mutations in the *hERG* gene. Functional expression studies have identified four classes of mechanisms underlying the loss-of-function phenotype observed in LQT2 patients: abnormalities in $K_v11.1$

synthesis (class 1); dysfunction in intracellular transport (protein trafficking) to the cell surface membrane (class 2); defects in channel gating (class 3); or abnormalities in permeation (class 4)[43].

It has been demonstrated that major differences between men and women exists in epidemiology, manifestation, pathophysiology, treatment, and outcome of CVD, including LQTS [48]. Hence, studying sex hormones and their interaction with the ion channel hERG is important. This disparity confirms that sex differences being important at the level of ion channel structure and function[49].

It was demonstrated that women with LQT2 are more likely than men to suffer cardiac event[49–51]. Moreover, it seems that men with loop mutation in *hERG* gene are more likely to suffer an event than those with no loop location; instead in women there is no correlation with the location of the mutation[50].

1.3 Polycystic Ovary Syndrome (PCOS)

Polycystic ovary syndrome (PCOS) is one of the most common endocrine and metabolic disorders in women of reproductive age[52]. This syndrome is highly heterogeneous and is defined by a combination of signs and symptoms of androgen excess (hirsutism and/or hyperandrogenemia) and ovulatory dysfunction (menstrual dysfunction and/or polycystic ovarian morphology (PCOM) due to an excessive number of preantral follicles in the ovaries) in the absence of other specific diagnoses. PCOS is frequently associated with abdominal adiposity, insulin resistance, obesity, metabolic disorders and cardiovascular risk factors[52–54].

Globally, the prevalence of PCOS ranges between 4% and 21% depending on the diagnostic criteria (table 1.2) and the population studied[53,55–57].

The exact cause of PCOS is unknown. However, it is understood to be a multifactorial condition with a genetic component[58], besides strong epigenetic and environmental influences, including diets and lifestyle factors[52]. An estimated 20-40% of first-degree female relatives of women with PCOS develop PCOS themselves compared to 4-6% prevalence in the general population[59].

Table 1.2. Polycystic Ovary Syndrome Classification.

Parameter	**NIH 1990**[60]	**ESHRE/ASRM 2003**[61,62]	**AE-PCOS 2006**[63,64]	**NIH 2012 extension of ESHRE/ASRM 2003***
Criteria	HA	HA	HA	HA
	OA	OD	Ovarian dysfunction (OD and/or PCOM)	OD
	\	PCOM	\	PCOM
Limitations	Two of two criteria required	Two of three criteria required	Two of two criteria required	Two of three criteria required
				Identification of specific phenotypes included: **Phenotype A:** HA + OD + PCOM **Phenotype B:** HA + OD **Phenotype C:** HA + PCOM **Phenotype D:** OD + PCOM

NIH, National Institutes of Health; ESHRE, European Society for Human Reproduction and Embryology; ASRM, American Society for Reproductive Medicine; AE-PCOS, Androgen Excess & PCOS Society; HA, hyperandrogenism; OA, oligo-anovulation; OD, ovulatory dysfunction; PCOM, polycystic ovarian morphology. Adapted from Lizneva et al[57]*.*
**https://prevention.nih.gov/research-priorities/research-needs-and-gaps/pathways-prevention/evidence-based-methodology-workshop-polycystic-ovary-syndrome-pcos*

Insulin resistance is not part of diagnostic criteria, despite it is present in up to 95% of obese women with PCOS and up to 75% of lean women with PCOS[65]. Notably, few prior studies and meta-analyses have shown that presence of insulin resistance and hyperinsulinemia increase the risk of cardiovascular diseases (CVD), coronary heart disease (CHD) and stroke, in women with PCOS. Results of these studies, which compare the degree of CVD risk in PCOS versus the general population, have demonstrated mixed findings[66–68].

Since 2002 it has investigated the QT intervals and QT dispersion in PCOS. Alpaslan et al., in 2002, demonstrated that QT interval prolongation or increased QT dispersion is not a part of the cardiac abnormalities in patients affected by PCOS[69]. Recently, other studies tried to study QT prolongation and dispersion in patients affected by LQTS and PCOS compared to age-matched healthy women. Gazi et al. demonstrates that, in patients affected by LQTS and PCOS, increase in insulin and estradiol levels can cause QTc prolongation whereas high testosterone levels cause QTc shortening[70]. Also, Vrtovec et al. obtained the same result[71].

1.3.1 Estrogens in cardiac myocytes

Three endogenous physiologic estrogens exist: estrone (E1), estradiol (E2) and estriol (E3). The predominant and most biologically active form of estrogen is 17β-estradiol (E2), formed from the aromatization, mediated by cytochrome p450 aromatase, of testosterone in multiple tissues (including bone, breast, adipose tissue, and the brain[72]) but predominantly in the ovaries of premenopausal women[27,73]. In this thesis work, the term estrogen refers to E2.

It was demonstrated that the aromatase is also expressed in the heart tissue and so the E2 can be produced also locally in cardiac cells[27,74–77].

Estrogen mediates its actions on the heart through three identified estrogen receptors (ERs). Estrogen receptor subtypes α (ERα; *ESR1*) and β (ERβ; *ESR2*) are classical nuclear hormone receptors, which bind estrogen and translocate to the nucleus to regulate target gene expression, called genomic mechanism[78–80].

The genomic action of estrogen signaling is mediated by ligand-dependent DNA or transcription factor binding and subsequent regulation of transcription. ERs function as dimers, both homodimers and heterodimers, binding to palindromic DNA sequences called estrogen response elements (EREs)[81]. Transcription regulation can also occur through the recruitment of coregulators, coactivators and/or corepressor, to enhance or inhibit, respectively, gene expression[79]. Moreover, ERs can interact with other transcription factors. A membrane-bound ER, distinct from ERα and ERβ, was identified as the orphan receptor GPR30 before being renamed G protein-coupled estrogen receptor (GPER)[81,82], which mediates a non-genomic mechanism. The non-genomic action mediates rapid signaling events, including cAMP production, calcium mobilization[83,84], ion channel activation (regulation of potassium channel)[85,86] and protein kinase activation with the resulting activation of secondary signaling cascades and effectors, which can also regulate transcription through or independent of ERs[81].

ERα and GPER are expressed at similar levels in male and female human cardiac tissue[87,88]. Different studies have been conducted to establish the ERβ expression in the human and rat heart, and results are conflicting. Some studies indicate that ERβ may be upregulated in the heart during disease or impact cardiac function through infiltrating cells rather than in cardiomyocytes[88–91]. Instead, other studies indicate that ERα and ERβ induce cardioprotection[92], or that ERβ has a dominant role[93] and another suggests physiological redundancy or compensation[94]. In table 1.3 are outlined the distinct features of the ER subtypes[95].

Table 1.3. Features and classification of estrogen receptors.

Features	**GPER**	**ERα**	**ERβ**
Cellular location	Cytosol[96] Plasma membrane[82]	Nucleus[97,98] Cytosol[99,100] Plasma membrane[100,101]	Nucleus[100] Cytosol[99] Plasma membrane[98,102]
Onset of physiological effects	Rapid actions (effects within seconds to minutes)[103]	Rapid and genomic action (effects within minutes to days)[102–106]	Rapid and genomic action (effects within minutes to days)[97,102,106,107]
Cardiovascular tissue distribution	Cardiac fibroblast[108] Vascular tissues[109] Cardiomyocytes[110]	Cardiac fibroblast[74] Vascular tissues[103,111] Cardiomyocytes[112,113]	Cardiac fibroblast[112] Vascular tissues[111] Cardiomyocytes (unresolved)
Relative abundance in cardiac cells	Highest[110]	Low[110]	Lowest[110]

GPER, G-protein-couples estrogen receptor; ERα, estrogen receptor α; ERβ, estrogen receptor β. Adapted from Machuki et al[95].

Epidemiological data suggest that estrogen is an important regulator of cardiovascular function; premenopausal women show decreased incidence of hypertension and coronary artery disease compared with age-matched men and postmenopausal women[114,115] and this led to the conclusion that estrogen protects against CVDs in premenopausal healthy woman[27,116], because it is an important regulator of diastolic cardiac function[117].

The main mechanisms affected by the loss of estrogen include: changes in mitochondrial metabolic function, induction of cardiac remodeling, enhancement of left ventricular hypertrophy, impairment of nitric oxide pathway/role of GPER, alteration of cellular Ca^{2+} and alteration of titin[117].

1.3.2 Effects of sex hormones on the QTc interval

Nearly 100 years ago, differences in QTc-interval were described between healthy adult males and females. The QTc-interval of females, after puberty, is longer than males[118]. The difference between males and females decreases with age, the QTc-interval increases faster in men in correlation with the gradual decrease of the level of testosterone[119]. The difference is correlated to changes in sex hormones levels, but the mechanisms on the repolarization are complex and still unresolved[36]. It has been demonstrated that testosterone decreases the I_{CaL} current and increases the potassium channel currents (I_{Ks}), resulting in a shorter QTc-interval. The testosterone, beside influencing I_{Ks} and shortening early repolarization, mostly affects the I_{CaL}[119]. In addition, progesterone decreases the I_{CaL} current and increases the I_{Ks} current shortening the QTc-interval[119]. Concerning estrogen, conflicting results have been described about the influence on the QTc interval. According to clinical data, estrogen seems to lengthen the early repolarization in animals, acting on the potassium channel current; however, this has not yet been supported by human studies[36].

Although the longer QTc-intervals in women is not associated with a higher incidence of SCD, females are certainly predisposed to malignant cardiac events if associated with QTc-interval prolongation diseases (i.e. LQTS). Females

affected by LQTS type 1 show no important changes in QTc-interval in time[51,120–122]. On the contrary, in most studies has been reported that females affected by LQTS type 2 show prolongation of QTc-interval[51,121,122]. In patients affected by LQTS type 3, both males and females, no evident changes in QTc-interval are seen. However, LQT3 females tend to have a slight prolongation in QTc-interval[51,121]. In one study, Anneken et al. provided mechanistic evidence for an increased *hERG* ion channel trafficking to the cell membrane under estrogen stimuli. Estrogen seems to increase chaperone (Hsc70/Hsp90) proteins interaction with *hERG* ion channel[123], improving the channel trafficking.

1.4 Severe Acute Respiratory Syndrome Coronavirus 2 (SARS-CoV-2)

1.4.1 SARS-CoV-2: main features

Severe acute respiratory syndrome coronavirus 2 (SARS-CoV-2) is a novel beta coronavirus (β-CoV) first identified in China in November 2019 and is the etiological agent of coronavirus disease 2019 (COVID-19). Among humans, coronaviruses are transmitted primarily through respiratory droplets, direct contact with contaminated surfaces and fecal–oral transmission. Direct transmission by respiratory droplets is reinforced by productive SARS-CoV-2 replication in both the upper and lower respiratory tracts, which increase human-to-human spread among close contacts exhibiting active coughing[124].

Coronaviruses (CoVs) are enveloped, single-stranded positive RNA viruses. SARS-CoV-2 genome is 29.8 Kb and comprises 14 open reading frames (ORFs), two-thirds of which encode nonstructural proteins involved in the replicase-transcriptase complex, one-third encodes for accessory and structural proteins[125]. The four structural proteins are spike (S), envelope (E), nucleocapsid (N) and membrane (M), of which S mediates SARS-CoV-2 entry into host cells interacting with angiotensin-converting enzyme 2 (ACE2) receptor (figure 1.6).

Figure 1.6. Schematic representation of SARS-CoV-2 particle structure.

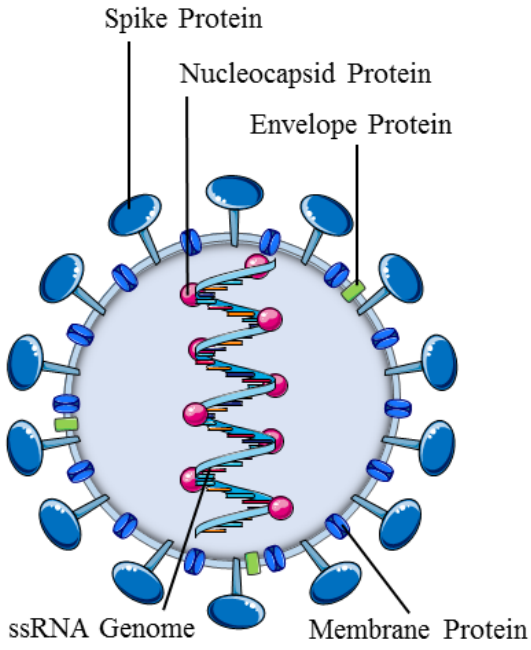

SARS-CoV-2 is composed of a positive-sense RNA genome and four structural proteins: spike (S), nucleocapsid (N), envelope (E) and membrane (M) proteins. Figure generated with Servier Medical ART (SMART), licensed under a Creative Commons Attribution 3.0 Unported License.

Spike has a receptor-binding domain (RBD) mediating direct contact with the host receptor ACE2. The extracellular domain is composed of two subunits S1 and S2, which mediate receptor binding and membrane fusion respectively[124]. The S1/S2 site in SARS-CoV-2 forms an exposed polybasic site that is proteolytically cleaved by cellular cathepsin L and/or the transmembrane protease serine 2 (TMPRSS2)[126]. The latter facilitates viral entry at the plasma membrane surface, whereas cathepsin L activates Spike in endosomes and can compensate for entry into cells lacking TMPRSS2[126]. Once the virus genome is released into the host cytosol, replicase genes are translated. The genomic and subgenomic RNAs are translated into accessory and viral structural proteins that are inserted in the rough endoplasmic reticulum. The proteins are inserted into the secretory pathway to the endoplasmic reticulum-Golgi intermediate compartment (ERGIC) for virion assembly[124]. Then the virus is released via exocytosis, sometimes without lysate the cells (figure 1.7).

Figure 1.7. SARS-CoV-2 lifecycle.

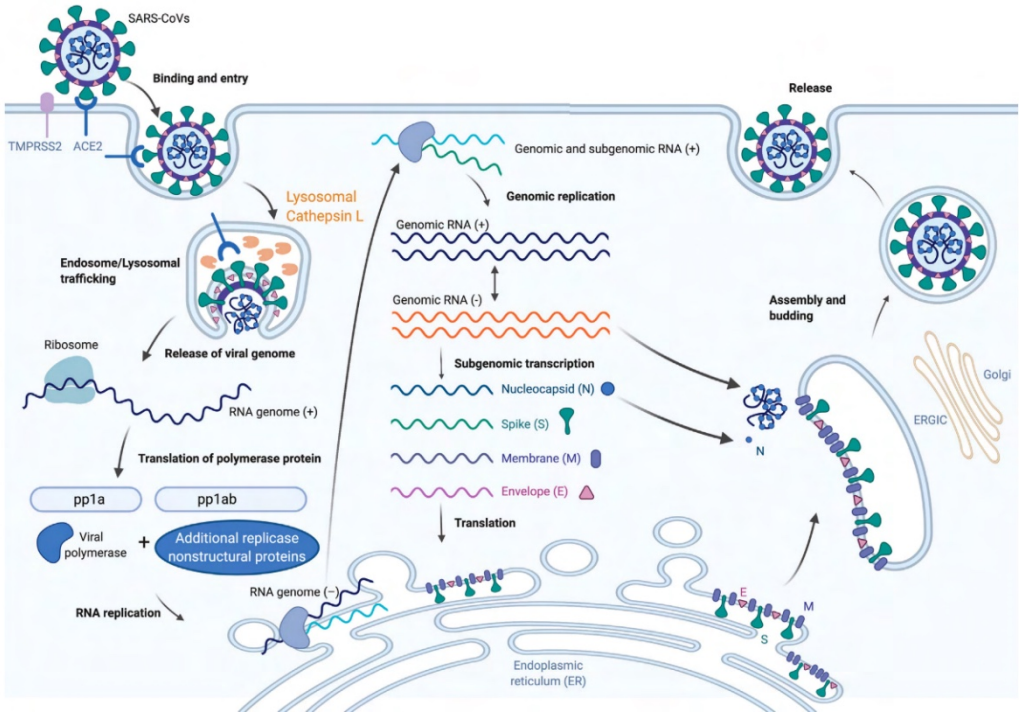

SARS-CoV-2 lifecycle starts by binding of the envelope Spike protein to its cognate receptor, angiotensin-converting enzyme 2 (ACE2). Efficient host cell entry depends on cleavage of the S1/S2 site by the surface transmembrane protease serine 2 (TMPRSS2) and/or endolysosomal cathepsin L, which mediate virus–cell membrane fusion at the cell surface and endosomal compartments, respectively. The RNA genome is released into the cytosol, where it is translated into the replicase proteins. The positive-strand genome serves as a template for full-length negative-strand RNA and subgenomic (sg)RNA. sgRNA translation results in accessory and structural proteins (indicated here as N, S, M, and E) that are inserted into the ERGIC for virion assembly. Finally, virions are secreted from the plasma membrane. Reproduced from Harrison et al[124].

Different *in vitro* studies reported that in some cell lines, such as Calu-3, 16HBE (both pulmonary cancer cell lines) and Caco2 (colorectal adenocarcinoma cell line) the viral replication occurs without the manifestation of a cytopathic effect[127,128]. The cytopathic effect is defined as cell rounding, detachment, fusion with adjacent cells to form a syncytium, and the appearance of nuclear or cytoplasmic inclusion bodies. In the African green monkey kidney epithelial cell line VERO E6, SARS-CoV-2 undergoes through a lytic cycle associated to a strong cytopathic effect (Takayama, 2020).

1.4.2 SARS-CoV-2 variants

Since the onset of the pandemic, many variants of SARS-CoV-2 have occurred[130]. Most of the variants of SARS-CoV-2 are results of point mutations in their nucleotides during replication, which are extremely significant for their transmission, virulence, antigenicity and evading antibody actions[131].

Initially, there were only few variants of SARS-CoV-2 due to the global absence of immunity against this pathogen and the low mutation rates of the coronaviruses which encode an enzyme with proofreading function that increases the fidelity of the replication process[131]. A new variant, with a single D614G mutation in Spike glycoprotein was detected in early March 2020. This new variant spreads globally over the next month due to increased transmissibility and virus replication[132,133].

Variants of SARS-CoV-2 have been classified into three groups: Variant of Interest (VOI), Variant of Concern (VOC), and Variant of High Consequence (VOHC). This classification is based on their specific genetic markers, transmission, and disease severity[130].

Variants that have been classified or that are still VOC are listed below.

Alpha (B.1.1.7) variant. The B.1.1.7 variant was unveiled in December 2020 in the United Kingdom (UK) in which was declared an increase in the incidence of SARS-CoV-2 infection. Since then, it has become the predominant variant and has largely replaced the circulating viruses. Epidemiological studies suggest that this variant spreads 56% faster than the wild-type strain[134]. Compared to ancestral viruses containing the D614G mutation, the B.1.1.7 variant has accumulated 23 mutations. Nearly half of reported changes (47%) occur in the spike gene[131].

Beta (B.1.351) variant. Starting from November 2020, the new variant B.1.351 was identified by the authorities from the Republic of South Africa. It replaced the circulating viruses becoming the dominant variant. Compared to the Wuhan reference strain, the South Africa's variant has 13 mutations. About 77% of these mutations are in the gene encoding the spike protein[135]. The two variants, B.1.1.7

and B.1.351, share the N501Y mutation that confers an increasing binding affinity of spike for ACE2 receptor, raising the viral transmission rate[131].

Gamma (P.1) variant. The third variant of SARS-CoV-2 is the P.1 variant and was isolated from four travelers who arrived in Tokyo from Brazil in January 2021. The P.1 variant has become the dominant circulating virus. This variant contains 12 mutations in the spike proteins. B.1.1.7 and B.1.351 have the N501Y mutation. The E484K mutation, which is shared with the B.1.351 variant, is the most worrying because it has been demonstrated that this mutation confers the ability to evade antibody-mediated immunity[136].

Delta (B.1.617.2) variant. The B.1.617.2 variant was identified in India in December 2020. Nowadays, Delta is the dominant circulating variant. It contains 7 mutations in the gene encoding for spike protein. The B.1.617.2 variant is characterized by its increased transmissibility, and major ability to evade antibody-mediated immunity[137].

Omicron (B.1.1.529) variant. The B.1.1.529 variant was identified in South Africa in November 2021. The Omicron variant is the most mutated variant among all the VOC. Its genome constitutes 18261 mutations, 97% of them are present in the coding region. The RDB of the spike proteins contains 30 mutations which two out of three are shared with Delta variant. The N501Y mutation in combination with Q498R mutation increase the RDB binding affinity with the ACE2 receptor and allow immunological escape. Indeed, the B.1.1.529 variant is responsible to the 4th wave of the COVID-19 outbreak[138].

1.4.3 Renin-Angiotensin System (RAS)

ACE2, the functional receptor for SARS-CoV-2 infection, is expressed in the lungs, small intestine, colon, gallbladder, testes, brain, esophagus, kidney, liver, heart, and blood vessels[139]. ACE2 is a key modulator of the renin-angiotensin system (RAS), which is a peptidergic system constitutively acting to execute biological function and to maintain physiological homeostasis.

When blood pressure decreases in the renal system, renin is released into the bloodstream. Renin converts angiotensinogen into angiotensin I (AngI), which is cleaved by angiotensin-converting enzyme (ACE) to form angiotensin II (AngII). This peptide acts on Ang II type 1 and type 2 receptors (AT1R and AT2R) promoting, when it binds AT1R, vasoconstriction, fibrosis, inflammation, salt and water reabsorption, oxidative stress and apoptosis. ACE2 counterbalances the hypertensive effects of AngII, converting it into angiotensin 1-7 (Ang1-7). Accordingly, Ang1-7 binds to Mas receptor promoting vasodilatation/anti-inflammatory effects (figure 1.8).

Figure 1.8. Renin–angiotensin system (RAS).

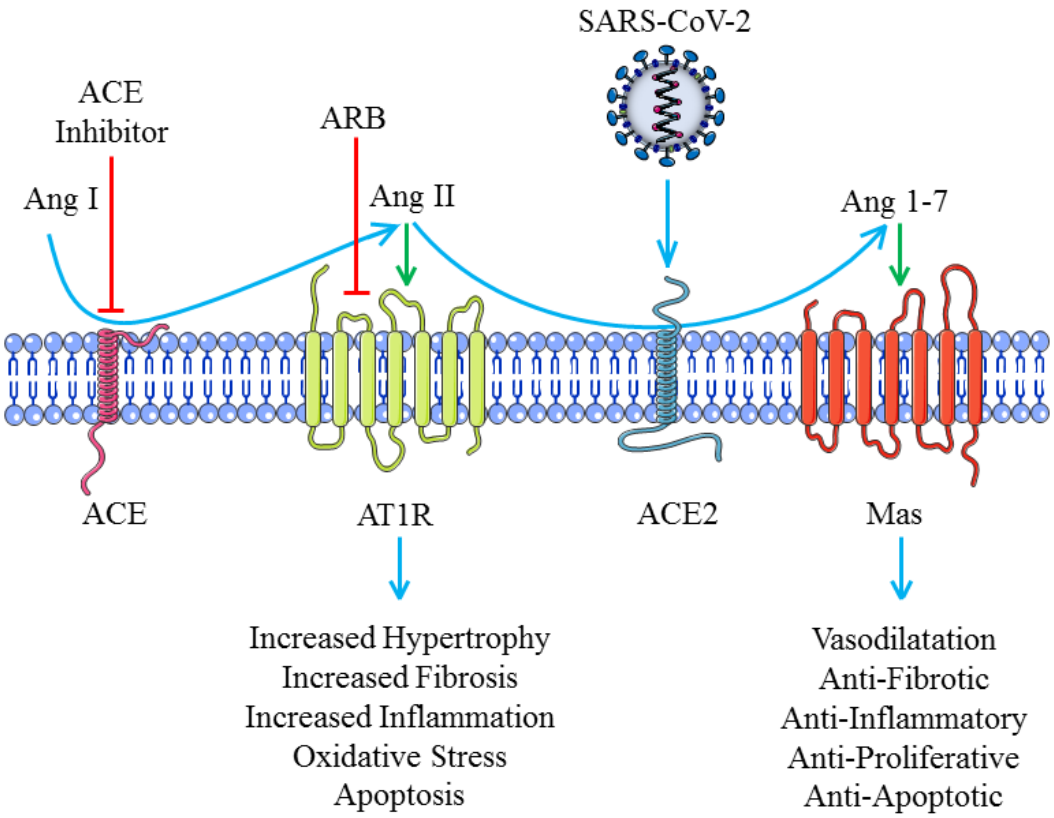

Ang I: angiotensin I; Ang II: angiotensin II; Ang 1-7: angiotensin 1-7; ACE: angiotensin-converting enzyme; ACE2: angiotensin-converting enzyme 2; AT1R: angiotensin II type 1 receptor; Mas: Mas receptor. Figure generated with Servier Medical ART (SMART), licensed under a Creative Commons Attribution 3.0 Unported License.

1.4.4 COVID-19 clinical manifestation

Coronavirus disease-2019 (COVID-19) has the characteristics of diverse clinical manifestations, indeed it is defined as a multiorgan disease. Generally, the SARS-CoV-2 virus invades the airway epithelium and then starts to replicate. When the viral load increases, the virus starts to leak the pulmonary vasculature tract invading the bloodstream and travelling to other organs expressing ACE2 receptor[140].

Immunity plays an important role in determining the severity of COVID-19. A high immune response may lead to a huge inflammatory process that leads to acute respiratory distress (ARDS) and multiple organ failure syndrome (MOFS), which are the most common causes of mortality in COVID-19[141].

Many factors can determine the severity of COVID-19, such as viral load, presence of comorbidities, genetic factors, age, sex, use of immune-suppressive agents, and immunity[141]. Examples of comorbidities are diabetes mellitus, chronic obstructive pulmonary disease, chronic lung disease, chronic kidney disease, cancer and hypertension[142].

At pulmonary level, two pathological mechanisms could explain ARDS in COVID-19 patients. The first mechanism involves the ACE2 receptor expressed on pneumocytes II, which are responsible to produce the pulmonary surfactant. Pulmonary surfactant is crucial in reducing surface tension in the lungs. When SARS-CoV-2 binds to the ACE2 receptor, it leads to damage and destruction of alveolar cells leading to an increase in the surface tension and predisposition to ARDS. The second mechanism considers the cytokine storm. Cytokine storm is a hyperimmune response that leads to an excessive release of proinflammatory cytokines that leads to multiple organ failure and ARDS[143].

Up to 30% of COVID-19 patients may develop cardiac damage. Major cardiac manifestations include arrhythmias, myocarditis, pericarditis, and acute coronary syndrome (ACS)[144]. Approximately 5–25% of hospitalized COVID-19 cases manifested elevation in cardiac Troponin T blood level, a biomarker of cardiac damage[145–148].

Two mechanisms lead to cardiac manifestations in COVID-19 patients. The first mechanism involved the ACE2 receptor. ACE2 receptor is highly expressed in cardiac tissue therefore SARS-CoV-2 may directly infect cardiac cells inducing myocardial damage[139]. The second mechanism is the consequence of ARDS and reduced pulmonary functionality. ARDS alters normal functionality of organs due to low oxygen saturation levels and low oxygen supply. Severe hypoxia can lead to cardiovascular injury and mortality risk. Moreover, SARS-CoV-2 infection elicits a systemic inflammation causing an increase in blood viscosity, endothelial dysfunction, activation of the coagulation cascade and atherosclerotic plaque rupture[149].

In particular, the hyper-inflammation triggered by SARS-CoV-2 infection can lead to myocarditis. Myocarditis is an acute inflammation of myocardium caused by infections, exposure to toxic substances and/or activation of the immune system. Some cases of fulminant myocarditis in COVID-19 patients have been reported. Nevertheless, in other two case reports, myocarditis was diagnosed in patients who were not initially suspected to have COVID-19. In the case report of Fried et al. the patient had no symptoms other than chest pressure but was eventually found to be SARS-CoV-2 positive and diagnosed with myocarditis[150]. In the case report by Gnecchi et al. a 16-year-old boy was admitted to the emergency department complaining of intense chest pain. He reported no other symptoms, only fever the day before, no medical history and no contact with anyone with confirmed COVID-19. He was tested for SARS-CoV-2 and resulted positive. He presented high levels of biomarkers for cardiac damage and was subsequently diagnosed with myocarditis[151,152]. Another study reported the case of a 69-year-old patient with flu-like symptoms rapidly degenerated into respiratory distress, hypotension and cardiac shock. Endomyocardial biopsy showed low-grade myocardial inflammation and viral particles were found in intestinal cytopathic macrophages and their surroundings[153]. This report demonstrates that SARS-CoV-2 localizes in cardiac tissue, despite the exact mechanism of myocardial injury has not been clear yet.

1.4.5 Pre-existing conditions

A significant percentage of COVID-19 patients admitted to hospital and later deceased showed one or more comorbidities. A study conducted by the Italian "Istituto Superiore di Sanità" (ISS) revealed that the presence of three or more comorbidities has the highest incidence of fatality (table 1.4).

Table 1.4. Most common comorbidities observed in SARS-CoV-2 positive deceased patients divided by gender.

	All		Women		Men	
Diseases	***N***	***%***	***N***	***%***	***N***	***%***
Ischemic heart disease	2,218	*28.0*	762	*23.7*	1,456	*31.0*
Atrial Fibrillation	1,958	*24.8*	835	*25.9*	1,123	*23.9*
Heart failure	1,245	*15.7*	578	*17.6*	667	*14.0*
Stroke	908	*11.5*	400	*12.4*	508	*10.8*
Hypertension	5,204	*65.8*	2,183	*67.8*	3,021	*64.4*
Type 2-Diabetes	2,317	*29.3*	882	*27.4*	1,435	*30.6*
Dementia	1,860	*23.5*	1,028	*31.9*	832	*17.7*
COPD (Chronic Obstructive Pulmonary Disease)	1,375	*17.4*	458	*14.2*	917	*19.5*
Active cancer in the past 5 years	1,291	*16.3*	469	*14.6*	822	*17.5*
Chronic liver disease	404	*5.1*	138	*4.3*	266	*5.7*
Dialysis	179	*2.3*	59	*1.8*	120	*2.6*
HIV Infection	18	*0.2*	2	*0.1*	16	*0.3*
Autoimmune diseases	366	*4.6*	202	*6.3*	164	*3.5*
Obesity	909	*11.5*	363	*11.3*	546	*11.6*
Number of comorbidities						
0 comorbidities	230	*2.9*	64	*2.0*	166	*3.5*
1 comorbidity	902	*11.4*	320	*9.9*	582	*12.4*
2 comorbidities	1,424	*18.0*	543	*16.9*	881	*18.8*
3 comorbidities and over	5,354	*67.7*	2,291	*71.2*	3,063	*65.3*
Complications from SARS-CoV-2 infection	N	*%*	N	*%*	N	*%*
Acute respiratory distress syndrome	7,264	*93.6*	2,906	*91.7*	4,358	*94.9*
Acute renal injury	1,929	*24.9*	674	*21.3*	1,255	*27.3*
Acute cardiac injury	792	*10.2*	292	*8.9*	500	*10.5*
Co-infection	1,562	*20.1*	602	*19.0*	960	*20.9*

(https://www.epicentro.iss.it/en/coronavirus/sars-cov-2-analysis-of-deaths)

Hypertension was the most common comorbidity detected in 64.4% of deceased patients. The two main classes of hypertensive drugs used to treat these patients are the RAS inhibitors angiotensin-converting enzyme inhibitors (ACEIs) and angiotensin II type 1 receptor blockers (ARBs), which block ACE and AT1R respectively. The impact of these drugs on the clinical course of COVID-19 is

controversial, indeed initially it has been proposed that patients should discontinue this medication. Some studies have shown that these drugs could significantly increase the expression of ACE2 and increase SARS-CoV-2 infectivity[154]. Most of the experiments that reported an increase in ACE2 expression were conducted on animal models, but in nearly all studies doses of ACEIs/ARBs used were greater than equivalent doses typically administered to human[155]. On the contrary, reviews and meta-analysis indicated that administration of RAS inhibitors was not associated with increased mortality or severity of COVID-19 patients[156]. The effects of ACE inhibitors and ARBs therapy toward the infection of SARS-CoV-2 need to be clarified.

1.4.6 COVID-19 treatment strategies

Therapies help to prevent the entry or disrupt the replication of viruses with the goal of minimizing patient infections, morbidity and facilitating a rapid recovery to full health[157]. Worldwide, different therapeutic strategies have been investigated in treating COVID-19. Principal treatments are listed below.

Antivirals. Compounds able to directly target SARS-CoV-2 and its lifecycle, excluding antibodies, are classified as antivirals.

Remdesivir, which is approved for COVID-19 treatment by U.S. Food and Drug Administration (FDA), is an antiviral that inhibits the RNA-dependent RNA polymerase of RNA viruses[158]. Hence, it inhibits viral replication through premature termination of RNA transcription.

Another antiviral not yet approved by the FDA is Favipiravir, which, like Remdesivir, inhibits RNA-dependent RNA polymerase[159]. The latest data evidence a lack of significance in mortality and any effect on the clinical course of COVID-19[160].

Lopinavir/ritonavir, an orally administered drug, is a combination of a viral protease (Lopinavir) and an inhibitor of cytochrome P450 (Ritonavir). Different clinical trials are ongoing, some were stopped early since there was no significant clinical benefit among treated and non-treated patients[161,162]. One

other which use this drug in a combination with a third antiviral (Ribavirin)[163] had a significant reduction in time to recovery, demonstrating the potential of using combination therapies.

At the end of 2021, two antiviral pills, Molnupiravir (MK-4482) produced by Merck and Paxlovid (PF-07321332 and Ritonavir) produced by Pfizer, are considered effective treatments. Molnupiravir, originally developed to treat Venezuelan equine encephalitis virus (VEEV), can induce mutations into the RNA reducing viral viability over the duration of infection[164]. In *in vitro* studies, on Calu-3 and VERO E6, Molnupiravir reduced viral titer[157]. On December 21, 2021, FDA approved Molnupiravir "for the treatment of mild-to-moderate coronavirus disease (COVID-19) in adults positive to SARS-CoV-2 viral testing. Molnupiravir should be initiated within five days of symptom onset." (https://www.fda.gov/news-events/press-announcements/coronavirus-covid-19-update-fda-authorizes-additional-oral-antiviral-treatment-covid-19-certain) Clinical trials and preliminary results showed that Molnupiravir reduced the risk of admission to hospital or death by 50%[165,166]. Medicines and Healthcare Products Regulatory Agency in UK was the first to approved Molnupiravir as clinical treatment for COVID-19[167]. Paxlovid is a combination of PF-07321332 protease inhibitor and Ritonavir that boosts the effectiveness of protease inhibitors. *In vitro* studies suggested that Paxlovid could have a high therapeutic impact. Different clinical trials are ongoing, but preliminary results from two completed clinical trial showed that Paxlovid reduce hospitalization or death by 89% compared to placebo in non-hospitalized high-risk adults affected by COVID-19[168]. Drug combinations may be key to treating early COVID-19; Molnupiravir and Paxlovid act on the virus in different ways making them together a potent strategy if resistance to one becomes widespread.

Anti-inflammatories and immunomodulatory drugs. Treatments able to limit the hyperimmune response are classified as anti-inflammatory and immunomodulatory. Many COVID-19 patients progress to ARDS, characterized by serious inflammation and release of inflammatory cytokines, which eventually lead to multiple organ failure[140]. Furthermore, patients develop

coagulopathy and thrombosis which increase the morbidity and the mortality of the disease[140].

Compound 21 (C21) is an agonist for the AT2R involved in the RAS system. In contrast to AT1R, AT2R has an anti-inflammatory effect. Clinically, C21 trials have demonstrated limited success; moreover, mortality is not significantly affected[157].

Whereas C21 agonizes AT2R, Losartan inhibits binding of angiotensin II to AT1R to limit its pro-inflammatory and thrombotic effects. Clinical trials concerning Losartan did not find significant differences in mortality nor changes in disease severity[169].

Dexamethasone is a corticosteroid used to treat inflammatory illnesses; indeed corticosteroids suppress expression and release of pro-inflammatory cytokines attenuating inflammatory response and reducing the damage associated with immune responses[170]. However, a meta-analysis of ten clinical trials found that the drug poses a risk of persistent immunosuppression at high doses increasing the incidence of secondary infections[171]. Thus, dexamethasone may be a possible therapeutic against COVID-19 when administered carefully and early in the onset of ARDS in patients with severe disease. Clinical trials are ongoing and show that dexamethasone decreased mortality only when associated with invasive mechanical ventilation or oxygen supplement[172].

Tocilizumab is a monoclonal antibody against IL-6 receptor, a pro-inflammatory cytokine. COVID-19 patients have a statistically significant increase in IL-6[173], which causes a muscle dysfunction and triggers a strong inflammatory response. However, tocilizumab clinical trials have not shown an improvement in mortality nor in hospital discharge[174].

Anticoagulants. Heparin is clinically used as an anticoagulant, it binds to antithrombin III (AT-III) by activating it. Active AT-III in turn inactivates thrombin, factor X and other proteases involved in blood clotting. Heparin has been approved for clinical use to treat and prevent blood coats in COVID-19 patients. About 100 clinical trials using heparin are ongoing and show that

heparin is a promising treatment strategy for critically ill COVID-19 patients hospitalized in Intensive Care Unit (ICU)[157]. Moreover, heparin may improve the lung function due to its mucolytic activities[175].

Hyperimmune plasma. Blood plasma obtained from recovered patients, also known as convalescent plasma, contains antibodies against the infectious virus that reduce disease severity[176,177]. Convalescent plasma, in *in vitro* studies, is capable of neutralizing SARS-CoV-2[178]. Clinical trials find divergent results in mortality rate, some, with a little sample size, show a decrease in mortality rate, instead others found no significant differences in mortality or clinical status[179,180].

Monoclonal antibodies against Spike protein. Bamlanivimab is a monoclonal antibody which targets epitopes on the RBD of the SARS-CoV-2 spike protein. Prior to the arrival of the Delta variant, this monoclonal antibody presented great clinical results, significantly reducing hospitalization and death[181]. A good strategy is a mAbs combination which targets different epitopes at the same time.

Antirheumatic drugs. Hydroxychloroquine (HCQ) is a weak base that has been used to treat malaria and at lower doses, is in clinical use to threat rheumatoid arthritis. It diffuses spontaneously and rapidly across the membranes of cells and organelles with acidic cytoplasmic vesicles such as endosomes, lysosomes, or Golgi vesicles and thereby increases their pH which leads to dysfunction of several enzyme[182]. HCQ showed antiviral properties in *in vitro* studies; the drug inhibits early endosome acidification and maturation into endolysosomes, resulting in retention of virions in early endosomes[183]. Despite its potential mechanism of action against SARS-CoV-2, clinical trials using HCQ monotherapy did not show a significant clinical benefit[184].

Cell-based therapy. The inflammatory nature of COVID-19 also points toward a solid rationale for the use of mesenchymal stromal cells (MSCs) as a possible new cell-based therapy. MSC are adult stem cells with capacity for self-renewal and multi-lineage differentiation. Initially described in the bone marrow, MSC are also present in other organs and tissues such as adipose tissue, cord blood, cord tissue and placenta[185]. From a therapeutic perspective, given their ease to

isolate, low immunogenicity, amenability to *ex vivo* expansion, and genetic modification, they are optimal candidate for tissue repair and regeneration[185].

MSC-based therapy has been successfully employed for the treatment of immune-mediated disorders, due to their ability to trafficking to the damaged tissue and down-modulate the inflammatory response[186]. Several clinical studies, including phase III trials, documented their efficacy in the control of graft-versus-host disease in recipients of allogeneic haematopoietic stem cell transplantation, and there are evidences also in other immune-mediated disorders[186]. In addition, there are existing pre-clinical and a few preliminary feasibility and safety clinical studies supporting further investigation of cell-based therapies, particularly with mesenchymal stromal cells (MSCs), or the MSC-derived secretome, for potential treatment of ARDS and acute myocarditis[186–188].

Current understanding of MSC mechanisms of action is that most of their beneficial effects in repair from injury occur through secretion of cytoprotective, repair-promoting, and immunoregulatory factors[189]. Some examples include the induction of M2 macrophages, inhibition of natural killer cell proliferation and their cytotoxic function, anti-inflammatory cytokine production, and promotion of T regulatory cell generation[187]. Overall, these immunomodulatory effects can facilitate the resolution of inflammatory processes, including those characterizing ARDS and acute myocarditis. Furthermore, MSCs have constitutively low immunogenicity allowing off-the-shelf allogeneic use and there is a strong track record of safety for use in a range of diseases. MSCs from different sources including bone marrow, adipose, cord blood, and placental tissues, have shown promising results in experimental models of lung diseases, following either systemic or direct endobronchial administration[187]. Phase I and II trials have demonstrated feasibility and safety of systemic administration of MSCs in non-COVID ARDS patients and inflammatory cardiomyopathy[188,190].

A pilot study conducted in China on seven patients affected by SARS-CoV-2 pneumonia has reported feasibility and safety of MSC therapy[191], and a total of 39 phase I/II trials testing MSC-therapy for COVID-19 are currently registered

in ClinicalTrials.gov. However, infusion of MSCs in the presence of active viremia has raised some critical issues regarding the possibility that the virus may infect MSCs, causing not only lack of efficacy but also possible deleterious effects. As alveolar epithelium and capillary endothelium are major sites of viral replication during COVID-19 disease, it was hypothesized that MSCs retained within the lungs and the capillaries, for instance after intravenous infusion, may rapidly undergo infection and relative virus-mediated lysis, with significant decrease in therapeutic efficiency. For this reason, determining if human MSCs can be infected by SARS-CoV-2 is of crucial importance. Indeed, stem cells are generally resistant to viral agents[190] but infection of MSCs by avian influenza or herpesviruses has been reported[192,193], and a similar concern has been raised for the SARS-CoV-2.

Whether human MSCs of any origin constitutively express ACE2 and/or TMPRSS2 is so far unclear. Leng et al claimed the absence of ACE2 and TMPRSS2 expression on the umbilical cord-derived MSC infused in their study[191], even though a clear demonstration was not reported. Moreover, if all human MSC types express or not ACE2 is still a matter of debate and solid data are missing.

Table 1.5. Summary of SARS-CoV-2 treatment strategies.

Treatment	Mechanism of action	Clinical benefit	Decrease in mortality
Antivirals			
Remdesivir	RNA-dependent RNA polymerase	Yes	Yes/No
Favipiravir	RNA-dependet RNA polymerase	Yes	No
Lopinavir/Ritonavir	Viral protease	Yes	No
Molnupiravir	RNA-dependet RNA polymerase	Yes	Yes
Paxlovid	Protease inhibitor	Yes	Yes

Anti-inflammatory Drugs			
Compound 21	AT2R	Yes	No
Losartan	AT1R	No	No
Dexamethasone	Inflammatory cytokine production	Yes	Yes
Tocilizumab	mAb against IL-6 receptor	No	No
Anticoagulant			
Heparin	Blood clotting	Yes	Yes
Hyperimmune Plasma			
Convalescent plasma	Polyclonal Abs against SARS-CoV-2	Yes/No	No
Monoclonal Antibodies against Spike protein			
Bamlanivimab	mAb against the receptor binding domain of the spike protein	Yes/No	Yes/No
Antirheumatic drugs			
Hydroxychloroquine	Endosomal acidification	No	No
Cell therapy			
Mesenchymal Stromal Cells (MSCs)	Down-modulate inflammatory response	Yes	N\A

Yes: the drug produced the column's effect; No: the drug failed to produce the column's effect; Yes/No: the drug produced negative and positive outcomes; N\A: data not available.

1.3.7 COVID-19 vaccines

Shortly after SARS-CoV-2 diffusion, spike was identified as the immunodominant antigen of the virus. It was demonstrated that the receptor-binding domain of the S1 subunit is targeted by neutralizing antibodies[194]. Several vaccine designs were evaluated and generated to stimulate the immune system against the S1 spike subunit. Different types of vaccines were designed: mRNA expressing the spike S1 subunit (Pfizer-BioNTech and Moderna);

adenoviral replication defective vectors expressing spike protein (AstraZeneca and Johnson&Johnson); spike synthetic protein/peptide (Novavax) and inactivated SARS-CoV-2 (Sinovac and Sinopharm). Published data demonstrated higher antibody responses to the mRNA vaccines and to Novavax protein subunit vaccine than other types[195]. However, the onset of new SARS-CoV-2 variants can modify the potency of neutralizing antibodies, compromising vaccine efficacy. Indeed, a significant increase in transmission between vaccinated people has been observed for Delta and Omicron variants, but the severity of disease is still much reduced, indicating the high vaccine effectiveness[195].

So far, only 62% of the world population is vaccinated, this is due to the difficult distribution of vaccine doses around the world, particularly in Africa and Latin America, or to a significant amount of people who cannot be vaccinated for age or health conditions. Moreover, there are still many people who do not want to get vaccinated contributing to keep the percentage relatively low. For those not vaccinated people who contracts COVID-19, and so at high risk, treatments remain an essential part of the COVID-19 fight [157].

2 AIMS

2.1 PROJECT 1: Generation of a biobank of somatic cells and hiPSCs from patients with inherited cardiovascular diseases

The goal of Project 1 was to contribute to the expansion of a biobank of patient-specific, de-identified cell lines, previously set-up by my lab, the Laboratory of Experimental Cardiology for Cell and Molecular Therapy, comprising 69 lines isolated from patients covering a broad spectrum of cardiovascular diseases (i.e. LQTS, Danon's disease, Emery-Dreifuss syndrome and other rare familiar cardiomyopathies), healthy controls, and non-cardiac disease controls.

The discovery of iPSCs and concurrent development of protocols for their cell-type specific differentiation have revolutionized studies of diseases and raised the possibility that personalized medicine may be achievable. For this reason, the demand for iPSC is quickly growing. However, not many iPSC banks exist in Italy. Moreover, the process of developing and testing iPSCs is complex and requires sophisticated technical procedures and expertise, not readily available in many laboratories. In the last few years, my Lab has developed the expertise to establish, test and characterizing iPSCs.

I now propose to implement that biobank and to use the iPSC technology to model rare cardiac diseases and test novel therapies.

A more general scope of project 1 is to improve the expertise of the lab in generating, characterizing, and differentiating iPSCs into cardiomyocytes. Specifically, most of the iPSC lines generated in my lab were reprogrammed starting from skin biopsy and using integrated retroviruses. During PhD, a new reprogramming method based on the use of non-integrating Sendai virus vectors (CytoTune™-iPS 2.0 Sendai Reprogramming Kit, Invitrogen®) was optimized on both skin fibroblasts and on the easier accessible peripheral blood mononuclear cells PBMCs).

I also worked on the optimization of the protocol for the differentiation of iPSCs into cardiomyocytes to increase their purity and maturation.

2.2 PROJECT 2: define the role of sex hormones as disease modifiers of LQTS in hiPSC-CMs from a patient affected by both LQT2 and PCOS

In project 2 it was chosen one of the hiPSC line generated for the biobank, to model the role of sex hormones as disease modifiers of LQTS. That hiPSC line derived from a patient affected by LQTS Type2 (class 3 mutation, c.1882G>A (p.Gly628Ser) [VCV000014427.1]), and by PCOS, associated with high levels of testosterone and low levels of estrogen. The first manifestation of LQT2 in this patient occurred during puberty, after starting an estro-progestin therapy, which was never regularly taken by the patient, especially when cardiac events occurred. Therefore, the aim of the project was to investigate how estrogens modulate the QT interval, with a particular focus on the temporal dynamic of ventricular repolarization changes, on the impact on early after depolarization (EAD) and ventricular arrhythmias susceptibility.

2.3 PROJECT 3: use of hiPSC-CM to model the cardiovascular complications of COVID-19

In project 3 hiPSC-CMs from healthy donors were used to clarify important aspects of SARS-CoV-2 pathogenicity and cardiotoxicity.

SARS-CoV-2 is the etiological agent of COVID-19 that was initially classified as a severe acute respiratory syndrome and has emerged as a global pandemic. Up to 30% of COVID-19 patients may develop cardiac damage due to acute myocarditis, acute coronary syndrome, or septic heart.

SARS-CoV-2 entry in host cells is mediated by the interaction between the viral Spike glycoprotein, and the host angiotensin-converting enzyme 2 (ACE2). ACE2 is expressed in several tissues included in the heart, where it serves as a key counter-regulator of the renin–angiotensin aldosterone system (RAAS). ACE2 converts Ang II to Ang 1–7, counterbalancing the fibrotic, oxidative, and pro-inflammatory effects of the Ang II/AT1R, and thus imparting protection against heart failure.

It has been reported in preclinical studies that some widely used anti-hypertensive drugs such as the ARB Valsartan and the ACEI Lisinopril may modulate ACE2 expression, therefore there is no consensus as to whether the risk and severity of SARS-CoV-2 infection might be increased or reduced with the use of such agents.

Accordingly, the aims of this project are: 1) prove that SARS-CoV-2 can directly infect hiPSC-CMs; 2) test if Valsartan and Lisinopril have any effects, protective or detrimental, on SARS-CoV-2 infection of hiPSC-CMs.

2.4 PROJECT 4: determine the safety of MSC as a possible stem cell therapy for the most severe forms of COVID-19

Human MSCs are currently under investigation for the treatment of COVID-19. However, the potential safety profile of hMSCs in this context had never been defined since none had described if they express ACE2 and TMPRSS2, the main host cell factors for SARS-CoV-2 entry, and if they can be infected by SARS-CoV-2. Therefore, the aim of this project was to evaluate for the first time whether hMSCs from various sources (amniotic membrane of human placenta, cord blood, cord tissue, bone marrow, and adipose tissue) express ACE2 and, most importantly, if they are permissive to SARS-CoV-2 infection.

3 PROJECT 1. Generation of a biobank of somatic cells and hiPSCs from patients with inherited cardiovascular diseases

3.1 Results

3.1.1 Biobank

The Laboratory of Experimental Cardiology, since 2011, has been collecting and storing in a biobank, samples of 69 patients covering a broad spectrum of cardiovascular diseases and non-cardiac disease controls. The first patients were enrolled thorough skin biopsy (SB) collection, after signing a specific informed consent form approved by the ethics committee of the Fondazione IRCCS Policlinico San Matteo in Pavia. Fibroblasts isolated from skin biopsies, were reprogrammed to iPSCs using traditional method based on retroviral vectors and culture on MEF feeder layer.

Starting from October 2018, I contributed to the expansion of that biobank, reaching a total of 122 patients enrolled and sample collected.

During the first year of the project, a lot of effort was spent for the optimization of hiPSC generation (see pages 109-116 for details), expansion (see pages 115-116 for details), and CM differentiation protocols (see pages 117-120 for details). At first, feeder-dependent hiPSC cultures were transitioned to feeder-free cultures in TeSR-E8 medium (STEMCELL Technologies™) and hESC qualified Matrigel matrix (Corning). Then fibroblast reprogramming was improved, by replacing the retrovirus-based protocol in use with a non-integrative one involving transfection of mRNAs. Finally, this protocol was replaced with a new one based on the use of non-integrative Sendai viral vectors (SeV). This protocol allows to reprogram not only the fibroblasts, but also the PBMCs isolated from peripheral blood (PB). Indeed, we started to collect PBMCs to facilitate the enrollment of more probands and their relatives.

A total of 38 patients were enrolled through PB, which 24 were probands and the other 14 samples were collected from family members. 6 patients were enrolled through both SB and PB collection, and 4 were probands.

A total of 30 iPSC lines were generated, of which 3 with mRNA methods and 8 with SeV technique.

To differentiate iPSCs into cardiomyocytes, differentiation protocols from feeder-free hiPSCs were optimized, testing a custom-made protocol based on the sequential use of glycogen synthase kinase 3 (GSK3) and beta-catenin inhibitors, and two commercially available kits with defined media: PSC Cardiomyocyte Differentiation Kit (Gibco™) and STEMdiff™ Cardiomyocyte Differentiation Kit (STEMCELL Technologies™).

4.1.2 iPSCs generation and characterization

The hiPSC lines generated in our laboratory were characterized following the steps required by international guidelines. In the following paragraphs are reported examples of hiPSC line characterization of two out of the three methods used to reprogram the cells of the biobank: retroviruses and SeV.

The characterization of an iPSC line reprogrammed with mRNA technique is reported in Project 2.

4.1.2.1 Characterization of iPSC generated by retroviruses

Patient clinical history:

LQT1.P4 iPSC line, unique stem cell line code PSMi006-A, was generated by reprogramming dermal fibroblasts isolated from skin biopsy of a 40-years-old woman affected by an autosomal recessive form of LQTS type 1 (AR-LQT1). The enrolled patient had a markedly prolonged QTc (QT corrected for heart rate of 576 ms), and she experienced several syncopal episodes and a documented episode of ventricular fibrillation triggered by emotional stress. The patient carries a homozygous mutation on the KCNQ1 gene: c.535 G/A, leading to the substitution of the glycine in position 179 with serine. Her two older sisters carry the same mutation in homozygosis; the firstborn died at age 19 after an intense emotional stress, the second born is still alive but experienced several cardiac episodes. Finally, her son is heterozygous for the mutation and asymptomatic[196].

hiPSC characterization:

Fibroblasts were reprogrammed by retroviral infection of OCT4, SOX2, KLF4 and c-MYC (see page 109 for protocol). The obtained hiPSCs were maintained on feeders, retaining embryonic stem cell (ES)-like morphology (figure 3.1C) and pluripotent features up to passage 50. Both patient's fibroblasts and hiPSCs present the disease-causing mutations on the KCNQ1 gene (figure 3.1A. The KCNQ1 coding sequence -CDS- used as a reference is the NCBI sequence NM_000218.2) and an identical DNA profile at seven polymorphic loci by Short

tandem Repeat (STR) analysis. The DNA karyotyping (300 g-bandings; see page 126 for details) revealed normal female chromosome asset (46, XX) (figure 3.1B). PSMi006-A uniformly expresses the human ES surface antigens Tumor Related Antigen-1-60 (TRA-1-60), Stage Specific Embryonic Antigen-3 and −4 (SSEA-3, SSEA-4) (figure 3.1C–D), and the pluripotent markers NANOG, OCT4, SOX2 (figure 3.1C–E), REX1, GDF3, ESG1, DPPA2, DPPA4 and NODAL (figure 1.1E). Likewise, it shows alkaline phosphatase (AP) activity (figure 3.1C; see page 127 for protocol). Table in figure 3.1D shows immunocytochemistry counting of anti Nanog-positive ($Nanog^{+}$) and anti TRA-1-60-positive ($TRA\text{-}1\text{-}60^{+}$) cells. The total number of cells in each of the fields analyzed was quantified by counting the nuclei stained with Hoechst 33258. RT-PCR in figure 3.1F (see pages 139-140 for details) shows no expression of the four viral transgenes (Tg) in naïve fibroblasts (HDF), clear expression of Tg OCT4, SOX2, KLF4 and cMYC in fibroblasts five days after transduction (OSKM) and silencing of the four Tg in PSMi006-A at passage 5. AR-LQT1 cell line spontaneously forms embryoid bodies (EBs) able to differentiate into cells belonging to the three germ layers: endoderm, mesoderm and ectoderm (figure 3.1G). In addition, we used the PSC Cardiomyocyte Differentiation Kit (Gibco™) to successfully differentiate this PSMi006-A line into spontaneously beating cardiac-like cells expressing typical cardiac markers: the sarcomeric proteins alpha-actinin (α-SA) and troponin I (TnI) (figure 3.1H, the insets show areas of cross-striation). We also excluded the presence of mycoplasma contamination (figure 3.1I; see page 149 for protocol)[196].

Figure 3.1. LQT1.P4 iPSC line characterization.

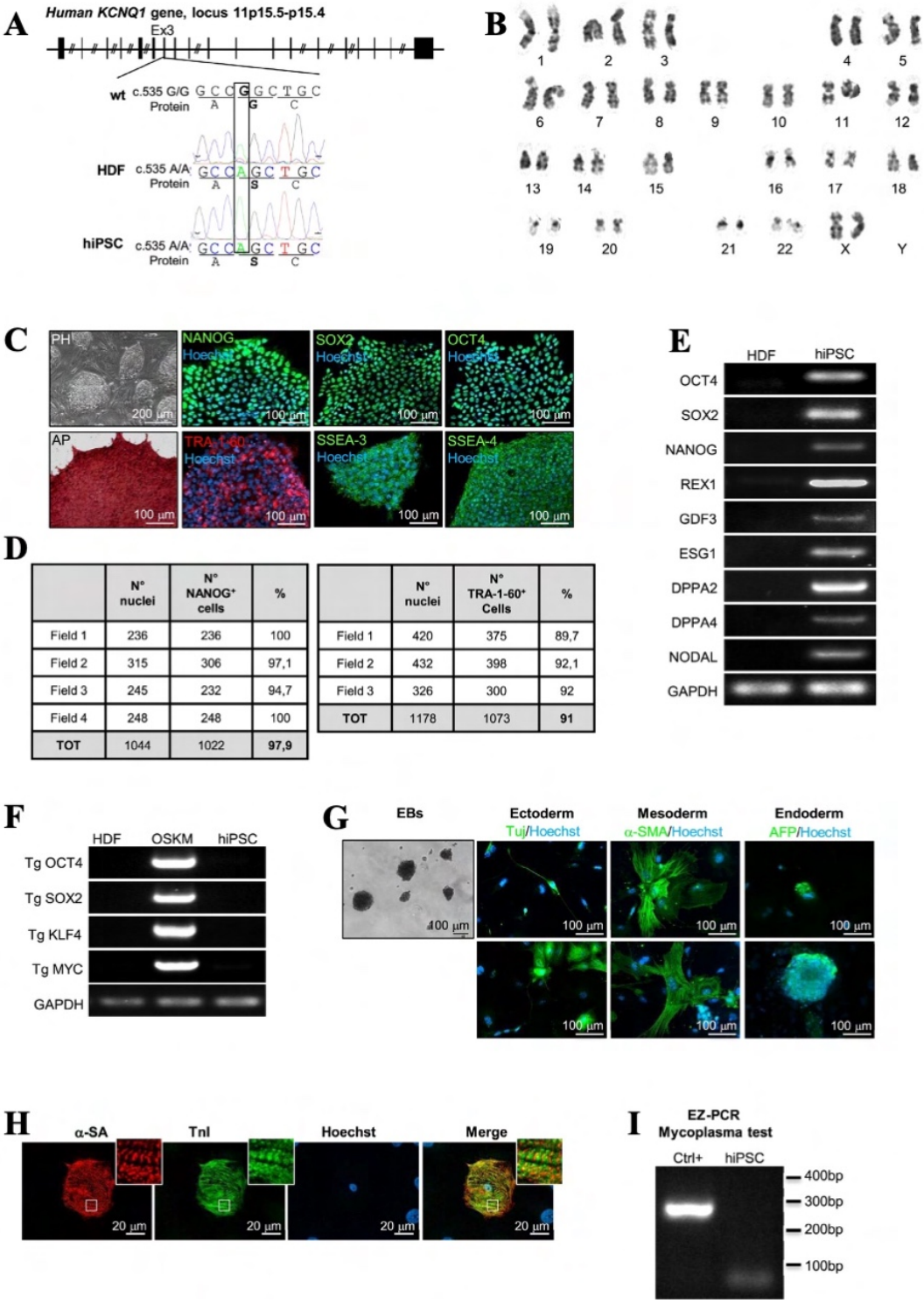

	N° nuclei	N° NANOG+ cells	%
Field 1	236	236	100
Field 2	315	306	97,1
Field 3	245	232	94,7
Field 4	248	248	100
TOT	1044	1022	**97,9**

	N° nuclei	N° TRA-1-60+ Cells	%
Field 1	420	375	89,7
Field 2	432	398	92,1
Field 3	326	300	92
TOT	1178	1073	**91**

(A) *DNA sequencing results showing the presence of the mutation 535 G>A in homozygous on the Exon 3 of KCNQ1 gene of HDF and hiPSC. The KCNQ1 coding sequence used as a reference is NM_000218.2.* ***(B)*** *Karyotype analysis of PSMi006-A (300 G-bandings).* ***(C)*** *PH: phase contrast image showing morphology. AP: alkaline phosphatase colorimetric staining. Immunofluorescence staining showing uniform expression of pluripotency markers; nuclei were counterstained with Hoechst (blue).* ***(D)*** *Immunocytochemistry counting of anti Nanog-positive (Nanog+) and anti TRA-1-60-positive (TRA-1-60+) cells.* ***(E)*** *RT-PCR analysis showing expression of the indicated markers of pluripotency in hiPSC, compared with HDF.* ***(F)*** *RT-PCR analysis showing no expression of the four Tg in HDF, expression of Tg*

five days after transduction (OSKM) and silencing of the four Tg in hiPSC. ***(G)*** *Far left panel: floating embryoid bodies (EBs) formed after 7 days of cell culture in suspension. Panels on the right: immunofluorescence staining for markers of the 3 germ layers in iPSC-derived EBs: Tuj for ectoderm; SMA for mesoderm, and AFP for endoderm.* ***(H)*** *Co-immunofluorescence staining for α-SA (red) and TnI (green) in cardiomyocytes differentiated from the PSMi006-A. Nuclei were counterstained with Hoechst (blue).* ***(I)*** *EZ-PCR test showing the absence of mycoplasma contamination in PSMi006-A. The positive control is provided by the kit. Scale bar: 100μM. Reproduced from Mura et al*[196]

4.1.2.2 Characterization of iPSC generated by SeV

Patient clinical history:

LQT16.P1 iPSC line was generated by reprogramming PBMCs isolated from peripheral blood of a 3-month-old baby affected by an autosomal dominant form of LQTS type 16 (AD-LQT16). The enrolled patient had a markedly prolonged QTc (QT corrected for heart rate of 606 ms) and experienced self-resolved episodes of TdP arrhythmias. The left ventricle is globular with a non-compaction appearance. The baby carries a heterozygous de novo mutation on the CALM3 gene: c.389 A/G, leading to the substitution of the aspartic acid in position 130 with asparagine.

hiPSC characterization:

PBMCs were reprogrammed by Sendai virus (SeV; see pages 112-116 for protocol details) infection of three vectors: polycistronic Klf4–Oct3/4–Sox2 (KOS), Klf4, and cMyc. The obtained hiPSCs were maintained as feeder-free culture, retaining embryonic stem cell (ES)-like morphology and pluripotent features. Both patient's PBMCs and hiPSCs present the disease-causing mutation on the CALM3 gene (figure 3.2A. The CALM3 coding sequence -CDS- used as a reference is the NCBI sequence NM_005184.4). The DNA karyotyping (300 g-bandings) (figure 3.2B) and the FISH on X and Y chromosome revealed normal female chromosome asset (46, XX) (figure 3.2C). LQT16.P1 uniformly expresses the human ES surface antigens Tumor Related Antigen-1-60 (TRA-1-60), Stage Specific Embryonic Antigen-3 and −4 (SSEA-3, SSEA-4) (figure 3.2D-E), and the pluripotent markers NANOG, OCT4, SOX2 (figure 3.2D-E), REX1, GDF3, ESG1, NODAL, DPPA2 and DPPA4 (figure 3.2E). Likewise, it shows alkaline phosphatase (AP) activity (figure 3.2D). RT-PCR in figure 3.2F shows clear expression of Sendai virus vector SeV, KOS,

KLF4 and cMyc in infected PBMC and loss of them in LQT16.P1 at passage 15. LQT16.P1 cell line spontaneously forms embryoid bodies (EBs) able to differentiate into cells belonging to the three germ layers: endoderm, mesoderm, and ectoderm (figure 3.2H). We also excluded the presence of mycoplasma contamination (figure 3.2G).

Figure 3.2. LQT16.P1 iPSC line characterization.

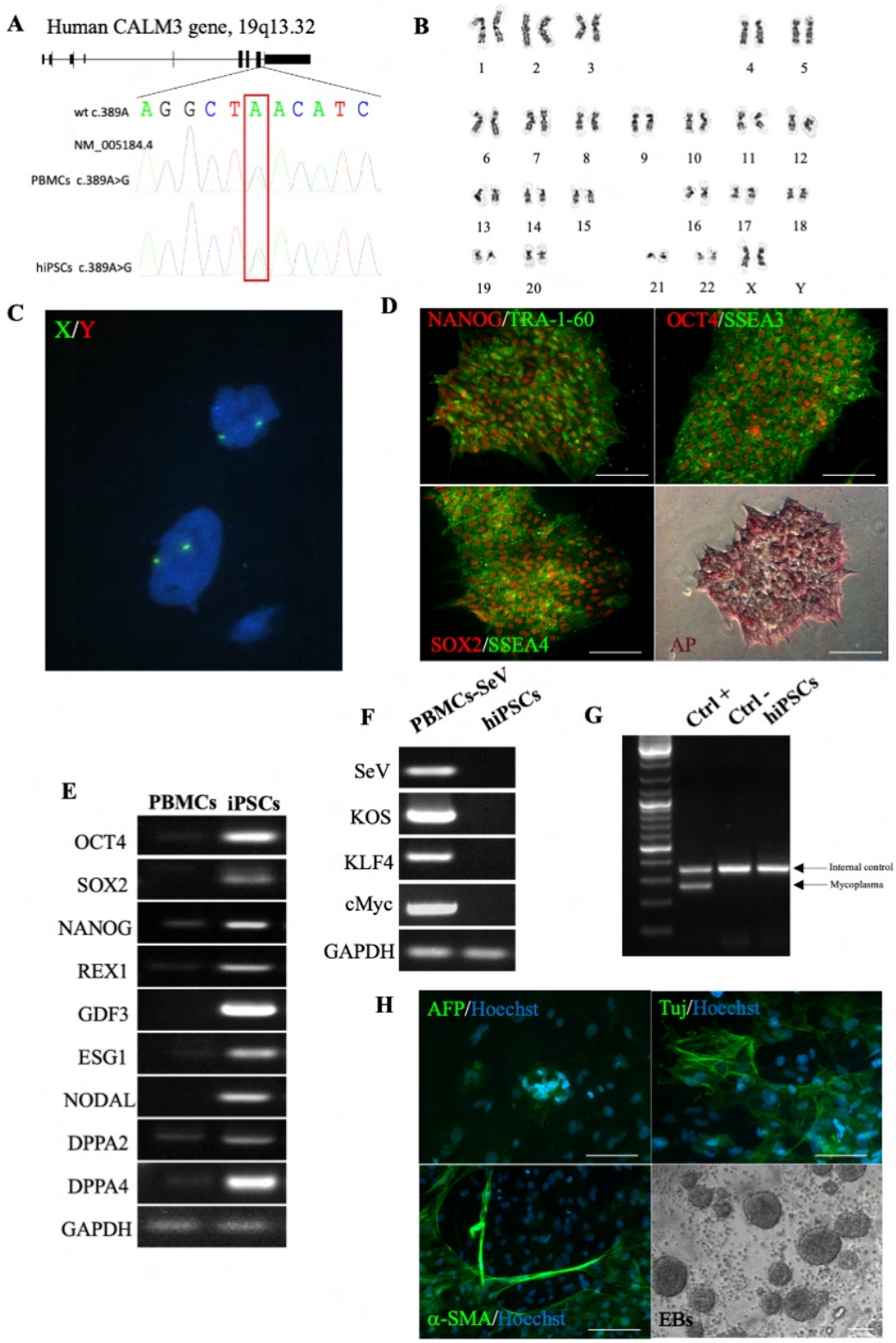

(A) *DNA sequencing results showing the presence of the mutation 389 A>G in heterozygous on the Exon 5 of CALM3 gene of PBMC and hiPSC. The CALM3 coding sequence used as a reference is NM_005184.4.* ***(B)*** *Karyotype analysis of LQT16.P1 (300 G-bandings).* ***(C)*** *FISH on X and Y chromosomes.* ***(D)*** *Immunofluorescence staining showing uniform expression of pluripotency markers; nuclei were*

counterstained with Hoechst (blue). AP: alkaline phosphatase colorimetric staining. ***(E)*** *RT-PCR analysis showing expression of the indicated markers of pluripotency in hiPSC compared with PBMC.* ***(F)*** *RT-PCR analysis showing expression of the four SeV after transduction and silencing of them in hiPSC.* ***(G)*** *EZ-PCR test showing the absence of mycoplasma contamination in LQT16.P1. The positive and negative controls are provided by the kit.* ***(H)*** *Immunofluorescence staining for markers of the 3 germ layers in iPSC-derived EBs: AFP for endoderm, Tuj for ectoderm and SMA for mesoderm. EBs: floating embryoid bodies formed after 7 days of cell culture in suspension. Scale bar: 100μM.*

4.1.3 Optimization of the protocol for iPSC-CMs generation

For the differentiation of the hiPSC lines into cardiomyocytes (iPSC-CMs), 3 methods were tested: the first one was a custom-made method based on small molecule inhibitors of GSK3β and Wnt signaling pathways, the other two were the commercially available kits PSC Cardiomyocyte Differentiation Kit (Gibco™) and STEMdiff™ Cardiomyocyte Differentiation Kit (STEMCELL Technologies™).

Custom-made method. With this method, the iPSCs were first committed to mesoderm through a GSK3 inhibitor CHIR99021 (CHIR). At day 3, O-acyltransferase Porcupine inhibitor (IWP2) was added for 48hrs to block Wnt protein secretion and activity, committing cells to cardiac mesoderm. Finally, cardiac maturation started after the seventh day and first beating cells appeared around day 10 (figure 3.3A). Based on literature data, the cardiomyocyte differentiation efficiency of this protocol is 98%[17]. (See page 118 for more protocol details).

PSC Cardiomyocyte Differentiation Kit. Within the first two days, cells were committed to mesoderm, then in the following two days mesoderm proceeded differentiation into cardiac mesoderm. Finally, cardiac maturation started after the fifth day until day 10 when first beating cardiomyocytes appeared (figure 3.3B). Based on literature data, the cardiomyocyte differentiation efficiency of this protocol is 85%[17]. (See page 119 for more protocol details).

STEMdiff™ Cardiomyocyte Differentiation Kit. Within the first two days, cells were committed to mesoderm, then in the following two days mesoderm proceeded differentiation into cardiac mesoderm. Finally, cardiac maturation started after the fourth day until day 8 when first beating cardiomyocytes

appeared (figure 3.3C). There are no literature data yet available about the cardiomyocyte differentiation efficiency of this protocol, but on the datasheet is reported an 80% of efficiency. (See pages 119-120 for more protocol details).

In my hands, the same amount of beating cardiomyocytes was obtained with all three protocols, but with the PSC Cardiomyocyte Differentiation Kit more reproducible results were obtained. Moreover, the kit is less expensive and less time-consuming than the other two and for those reasons it was chosen to carry out all the experiments presented in projects 2 and 3.

About the efficiency, only 50%-60% of cells differentiated with the PSC Cardiomyocyte Differentiation Kit were cardiac troponin-positive cardiomyocytes (figure 3.4A). To increase cardiomyocyte purity, a metabolic selection by glucose starvation was performed for three days, a condition that allows survival of cardiomyocytes only. After this selection, a purity of about 90-95% was reached (figure 3.4B).

Figure 3.3. Diagrams of the three differentiation protocols tested.

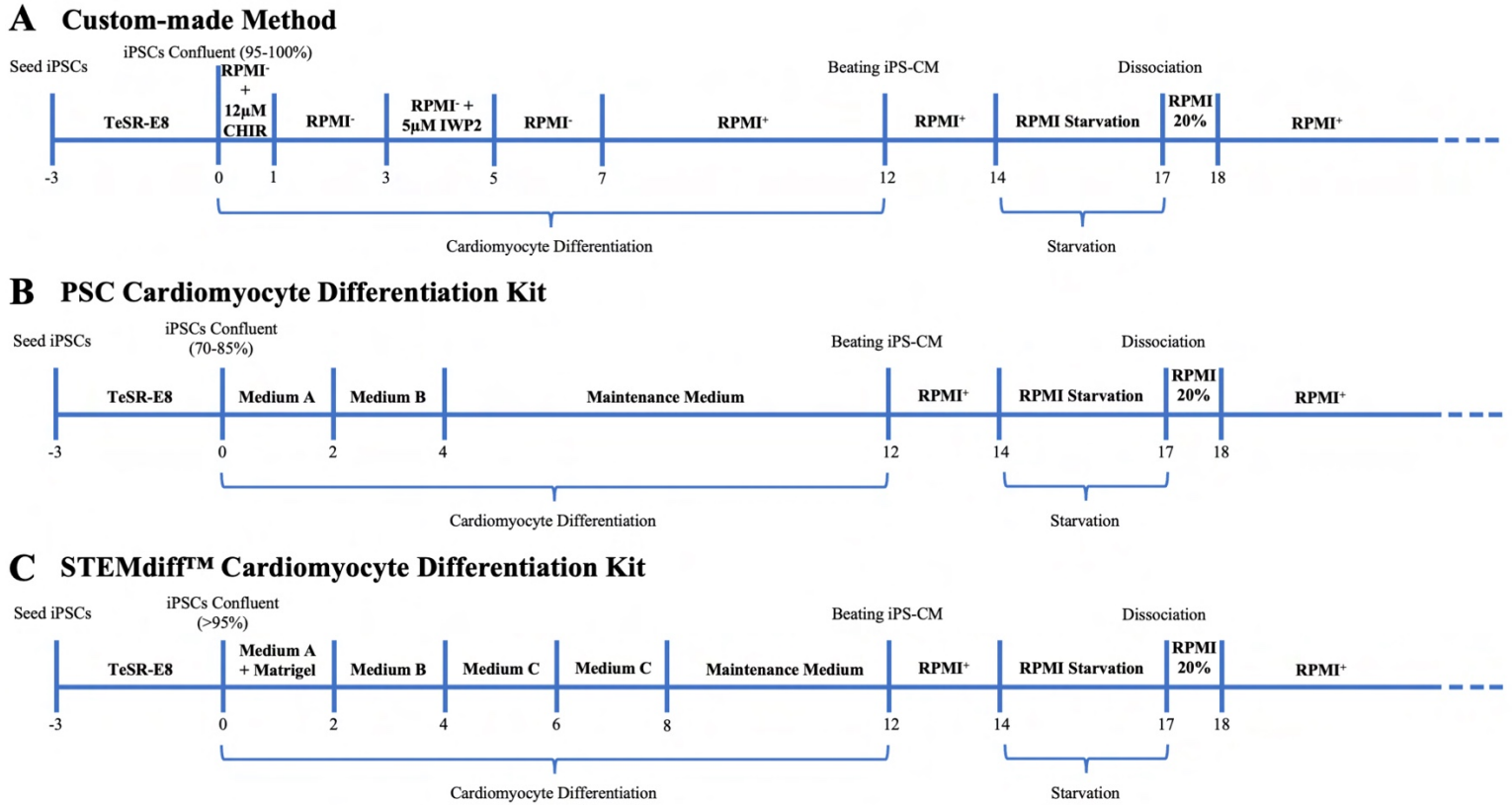

(A) *Custom-made method. RPMI-, RPMI1640 with 1X B27 Supplement Minus Insulin; CHIR, CHIR99021; IWP2; O-acyltransferase Porcupine inhibitor; RPMI+, RPMI1640 with 1X B27 Supplement; RPMI Starvation, RPMI1640 no glucose with 1X B27 Supplement; RPMI 20%, RPMI1640 with 20% FBS.* ***(B)*** *PSC Cardiomyocyte Differentiation Kit. Medium A, Medium B and Maintenance Medium are components of the kit; RPMI+, RPMI1640 with 1X B27 Supplement; RPMI Starvation, RPMI1640 no glucose with 1X B27 Supplement; RPMI 20%, RPMI1640 with 20% FBS.* ***(C)*** *STEMdiff™ Cardiomyocyte Differentiation Kit. Medium A, Medium B, Medium C and Maintenance Medium are components of the kit; RPMI+, RPMI1640 with 1X B27 Supplement; RPMI Starvation, RPMI1640 no glucose with 1X B27 Supplement; RPMI 20%, RPMI1640 with 20% FBS.*

Figure 3.4. hiPSC-CMs starvation.

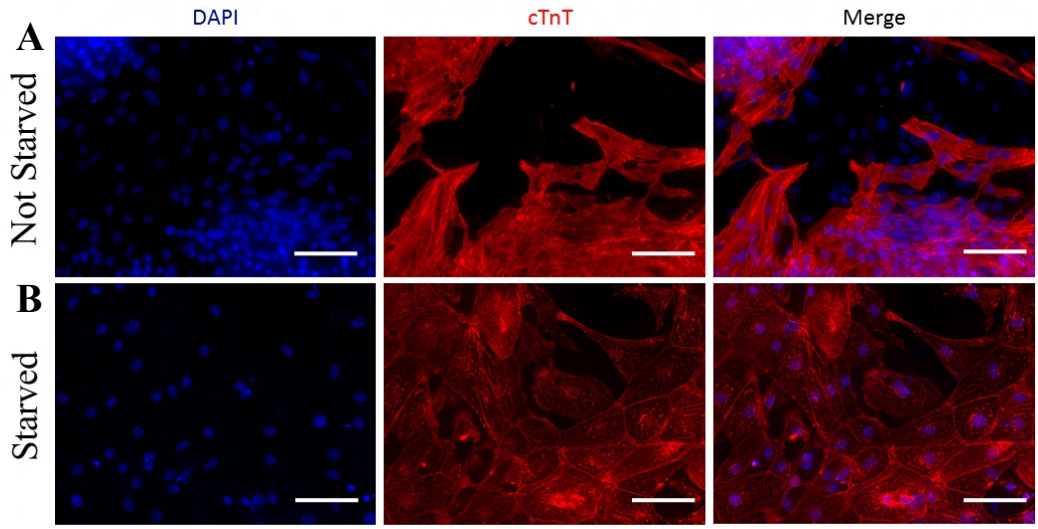

*Immunofluorescence images of iPSC-CMs differentiated with the PSC Cardiomyocyte Differentiation Kit before starvation **(A)** and after starvation **(B)**. Scale bar: 100µM.*

3.2 Discussion

Induced pluripotent stem cells (iPSC) are an important tool to model genetic disease and to test pharmacological/molecular therapies. Collection of hundreds to thousands of cell lines, also known as biobank, allow creating a compendium of cell systems, ideal for "population on a dish" mechanistic studies[12]. Indeed, for drug discovery and development, the possibility to test new compounds on high numbers of differentiated hiPSCs, enable recapitulating the human phenotype variability more closely than other previously used engineered cell systems.

Starting from 2011, the Laboratory of Experimental Cardiology has generated a biobank of a total of 122 patients, of which 78 were enrolled through skin biopsy collection, 38 were enrolled through peripheral blood collection and 6 through both methods. 35 of these somatic cell lines were reprogrammed to iPSCs.

During my PhD, the reprogramming protocol was optimized by testing two new integration-free techniques: transfection of fibroblasts with mRNAs and infection of both fibroblasts and PBMCs with Sendai vectors. Since the collection of blood is much less invasive than skin biopsy, the possibility to reprogram PBMCs facilitated the enrollment of more probands and their relatives to our studies. Moreover, the cardiomyocyte differentiation protocol was optimized, choosing the best one among three different methods. The PSC Cardiomyocyte differentiation kit gave more reproducible results between different hiPSC clones and was also less expensive and less time-consuming than the other two protocols.

hiPSC lines belonging to a biobank should meet high quality and safety standards. Accordingly, all the hiPSC lines generated in our laboratory were highly characterized[196–202]. In particular:

- The hiPSC lines' identity was verified by short tandem repeat (STR) profiling.
- The disease-causing mutation was still present in the generated cell lines.

- The cell lines presented a normal karyotype stable over passages (figure 3.1B and figure 3.2B-C).
- The expression of surface and nuclear pluripotent markers was verified with different assays (figure 3.1C-E and figure 3.2C-D).
- The expression of viral Tg (OCT4, SOX2, KLF4 and cMYC) was lost in hiPSC lines (figure 3.1.F).
- hiPSCs were able to differentiate into the three germ layers after EB formation (figure 3.1G and figure 3.2H).
- Mycoplasma contamination was excluded (figure 3.1I and figure 3.2H).

Biobank can be useful also for drug repurposing studies. For instance, the Laboratory of Experimental Cardiology demonstrated that a drug currently used to treat cystic fibrosis, Lumacaftor (LUM), can rescue the pathological phenotype of iPSC-CMs derived from LQT2 patients, suggesting a novel therapeutic option in patients not protected by β-blockers[203].

Moreover, the banking of samples from an entire family allows to study the effect of 'modifier genes', which may modulate the phenotypic manifestations of target genes in an epistatic manner. The study of a family may help to unravel why in family members carrying the same disease-causing mutations, the clinical manifestations may vary from benign to highly malignant. For example, my colleagues performed studies on iPSC-CMs of symptomatic and asymptomatic KCNQ1-A341V mutation carriers, with or without the minor alleles of NOS1AP SNPs rs16847548 and rs4657139 respectively, unravelling the cellular impact of the SNPs (from modifier genes to cellular mechanisms)[204]. Conversely, they also characterized iPSC-CMs from symptomatic and asymptomatic patients carrying the KCNQ1-Y111C mutation, and the molecular differences observed drove to the identification of a new protective modifier gene (from cellular mechanisms to modifier genes)[204,205].

3.3 Conclusion

Working on the expansion of a biobank allowed me to improve skills in generation, characterization, and differentiation of iPSCs which were important to develop the research lines presented in project 2 and 3. Overall, our biobank of cells affected by inherited cardiac disease have been and will be exploited for studies of disease modeling, drug discovery, and drug repurposing

4 PROJECT 2. Define the role of sex hormones as disease modifiers of LQTS in hiPSC-CMs from a patient affected by both LQT2 and PCOS

4.1 Results

4.1.1 Patient clinical history

LQT2.P6 line was generated by reprogramming dermal fibroblasts of a 26-year-old woman affected by a dominant-negative form of Long QT Syndrome type 2 (LQT2), class 3. Furthermore, the young patient was on hormonal replacement therapy (ORT, estro-progestinic) for the symptomatic PCOS since the age of 14. At the age of 21, after an almost uneventful life, she developed a severe electrical storm as first clinical manifestation of LQTS, in the setting of a very prolonged QTc (QT corrected for heart rate of 650 ms) with frequent ventricular ectopic beats. Genetic screening revealed the presence of a heterozygous c.1881 G/A mutation on the KCNH2 gene, leading to the substitution of the glycine in position 628 with serine [VCV000014427.1]. When enrolled, the girl was taking ORT very irregularly after a period of regular taking. Based on the presumed role in favoring/triggering the life-threatening ventricular arrhythmias, ORT was stopped. Since then, the patient has maintained asymptomatic for more than 18 months, despite persistency of a QTc interval above 550ms. PCOS has significantly worsened without ORT (testosterone levels rose, and estrogens levels went down). Patient's mother was drug addicted, who died suddenly at the age of 29 while undergoing methadone therapy. First degree cousins, one male and one female, on the maternal side were asymptomatic for major events, but experienced paroxysmal atrial fibrillation (PAF) and syncope. In male cousin, recently, Brugada Syndrome pattern was documented. On the contrary, father's family history cannot be reconstructed due to lack of information.

4.1.2 hiPSC generation and characterization

Patient's fibroblasts were reprogrammed through transfection of RNA vectors with the ReproRNA™-OKSGM kit (StemCell™ Technologies) (figure 4.1A; see page 110-111 for protocol details). The obtained hiPSCs were maintained on feeders, retaining embryonic stem cell (ES)-like morphology (figure 4.1B-C). Around passage 10, hiPSCs were passed from a feeder-dependent to a feeder-free cultivation (figure 4.1D; see page 116 for details).

Both patient's fibroblasts and hiPSCs present the disease-causing mutation on the KCNH2 gene (figure 4.2. The KCNH2 coding sequence -CDS- used as a reference is the NCBI sequence NM 000238.4). The DNA karyotyping (300 g-bandings) revealed normal female chromosome asset (46, XX) (figure 4.3; see page 126 for details).

LQT2.P6 uniformly expresses the human ES surface antigens Tumor Related Antigen-1-60 (TRA-1-60), Stage Specific Embryonic Antigen-3 and -4 (SSEA-3, SSEA-4) and the pluripotency nuclear markers NANOG, SOX2 and OCT4 (figure 4.4A). Furthermore, figure 4.4B showed the presence of alkaline phosphatase enzymatic activity revealed by a colorimetric assay in the hiPSC line (figure 4.4B; see page 127 for protocol details). These results were confirmed by an expression screening of the stem cell genes performed by RT-PCR on the RNA extracted from the clones (see pages 139-140 for details). The expression of the OCT4, SOX2, NANOG, REX1, GDF3, ESG1, NODAL, DPPA2 and DPPA4 stem cell genes was detected in the hiPSCs but not in parental HDFs, tested as a negative control (figure 4.5). The equal expression of the housekeeping GAPDH gene in HDFs and hiPSCs proves that the amount of RNA tested was the same between the various cell types, and therefore the observed differences were attributable to an induction of the expression of pluripotency markers after reprogramming.

LQT2.P6 cell line spontaneously forms embryoid bodies (EBs) able to differentiate into cells belonging to the three germ layers: endoderm, mesoderm and ectoderm (figure 4.6). Mycoplasma contamination was excluded (figure 4.7; see page 149 for protocol details).

Figure 4.1. Reprogramming protocol.

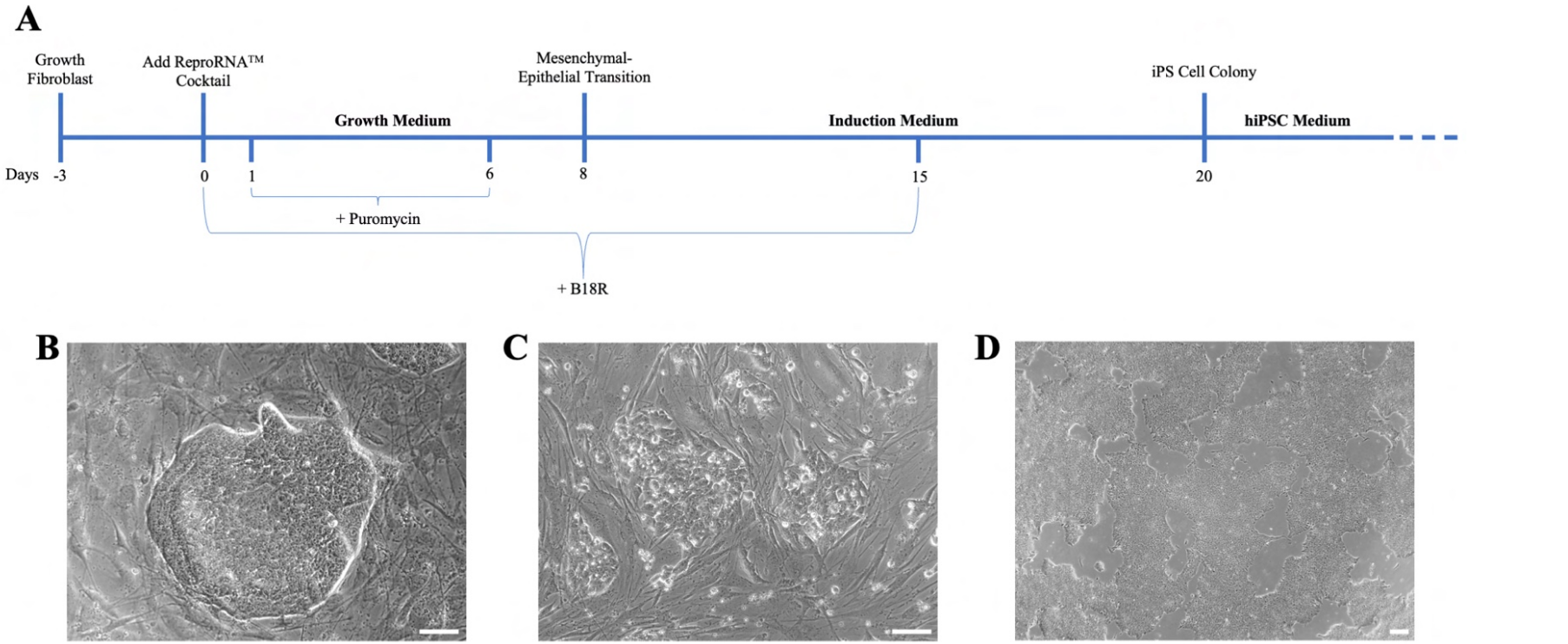

(A) *ReproRNA™-OKSGM protocol. ReproRNA™ Cocktail: ReproRNA™-OKSGM, Opti-MEM® I Reduced-Serum Medium, ReproRNA™ Transfection Supplement, ReproRNA™ Transfection Reagent; Growth Medium: DMEM supplemented with 10% FBS, 1% L-Glutamine and 175 ng/mL Recombinant B18R protein (B18R); Induction Medium: DMEM/F12 with 10% FBS, 10% KO-SR, 1% L-Glutamine, 100 U/mL penicillin, 100 mg/mL streptomycin, 1% NEAA, 0.1 mM β-mercaptoethanol, 10 ng/mL bFGF and 1 mM valproic acid; hiPSC Medium: DMEM/F12 with 20% KO-SR, 1% L-Glutamine, 100 U/ mL penicillin, 100 mg/mL streptomycin, 1% NEAA, 0,1 mM β-mercaptoethanol and 10 ng/mL bFGF. iPS cell colony on MEF-feeder at p0 (**B**), at p2 (**C**) and after adaption of feeder-free cultivation (**D**). Scale bar: 100µM.*

Figure 4.2. Disease-causing mutation on KCNH2 gene.

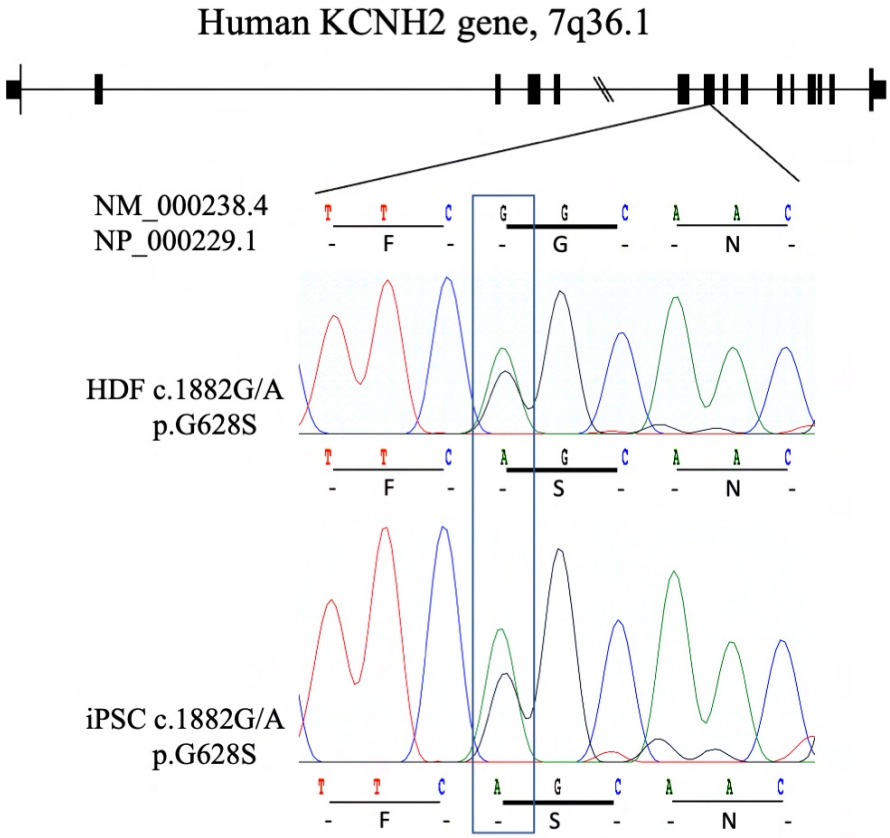

DNA sequencing results showing the presence of the mutation 1882 G>A in heterozygous on the Exon 7 of KCNH2 gene of HDF and hiPSCs. The KCNH2 coding sequence used as a reference is NM_000238.4.

Figure 4.3. Karyotyping.

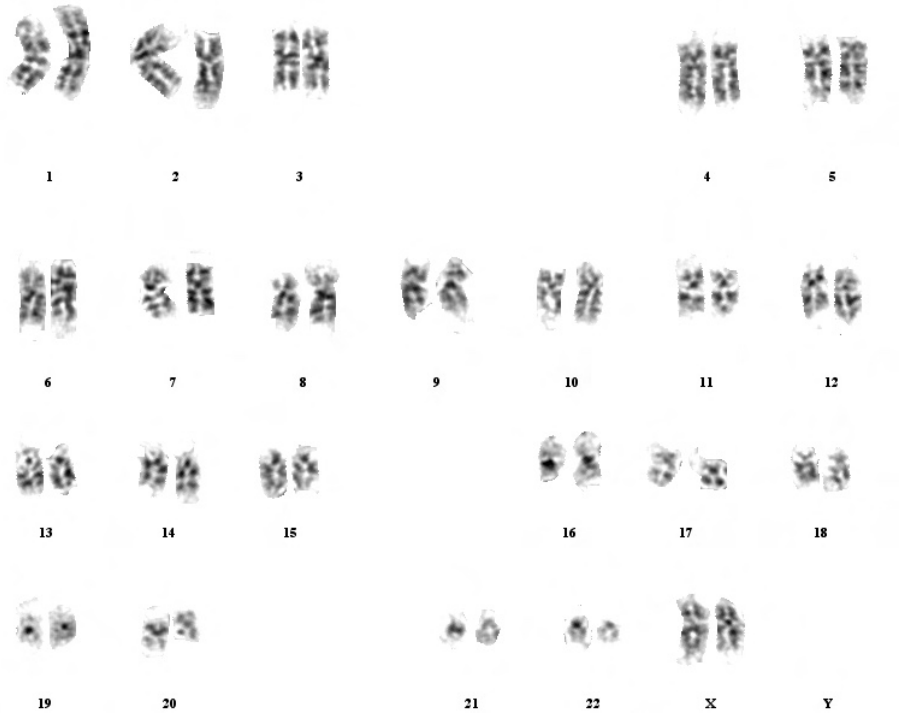

Karyotype analysis of LQT2.P6 (300 G-bandings).

Figure 4.4. Expression of pluripotency markers in hiPSCs.

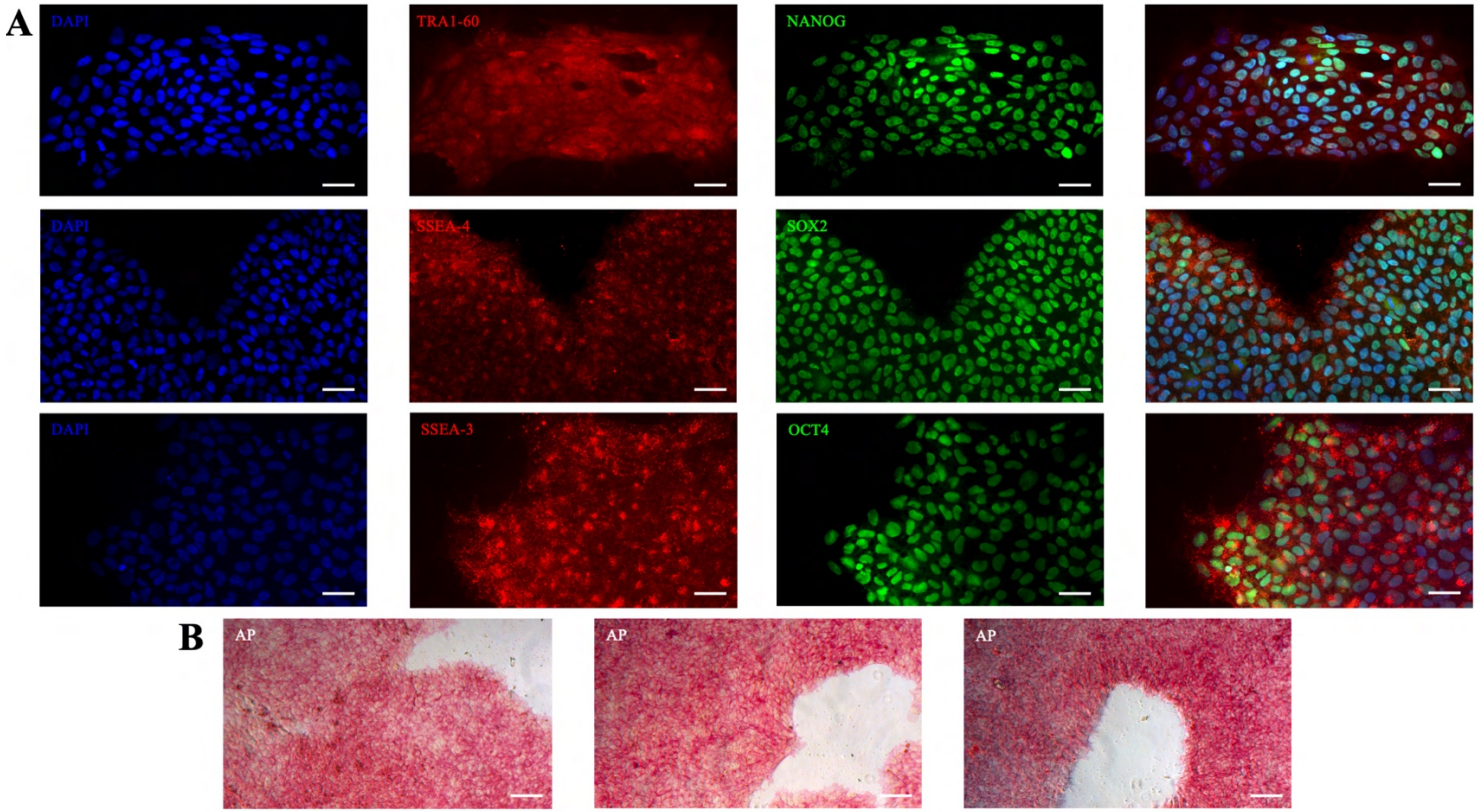

(A) *Indirect immunofluorescence of the surface antigens TRA1-60, SSEA-3 and SSEA-4 (reed) and of the nuclear markers NANOG, SOX2 and OCT4 (green). Nuclei were counterstained with DAPI (blue). Scale bar: 50 µm.* ***(B)*** *Colorimetric assay of alkaline phosphatase (AP) activity. Scale bar: 100µm.*

Figure 4.5. Expression of pluripotency markers in hiPSCs by RT-PCR.

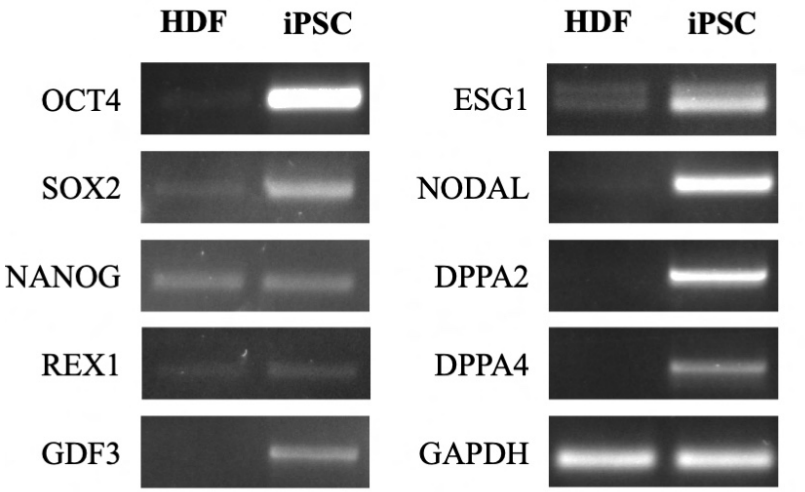

RT-PCR analysis of endogenous pluripotency markers in hiPSCs and non-reprogrammed HDFs. Endogenous GAPDH housekeeping gene expression was used as a loading control.

Figure 4.6. EBs differentiation.

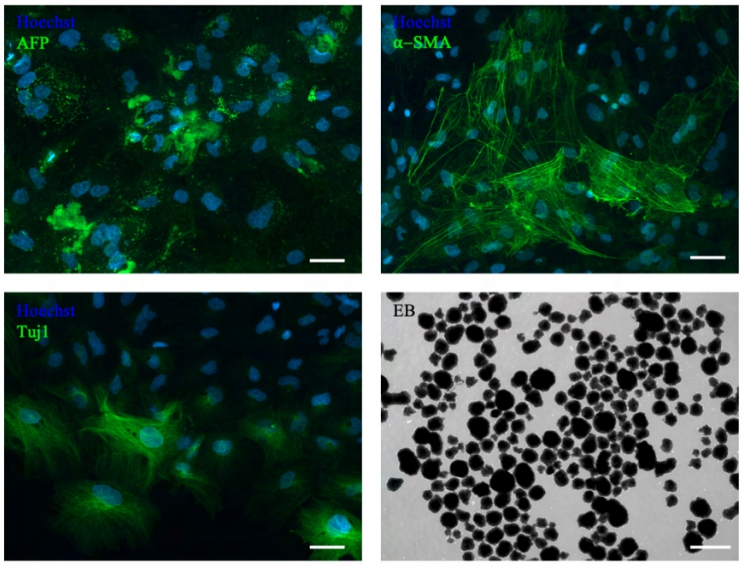

Immunofluorescence staining for markers of the 3 germ layers in iPSC-derived EBs: AFP for endoderm, Tuj1 for ectoderm and α-SMA for mesoderm. Scale bar: 50 µm. EBs: floating embryoid bodies formed after 7 days of cell culture in suspension. Scale bar: 200 µm.

Figure 4.7. Mycoplasma test.

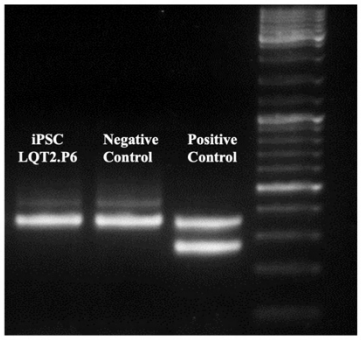

EZ-PCR test showing the absence of mycoplasma contamination in LQT2.P6. Negative and Positive controls are provided by the kit.

4.1.3 Functional studies on hiPSC-CMs

The PSC Cardiomyocyte Differentiation Kit (Gibco™; see page 119 for protocol details) was used to successfully differentiate this hiPSC line into spontaneously beating cardiac-like cells expressing typical cardiac markers such as troponin T (cTnT) (figure 4.8).

After 30 days from day 0 of differentiation, it was assessed if cardiomyocytes derived from LQT2.P6 iPSCs express the estrogen receptors (figure 4.9). Estrogen α and β receptors, which mediate the genomic effect, shows a peri-nuclear localization (figure 4.9) whereas the GPER receptor, which acts through non-genomic pathway, shows a cytoplasmatic localization (figure 4.9), as already reported for cells in basal condition (not stimulated).

Figure 4.8. Immunofluorescence images of hiPSC-CMs.

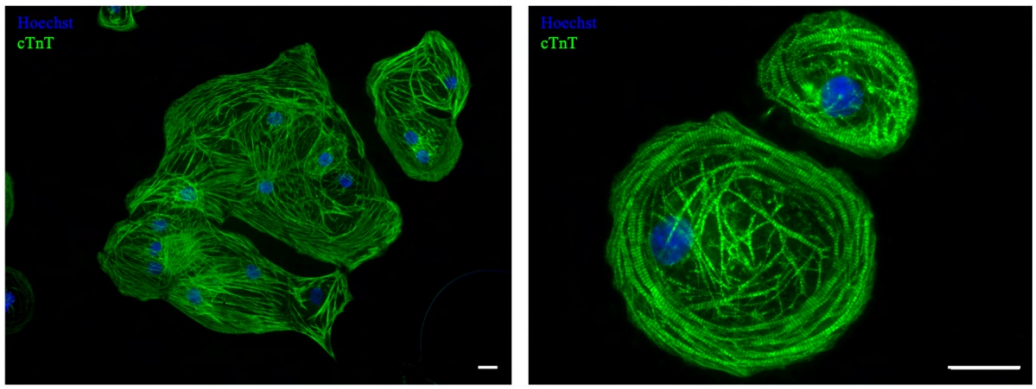

Immunofluorescence staining for cardiac troponin T (cTnT) in cardiomyocytes differentiated from the LQT2.P6 iPSCs. Nuclei were counterstained with Hoechst. Scale bar: 20 µm.

Figure 4.9. Immunofluorescence images of estrogen receptors.

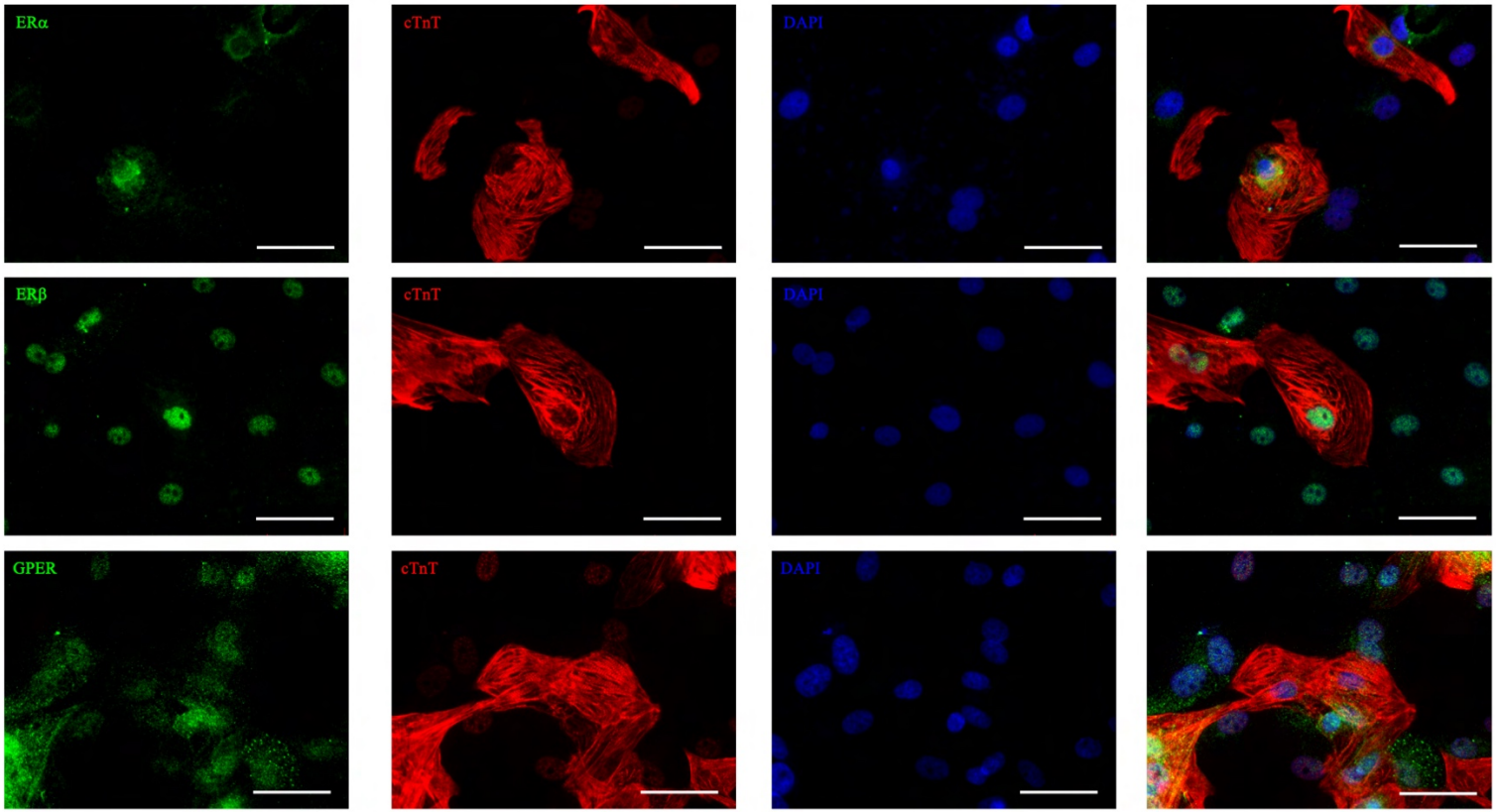

Immunofluorescence staining for estrogen receptor α (ERα), estrogen receptor β (ERβ) and G-coupled estrogen receptor (GPER) in cardiomyocytes differentiated from the LQT2.P6 iPSCs. Nuclei were counterstained with DAPI. Scale bar: 50 µm.

4.1.3.1 Comparison between RPMI and HFM media

Before E2 treatment, Hormone Free Medium (HFM, for composition description see page 119) containing very low levels of steroids and no phenol red, was tested if is more suitable than hiPSC-CM maintenance medium (RPMI 1640 supplemented with B27, hereafter named RPMI) to perform estrogenic stimulation of hiPSC-CM. Indeed, it was reported that phenol red may cause partial estrogenic stimulation due to structural resemblance to some nonsteroidal estrogens[206]. Therefore, it was checked if the estrogenic pathway is silenced in HFM compared to RPMI.

After 15 days of culture in HFM, it was initially evaluated if medium affects cTnT expression compared to RPMI maintenance (figure 4.10). Then, the cell viability was evaluated by In Cell Western (ICW; see page 129 for details) comparing integrated intensity of cTnT (figure 4.10). As shown in figure 4.10, HFM medium does not affect iPSC-CMs viability, and it is comparable to RPMI.

Figure 4.10. LQT2.P6 viability after 15 days of RPMI or HFM maintenance.

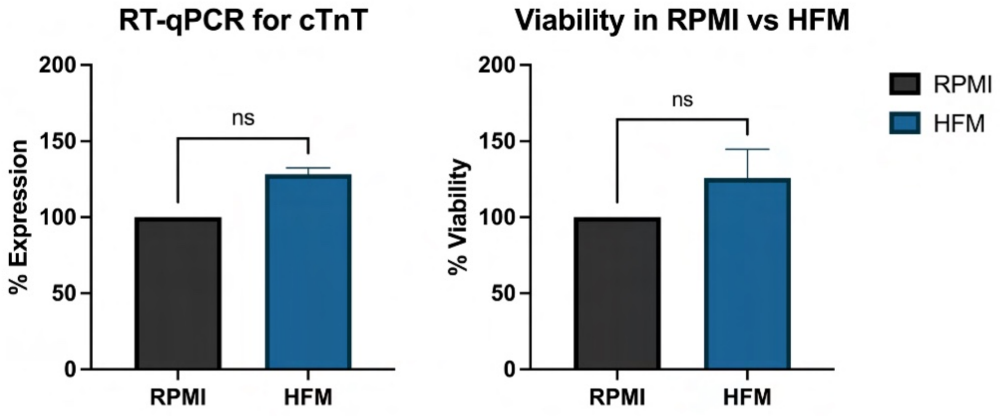

On the right, relative quantification by RT-qPCR of cTnT mRNA levels in LQT2.P6 hiPSC-CMs maintained in RPMI (black) and HFM (blue). The GAPDH was used as reference gene of the $2^{-\Delta\Delta Ct}$ method of RT-qPCR. On the left, ICW results obtained through integrated intensity of cTnT. Cardiomyocytes maintained 15 days in RPMI medium was normalized to 100% of cell viability. For both experiments each sample was loaded in sextupled. Statistical analyses were conducted using GraphPad Prism 9 (GraphPad) and significance was determined by Student's t test. The "ns" stands for not statistically significant.

To evaluate if HFM has an effect on estrogen receptor expression, the RT-qPCR (see pages 141-143 for details) was performed. The GAPDH was used as reference gene. Estrogen receptor expression in RPMI was normalized to 100%.

As depicted in figure 4.11 HFM significantly increases the ERα expression ($p<0.001$), whereas the ERβ and GPER expression are not affected by HFM medium.

Figure 4.11. Estrogen receptors expression level between RPMI and HFM.

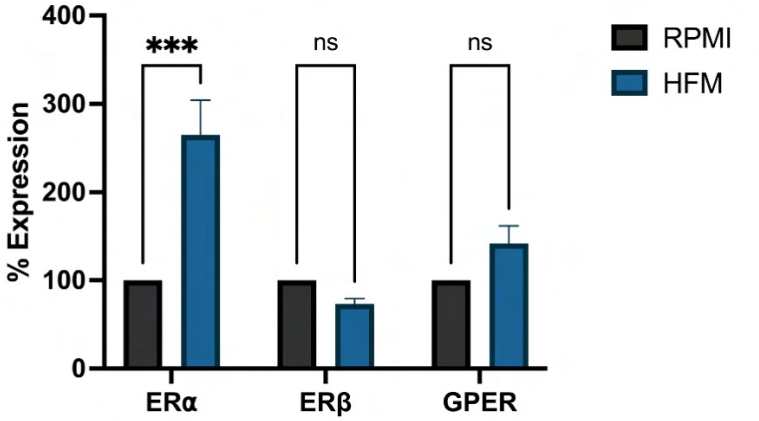

*Relative quantification by RT-qPCR and the $2^{-\Delta\Delta Ct}$ method of ERα, ERβ and GPER mRNA levels in LQT2.P6 hiPSC-CMs maintained in RPMI (black) and HFM (blue). The GAPDH was used as reference gene of the $2^{-\Delta\Delta Ct}$ method of RT-qPCR. Each sample was loaded in triplicate. Statistical analyses were conducted using GraphPad Prism 9 (GraphPad) and significance was determined by two-way ANOVA. The asterisks indicate the statistical significance: *** p-val<0.001. The "ns" stands for not statistically significant.*

Finally, the expression of GPER and hERG was investigated in cardiomyocytes derived from LQT2.P6 through RT-qPCR and the ICW (figure 4.12). GAPDH was used as reference gene and RPMI was normalized to 100%. As shown in figure 4.12 the ICW reveals a statistically significant increase ($p<0.05$) in GPER expression in cardiomyocytes maintained for 15 days in HFM. There are no statistically significant differences between hERG expression levels in the two media. These data suggested that HFM increases the expression of estrogenic receptors not blunting the estrogenic pathway, so the next experiments were performed maintaining cardiomyocytes in RPMI.

Figure 4.12. GPER and hERG expression level between RPMI and HFM.

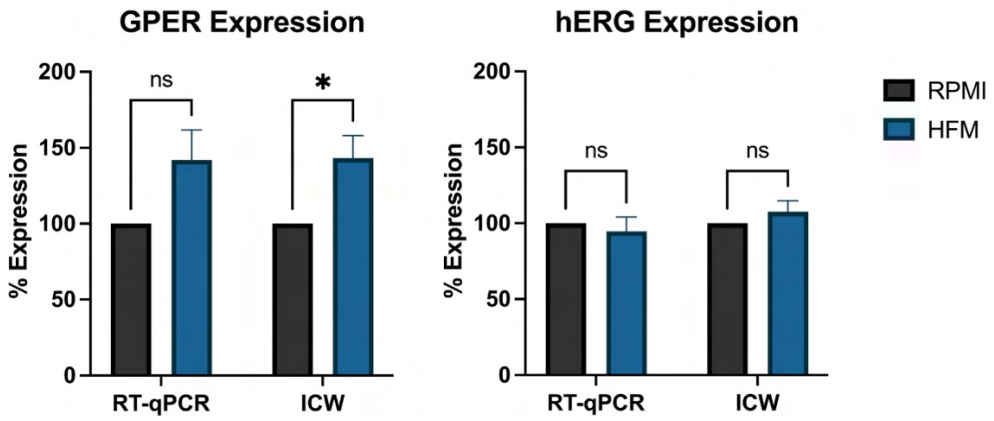

*Relative quantification by RT-qPCR and ICW of GPER (left) and hERG (right) in LQT2.P6 hiPSC-CMs maintained in RPMI (black) and HFM (blue). The GAPDH was used as reference gene of the $2^{-\Delta\Delta Ct}$ method of RT-qPCR. Each sample was loaded in triplicate. Statistical analyses were conducted using GraphPad Prism 9 (GraphPad) and significance was determined by two-way ANOVA. The asterisks indicate the statistical significance: * p-val<0.05. The "ns" stands for not statistically significant.*

4.1.3.1 Estrogen (E2) stimulation

Cardiomyocytes derived from LQT2.P6 hiPSC and a wild-type control (CTRL) were stimulated for 10 minutes with 10 nM of estrogen (E2; see page 135 for details). The not-stimulated controls of each cell line were normalized to 100% of expression ("Basal"). Differences in GPER expression were evaluated performing both RT-qPCR and ICW (figure 4.13). Both assays demonstrate a statistically significant increase in GPER expression in CTRL cardiomyocytes after stimulation ($p<0.001$ in RT-qPCR, $p<0.05$ in ICW, figure 4.13). On the contrary, a not statistically significant difference is detected in cardiomyocytes derived from the patient between stimulated and not-stimulated (figure 4.13). A statistically difference between stimulated cardiomyocytes derived from patient and wt is detected through both assays ($p<0.001$ in RT-qPCR, $p<0.01$ in ICW; figure 4.13)

Figure 4.13. GPER expression after E2 stimulation.

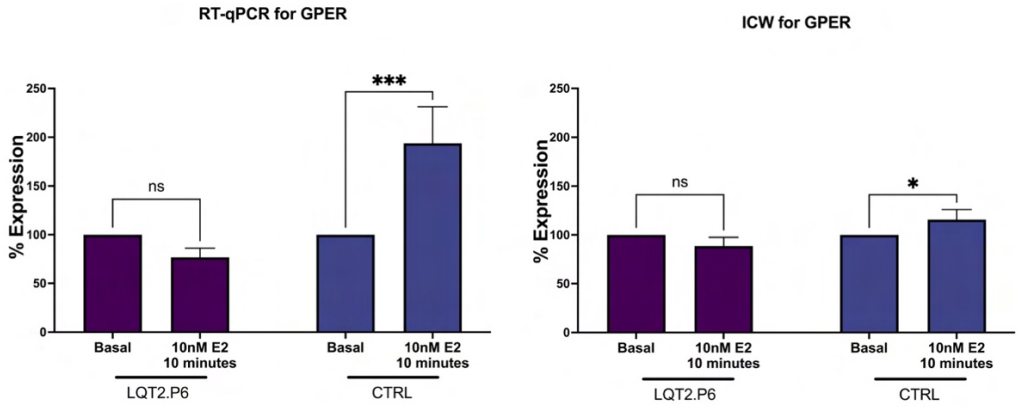

*Relative quantification by RT-qPCR (left) and ICW (right) of GPER in LQT2.P6 and CTRL hiPSC-CMs not stimulated (basal) and stimulated with 10 nM of E2 for 10 minutes. The GAPDH was used as reference gene of the $2^{-\Delta\Delta Ct}$ method of RT-qPCR. Each sample was loaded in triplicate. Statistical analyses were conducted using GraphPad Prism 9 (GraphPad) and significance was determined by two-way ANOVA. The asterisks indicate the statistical significance: * p-val<0.05, ** p-val<0.01, *** p-val<0.001. The "ns" stands for not statistically significant.*

Electrophysiological studies, carried out by prof. Antonio Zaza laboratory team, on LQT2.P6 and CTRL cardiomyocytes allow to understand function differences under E2 stimulation. Membrane potential of hiPSC-CMs was recorded during pacing at 1 Hz in native condition reaching a diastolic membrane potential (Ediast) of around -50 mV (see page 156 for details). During 10 nM E2 stimulation, LQT2.P6 cardiomyocytes show a very fast and reversible reduction in the magnitude of the action potential (figure 4.14). On the contrary, any difference is detected in cardiomyocytes derived from CTRL.

Figure 4.14. LQT2.P6 membrane potential recording during E2 stimulation.

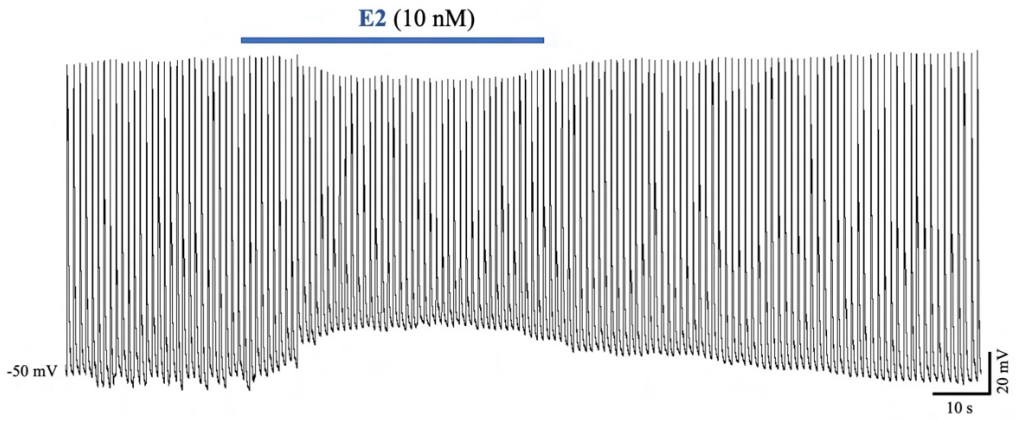

Effects of 10 nM concentrations of E2 on action potentials recorded from patch-clamped LQT2.P6 ventricular cardiomyocytes.

At the end, to evaluate any change the expression of hERG was studied through RT-qPCR and ICW. LQT2.P6 cardiomyocytes show a statistically significant decrease in expression after E2 stimulation ($p<0.01$ in both RT-qPCR and ICW; figure 4.15). On the contrary, CTRL cardiomyocytes have not significant difference in expression between basal and stimulated (figure 4.15). ICW assay evidences a significant difference in hERG expression between stimulated LQT2.P6 and CTRL cardiomyocytes (figure 4.15).

Figure 4.15. hERG expression after E2 stimulation.

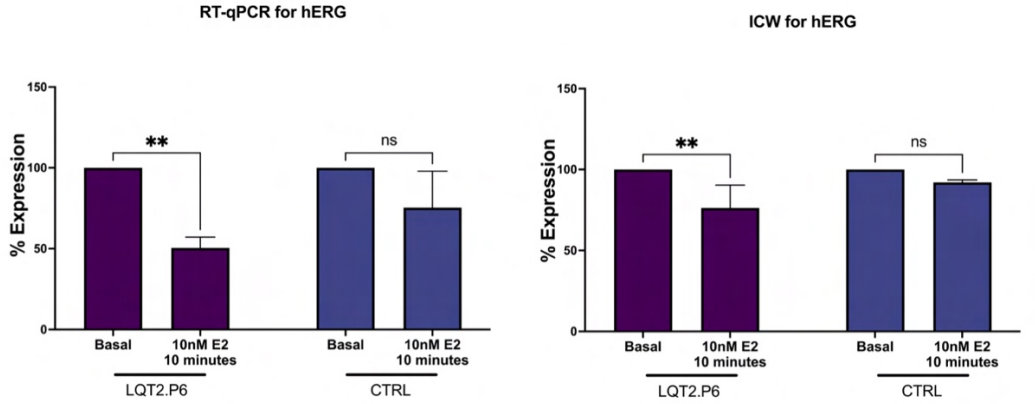

Relative quantification by RT-qPCR (left) and ICW (right) of hERG in LQT2.P6 and CTRL hiPSC-CMs not stimulated (basal) and stimulated with 10 nM of E2 for 10 minutes. The GAPDH was used as reference gene of the $2^{-\Delta\Delta Ct}$ method of RT-qPCR. Each sample was loaded in triplicate. Statistical analyses were

*conducted using GraphPad Prism 9 (GraphPad) and significance was determined by two-way ANOVA. The asterisks indicate the statistical significance: * p-val<0.05, ** p-val<0.01. The "ns" stands for not statistically significant.*

4.2 Discussion

Estrogen is an important regulator of cardiovascular function. Epidemiological data suggest that premenopausal women show decreased incidence of hypertension and coronary artery disease compared with age-matched men and postmenopausal women[114,115]. Estrogen mediates its actions on the heart through three identified estrogen receptors (ERs): ERα (ESR1) and ERβ (ESR2), which are classical nuclear hormone receptors, and GPER which mediates a non-genomic mechanism[80,207]. The non-genomic action mediates rapid signaling events such as calcium mobilization[83,84] and regulation of potassium channels[85,86].

Differences in QTc-interval were described between healthy adult males and females, with longer QTc-interval in post-puberty females than in age-matched males[118]. The difference is correlated to changes in sex hormones levels, but the mechanisms on the repolarization are complex and still unresolved[36]. Conflicting results have been described about the influence of estrogen on the QTc-interval. Estrogen, according to clinical data, seems to lengthen the early repolarization in animals, acting on the potassium channel current; however, this has not been yet supported by human studies[36]. Although the longer QTc-intervals in women is not associated with a higher incidence of SCD, females are certainly predisposed to malignant cardiac events if associated with QTc-interval prolongation diseases (i.e. LQTS).

In this thesis work the hiPSC line from a female patient, affected by LQTS type 2 (class 3 mutation) and PCOS, was generated to model the role of sex hormones as disease modifier of LQTS. The first manifestation of LQT2 in this patient occurred during puberty, after starting an estro-progestin therapy, which was never regularly taken by the patient, especially when cardiac events occurred. Fibroblasts isolated from skin biopsy, were reprogrammed to iPSCs using reprogramming RNA vectors and culture on MEF feeder layer (figure 4.1). Around passage 10, LQT2.P6 hiPSCs were passed from a feeder-dependent to a feeder-free cultivation (figure 4.1D).

After about 18 passages the cell line was highly characterized. In particular:

- The disease-causing mutation was still present (figure 4.2), in particular the G to A substitution at position 1882 on *KCNH2* gene results in substitution of serine for a highly conserved glycine at codon 628 (G628S), altering the pore-forming domain[208].

- The cells presented a normal karyotype stable over passages (figure 4.3).

- The expression of surface and nuclear pluripotent markers was verified (figure 4.4 and figure 4.5).

- hiPSCs were able to differentiate into the three germ layers after EB formation (figure 4.6).

- Mycoplasma contamination was excluded (figure 4.7).

The PSC Cardiomyocyte Differentiation Kit (Gibco™) was used to generate iPSC-CMs (figure 4.8).

Initially, the expression of estrogen receptor ERα, Erβ and GPER in hiPSC-CMs was investigated through immunofluorescence assay (figure 4.9). As reported in literature, the two nuclear receptors ERα and ERβ show a peri-nuclear localization[95] (figure 4.9). On the contrary, the GPER receptor, which acts through non-genomic pathway, shows a cytoplasmatic localization[95] (figure 4.9).

Huo et al., to study the effects of sex hormones on cardiomyocytes, developed a HFM, which contained very low levels of sex steroids and phenol red[206]. They demonstrated that hiPSC-CMs maintained for 15 days in this culture medium shown a little effect on cell viability; my data show that there is not statistically significance difference between the viability of hiPSC-CMs maintained in RPMI or HFM (figure 4.10). Moreover, Huo et al. assert that HFM is able to decrease the expression of ERα; my data, on the contrary, demonstrate that HFM maintenance increases the ERα expression (figure 4.11) and the GPER expression (figure 4.12). Furthermore, cardiomyocytes maintained in HFM were very less hyperpolarized than those maintained in RPMI (data not shown). Thus,

the best medium to maintain and study estrogen interaction with hiPSC-CMs is the RPMI medium.

To investigate how sex hormones modulate the QT interval, with a particular focus on the temporal dynamic of ventricular repolarization changes (from the beat-to-beat variability, to the middle and long-term variability) and on the impact on early after depolarization (EAD) and ventricular arrhythmias susceptibility, the non-genomic pathway mediated by GPER was studied.

In particular, the GPER expression level after 10 minutes of 10nM of β-estradiol (E2) stimulation was measured. The expression was compared between LQT2.P6 and wild type (CTRL) hiPSC-CMs maintained in RPMI and then the GPER expression level was measured through 2 specific assays: RT-qPCR and ICW. Figure 4.13 shows that in patient's cardiomyocytes there is not a statistically significant difference in GPER expression between not-stimulated (Basal) and stimulated (10nM E2 10 minutes) cells. The result is confirmed through both RT-qPCR and ICW (figure 4.13). On the contrary, in CTRL hiPSC-CMs the GPER expression statistically increases after stimulation with 10nM of E2 for 10 minutes (figure 4.13). The difference between stimulated LQT2.P6 cardiomyocytes and stimulated CTRL cardiomyocytes is statistically significant with both assays (figure 4.13). Sex hormones regulate ionic currents via either genomic and/or non-genomic pathways[206]. The non-genomic pathway is faster than genomic one. Indeed, the electrophysiological analysis reported in figure 4.14 shows a fast and reversible reduction in the magnitude of the action potentials of LQT2.P6 cardiomyocytes during E2 stimulation. Kurokowa et al. demonstrate, in guinea pig cardiomyocytes, that E2 suppresses hERG currents by modulating the gating kinetics rather than by blocking the channel pore[209].

To reveal the potential mechanism of sex-related differences in drug-induced arrhythmias, any difference in the expression of *KCNH2* gene, which encodes for the hERG ion channel, was measured after 10nM E2 stimulation. Data suggest that 10nM E2 stimulation statistically decrease the expression of hERG in LQT2.P6 cardiomyocytes; on the contrary, CTRL hiPSC-CMs do not shown any difference in hERG expression after E2 stimulation (figure 4.15). The E2

effect includes the transcriptional regulation of some K^+ channels, but not the hERG channel[210,211]. In addition, it was also reported that E2 augments membrane trafficking of hERG by enhancing interaction to heat shock proteins (Hsc70/Hsp90) in non-genomic pathway[123].

Anneken et al. provided mechanistic evidence for an increased hERG ion channel trafficking to the cell membrane under estrogen stimuli. Estrogen seems to increase chaperone (Hsc70/Hsp90) proteins interaction with hERG ion channel[123], improving the channel trafficking.

Studies about this project are ongoing. In the next months the molecular and electrophysiological characterization of wt and LQT2.P6 cardiomyocytes under E2 stimulation will be completed to understand if there is a different response to estrogens or a different predisposition to arrhythmia in concomitance with a defect on the I_{Kr} current. To evaluate if the data obtained are mutation-specific, or are related to the genetic background of the patient, two isogenic cell lines will be generated by CRISPR-Cas9 technology, will be differentiated into cardiomyocytes and will be studied: 1) LQT2.P6-corrected line in which the c.1882 A>G *KCNH2* mutation will be edited; 2) wt-corrected line in which the c.1882 A>G *KCNH2* mutation will be inserted in a wt hiPSC line not affected by PCOS. Finally, these data will also be validated on other hiPSC-CM of LQTS patients who experienced or did not experience cardiac events after hormone therapy.

4.3 Conclusion

The LQT2.P6 hiSPC-CMs are useful to study estrogen non-genomic effects which have recently been suggested as novel potential cause of the higher susceptibility to drug-induced LQTS in women.

5 PROJECT 3. Use of hiPSC-CM to model the cardiovascular complications of COVID-19

5.1 Results

5.1.1 SARS-CoV-2 infection of hiPSC-CM and pulmonary cells

The pulmonary cell line 16HBE, the hiPSC-CMs and VERO-E6 as a positive control cell line, were infected with the previously titrated SARS-CoV-2 Italian reference strain (D614G, B.1; GISIAD: EPI_ISL_568579), isolated from an infected patient[212] (see page 135 for infection protocol details). After infection, cells were scored every other day at light microscope to detect cytopathic effect (CPE). At 72 hours post infection, supernatant from each well was collected and titrated on VERO E6 cells to detect the presence of active viral particles (see page 136 for viral titration details).

A significantly decrease in viability after virus infection was detected in VERO E6 (~-64%, $p<0.05$; figure 5.1A-C) and hiPSC-CMs (~-35%, $p<0.01$; figure 5.2B). On the contrary, in 16HBE cells SARS-CoV-2 infection did not elicit CPE (figure 5.2A) observed with other respiratory viruses. The virus was able to replicate and be released from all the three types of infected cells[127](figure 5.1D-F and figure 5.2C-D).

5.1.2 ACEI and ARB effects on SARS-CoV-2 infection

In a pilot experiment, we tested Lisinopril and Valsartan at both concentrations on VERO E6 cells in three different ways: treatment before SARS-CoV-2 infection (discontinuation), treatment before and after SARS-CoV-2 infection (continuation) and treatment after virus infection (initiation). As shown in figure 5.1, significant increase in viability of VERO E6 cells, after SARS-CoV-2 infection, was obtained with discontinuation (+68.83%) and continuation (+55.45%) of Valsartan treatment at the highest concentration compared to "Not treated" sample; initiation of it, after SARS-CoV-2 infection, had neutral effect. Lisinopril, at both concentrations, had neutral effect in the 3 strategies of

administration. To test if SARS-CoV-2 replicates into cell lines and is released in the supernatant, conditioned media were collected 72 hours post infection and titrated in a reinoculation experiment (figures 5.1D-F). Importantly, a hundred-fold reduction of viral titer was observed in the supernatants of VERO-E6 infected with SARS-CoV-2 and treated in continuation with 50µM of Valsartan (figure 5.1E), whereas no changes were observed for the other treatment conditions.

Accordingly, to these results, 16HBE and hiPSC-CMs were treated with the two drugs using a continuation protocol, that is before and after SARS-CoV-2 infection. As observed in VERO-E6 cells, treatment with Valsartan at the highest concentration significantly increased hiPSC-CMs viability (+10%; figure 5.2B). As regards 16HBE cells, they did not show any statistically significant increase or decrease in viability after each treatment (figure 5.2A).

Again, to assess SARS-CoV-2 replication, conditioned media from each cell type were collected post infection and titrated in a reinoculation experiment on VERO E6 cells (figures 5.2C-D). As observed in the pilot experiment, a significant reduction of viral titer was observed only in the supernatants of 16HBE and hiPSC-CMs treated in continuation with Valsartan 50µM.
In summary, treatment in continuation with Valsartan at the highest concentration increase both cardiac and pulmonary cell viability after infection, and reduce the number of viral particles released.

5.1.3 ACEI and ARB effects on SARS-CoV-2 replication

To assess if the reduction of viral titer in the supernatants of cells treated with Valsartan is imputable to an inhibitory effect on the SARS-CoV-2 Main protease (M^{pro}), an *in vitro* time-point based assay was performed (see page 137 for details). The compound GC376, a known inhibitor of SARS-CoV-2 M^{pro}, was used as a control inhibitor. As shown in table 5.1, neither Valsartan nor Lisinopril influence the SARS-CoV-2 main protease activity.

Figure 5.1. SARS-CoV-2 infection and virus titer in VERO E6 after ACEi/ARB treatment.

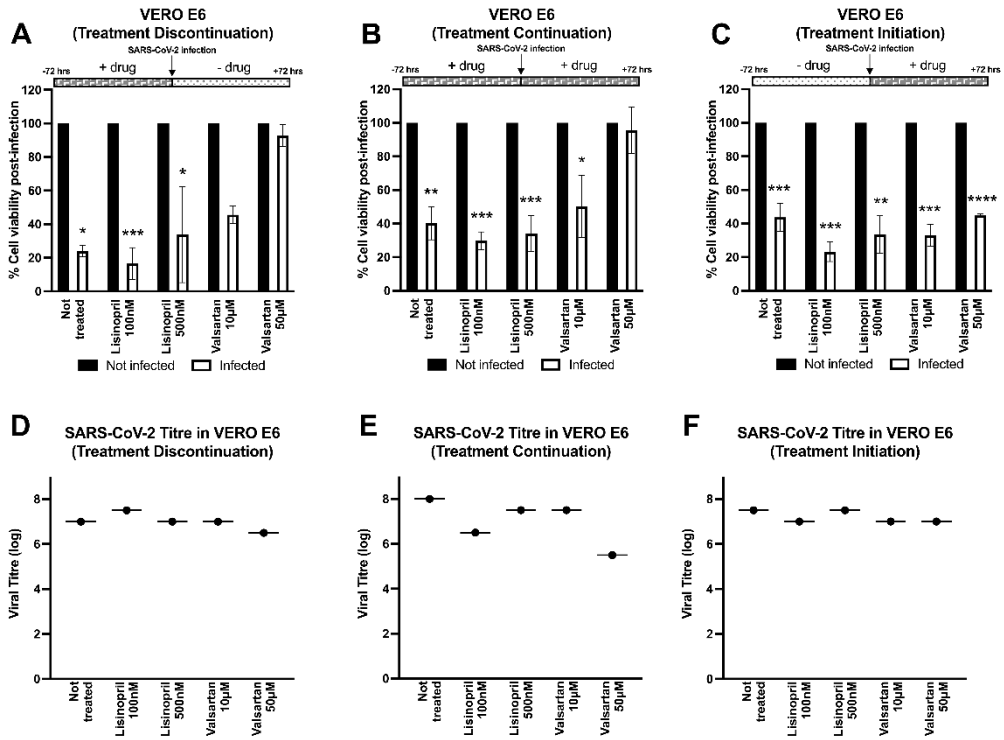

*VERO E6 seeded in a black F-bottom transparent 96-wells plate, were treated for 72 hours with Lisinopril or Valsartan, both at minimum and maximum plasma concentration before SARS-CoV-2 infection. One "Not treated" control sample was added. VERO E6 cells were treated with drugs with 3 different approaches: discontinuation **(A)**, continuation **(B)** or initiation **(C)** of treatment. For each drug condition of VERO E6 (n=6), half of wells were infected for 1 hour with 1000 $TCID_{50}$/mL of SARS-CoV-2 and 72 hours post-infection cells were fixed with 4% paraformaldehyde and viability was measured with the infrared BioTracker 650 Red Nuclear Dye. Percentage of viability of each condition was obtained normalizing to 100% uninfected cells (black bars). Statistical analyses were conducted using GraphPad Prism 9 and significance was determined by Student's t test. The asterisks indicate the statistical significance: * p-val<0.05, ** p-val<0.01, *** p-val<0.001 and **** p-val<0.0001. **(D-F)** Microneutralization assay results for SARS-CoV-2 titration (n=2).*

Table 5.1. Time-dependent inhibition assay.

Compound	**100 µM (c.f.)**	**10 µM (c.f.)**	**ID50**	**Notes**
GC376	100% inhibition	99.8%	0.138±0.04 µM	Positive control
Lisinopril	No inhibition	No inhibition		
Valsartan	No inhibition	1.22%		

Lisinopril and Valsartan inhibition against M^{pro} was tested through time point-based assay. GC376 was used as positive control.

Figure 5.2. SARS-CoV-2 infection and virus titer 16HBE and hiPSC-CMs after ACEi/ARB treatment.

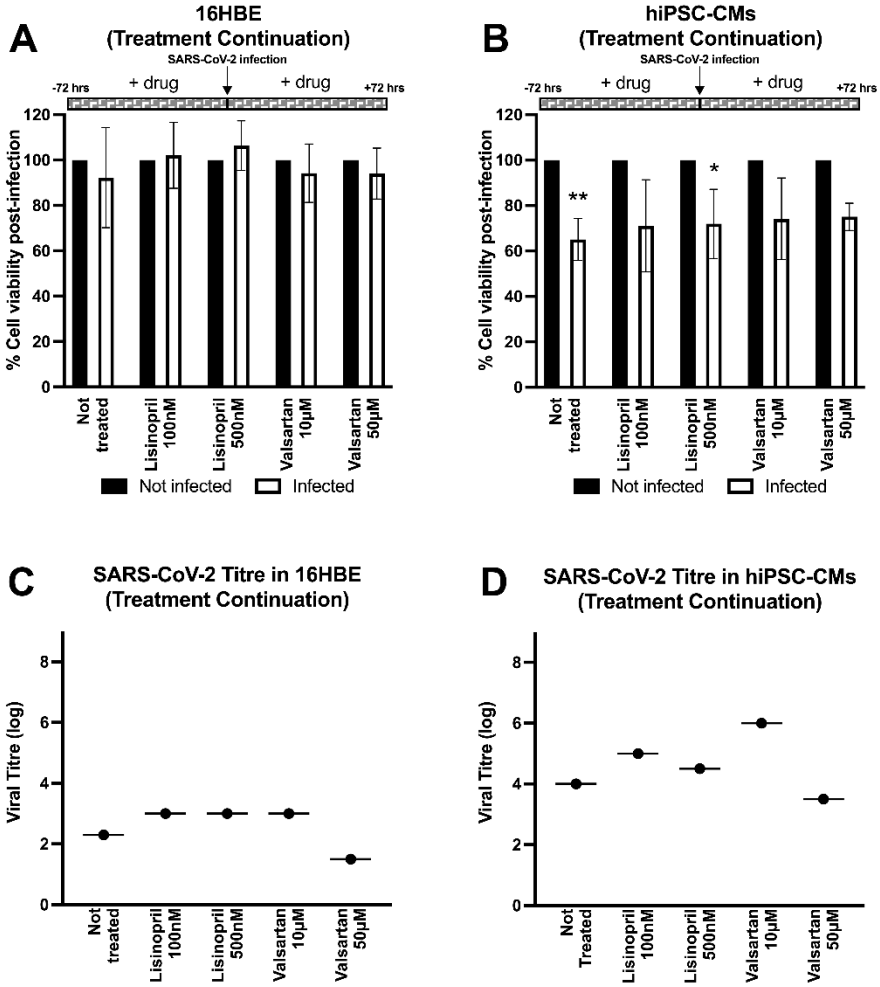

*16HBE **(A)** and hiPSC-CMs **(B)** seeded in a black F-bottom transparent 96-wells plate, were treated for 72 hours with Lisinopril or Valsartan, both at minimum and maximum plasma concentration before SARS-CoV-2 infection. One "Not treated" control sample was added. 16HBE and hiPSC-CMs were treated before and after SARS-CoV-2 infection. For each drug condition of 16HBE (n=12) and hiPSC-CMs (n=12), half of wells were infected for 1 hour with 1000 $TCID_{50}$/mL of SARS-CoV-2 and 72 hours post-infection cells were fixed with 4% paraformaldehyde and viability was measured with the infrared BioTracker 650 Red Nuclear Dye. Percentage of viability of each condition was obtained normalizing to 100% uninfected cells (black bars). Statistical analyses were conducted using GraphPad Prism 9 and significance was determined by Student's t test. The asterisks indicate the statistical significance: * p-val<0.05, ** p-val<0.01. **(C-D)** Microneutralization assay results for SARS-CoV-2 titration in 16HBE (n=3) **(C)** and hiPSC-CMs (n=3) **(D)**.*

5.1.4 ACE2 expression after ACEI and ARB treatment

To assess if Valsartan may reduce the permissivity of cardiac and pulmonary cells to SARS-CoV-2, we assessed ACE2 expression in VERO E6, 16HBE and hiPSC-CMs. After normalising the "Not treated" sample of the three cell lines to 100%, the ACE2 mRNA level after 72 hours of each treatment was measured. After Valsartan 50μM treatment, the ACE2 expression was significantly decreased in VERO E6 cells (-64.68%, $p<0.01$; figure 5.3A), 16HBE cells (-53.72%, $p<0.05$; figure 5.3B) and hiPSC-CMs (-49.48, $p<0.01$; figure 5.3C). ACE2 protein content in cell lysates of VERO E6 cells (figure 5.3D), 16HBE cells (figure 5.3E) and hiPSC-CMs (figure 5.3F) was detected by Western Blot (see pages 153-154 for details). In agreement with what observed at RNA levels, also the ACE2 protein content treated with Valsartan 50μM was decreased in lysates of VERO E6, 16HBE and hiPSC-CMs.

Figure 5.3. ACE2 expression in VERO E6, 16HBE and hiPSC-CMs after drug treatment.

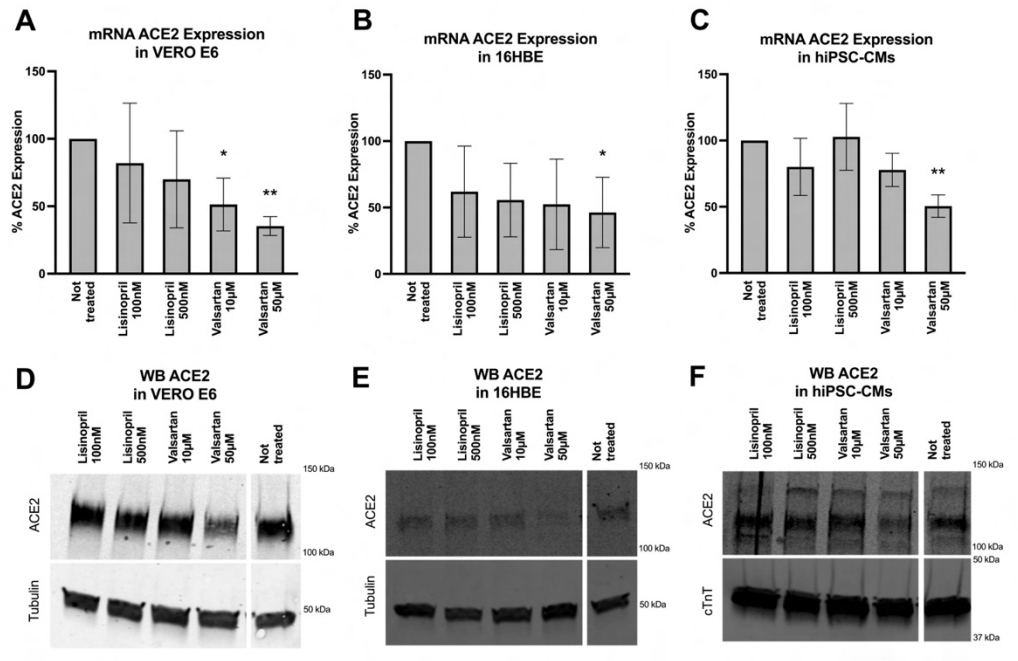

*Relative quantification of mRNA levels (**A-C**) and protein content (**D-F**) of ACE2, after 72 hours of treatment, in VERO E6 (**A,D**), 16HBE (**B,E**) and iPSC-CMs (**C,F**). The GAPDH was used as reference*

*gene of the $2^{-\Delta\Delta Ct}$ method of RT-qPCR. Each sample was loaded in quadruplicate. Statistical analyses were conducted using GraphPad Prism 9 and significance was determined by one-way ANOVA. The asterisks indicate the statistical significance: * p-val<0.05 and ** p-val<0.01. Tubulin was used as loading control for cell lysates of VERO E6 and 16HBE. Cardiac troponin T was used as loading control for cell lysates of hiPSC-CMs.*

5.2 Discussion

The recent emergence of the COVID-19 pandemic raised issue about safety of ACEI and ARB drugs in patients with COVID-19, due to the hypothesis that RAS inhibitors may upregulate ACE2 expression, the SARS-CoV-2 receptor on target cells, increasing SARS-CoV-2 infectivity[154]. Most of the experiments that reported an increase in ACE2 expression were conducted on animal models, but in nearly all studies doses of ACEIs/ARBs used were greater than equivalent doses typically administered to human[155]. Since the beginning of the COVID-19 pandemic, different studies and clinical trials have been conducted to clarify the effects of discontinuation, continuation, or initiation of these drugs in COVID-19 patients. Consequently, we decided to test *in vitro* the effects of ACEI (Lisinopril) and ARB (Valsartan). RAS inhibitors were tested, each at the lowest and highest plasma concentration, on VERO E6 cells, which are the master replicative line for SARS-CoV-2; 16HBE cells, as pulmonary model and hiPSC-CMs, as heart model.

Initially, it was assessed that VERO E6 cells[213], hiPSC-CMs[32] and 16HBE cells could be infected by SARS-CoV-2. A statistically significant reduction in viability after virus infection was detected in VERO E6 (figure 5.1A-C) and hiPSC-CMs (figure 5.2B). On the contrary, in 16HBE cells SARS-CoV-2 infection did not elicit CPE (figure 5.2A) observed with other respiratory viruses, but the virus was able to replicate and be released from infected cells[128] (figure 5.1D-F and figure 5.2C-D).

To recreate, *in vitro*, discontinuation, continuation or initiation of ARB and ACEI treatment 3 strategies of drug administration were adopted on VERO E6: treatment before SARS-CoV-2 infection, treatment before and after SARS-CoV-2 infection and treatment after virus infection. As shown in figure 5.1, significant increase in viability of VERO E6 cells, after SARS-CoV-2 infection, was obtained with discontinuation and continuation of Valsartan treatment at highest concentration compared to “Not treated” sample; initiation of it, after SARS-CoV-2 infection, had neutral effect. Lisinopril, at both concentrations, had neutral effect in the 3 strategies of administration. Most importantly viral titer in

the supernatants of VERO-E6 infected with SARS-CoV-2 and treated in continuation with 50μM of Valsartan is strongly reduced (figure 5.1E).

Therefore, RAS inhibitors, at both concentrations, were tested on 16HBE and hiPSC-CMs in treatment continuation. As observed in VERO E6 cells, treatment with Valsartan at highest concentration significantly increased cell viability (figure 5.2B) and reduced viral titer in the supernatants of both hiPSC-CMs and 16HBE (figure 5.2C-D).

Alnajjar et al. reported that Valsartan could exert a moderate inhibitory effect on virus Main protease (M^{pro}) [214]. Any Valsartan effect was not observed when added after virus infection, suggesting that it act on virus entry more than viral replication. As a confirmation, we demonstrated through a time-point based assay, that Valsartan had no effect on the M^{pro} (table 5.1).

On the contrary, ACE2 mRNA and protein levels were significantly decreased in VERO E6, 16HBE and hiPSC-CMs treated with the highest concentration of Valsartan (figure 5.3), indicating that Valsartan may reduce the permissivity of these cell types to SARS-CoV-2 infection.

5.3 Conclusion

Our data suggest that ACEi and ARBs do not worsen the SARS-CoV-2 infection. This is in agreement with two clinical trials reporting no increased risk with continuation of ACEI and/or ARB therapy[215,216]. Most relevant, the treatment with Valsartan at highest plasma concentration (50μM) seems to be protective against SARS-CoV-2 infection. This finding may explain why ARB users had a 9% lower relative risk of all-cause hospitalization or mortality compared to patients treated with ACEI[217].

6 PROJECT 4. Determine the safety of MSC as a possible stem cell therapy for the most severe forms of COVID-19

6.1 Results

6.1.1 MSC isolation and characterization

The MSC lines used in this study were both adult and fetal MSC. Adult MSC were isolated from bone marrow (BM-MSC) and adipose tissue (AT-MSC); fetal MSC were isolated from amniotic membrane of human placenta (A-MSC), cord blood (CB-MSC) and cord tissue (CT-MSC). A-MSC and BM-MSC were isolated in my lab whereas AT-MSC, CB-MSC and CT-MSC were isolated by our collaborator dr. Maria Antonietta Avanzini from the Cell Factory of the Fondazione IRCCS Policlinico San Matteo in Pavia.

All the MSCs fulfill the criteria set by the ISCT[218]. Hereafter, isolation and characterization of A-MSC is described as a reference.

A-MSC were isolated from amnios (figure 6.1A) and seeded on plastic dishes. After the first change of medium few MSCs, with the typical spindle-shaped morphology, were observed in co-culture with other cell types of different morphology, including epithelial cells (figure 6.1B1). After the first passage contaminant cells were lost and MSCs started to form colonies (figure 6.1B2). In panel 3 (figure 6.1B3) is shown a pure culture of A-MSCs at 80% of confluence.

The analysis by flow cytometry (see page 126 for details) proved that isolated A-MSC express the typical MSC membrane antigens, in accordance with the criteria established by ISCT[218]. As expected, MSC are positive for CD90, CD73 and CD105 antigens (figure 6.2A1) and negative for CD14, CD20, CD34 and CD45 antigens (figure 6.2A2). As for the histocompatibility antigens A-MSC were found to be negative for HLA DR and positive for HLA ABC (figure 6.2A3), confirming that they had an immune privileged phenotype.

Another feature associated with the mesenchymal phenotype is the ability to differentiate into adipocytes, osteoblasts and chondroblasts (see pages 122-125 for details). Our A-MSCs, when grown in specific differentiation media, were able to: form chondroblast spheroids expressing proteoglycans, as revealed by staining with the Alcian Blue dye (figure 6.2B1), differentiate into adipocytes containing lipid droplets, visualized with Oil red O (figure 6.2B2) and in osteoblasts as shown by the Van Kossa stain which reveals the presence of calcium phosphates (figure 6.2B3). Moreover, the DNA karyotyping revealed normal chromosome asset (46, XX) (figure 6.2C).

Figure 6.1. A-MSC isolation and culture.

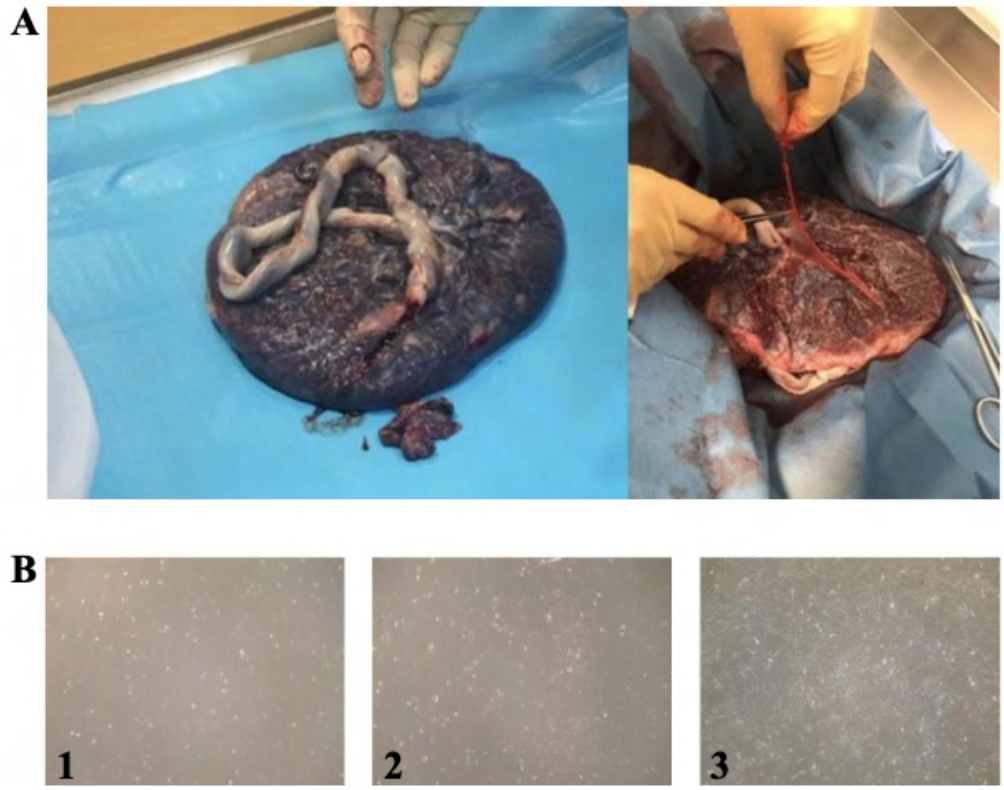

***(A)** Photograph of a human placenta. On the left, image of an intact placenta with the umbilical cord still attached. The chorionic disk of fetal origin faces outwards. On the left, the amnios partially lifted from the chorion. **(B)** Culture of A-MSCs. In panel 1, A-MSCsat p0 are observed in culture along with other cell types. In panel 2, culture of only A-MSCs at the first passage which begin to form colonies. Panel 3 shows a culture of A-MSC at the second passage at 80% of confluence.*

Figure 6.2. A-MSC characterization.

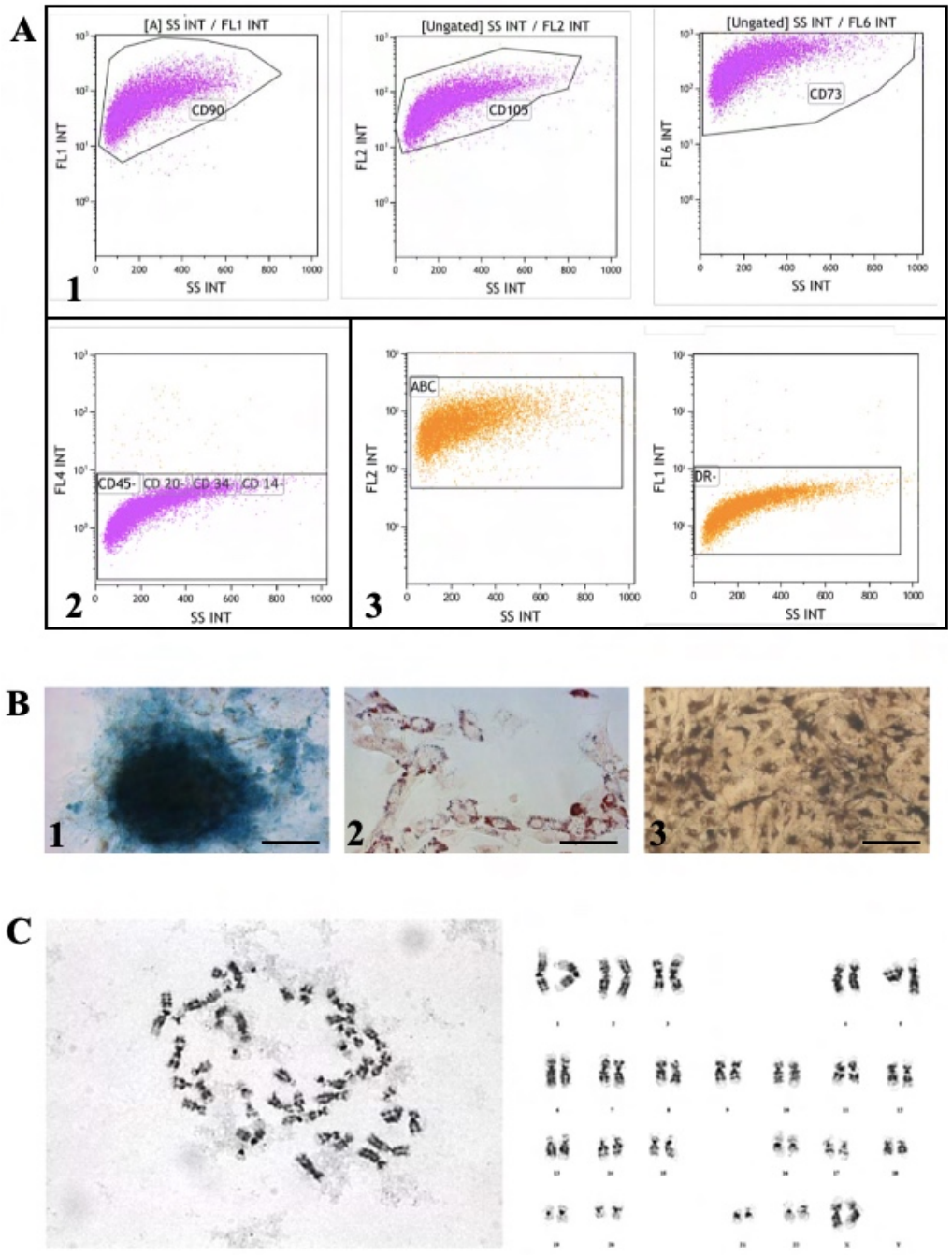

(A) *Phenotyping of A-MSCs by flow cytometry. Primary cultures of A-MSC were analyzed by flow cytometry, after labeling with the mix of fluorochrome conjugates of the MSC phenotyping kit (Miltenyi Biotech): anti-CD73 conjugated to fluorochrome allophycocyanin (APC), anti-CD90 conjugated to isothiocyanate of fluorescein (FITC), anti-CD105 conjugated to phycoerythrin (PE), anti CD14, CD20, CD34 and CD45 all conjugated to perinine-chlorophyll (PreCP). In the scatter plots presented, each dot represents a single cell. On the ordinary axis we have the intensity of the fluorescent signal on a logarithmic scale. On the abscissa axis there is the granularity and complexity of the cells. In panel 1 we observe the positivity for CD90, CD105 and CD73 given by the signal intensity of the fluorochromes FITC, PE and APC. In panel 2, the absence of PerCP dye signal indicates negativity for CD45, CD20, CD34 and CD14. In panel 3, the A-MSCs have been labeled with anti HLA DR-FITC and anti HLA ABC-PE: on the left is observed the positivity for HLA-ABC while on the right negative for HLA DR.* ***(B)*** *Differentiation into adipocytes, osteoblasts and chondroblasts. Photographs representative of the differentiation capacity of A-*

MSC. Chondroblasts were revealed with Alcian Blue (1), adipocytes with Oil red O (2) and osteoblasts with Von Kossa (3). Scale bar: 100µm. ***(C)*** *A-MSC karyotype showing a diploid chromosomal set 46 XX devoid of structural and numerical anomalies.*

6.1.2 Analysis of ACE2 and TMPRSS2 expression

ACE2 and TMPRSS2 expression were assessed on 4 lines of A-MSCs, 2 lines of CB-MSC and 2 lines of CT-MSC as fetal MSC; 4 lines of BM-MSC and 1 line of AT-MSC as adult MSC. The lung epithelial cell line Calu-3, which expresses high levels of both ACE2 and TMPRSS2 and is permissive to SARS-CoV-2 infection and non-lytic replication[219], was used as positive control[220].

Compared with Calu-3, the levels of ACE2 and TMPRSS2 mRNAs in all MSC lines considered were around 100-fold and 200-fold lower, respectively (figure 6.3A; see page 141 for details about qRT-PCR). ACE2 and TMPRSS2 protein expression in MSC lysates was undetectable by Western blot (figure 6.3B; see pages 153-154 for WB details). Finally, we were unable to detect any soluble amount of ACE2 in MSC-derived conditioned media by both Western blot and ELISA (figure 6.3B, C; see page 155 for ELISA details)[220].

Figure 6.3. hACE2 and TMPRSS2 expression in human MSCs from fetal and adult tissues.

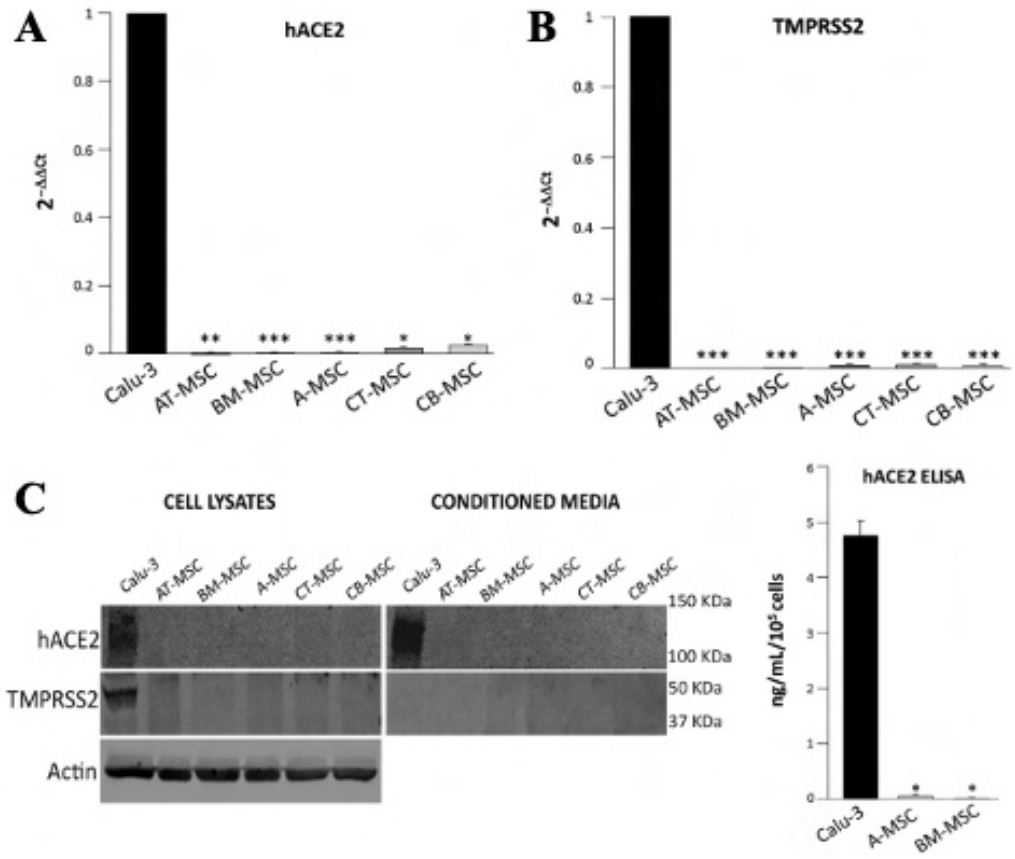

(A) *Relative quantification by RT-qPCR and the $2^{-\Delta\Delta Ct}$ method of ACE2 (left) and TMPRSS2 (right) mRNA levels in MSCs from cord blood (CB-MSC, n=2 lines), cord tissue (CT-MSC, n=2 lines), amnios (A-MSC, n=4 lines), bone marrow (BM-MSC, n=4 lines), and adipose tissue (AT-MSC, n=2 RNA samples from the same line), compared with the Calu-3 cell line. Each sample was loaded in triplicate. Columns represent mean $2^{-\Delta\Delta Ct}$ values and SD. The GAPDH was used as a reference gene. *P < .05, **P < .01, ***P < .001 vs Calu-3.* ***(B)*** *Representative Western blot of hACE2 and TMPRSS2 in cell lysates (left) and serum free 48 hours-conditioned media (right) of the different MSC types, and the positive control cell line Calu-3. Actin was used as loading control for cell lysates. The amount of conditioned media loaded for each sample was obtained from 1×10^5 cells.* ***(C)*** *ACE2 protein quantification by ELISA assay in serum-free 48 hours-conditioned media generated by 1×10^5 MSCs. The bars represent the mean and SD of triplicates obtained from a single line of Calu-3 and 4 distinct lines of both A-MSCs and BM-MSCs. *P < .001 vs Calu-3. MSCs, mesenchymal stromal cells. Reproduced from Avanzini et al*[220].

6.1.3 Infection of A-MSCs and BM-MSCs with spike-pseudotyped retrovirus

To substantiate the absence of ACE2 and TMPRSS2 in fetal and adult MSCs, both A-MSCs and BM-MSCs were transduced, as representative cell populations, with a replication-defective, GFP-tagged, pseudotyped retrovirus bearing the SARS-CoV-2 spike envelope protein (see page 138 for details). This

pseudovirus does not go through a lytic replication and does not induce CPE, but it shares the same host cell factors for viral entry with the authentic SARS-CoV-2. As expected, Calu-3 were infected by the spike-pseudotyped virus and turned green, confirming that the assay properly worked (figure 6.4). On the contrary, neither A-MSCs nor BM- MSCs were infected by the pseudovirus (figure 6.4). A-MSCs, BM- MSCs, and Calu-3 were all susceptible to entry driven by the pantropic VSV-G, confirming the specificity of the assay (figure 6.4). Finally, immunofluorescent analysis confirmed the expression of ACE2 and TMPRSS2 only in the permissive cell line Calu-3, whereas no expression was documented in fetal and adult human MSCs (figure 6.4)[220].

Figure 6.4. MSC infection with a SARS-CoV-2 Spike pseudovirus.

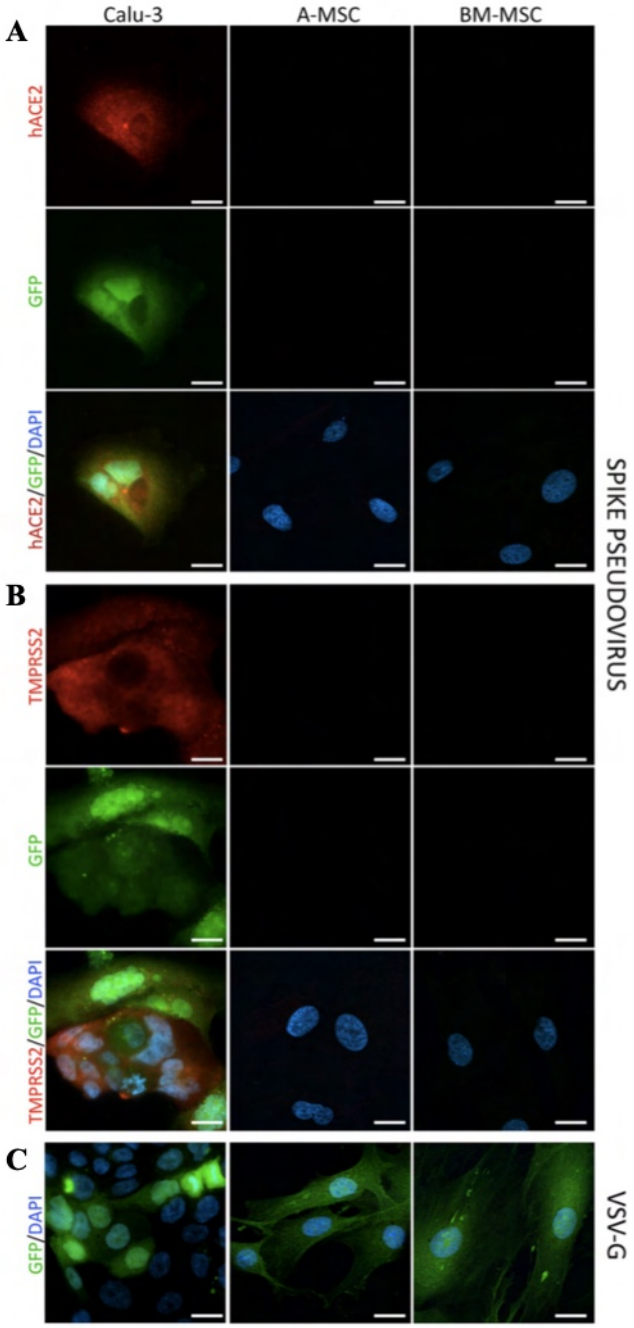

A-MSCs, BM-MSCs, and Calu-3 were transduced with a replication- defective, green fluorescent protein (GFP)-tagged, pseudotyped retrovirus bearing the SARS-CoV-2 spike envelope protein (Spike pseudovirus; ***A, B****), or the pantropic vesicular stomatitis virus glycoprotein (VSV-G;* ***C****). The green signal is present if cells are infected. Costaining for ACE2* ***(A)*** *or TMPRSS2* ***(B)*** *is shown in red. Nuclei were counterstained with the nuclear dye DAPI (Blue). Scale bar: 20 µm. Reproduced from Avanzini et al*[220].

6.1.4 Infection with SARS-CoV-2

To exclude that SARS-CoV-2 can infect MSCs through other host factors/receptors, fetal and adult human MSCs of different origin were infected with a SARS-CoV-2 wild strain (see page 135 for infection details) under two different conditions: as adherent monolayer or cellular suspension (figure 6.5A). All MSCs infected in adhesion showed the typical spindle shape morphology with no signs of CPE (figure 6.5B). Also, MSCs infected in suspension and seeded in 24 well-plates were found adherent to plastic and showed no CPE starting from the day post inoculum up to 7 days. Conversely, a 100% CPE was detected in the control VERO E6 cell line (figure 6.5B). As expected,[219] any CPE was observed in Calu-3 cells for the entire observation period (figure 6.5B). At 7 days after infection, supernatants from all experiments were collected and tested in a re-inoculation experiment in VERO E6 cells (figure 6.5A; see page 136 for viral titration protocol). As expected, a typical CPE was evident in all the wells inoculated with supernatants collected from infected VERO-E6 and Calu-3 cultures (figure 6.5C). On the contrary, none of the supernatant collected from the different MSC cell lines induced CPE, demonstrating the absence of viral replication inside the MSC lines and, consequently, the absence of SARS-CoV-2 infection (figure 6.5C)[220].

Figure 6.5. MSC infection with SARS-CoV-2.

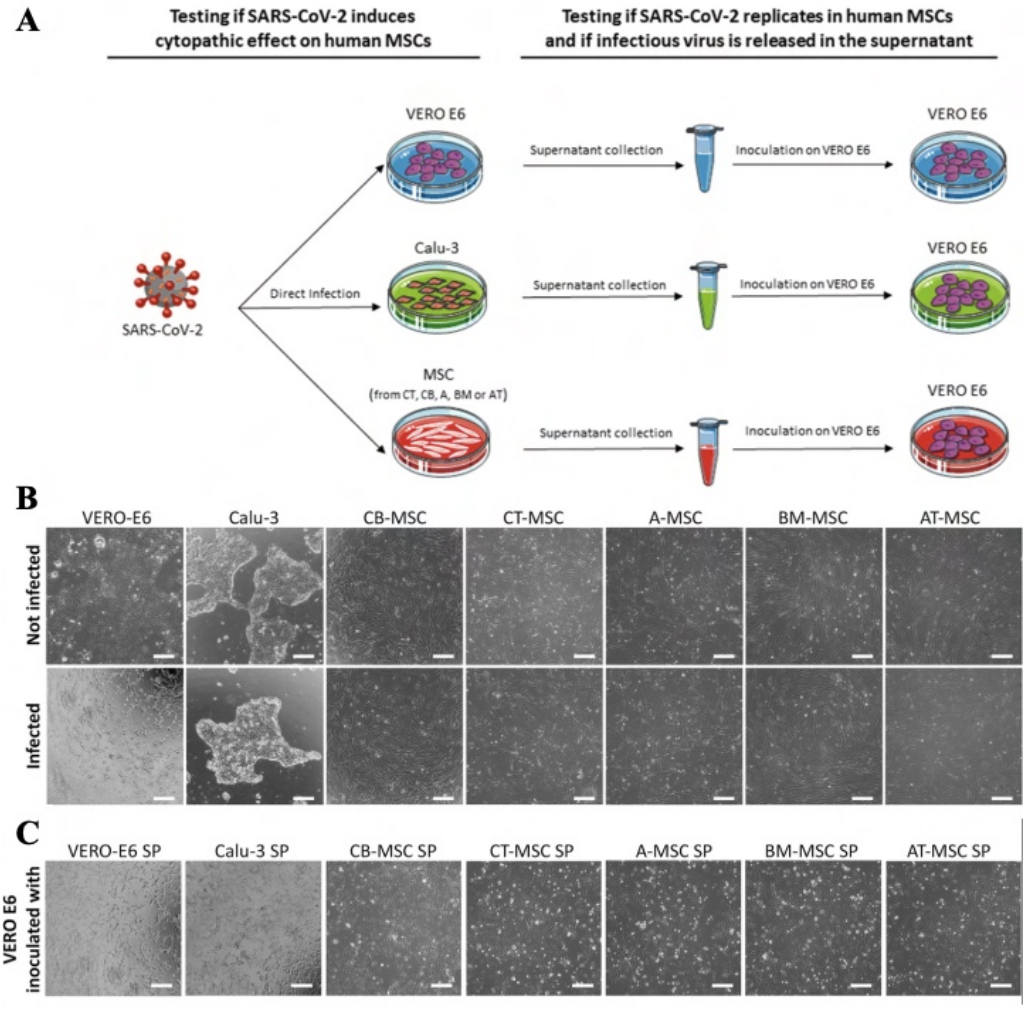

(A) *Experimental design. First, MSCs from CB, CT, A, BM and AT, and the permissive cell lines VERO E6 and Calu-3 were incubated with SARS-CoV-2 wild-type strain. CPE defined as cell rounding, detachment, degeneration, and/or syncytium formation was assessed by microscopic analysis, and the cells maintained in culture for 7 days, changing the medium every 3 days. Then, supernatants were collected and tested in a reinoculation experiment on VERO E6.* ***(B)*** *Representative phase contrast images of VERO-E6, Calu-3, and hMSCs before (not infected—upper panels) and after exposure to SARS-CoV-2 (infected—lower panels). Scale bar: 200µm. hMSCs and Calu-3 showed no signs of CPE and maintained their typical spindle-shaped and epithelial morphology, respectively, whereas VERO E6 displayed clear signs of CPE, since almost all the cells were round or fused into syncytia or detached.* ***(C)*** *Representative phase contrast images of VERO E6 cells after exposure to supernatant generated by the infected cell lines respectively indicated on top of each frame. Scale bar: 200µm. CPE, cytopathic effect; hMSCs, human mesenchymal stromal cells; MSCs, mesenchymal stromal cells. Reproduced from Avanzini et al*[220].

6.2 Discussion

Stem cells are generally resistant to viral agents[190] but infection of MSCs by avian influenza or herpesviruses has been reported[192,193], therefore a similar concern has been raised for the SARS-CoV-2. So far, evaluation of MSC infectiveness by coronaviruses, particularly by SARS- CoV-2, has not yet been investigated and described. There is only one study in which absence of the viral host cell factors ACE2 and TMPRSS2 expression on human umbilical cord blood-derived MSCs is claimed, but this cannot be considered a surrogate indicating a condition of refractoriness to infection[191]. Indeed, the presence on MSCs of a different receptor able to mediate viral entry cannot be ruled out. Moreover, if all human MSC types express or not ACE2 is still a matter of debate and solid data are missing[220].

MSC from the amniotic membrane of the human placenta, A-MSC, were isolated and maintained (figure 6.1). The A-MSCs were positive for membrane antigens CD105, CD73, CD90 and HLA ABC, and negative for CD45, CD34, CD14, CD20 and HLA DR (figure 6.2A). They were also able to differentiate into chondroblasts, adipocytes and osteoblasts after appropriate stimulation (figure 6.2B). As a further verification the karyotype was carried out which was found to be free of numerical or structural chromosomal abnormalities (figure 6.2C). These results demonstrate that the protocol used in the laboratory to isolate A-MSCs is reliable, allowing to obtain pure A-MSC populations.

Also, the other MSC lines (CB-MSC[221], CT-MSC[222], BM-MSC[223], AT-MSC[224]) used for this study were characterized confirming that they fulfill the criteria set by the ISCT[218].

Following confirmation of the mesenchymal identity of the isolated lines, using a variety of assays, we unequivocally demonstrated that human MSCs do express neither ACE2 nor TMPRSS2. Most importantly, using a direct infection assay, our study provides the first evidence that human MSCs derived from fetal and adult tissues are not permissive to SARS-CoV-2 infection[220].

6.3 Conclusion

Data obtained demonstrate that MSCs derived from different human tissues are resistant to SARS-CoV-2 infection are important to support the use of MSCs as a possible useful tool to down-modulate the immune hyper-activation in COVID-19 patients, and to contrast the pro-fibrotic mechanisms that lead to the severe long-term pulmonary sequelae increasingly observed in patients recovering from acute infection[220].

7 MATERIALS AND METHODS

7.1 Cell culture methods

In this thesis work different cell types were used: human dermal fibroblasts (HDF) [Project 1 and 2], peripheral blood mononuclear cells (PBMC) [Project 1], murine embryonic fibroblasts (MEF) [Project 1], hiPSCs [Project 1, 2 and 3], embryoid bodies (EB) [Project 1 and 2], hiPSC-CMs [Project 1, 2 and 3], lung epithelial cancer cell lines 16HBE and Calu-3 [Project 3 and 4, respectively], african green monkey-derived epithelial kidney cells (VERO E6) [Project 3 and 4] and mesenchymal stromal cells (MSCs) [Project 4]. Each cell type requires specific medium and culture conditions.

7.1.1 Human Dermal Fibroblasts (HDF)

Skin biopsies were collected from patients after obtaining written informed consent, approved by the Ethics Committee of Fondazione IRCCS Policlinico San Matteo, for both biopsy collection, reprogramming and conservation.

To obtain HDF, skin biopsy was cut into small pieces and placed in a 60 mm dish, covered with 2 mL of HDF medium composed by Dulbecco's Modified Eagle's Medium (DMEM, Euroclone) with 10% Fetal Bovine Serum (FBS, Sigma-Aldrich®), 2 mM L-Glutamine (Gibco®), 100 U/mL penicillin and 100 mg/mL streptomycin (Gibco®), 1% Non-Essential Amino Acids (NEAA, Gibco®), 1% sodium pyruvate (Gibco®), 0.2% Mycozap Plus PR (Lonza®), and incubated at 37°C, 5% CO_2. Thereafter, 2 mL of HDF medium was changed every 2-3 days until HDF outgrowth was observed. When they reach the confluence, they were split with 0.05% Trypsin (Gibco®) for 5 minutes at 37°C, 5% CO_2. Trypsin (Gibco®) was inactivated by adding a double volume of medium and cells were centrifuged at 300 rcf for 5 minutes. Pellet was resuspended in HDF medium to be seeded at the desired cell density or was resuspended in DMEM supplemented with 50% FBS (Sigma-Aldrich®) and 10%

Dimethylsulfoxide (DMSO, Sigma-Aldrich®) to be frozen in liquid nitrogen for long term storage.

7.1.2 Peripheral Blood Mononuclear Cells (PBMC)

Peripheral blood samples were obtained from patients after obtaining written informed consent, approved by the Ethics Committee of Fondazione IRCCS Policlinico San Matteo, for both PBMC collection, reprogramming and conservation.

PBMCs were isolated from fresh whole blood using Ficoll®-Paque PREMIUM (GE Healthcare) solution gradient. Ficoll®-Paque PREMIUM was added to a 15 mL centrifuge tube and then blood sample, previously diluted 1:2 with PBS 1X, was carefully added dropwise on Ficoll®-Paque PREMIUM (GE Healthcare). It was important to maintain a 3:4 ratio of Ficoll®-Paque PREMIUM (GE Healthcare) and diluted blood, respectively. Sample was centrifuged at 400rcf for 30 to 40 minutes at 18°C, and centrifuge brake disabled. The layer containing mononuclear cells was transferred to a sterile centrifuge tube using a sterile pipette, and then washed three times with three volumes of PBS 1X and centrifuge at 400 rcf for 15 minutes at 18°C, brake on. The supernatant was discarded, and the pellet was finally resuspended in PBMC medium composed by Stem-Pro™-34 SFM (Gibco®) supplemented with 100 U/mL penicillin and 100 mg/mL streptomycin (Gibco®), 100 ng/mL Stem Cell Factor (SCF, Gibco®), 100 ng/mL FMS-like Tyrosine Kinase 3 (FLT-3, Gibco®), 20 ng/mL Interleukin 3 (IL-3, Gibco®) and 20 ng/mL Interleukin 6 (IL-6, Gibco®).

For long storage, PBMCs were resuspended in Cryostor CS10 (Biolife Solution®) in cryovials (Nalgene®) to be frozen in liquid nitrogen.

7.1.3 Mitotically inactivated MEF (iMEF)

iMEF were used as feeder layer for generation and maintenance of hiPSCs with a feeder-dependent protocol. MEF were isolated from mouse CD1 embryos at

13th weeks of gestation and criopreserved at passage 1. To prepare the stocks of mitotically-inactivated feeders, proliferating 5x10^6 MEFs were thawed and seeded in a 175cm^2 flask. When cells became confluent, they were split in four 175cm^2 flasks, and when they again reached the confluency, they were split in two 10-layer flasks. When cells became confluent (passage 4), they were detached with 0.05% trypsin/EDTA, collected by centrifugation, resuspended in 15 ml of HDF culture medium, and divided in 3 tubes for irradiation (Cellstar). Cells into tubes were irradiated at 3000 rad, and then mixed together, counted by using Trypan blue 0.4% to distinguish between live and dead cells, and finally frozen in criovials at 2.5 x 10^6 cells/vial. One to two days before initiating or passaging iPSC culture, iMEFs were thawed and seeded at 3x10^{4}cells/cm^2 on a gelatin-coated culture vessels in HDF medium (see par. 3.1.1 for the recipe). To do the coating of plates with gelatin, the whole surface of culture vessels was covered with 0.1% gelatin solution and incubated for at least 30 minutes at room temperature. Gelatin solution was then removed from the culture vessel by aspiration just prior to use, to avoid air-drying.

7.1.4 hiPSCs

In this PhD thesis work, hiPSC were generated by three different methods and starting from two different cell types. Initially, HDF were reprogrammed to hiPSCs using retroviral vectors and a feeder-dependent protocol. Then, HDF were reprogrammed with a non-integrative RNA-based vector on MEF feeder-layer. Later, this protocol was replaced with a new one based on the use of non-integrative Sendai viral vectors (SeV) and a feeder-free culture able to reprogram both HDF and PBMC.

Feeder-dependent hiPSC cultures were maintained in hiPSC medium, composed by DMEM/F12 supplemented with 20% Knockout Serum Replacement (KO-SR), 2 mM L-glutamine, 100 U/mL penicillin, 100 mg/mL streptomycin, 1% NEAA, 0,1 mM β-mercaptoethanol and 10 ng/mL basic Fibroblast Growth Factor (bFGF) (all purchased from Gibco®).

On the contrary, feeder-free hiPSCs were plated on Matrigel® hESC-qualified Matrix (Corning®) and cultivated in TeSR™-E8™ medium (StemCell™ Technologies). Matrigel® (Corning®) was aliquoted and conserved at -20°C. Matrigel® aliquots were thawed on ice, diluted in DMEM/F12 (Gibco®) at the dilution factor indicated on the datasheet, distributed into the culture plates, and incubated for at least 1 hour at room temperature. Matrigel®-coating was aspirated immediately before seeding the cells.

7.1.4.1 Reprogramming protocol with retroviral vectors

The four retroviral vectors pMXs-hOCT3/4 (#17217), pMXs-hSOX-2 (#17218), pMXs-hcMYC (#17220) and pMXs-hKLF4 (#17219) and the packaging plasmid pCL-Eco (#12371) were obtained from Addgene. Viral particles were packaged into the 293T cell line (Clontech). Briefly, 293T cells were seeded into four 75 cm^2 flasks at the density of $4x10^6$ cells/flask. After 24 hours, the cells were co-transfected, using the Calcium/Phosphate method, with 20 µg of pCL-Eco and 20 µg of one of the four pMXs viral vectors in each flask. Viral supernatants (10 mL) were harvested after 48 and 72 hours from transfection, filtered with 0.45 µm PVDF Durapore® filters (Millipore®), and immediately used for HDF infection.

Day -1: HDF between passage 2 to 4 were harvested and seeded on 6-multiwell plate at the density of $1x10^5$ cells/well. Cells were incubated at 37°C with a humidified atmosphere of 5% CO_2.

Day 0: First round of infection (12 hours) was performed with 2.5 mL of each viral supernatant collected at 48 hours in the presence of 4 µg/mL of polybrene (Sigma-Aldrich®). Cells were incubated overnight at 37°C with a humidified atmosphere of 5% CO_2.

Day 1: In the morning, the spent medium containing viral supernatants was replaced with fresh HDF medium. In the evening, second round of infection (12 hours) was performed. HDF medium was aspirated and replaced with fresh viral supernatants (2.5 mL) collected after 72 hours

in the presence of 4 µg/mL of polybrene (Sigma-Aldrich®). Cells were incubated overnight at 37°C with a humidified atmosphere of 5% CO_2.

Day 2: In the morning, the spent medium was aspirated and replaced with DFBS Medium composed of DMEM/F12 (Gibco®), 20% FBS (Gibco®), 2 mM L-glutamine (Gibco®), 100 U/mL penicillin and 100 mg/mL streptomycin (Gibco®), 1% NEAA (Gibco®), and 10 ng/mL basic Fibroblast Growth Factor (bFGF, Sigma-Aldrich®). DFBS was changed daily.

Day 6: Reprogrammed HDFs were seeded on a layer of iMEF in 10 cm culture dishes in DFBS medium.

Day 7: DFBS Medium was replaced with Induction Medium composed of DMEM/F12 (Gibco®), 10% FBS (Gibco®), 10% KO-SR (Gibco®), 2 mM L-glutamine (Gibco®), 100 U/mL penicillin (Gibco®), 100 mg/mL streptomycin (Gibco®), 1% NEAA (Gibco®), 0.1 mM β-mercaptoethanol (Gibco®), 10 ng/mL bFGF (Gibco®) and 1 mM valproic acid (VPA, Sigma-Aldrich®). Induction Medium was changed every day.

Day 14: After one week, Induction Medium was replaced with hiPSC Medium, which was renewed daily.

Day 20: First hiPSC colonies appeared and were ready to be manually isolated with a pulled glass pipette. Then, a 200 µL micropipette with filtered pipette tip was used to aspirate colony fragments that were immediately plate on feeder-layer of iMEF and containing fresh hiPSCs Medium supplemented with 10 µM of ROCK Y-27632 inhibitor (StemCell™ Technologies).

7.1.4.2 Reprogramming protocol with RNA based vectors

ReproRNA™-OKSGM kit was purchased from StemCell™ Technologies. $1x10^5$ HDFs were seeded in a well of 6-multiwell plate and were incubated at 37°C, 5% CO_2 overnight.

Day 0: HDF were washed with 2 mL sterile PBS 1X. 1 mL of HDF medium supplemented with 175 ng/mL Human Recombinant Carrier-Free (B18R, Sigma-Aldrich®) was added to each well and incubated for 20 minutes at 37°C, 5% CO_2. ReproRNA™ Cocktail was prepared using solutions supplied by the kit. To prepare the Cocktail for each well the following components were added in a sterile tube in this order: 1 µL ReproRNA™-OKSGM vector, 100 µL Opti-MEM® I Reduced-Serum Medium (Gibco®), 2 µL ReproRNA™ Transfection Supplement and 2 µL ReproRNA™ Transfection Reagent. The solution was incubated at room temperature (15-25°C) for 5 minutes. ReproRNA™ Cocktail was added dropwise to each well and incubated overnight.

Day 1: Medium containing ReproRNA™ Cocktail was aspirated and 1.5 mL HDF Medium supplemented with B18R (Sigma-Aldrich®) and 0.8 µg/mL Puromycin was added. The addition of Puromycin allows the removal of fibroblasts that have not been transfected with ReproRNA™-OKSGM. The plate was incubated 37°C and 5% CO_2 overnight.

Day 2-5: A daily medium change with 1.5 mL of fresh HDF Medium supplemented with B18R (Sigma-Aldrich®) and 0.8 µg/mL Puromycin was performed and incubated at 37°C and 5% CO_2.

Day 6-7: Reprogrammed fibroblasts were seeded on a layer of iMEF and a daily medium change with 1.5 mL of fresh HDF Medium with B18R (Sigma-Aldrich®) without Puromycin was performed and incubated at 37°C and 5% CO_2.

Day 8: HDF Medium with B18R (Sigma-Aldrich®) was aspirated and 1.5 mL of Induction Medium with B18R (Sigma-Aldrich®) was added in each well and incubated at 37°C and 5% CO_2 overnight.

Day 15: After one week, Induction Medium was replaced with hiPSC Medium supplemented with B18R (Sigma-Aldrich®), which was renewed daily.

Day 20: A daily medium change with hiPSCs Medium without B18R was performed until hiPSC colonies form and were ready to be manually

isolated with a pulled glass pipette. Then, a 200 µL micropipette with filtered pipette tip was used to scrape and aspirate colony fragments that were immediately plate on feeder-layer of iMEF and containing hiPSCs Medium supplemented with 10 µM of ROCK Y-27632 inhibitor (StemCell™ Technologies).

7.1.4.3 Sendai virus vector reprogramming protocol

HDFs or PBMCs were reprogrammed using CytoTune®-iPS 2.0 Reprogramming System which uses vectors based on a modified, non-transmissible form of Sendai virus (SeV) to safely and effectively deliver and express key genetic factors necessary for reprogramming somatic cells into iPSCs. In contrast to most available protocols, relying on integrative viral vectors, the CytoTune®-iPS 2.0 Reprogramming System uses vectors that were non-integrating and remain in the cytoplasm (i.e., they were zero-footprint). In addition, the host cell can be cleared of the vectors and reprogramming factor genes by exploiting the cytoplasmic nature of SeV and the functional temperature sensitivity mutations introduced into the key viral proteins.

<u>HDF reprogramming:</u>

Day -2: HDFs were seeded in wells of a 6-well plate at $3x10^5$ cells/well to achieve 50-80% confluence on the day of transduction. Cells were incubated at 37°C with a humidified atmosphere of 5% CO_2.

Day 0: CytoTune®-iPS 2.0 Sendai reprogramming tubes were thawed. Cells were transduced by adding the KOS (KLF4, OCT4, SOX2) polycistronic virus and the c-Myc virus at a MOI of 5, and the Klf4 virus at a MOI of 3 in a total volume of 1 mL complete DMEM, following the equation written below.

$$\text{Volume of virus } (\mu L) = \frac{\text{MOI } \left(\frac{\text{CIU}}{\text{cell}}\right) \times \text{ number of cells}}{\text{titer of virus } \left(\frac{\text{CIU}}{\text{mL}}\right) \times 10^{-3} \left(\frac{\mu L}{\text{mL}}\right)}$$

The reprogramming virus mixture was added to the well containing the cells. Cells were incubated overnight in a 37°C incubator.

Day 1: 24 hours after transduction HDF medium was replaced with fresh complete DMEM. Fibroblast were at 37°C, 5% CO_2 for 6 days changing medium every other day. A drastic cell death (>50%) was observed.

Day 7: Fibroblast cells were harvested and seeded on plates coated with Matrigel® (Corning®) with a density from $1x10^5$ to $5x10^5$ live cells per dish in HDF medium. The cells were incubated at 37°C, 5% CO_2. As a positive control in the RT-qPCR detection of the SeV genome, RNA from an aliquot of reprogrammed HDFs was extracted.

Day 8-28: 24 hours later (day 8), the medium was switched to TeSR™-E8™ medium (StemCell™ Technologies) and replaced everyday thereafter. Starting from day 12 post-transduction, colonies should have grown to an appropriate size for transfer. Colonies were picked manually and transferred onto prepared 12- or 24-well Matrigel®-coated (Corning®) culture plates.

PBMC reprogramming

Day -4: Four days before transduction, PBMCs were thawed and gently transferred into a 15-ml conical tube. PBMCs were slowly (dropwise) added to 5-10 mL of pre-warmed PBMC medium (cytokines were freshly added daily). Cell viability was determined by counting with tripan blue. Cell suspension was centrifuged at 200rcf for 10 minutes, the supernatant was discarded, and the cells were resuspended in PBMC medium at $5x10^5$ cells/mL. In the middle section of a 24-well plate 1 mL of cell suspension was added. Cells were incubated at 37°C with a humidified atmosphere of 5% CO_2.

Day -3 to -1: A daily medium change with PBMC medium was performed removing 0.5 mL of medium and adding 0.5 mL of fresh medium trying to not disturb the cells.

Day 0: The viability and total number of cells was measured. Generally, $3x10^5$ PBMCs per sample were transduced.

CytoTune®-iPS 2.0 Sendai reprogramming tubes were thawed. Cells were transduced by adding the KOS (KLF4, OCT4, SOX2) polycistronic virus and the c-Myc virus at a MOI of 5, and the Klf4 virus at a MOI of 3 in a total volume in a total volume of 1 mL, following the equation written below.

$$\text{Volume of virus } (\mu L) = \frac{\text{MOI } \left(\frac{\text{CIU}}{\text{cell}}\right) \times \text{ number of cells}}{\text{titer of virus } \left(\frac{\text{CIU}}{\text{mL}}\right) \times 10^{-3} \left(\frac{\mu L}{\text{mL}}\right)}$$

Transduction and reprogramming efficiencies of PBMCs were greatly increased by a centrifugation step at this point. Centrifuge at 2250rpm for 30 minutes at room temperature. When the centrifugation was complete, the pellet was resuspended in the same medium containing the virus and an additional 1 ml of PBMC medium was added to the well and plated in a 12-well tissue culture plate incubating overnight at 37°C.

Day 1: 24 hours after transduction PBMCs and medium were removed from the culture plate and transferred to a 15 mL centrifuge tube. The well was gently rinsed with 1 mL of medium to ensure most of the cells were harvested. To remove the CytoTune® Sendai viruses, cells were centrifuged at 200rcf for 10 minutes, supernatant was aspirated and cells were resuspended in 0.5 mL of complete StemPro®-34 medium containing the appropriate cytokines in a 24-well plate.

A drastic cell death (>60%) was observed. Cells were cultured at 37°C, 5% CO_2 for 2 days.

Day 3: PBMCs were counted using the desired method and seeded on plate coated with Matrigel® (Corning®) with a density from $1x10^4$ to $5x10^5$ live cells per dish in 2 mL of complete StemPro®-34 medium without the cytokines. The cells were incubated at 37°C, 5% CO_2. As a positive

control in the RT-qPCR detection of the SeV genome, RNA from an aliquot of reprogrammed PBMCs was extracted.

Day 3-6: Every other day, 1 mL (half) of the spent medium was removed from PBMCs and replaced with 1 mL of fresh complete StemPro®-34 medium without cytokines working with care to not disturb the cells.

Day 7: To start the transition of the cells to the new culture medium, 1 mL (half) of StemPro®-34 medium was removed from the cells and replaced with 1 mL of TeSR™-E8™ medium (StemCell™ Technologies).

Day 8-28: 24 hours later (day 8), the full volume of medium to TeSR™-E8™ medium (StemCell™ Technologies) was changed, and the spent medium was replaced everyday thereafter. Day 15 to 21 after transduction, colonies should have grown to an appropriate size for transfer. Colonies were picked manually and transferred onto prepared 12- or 24-well Matrigel®-coated (Corning®) culture plates.

Spent medium was replaced every day, for feeder-dependent culture, or every other day for feeder-free colonies. Passaging of hiPSC was performed once a week, at 1:3 split ratio. Differentiated cells were manually removed before the passage. Feedere-dependent iPSCs were detached using a dissociation buffer composed by 1 mg/mL collagenase IV (Invitrogen®), 0.25% Trypsin (Gibco®), 20% KO-SR (Gibco®), 1 mM $CaCl_2$ all diluted in PBS 1X. After 2 minutes of incubation at 37°C, 5% CO_2, the edges of the colonies started to pull away from the plate. Dissociation buffer was, then, aspirated and cells washed gently three times with PBS 1X. Colonies were peeled off the surface of the dish pipetting up and down the medium.

To detach and pass hiPSCs grown on Matrigel®-coated (Corning®) plates the ReLeSR™ (StemCell™ Technologies) reagent was used. A thin layer of reagent was added in each well, when the edges of colonies start to pull away, at least two washes with fresh TeSR™-E8™ medium (StemCell™ Technologies) were performed.

Collected cells were split on plates with fresh feeder-layer or fresh Matrigel® (Corning®) coating. Otherwise, cells can be stored in liquid nitrogen: after centrifugation at 200rcf for 5 minutes, the pellet was resuspended in Cryostor CS10 (Biolife Solution®) in cryovials (Nalgene®).

7.1.4.4 hiPSCs thawing

To thaw hiPSCs, cryovials were put in a water-bath at 37°C until a small ice pellet remains. Very gently, cells were added dropwise, from the cryovials (Nalgene®), into a 15 mL conical centrifuge tube containing 9.5 mL pre-warmed hiPSC Medium or TeSR™-E8™ medium (StemCell™ Technologies) for feeder-dependent or feeder-free culture, respectively. Cells were centrifuged at 200rcf for 5 minutes and the pellet was resuspended in hiPSCs Medium or TeSR™-E8™ medium (StemCell™ Technologies) with 10 μM ROCK Y-27632 inhibitor (StemCell™ Technologies). Thawed colonies were added onto a dish cover by feeder layers or Matrigel® (Corning®) coating and put in a humidified incubator at 37°C, 5% CO_2. Medium was replaced after 24-48 hours and ROCK Y-27632 (StemCell™ Technologies) was no more added.

7.1.4.5 Passage from a feeder-dependent to a feeder-free cultivation

To pass cells from a feeder-dependent to a feeder-free cultivation, Biolaminin 521 LN (LN521) (Biolamina) was employed.

LN521 (Biolamina) was a full-length, human, recombinant laminin 521 cell culture substrate, that provides an optimal environment for passing feeder-dependent to feeder-free hiPSC colonies.

Plates were coated with 100 μg/mL of LN521 (Biolamina), diluted in PBS 1X with Ca^{2+} and Mg^{+}, and incubated at 4°C overnight. hiPSC colonies were detached using 1 mg/mL collagenase IV (Invitrogen®), 0.25% Trypsin (Gibco®), 20% KO-SR (Gibco®), 1 mM $CaCl_2$ all diluted in PBS 1X. Cells were incubated for 45 minutes at 37°C, 5% CO_2. 1 mL of TeSR™-E8™ (StemCell™ Technologies) was added to peel off colonies from the surface of the dish

pipetting up and down the medium. Cells were collected in a 15 mL centrifuge tube and let them settle for 5 minutes. Carefully, the supernatant was discarded, and cells were resuspended in TeSR™-E8™ (StemCell™ Technologies) medium. The cell suspension was plated on LN521-coated (Biolamina) plates using TeSR™-E8™ (StemCell™ Technologies) medium with 10 μM ROCK Y-27632 inhibitor (StemCell™ Technologies). Medium was replaced every 24-48 hours and ROCK Y-27632 (StemCell™ Technologies) was no more added. When hiPSC colonies reach the proper confluence (~70-90%), they were passed on Matrigel®-coated (Corning®) plates.

7.1.5 Embryoid Bodies (EBs)

Embryoid bodies (EBs) are three-dimensional aggregates of pluripotent stem cells induced by suspension culture. During embryoid bodies formation, hiPSCs, if pluripotent, can differentiate into cells belonging to the three-germ layers. hiPSCs were detached using the specific dissociation buffer previously described and grown for 4 days (humidified incubator at 37°C, 5% CO_2) in plates treated with 5% polyhema (Sigma-Aldrich®) that is non-adherent condition. Then EBs were maintained in a modified hiPSCs Medium deprived of bFGF and containing 20% FBS (Gibco®) instead of KO-SR (Gibco®). Forming EBs were then transferred on 0.1% gelatin coated dishes to allow differentiation in adhesion for additional 7 days in the same medium.

7.1.6 hiPSC-derived cardiomyocytes (hiPSC-CMs)

To differentiate hiPSC into CMs three different protocols were tested: a custom-made protocol based on the sequential use of glycogen synthase kinase 3 (GSK3) and beta-catenin inhibitors (RPMI/B27 differentiation Protocol), and two commercially available kits with defined media: PSC Cardiomyocyte Differentiation Kit (Gibco™) and STEMdiff™ Cardiomyocyte Differentiation Kit (STEMCELL Technologies™).

7.1.6.1 RPMI/B27 differentiation protocol

Day 0: RPMI 1640 Medium (Gibco®) with 1X B27 supplement Minus Insulin (Gibco®), 50 U/ mL penicillin (Gibco®), 100 mg/mL streptomycin (Gibco®) and 12 µM CHIR99021 (CHIR, Selleckem) was added to hiPSC culture at 95-100% confluence and put in a humidified incubator at 37°C, 5% CO_2. CHIR99021 is a selective small molecule GSK3 inhibitor that activates Wnt signaling.

Day 1: the spent medium containing CHIR was aspirated and replaced with RPMI 1640 Medium (Gibco®) with 1X B27 Minus Insulin supplement (Gibco®), 50 U/ mL penicillin (Gibco®) and 100 mg/mL streptomycin (Gibco®). The plate was put in a humidified incubator at 37°C, 5% CO_2.

Day 3: the spent medium was replaced with RPMI 1640 Medium (Gibco®) with 1X B27 Minus Insulin supplement (Gibco®), 50 U/ mL penicillin (Gibco®), 100 mg/mL streptomycin (Gibco®) and 5 µM O-acyltransferase Porcupine inhibitor (IWP2, Sigma-Aldrich®) and incubated for 2 days at 37°C, 5% CO_2. Inhibition of Porcupine prevents Wnt secretion and thus blocks activation of the Wnt signaling pathway. Consistent with the missing Wnt ligand, levels of phosphorylated Lrp6 and Dvl2 are decreased in the presence of IWP-2 and β-catenin cannot accumulate.

Day 5: RPMI 1640 Medium (Gibco®) with 1X B27 Minus Insulin supplement (Gibco®), 50 U/ mL penicillin (Gibco®) and 100 mg/mL streptomycin (Gibco®) was added after the spent medium was aspirated and the plate was put in a humidified incubator at 37°C, 5% CO_2.

Day 7-10: RPMI 1640 Medium (Gibco®) with 1X B27 Supplement containing insulin (Gibco®), 50 U/ mL penicillin (Gibco®) and 100 mg/mL streptomycin (Gibco®) was changed every other day.

Day 10-15: spontaneously contracting syncytium of troponin T cardiac type 2 (TNNT2/cTnT) positive cardiomyocytes were present and ready for use in various research applications.

7.1.6.2 PSC cardiomyocytes differentiation protocol

The PSC Cardiomyocyte Differentiation Kit (Gibco®) is a complete ready-to-use xeno-free system for the efficient differentiation of human pluripotent stem cells (PSCs) into contracting cardiomyocytes within 10 days of initiating differentiation. The kit consists of three media: A, B and Maintenance.

Day 0: pre-warmed Cardiomyocyte Differentiation Medium A was added to hiPSC culture at 70-85% confluence and put in a humidified incubator at 37°C, 5% CO_2.

Day 2: the spent medium A was replaced with pre-warmed Cardiomyocyte Differentiation Medium B and cells were put to the 37°C incubator with a humidified atmosphere of 5% CO_2.

Day 4-10: replace Cardiomyocyte Differentiation Medium B with Cardiomyocyte Maintenance Medium. Return cells to the 37°C incubator with a humidified atmosphere of 5% CO_2. Cells were refed every other day.

Day 10-12: Spontaneously contracting syncytium of troponin T cardiac type 2 (TNNT2/cTnT) positive cardiomyocytes were present and ready for use in various research applications.

7.1.6.3 STEMdiff™ cardiomyocyte differentiation protocol

The STEMdiff™ Cardiomyocyte Differentiation Kit (STEMCELL Technologies™) was a complete xeno-free system for the efficient differentiation of hiPSC into contracting cardiomyocytes within 10 days of initiating differentiation. The kit consists of STEMdiff™ Cardiomyocyte Differentiation Basal Medium (STEMCELL Technologies™) to which 1X STEMdiff™ Cardiomyocyte Differentiation Supplement A (Medium A) or 1X STEMdiff™ Cardiomyocyte Differentiation Supplement B (Medium B) or 1X STEMdiff™ Cardiomyocyte Differentiation Supplement C (Medium C) were added. The kit comprises also STEMdiff™ Cardiomyocyte Maintenance Basal Medium (STEMCELL Technologies™) to which 1X STEMdiff™

Cardiomyocyte Maintenance Supplement (Medium Maintenance) must be added.

Day 0: STEMdiff™ Cardiomyocyte Medium A supplemented with Matrigel® (Corning®) (1:100) was added to hiPSC culture at >95% confluence and put in a humidified incubator at 37°C, 5% CO_2.

Day 2: the spent medium was replaced with STEMdiff™ Cardiomyocyte Medium B. Cells were put to the 37°C incubator with a humidified atmosphere of 5% CO_2.

Day 4: STEMdiff™ Cardiomyocyte Medium B was replaced with STEMdiff™ Cardiomyocyte Medium C. Cells were incubated at 37°C, 5% CO_2.

Day 6: Spent medium C was replaced with fresh medium C. Cells were incubated at 37°C, 5% CO_2.

Day 8-10: the spent medium was aspirated and replaced with STEMdiff™ Cardiomyocyte Medium Maintenance and changed every other day.

Day 12: Spontaneously contracting syncytium of troponin T cardiac type 2 (TNNT2/cTnT) positive cardiomyocytes were present and ready for use in various research applications.

For all the three protocols, beating cardiomyocytes were selected by glucose deprivation, that is incubation in RPMI 1640 Medium no glucose (Gibco®) with 1X B27 Supplement (Gibco®), from day 14 to day 17.

At 18th day, hiPSC-CMs were dissociated. The spent medium was aspirated and cells were washed once with PBS 1X. 1 mL of dissociation enzyme TrypLE™ Express 1X (Gibco®) was added per well of 6-multiwell plate. Plates were incubated in a humidified incubator for 10 minutes at 37°C, 5% CO_2. TrypLE™ Express 1X (Gibco®) was aspirated and cells were collected in 15 mL centrifuge tube with RPMI 1640 Medium (Gibco®) supplemented with 20% FBS (Gibco®) and 10 μM ROCK Y-27632 inhibitor (StemCell™ Technologies). Cells were centrifuged at 100rcf for 5 minutes. The supernatant was aspirated to remove any residual enzyme. Then, CMs pellet was resuspended in RPMI 1640 Medium

(Gibco®), with 20% FBS (Gibco®) and 10 μM ROCK Y-27632 inhibitor (StemCell™ Technologies), by pipetting up and down a few times and seeded on Matrigel®-coated (Corning®) dishes at density of ~260.000 cells/cm^2. Cells were refed every other day with RPMI 1640 Medium (Gibco®) with 1X B27 Supplement (Gibco®), 50 U/ mL penicillin (Gibco®) and 100 mg/mL streptomycin (Gibco®). CMs were maintained at 37°C, 5% CO_2.

In Project 2, hiPSC-CMs were maintained in Hormone Free Medium (HFM). The HFM is composed of DMEM basal medium (no glucose, no phenol red; Gibco®), 2 mM glutamine, 5 mM HEPES, 1 mM sodium pyruvate (Gibco®), 10 mM galactose, 1X ITS-3 (insulin-transferrin-selenium with fatty acid-albumin supplements, Sigma-Aldrich®), and 10% charcoal stripped fetal bovine serum (Gibco®).

7.1.7 Pulmonary cells

16HBE (SCC150, Sigma-Aldrich®) and Calu-3 (HTB-55™, ATCC®) are epithelial cell lines derived from human bronchi and lung adenocarcinoma, respectively. 16HBE cells were cultured in DMEM (Euroclone) with 10% FBS (Sigma-Aldrich®), 2 mM L-Glutamine (Gibco®), 100 U/mL penicillin and 100 mg/mL streptomycin (Gibco®), 1% Non-Essential Amino Acids (NEAA, Gibco®), 1% sodium pyruvate (Gibco®), 0.2% Mycozap Plus PR (Lonza®), and incubated at 37°C, 5% CO_2. Calu-3 cells were maintained in Eagle's Minimum Essential Medium (EMEM, ATCC®) supplemented with 10% FBS (Sigma-Aldrich®) and 100 U/mL penicillin and 100 mg/mL streptomycin (Gibco®) as recommended by ATCC®.

Media were changed every 2-3 days until cell outgrowth was observed. Subsequently, cells were expanded and further processed.

When 16HBE or Calu-3 reach the confluence, they were split with 0.05% Trypsin (Gibco®) for 5 minutes at 37°C, 5% CO_2. Trypsin (Gibco®) was inactivated by adding a double volume of medium and centrifuge at 300 rcf for 5 minutes. Pellets were resuspended in complete media, and cells were seeded

at the desired cell density. For long storage in liquid nitrogen, cells were resuspended in complete DMEM, for 16HBE cells, or EMEM, for Calu-3 cells, supplemented with 50% FBS (Sigma-Aldrich®) and 10% DMSO (Sigma-Aldrich®) and aliquoted in cryovials (Nalgene®).

7.1.8 VERO E6 cells

VERO E6 (CRL-1586™, ATCC®) are African green monkey kidney epithelial cells, widely used to replicate and isolate viruses, among them the SARS-CoV-2. This cell line was cultured in DMEM (Euroclone) with 10% FBS (Sigma-Aldrich®), 2 mM L-Glutamine (Gibco®), 100 U/mL penicillin and 100 mg/mL streptomycin (Gibco®), 1% NEAA (Gibco®), 1% sodium pyruvate (Gibco®) for 24-48 hours after seeding, then maintained in DMEM (Euroclone) with 2% FBS (Sigma-Aldrich®), 2 mM L-Glutamine (Gibco®), 100 U/mL penicillin and 100 mg/mL streptomycin (Gibco®), 1% NEAA (Gibco®) and 1% sodium pyruvate (Gibco®).

Medium was changed every 2-3 days until cell outgrowth was observed. Subsequently, cells were expanded and further processed.

When VERO E6 cells reach the confluence were split with 0.05% Trypsin (Gibco®) for 5 minutes at 37°C, 5% CO_2. Trypsin (Gibco®) was inactivated by adding a double volume of medium and centrifuge at 300rcf for 5 minutes. Cell pellet was resuspended in complete DMEM and cells were seeded at the desired cell density. For long storage in liquid nitrogen, pellet was resuspended in DMEM supplemented with 50% FBS (Sigma-Aldrich®) and 10% DMSO (Sigma-Aldrich®) and transferred in cryovials (Nalgene®).

7.1.9 Mesenchymal Stem Cells (MSCs)

The placentas were obtained from pregnant women undergoing scheduled caesarean delivery at the Department of Gynecology and Obstetrics of the Fondazione IRCCS Policlinico San Matteo, after signing the informed consent

approved by the Ethics Committee. The amniotic leaflet, located on the chorionic face of the placenta, was manually collected in the first hour after delivery. The amniotic membrane was separated from the chorion to avoid contamination by maternal cells of the deciduous portion.

The amniotic membrane was collected in a 50 mL conical centrifuge tube containing PBS 1X, 100 U/mL penicillin and 100 mg/mL streptomycin (Gibco®). Once collected, the membrane was transferred to 10 cm diameter dish and washed several times with PBS 1X, 100 U/mL penicillin and 100 mg/mL streptomycin (Gibco®) to eliminate residual blood until a white colored membrane was obtained. Then, the amnion was weighed on an analytical scale and, on the basis of the measured weight, the amount of Trypsin (Gibco®) to be used for enzymatic digestion was calculated, i.e., 2.5 mL of 0.25% Trypsin (Gibco®) in Hank's balanced saline solution (HBSS, Euroclone) per gram of amnion was used. The amnion was then roughly cut to facilitate the release of the cells, placed inside a 50 mL conical centrifuge tube in HBSS and incubated for 30 minutes at 37°C in the presence of 0.25% Trypsin (Gibco®).

After the first enzymatic digestion, the amnion was further fragmented, suspended in HBSS and digested a second time with collagenase 100 U/mL (Sigma-Aldrich®) for an hour and a half at 37°C.

At the end of the second enzymatic digestion, a filtration was carried out using 100 μm nylon filters (BD Falcon®). The filtrate was centrifuged at 300rcf for 15 minutes. The cell pellet was resuspended in Minimum Essential Eagle Medium (α-MEM, Biowest®) with the addition of 20% FBS (Sigma-Aldrich®), 100 U/mL penicillin and 100 mg/mL streptomycin (Gibco®) and plated in culture dishes.

Growth of a mixed population of cells including blood cells in suspension, and epithelial and mesenchymal stem cells adhered to the plastic was observed in the first days of culture. The cells in suspension were eliminated after the first change of medium by aspiration, while to select the MSCs, Cell Dissociation Solution (Biological Industries) was used, which acts more on the MSCs than the epithelial cells that tend to stick to the plastic more firmly. Towards the third step, pure MSC cultures were obtained which assumed the typical fibroblast-like

morphology. When the cell line was stable, the amount of FBS in α-MEM was reduced to 10%. The MSCs derived from amnion (A-MSCs) were expanded maintaining a seeding density of $1x10^3$ cells/cm^2 at each passage. At each passage, they were counted to study the growth rate and a portion was frozen in liquid nitrogen in CryoStem™ MSC Freezing solution (Biological Industries), in aliquots of minimum $5x10^5$ and a maximum of $3x10^6$ cells.

The International Society for Cell and Molecular Therapy (ISCT) has established three criteria to define a cell as MSC. The first one is the ability to adhere to the plastic of the culture plate, a feature that makes MSCs easy to isolate. Then, MSCs should be positive for the membrane antigens CD105 (endoglin), CD73 (ecto 5'nucleotidase) and CD90 (Thy-1), and negative for the antigens CD45 (which is a pan-leukocyte marker), CD34 (typical of hematopoietic progenitors), CD14 or CD11b (which are abundantly expressed in macrophages and monocytes), CD79a or CD19 (typical membrane antigens of B cells) and HLA class II. Finally, MSC should be able to differentiate in osteoblasts, adipocytes and chondrocytes, after induction with specific culture media.

7.1.9.1 Chondrogenic differentiation protocol

To induce the differentiation of mesenchymal stem cells into chondroblasts, $2.5x10^5$ MSCs were resuspended in 500 µL of α-MEM (Biowest®) with 10% FBS (Sigma-Aldrich®), 100 U/mL penicillin (Gibco®), 100 mg/mL streptomycin (Gibco®), 100 µM Dexamethasone (Sigma-Aldrich®), 10% Insulin-Transferrin-Selenium (ITS-A, Gibco®), 1 µg/mL Ascorbic Acid (Sigma-Aldrich®), 1% Sodium Pyruvate (Carlo Erba) and 10 ng/mL TGF-β3 (Miltenyi Biotech). The suspension was transferred into a 1.5 mL tube which was placed in an incubator at 37 ° C with the lid ajar. This medium induced the formation of 3D aggregates, called spheroids.

On the third day, 300 µL of medium was replaced with an equal volume of fresh medium. On the fourth day the spheroids were resuspended and centrifuged at 1200 rpm for 5 minutes, then they were plated in 4-well plates. The medium was changed 3 times a week for 15 days.

Then, the cells were fixed with 4% Paraformaldehyde for 15 minutes. At the end of the fixation two washes in PBS1X were performed and cells were stained with 1% Alcian Blue solution in 3% acetic acid (Sigma-Aldrich®) for 45 minutes. This dye highlights, in blues, the proteoglycans, typical constituents of cartilage.

7.1.3.2 Adipogenic differentiation protocol

To differentiate MSCs into adipocytes, MSCs were detached, counted and seeded at a density of 6 x 10^4 cells/well in 24- or 4-well plates. The day after, the medium was replaced with α-MEM (Biowest®) supplemented with 10% FBS (Sigma-Aldrich®), 100 U/mL penicillin (Gibco®), 100 mg/mL streptomycin (Gibco®), 100 µM Dexamethasone (Sigma-Aldrich®), 50 mM Isobutyl-Methyl-Xanthine (Sigma-Aldrich®), 10 µg/mL Insulin (Gibco®), 200 µM Indomethacin (Sigma-Aldrich®) and 1% Sodium Pyruvate (Carlo Erba).

This medium was changed three times a week for ten days. The formation of lipid droplets inside the cells was observed under an optical microscope. Then cells were fixed in 4% PFA for 15 minutes and stained in Oil-Red-O as follows. A stock solution of 3 mg/mL Oil-Red-O (Sigma-Aldrich®) in isopropanol was diluted with distilled water with a 2:3 ratio. Fixed MSCs were washed with PBS 1X and incubated at room temperature with 500 µL of diluted Oil-red-O for 30 minutes. At the end the cells were washed abundantly with PBS 1X. Oil-red-O is a permeable dye that stain the lipid droplets inside the cells in red.

7.1.3.3 Osteogenic differentiation protocol

To induce osteogenic differentiation 4x10^4 MSCs were plated in each well of a 24- or 4-well plate, in α-MEM (Biowest®) supplemented with 10% FBS (Sigma-Aldrich®), 100 U/mL penicillin (Gibco®), 100 mg/mL streptomycin (Gibco®) and 0.2% Mycozap Plus PR (Lonza®). The day after the medium was switched to StemPro™ Osteogenesis Differentiation Kit (Gibco®) commercial medium, and changed three times per week for the following twenty days.

The cells were then fixed in 4% PFA for 15 minutes and then stained to reveal the presence of calcium phosphate crystals typically produced by osteoblasts. The staining was carried out using 400 µL of Von Kossa solution (5% $AgNO_3$ in water) which reacts with calcium phosphates to form silver phosphate, which is reduced following exposure to the UV transilluminator for 1 minute. The reduction to the transilluminator makes the metallic silver visible and balck.

7.2 Cell biology techniques

7.2.1 Karyotyping

Dividing cells were blocked in metaphase (at the greatest chromosome condensation) by exposure to 10 µg/mL Demecolcine solution (Sigma-Aldrich®) for 2 hours. The reagent was then removed, and the cells washed with PBS 1X. Both hiPSCs or MSCs were then detached with 0.05% Trypsin (Gibco®) and provided to the Laboratory of Oncohaematological Cytogenetic and Molecular Diagnostics, Division of Haematology, Fondazione IRCCS Policlinico San Matteo, for karyotyping using the Giemsa trypsin G-banding (GTG-banding) technique. Chromosome identification and karyotype description were made in accordance with the International System for Chromosome Nomenclature (ISCN, 2016).

7.2.2 Flow cytometry

To check if the MSCs [project 4] meet the ISCT criteria, they were analyzed by flow cytometer, after labeling with the MSC Phenotyping Kit (Miltenyi Biotech). The kit contains a mixture of the following monoclonal antibodies: anti-CD14, anti-CD20, anti-CD34, anti-CD45 conjugated to the protein complex peridine chlorophyll (PerCP), anti-CD73 conjugated to allophycocyanin (APC), anti-CD90 conjugated to fluorescein isothiocyanate (FITC) and anti-CD105 conjugated to phycoerythrin (PE). To carry out the labeling, $1x10^6$ MSCs were centrifuged, resuspended in 100 µL of PBS 1X and incubated for 10 minutes in

the dark at 4°C with 10 µL of the MSC Phenotyping Cocktail. In parallel, other $1x10^6$ cells were labeled with 10 µL of monoclonal antibodies anti HLA a-b-c conjugated to PE (Miltenyi Biotech), and HLA DR conjugated to isothioFITC (Miltenyi Biotech) in an equal volume and under the same experimental conditions.

At the end of the 10 minutes incubation, the cells were analyzed on the Navios EX (Beckman Coulter Life Sciences) flow cytometer in the Immuno-Hematology and Transfusion Laboratory of the Fondazione IRCCS Policlinico San Matteo, and the results analyzed with the Kaluza Analysis Software program.

7.2.3 Alkaline Phosphatase (AP) activity assay

AP is a marker of pluripotency that should be expressed by hiPSC. Its activity was evaluated with the Alkaline Phosphatase Staining kit II (Stemgent™) as follows.

I. AP Substrate Solution preparation:

- Mix 500 µL of Solution A (Stemgent™) with 500 µL of Solution B (Stemgent™).
- Incubate at room temperature for 2 minutes.
- Add 500 µL of Solution C (Stemgent™).
- Use within 30 minutes after preparation.

II. AP staining protocol:

- Grow hiPSCs on glass coverslips coated with 0.1% of gelatine.
- Wash cells once with PBS 1X and incubate them 2 minutes at room temperature with Fix Solution (Stemgent™).
- Wash once with PBS 1X supplemented with 0.05% Tween®20 (PBST).
- Add AP Substrate Solution (Stemgent™) and incubate in the dark for 20 minutes at room temperature.
- Stop the reaction with PBST.

- AP expression will result in a red or purple stain, while the absence of AP expression will result in no stain.

7.2.4 Immunofluorescence staining

For my PhD thesis work, immunofluorescence was used to evaluate the expression of specific antigens (listed in Table 3.1).

Once the cells were subconfluent, the immunofluorescence protocol was started:

Fixation

- Aspirate medium and wash with PBS 1X.
- Fix cells in 4% paraformaldehyde (PFA, Affymetrix) in PBS 1X at room temperature for 5 minutes.
- Aspirate 4% PFA (Affymetrix) and wash once in PBS 1X.

Permeabilization

- Permeabilize with 0.1% Triton X-100 (Sigma-Aldrich®) in PBS 1X for 5 minutes at room temperature
- Aspirate 0.1% Triton X-100 (Sigma-Aldrich®) and was once in PBS 1X

Blocking

- Block aspecific signals in 1% bovine serum albumin (BSA, Sigma-Aldrich®) in PBS for 1 hour at room temperature.

Primary antibody

- Incubate for 1 hour at room temperature with the primary antibody (Table 7.1) diluted in blocking solution.
- Aspirate the solution with the primary antibody and wash with PBS 1X for 2 minutes. Repeat three times.

Secondary antibody

- Incubate for 1 hour at room temperature with an appropriate secondary antibody (Table 7.1).
- Aspirate the solution with the secondary antibody and wash with PBS 1X for

2 minutes. Repeat three times.

- To stain nuclei, incubate for 5 minutes at room temperature with Hoechst 33342 diluted 1:1000 in PBS 1X.

Mounting

- Carefully collect the coverslip and quickly wash in distilled water.
- Mount the coverslip with a drop of Mowiol® (Sigma-Aldrich®) mounting solution or with mounting medium ProLong™ Gold antifade reagent with DAPI (Invitrogen®).
- Incubate overnight at room temperature.

Images were acquired using the Carl Zeiss fluorescence microscope Observer.Z1 equipped with the Apotome system and AxioVision 6.0 software (Zeiss).

7.2.5 In Cell Western (ICW) assay

The In-Cell Western Assay is a quantitative immunofluorescence assay performed in 96-well plates that combines the specificity of Western blotting with the replicability and throughput of ELISA. ICW Assays allow to: *i*) detect proteins in fixed and permeabilized cells using target-specific primary antibodies and IRDye® Secondary Antibodies; *ii*) quantify multiple targets using spectrally distinct fluorescent dye conjugates; *iii*) accurately measure relative protein levels in many samples; *iv*) detect proteins in situ in a relevant cellular context; *v*) normalize to cell number, allowing for accurate quantification and comparison of protein expression between wells.

In this thesis, ICW was performed to quantify cell viability or drug-toxicity and the expression of specific antigens.

The ICW protocol is based on standard immunofluorescent methods.

Fixation

- Culture cells in black 96-well plates with transparent flat bottom.
- Fix cells in 4% PFA (Affymetrix) in PBS 1X at room temperature for 15

minutes.

- Wash once in PBS 1X.

Permeabilization

- Permeabilize with 0.1% Triton X-100 (Sigma-Aldrich®) in PBS 1X for 5 minutes at room temperature with agitation (50 rpm).
- Repeat permeabilization for a total of five washes.

Blocking

- Block cells by adding Odyssey® Blocking Buffer (OBB, Li-COR®) to each well.
- Allow blocking for 1.5 hours at room temperature with moderate shaking on a rotator (50 rpm).
- Remove OBB (Li-COR®) from the blocking step.

Primary antibody

- Incubate with primary antibody diluted in OBB (Li-COR®) for 2 hours with agitation at room temperature. For greatest sensitivity continue incubation overnight at 4°C with no shaking.

Secondary antibody

- Wash five times with PBS 1X supplemented with 0.1% Tween®20 (PBST) for 5 minutes with agitation.
- Incubate with IRDye 680 or IRDye 800-conjugated secondary antibodies (Li-COR®) diluted 1:500 in OBB (Li-COR®) for 1 hour with gentle shaking at room temperature. Protect plate from light during incubation.
- Wash five times with PBST for 5 minutes with agitation. To stain nuclei in order to assess cells viability perform the last wash with BioTracker™ 650 Red Nuclear Dye (Sigma-Aldrich®) diluted 1:1000 in PBS 1X.
- After final wash, remove wash solution completely from wells. Turn the plate upside down and tap gently on a paper towel to remove traces of wash buffer.

Plate scan

- Scan the plates immediately using the Odyssey® Infrared Imaging System (Li-

COR®). Fluorescence intensities were measured from circular gates placed around the wells, which helps to avoid auto-fluorescence from the well walls. To perform absolute quantification the background fluorescence of empty wells is subtracted from the signal intensities. For statistical analysis, integrated fluorescence intensities in wells were analyzed using the Odyssey infrared Imaging System software (Li-COR®) provided with the imager station.

Table 7.1 Antibodies dilution for immunofluorescence staining and ICW

Type	Antibody	Specie	Dilution	Catalog Number	Company	Project
Pluripotency markers	anti-NANOG	Rabbit	1:200	09-0020	Stemgent™	1 and 2
	anti-OCT3/4	Mouse	1:500	sc-5279	Santa Cruz Biotechnologies	1 and 2
	anti-SOX2	Mouse	1:500	MAB2018	R&D System	1 and 2
	anti-TRA-1-60	Mouse	1:100	09-0010	Stemgent™	1 and 2
	anti-SSEA-3	Rat	1:100	MAB4303	Millipore®	1 and 2
	anti-SSEA-4	Mouse	1:100	09-0006	Stemgent™	1 and 2
Differentiation markers (EBs)	anti-TujIII	Mouse	1:500	MMS-435P	Covance	1 and 2
	anti-αSMA	Mouse	1:1000	CBL171	Millipore®	1 and 2
	anti-AFP	Mouse	1:500	SCR030	Millipore®	1 and 2
Differentiation markers (CMs)	anti-cTnT	Rabbit	1:250	ab45932	Abcam	1, 2 and 3
	anti-cTnT	Mouse	1:200	MA5-12960	Sigma-Aldrich®	1, 2 and 3
	anti-ACNT1	Mouse	1:800	A7811	Sigma-Aldrich®	1, 2 and 3
	anti-cTnI	Rabbit	1:250	Ab52862	Abcam	1
Hormone receptors	anti-ERα	Rabbit	1:200	D6R2W	Cell Signaling®	2

	anti-ERβ	Mouse	1:100	ab288	Abcam	2
	anti-GPER	Rabbit	1:200	GTX107748	GeneTex	2
	anti-Progesterone	Rabbit	1:80	D8Q2J	Cell Signaling®	2
	anti-Testosterone	Rabbit	1:800	D6F11	Cell Signaling®	2
K channel	anti-hERG	Rabbit	1:100	SC-20130	Santa Cruz Biotechnologies	2
SARS-CoV-2 target	anti-ACE2	Rabbit	1:200	GTX01160	GenTex	3 and 4
	anti-TMPRSS2	Rabbit	1:200	GTX100743	GenTex	4
Immunofluorescence secondary antibodies	Alexa Fluor™ 488 anti-rabbit IgG	Goat	1:500	A32731	Thermo Fisher Scientific™	1, 2, 3 and 4
	Alexa Fluor™ 546 anti-rabbit IgG	Goat	1:500	A11003	Thermo Fisher Scientific™	1, 2, 3 and 4
	Alexa Fluor™ 488 anti-mouse IgG	Goat	1:500	A32723	Thermo Fisher Scientific™	1, 2, 3 and 4
	Alexa Fluor™ 546 anti-mouse IgG	Goat	1:500	A11035	Thermo Fisher Scientific™	1, 2, 3 and 4
	Alexa Fluor™ 488 anti-rat IgG	Goat	1:500	A48262	Thermo Fisher Scientific™	1 and 2

	Alexa Fluor™ 546 anti-rat IgG	Goat	1:500	A11081	Thermo Fisher Scientific™	1 and 2
ICW secondary antibodies	IRDye® 800 anti-rabbit	Goat	1:500	926-32211	LI-COR®	2 and 3
	IRDye® 680 anti-rabbit	Goat	1:500	926-32221	LI-COR®	2 and 3
	IRDye® 800 anti-mouse	Goat	1:500	926-32210	LI-COR®	2 and 3
	IRDye® 680 anti-mouse	Goat	1:500	926-32220	LI-COR®	2 and 3

7.2.6 17β-estradiol (E2) stimulation

In project 2, hiPSC-CMs were stimulated with 10 nM of 17β-estradiol (E2; E2758, Sigma-Aldrich®). The "unstimulated" sample was used as control.

7.2.7 Lisinopril and Valsartan treatment

In project 3, VERO E6, 16HBE and hiPSC-CMs were treated with Lisinopril (ACEi; ab142316, Abcam) and Valsartan (ARB; 331-20973-1, RayBiotech) at minimum and maximum serum concentrations (100 nM and 500 nM for Lisinopril and 10 μM and 50 μM for Valsartan). As control, for each cell line, one Not Treated sample was added.

Three different treatment protocols were tested:

- Discontinuation: drug treatment was started 72 hours before SARS-CoV-2 infection and discontinued after infection.

- Continuation: drug treatment was started 72 hours before SARS-CoV-2 infection and continued after infection for other 72 hours.

- Initiation: drug treatment was started immediately after SARS-CoV-2 inoculation and maintained for 72 hours.

7.2.8 SARS-CoV-2 infection

SARS-CoV-2 infection was performed for project 3 and 4 of this thesis work. All the experiments with this virus were carried out inside biosafety cabins in the biosafety level 3 facility, by the staff of the Virology Department of the Fondazione IRCCS Policlinico San Matteo.

VERO E6, 16HBE, hiPSC-CMs, (project 3), Calu-3 and MSCs (project 4) were infected with the previously titrated SARS-CoV-2 Italian reference strain (D614G, B.1; GISIAD: EPI_ISL_568579), isolated from an infected patient[212].

In project 3, VERO E6 (n=6), 16HBE (n=12) and hiPSC-CMs (n=12) cell lines were seeded in black 96-well flat-bottom tissue-culture microtiter plates. VERO E6 cells were seeded at a density of $5x10^3$ cells/well, hiPSC-CMs were seeded at a density of $2x10^4$ cells/well, while 16HBE were seeded at a density of $1x10^4$ cells/well. Half of the wells for all conditions and cell lines, were infected with 1000 $TCID_{50}$ of SARS-CoV-2. The other half of the wells were used as a positive control for cell growth. The wells to be infected were incubated with the virus for 1 hour at 33°C and 5% CO_2, the inoculum was removed and fresh medium supplemented or not with drugs, was added in both infected and uninfected wells, prior to incubation at the same conditions.

In project 4, both Calu-3 and MSCs were seeded in 24-well culture microplates at different concentration ($1x10^5$, $5x10^4$ and $2.5x10^4$) and incubated at 37°C, 5% CO_2 to allow plastic adhesion. Sub confluent cells were infected with 100 $TCID_{50}$ of SARS-CoV-2. The virus was incubated for 48 hours and removed by changing the medium.

For both projects, after SARS-CoV-2 infection, cells were scored every other day at light microscope to detect cytopathic effect (CPE). At 72 hours post infection, supernatant from each well was titrated on VERO E6 cells. The black plates, of project 3, containing the remaining cells were fixed with 100µL Paraformaldehyde 4% in PBS 1X for 30 minutes at room temperature for further testing.

7.2.9 Viral titration

Spent medium from each infected cell line was serially diluted 10-fold with serum-free DMEM (Corning). Different dilutions (100 µL per well) of the supernatants were added to eight parallel wells of a transparent 96-well plate, after which 100 µL

of VERO E6 cell suspension was added to each well at a concentration of 2.5×10^5 cells/mL. Then, the 96-well plate was placed in an atmosphere of 5% CO_2 and incubated at 37°C for 72 hours. A microneutralization assay for viral titration was performed. Briefly, the cells were fixed and stained with 0.2% crystal violet solution (Merck) and 5% formaldehyde (Carlo Erba). The titer was calculated with the Reed–Muench method[225].

7.2.10 Time-dependent inhibition assay

In project 3, to study any inhibition effect of Lisinopril or Valsartan on the SARS-CoV-2 Main protease (M^{pro}) a time-point based assay was performed by our collaborators dr Deidda and Crespan of the Institute of Molecular Genetics IGM-CNR "Luigi Luca Cavalli-Sforza". Briefly, the FRET peptide substrate HiLyte Fluor488–ESATLQSGLRKAK–QXL520-NH2 (Anaspec) was used as a substrate and its cleavage by WT M^{pro} brought an increase in fluorescence intensity. This increase was monitored overtime at an excitation wavelength of 475 nm and an emission wavelength of 500-550 nm by using Glomax Discover Microplate reader (Promega). Assays were performed in assay buffer containing 20 mM HEPES pH 7.5, 150 mM NaCl, 4% glycerol, 2 mM DTT, 0.4 mM EDTA. The final assay volume was 50 µL and all the experiments were performed in duplicate by serving of a black 384-well microplate.

Both Lisinopril and Valsartan were dissolved initially at concentrations of 10 µM and 100 µM for early screening by pre-incubating with 0.25-0.5 µM of WT M^{pro} H6 (or WT M^{pro}) enzyme for 10-15 minutes at room temperature. After this time, the reaction was initiated by adding 20 µl of the substrate at a final concentration of 2 µM and monitored every 5 minutes at 30°C. The compound GC376, a known inhibitor of SARS-CoV-2 M^{pro}, was used as a control inhibitor at a concentration of 10 and 1 µM. Under these reaction conditions, this compound inhibited WT M^{pro} enzyme respectively 99% and 97%. The negative control sample contained storage

Buffer in place of WT M^{pro} and 5% DMSO whereas full enzyme activity of WT M^{pro} was assigned in presence of the enzyme (zero per cent inhibition or positive control) and 5% DMSO. Positive controls were referred to calculate the per cent inhibition at each compound concentration. Lisinopril and Valsartan were also checked if they interfered with blank subtraction.

7.2.11 MSCs conditioned medium collection

Conditioned media from MSCs [project 4] were collected as follows: 90% confluent cells were fed with α-MEM (Biowest®) with the addition of 100 U/mL penicillin and 100 mg/mL streptomycin (Gibco®) without FBS and incubated for 48 hours at 37°C. Cells were detached and counted for normalization purposes. The medium was collected and centrifuged at 300 rcf for 10 minutes to remove cell debris. Supernatant was transferred to Amicon® Ultra-15 filter tube (3 kDa Molecular Weight Cut-Off) (Millipore®) and concentrated by centrifugation at the highest speed for 45 minutes at 4°C.

7.2.12 SARS-CoV-2 Spike pseudotyped retrovirus production and infection

SARS-CoV-2 spike pseudotyped lentiviral particles used in project 4 were produced in 293T cells (Thermo Fisher Scientific™). Briefly, 293T were split in 75 cm^2 flasks at the seeding density of 4 x 10^6 cells/flask, complete DMEM (Biowest®). The day after, they were co-trasfected with 15 µg of each of the following plasmids, using the Calcium/Phosphate method: a replication-deficient retroviral vector FCQ pMM2-eGFP expressing the GFP (green fluorescent protein); a packaging vector pUMVC (8449, Addgene), and an envelope vector 2019-nCoV Spike ORF mammalian expression plasmid (VG40589-UT, Sino Biologicals), or pCMV-VSV-G (8454, Addgene) expressing the vescicular stomatitis virus glycoprotein (VSV-G) as a control. Viral supernatants (10 mL) were harvested after 48 and 72 hours

from transfection, filtered with 0.45 μm PVDF Durapore® filters (Millipore®), to remove cell debris. 1 mL of each virus was used to infect 2.5 x 10^4 cells, seeded in a 24-well plate.

7.3 Molecular Biology Techniques

7.3.1 RNA extraction from cultured cells

Total RNA was extracted from cells with PureZOL™ RNA isolation reagent (Bio-Rad). The reagent is a monophasic solution of phenol and guanidine isocyanate that facilitates immediate and effective inhibition of RNase activity, while lysing cells and eliminating other cellular components. Following the addition of chloroform and subsequent centrifugation, the homogenate separates into an aqueous phase, an interphase and an organic phase. RNA was recovered in the aqueous phase with the addition of isopropyl alcohol and was subsequently washed in ethanol and solubilized in RNase-free water.

The specific protocol:

- Aspirate spent medium from the cells and wash twice with PBS 1X.
- Add 1 mL (per well of 6-multiwell plate) of PureZOL™ RNA isolation reagent (Bio-Rad).
- Incubate the lysate at room temperature for 5 minutes once the sample has been disrupted, to allow the complete dissociation of nucleoprotein complexes.
- Gently pipette up and down to detach all cells and collect them in 1,5 mL microcentrifuge tube.
- Add 200 μL of chloroform per 1 mL of PureZOL™ (Bio-Rad) used.
- Energetically shake for 15 seconds.
- Incubate for 10 minutes at room temperature while periodically mixing the sample.
- Centrifuge at 12.000 rcf for 15 minutes at 4°C.

- After centrifugation the three phases were visible. Carefully collect the aqueous phase, without disturbing the interphase, in a new 1.5 mL microcentrifuge tube.
- Add 500 µL of isopropanol per mL of PureZOL™ (Bio-Rad) to favor RNA precipitation.
- Incubate overnight at -20°C.
- Centrifuge at 12.000 rcf for 30 minutes at 4°C.
- The RNA will appear as an opalescent pellet on the side and bottom of the tube. Carefully discard the supernatant.
- To wash the RNA pellet, add 1 mL of 75% ethanol for every 1 mL of PureZOL™ (Bio-Rad) used.
- Centrifuge at 7.500 rcf for 10 minutes at 4°C.
- Discard the supernatant.
- Air-dry the RNA pellet.
- Resuspend the pellet in 20 µL of diethyl pyrocarbonate (DEPC) water.
- To dissolve RNA, samples were vortex for 10 minutes at room temperature and then incubated at 60°C for 10 minutes.

RNA was quantified using NanoDrop® ND 1000 Spectrophotometer (Thermo Fisher Scientific™).

7.3.2 Reverse transcription of RNA to cDNA

To synthesize cDNA from total RNA the Superscript IV Reverse Transcriptase (ThermoFisher Scientific) was used, following manufacturer's instructions.

To reverse transcribe mRNAs among all RNAs, it was used oligo dT which selectively binds poly-A tail that is located at the 3'OH of most pre-mRNA, or Random Primers which hybridize to mRNA with or without poly-A tail.

The RT-PCR protocol used was based on 3 phases and the final volume of the reaction was 20 µL.

Primer annealing to template RNA

- Add in a reaction tube 1 µL of 50 µM oligo dT or 50 µM Random Primers, 1 µL of 10 mM dNTPs mix, 500 ng template RNA, and nuclease-free water to 13 µL.
- Mix and briefly centrifuge the components.
- Heat the RNA primer mix at 65°C for 5 minutes, and then incubate on ice at least 1 minutes.

RT reaction mix preparation

- Combine the following components in a reaction tube: 4 µL of 5X SuperScript® IV buffer (Thermo Fisher Scientific™), 1 µL of 100 mM dithiothreitol (DTT) important to stabilise reverse transcriptase, 1 µL recombinant RNase inhibitor OUT and 1 µL of the enzyme Superscript IV reverse transcriptase (200 U/µL).
- The two mixes were joined.

Reaction Incubation

- Incubate the combined reactions mixture at 55°C for 10 minutes.
- Inactivate the reaction by incubating at 80°C for 10 minutes.
- To remove untrascibed RNA, add 1 µL of RNase H to the sample and incubate at 37°C for 20 minutes.

Obtained cDNA can be amplified by PCR or stored at -20°C.

7.3.3 Quantitative Real-Time PCR (qRT-PCR)

For my thesis work, cDNA was amplified and quantified by Real-Time PCR, using the 7900HT Fast Real-Time PCR System (Applied Biosystem). The amplification was performed employing commercial primer pairs or primers designed by using the 'Primer3 input' software. The specificity of each primer was confirmed using the BLAST software (NCBI). In Table 7.2 are gathered primers sequences and product sizes. Commercial primers used in this thesis work are human ACE2 (HP100185,

Sino Biologicals), TMPRSS2 (HP101690, Sino Biologicals) and GPER (HP101148, Sino Biologicals). DNA polymerase, buffer, deoxynucleotide triphosphates (dNTP) mix, $MgCl_2$ and fluorochrome are contained in SYBR™ Green Master Mix (Applied Biosystem). The mix reaction recipe is indicated in the table 7.3 and the real-time stages are indicated in table 7.4.

Table 7.2 qRT-PCR primer sequences and product sizes

Target	Sequence (5' – 3')	PCR Product Length (bp)	Tm (C°)	Project
TNNT2	fw- agtgggaagaggcagactga	154	60	2 and 3
	rev- cgaacttctctgcctccaag			
GAPDH	fw- catgttccaatatgattccaccc	142	60	2, 3 and 4
	rev- gggatctcgctcctggaagat			
ESR1	fw- gccaggctttgtggatttga	204	60	2
	rev- gatgtagccagcagcatgtc			
ESR2	fw- tccctggtgtgaagcaagat	190	60	2
	rev- tccttcacacgaccagactc			
KCNH2	fw- gtgctgaagggcttccctga	146	60	2 and 3
	rev- ggtgcatgtgtggtcttgaa			

Table 7.3 Amount of qRT-PCR reagents

Components	Volume
SYBR™ Green Master Mix (2X)	12.5 µL
Primer Forward (10 µM)*	0.5 µL
Primer Revers (10 µM)*	0.5 µL
cDNA	2 µL
H_2O	9.5 µL
Final Volume	**25 µL**

*For commercial primer pairs (1 nM) a volume of 1 µL was used.

Table 7.4 Real-time Stages

Stage 1	**Stage 2**	**Stage 3**	**Stage 4**
50°C x 2 minutes	95°C x 10 minutes	95°C x 15 seconds 60°C x 1 minute	95°C x 15 seconds 60°C x 15 seconds

Obtained data were exported using the associated SDS 3.2 software (Applied Biosystem) in text format. Relative gene expression was quantified normalizing the Ct values to housekeeping gene (GAPDH or cTnT) and then compared. First, the difference between the Ct values (ΔCt) of the gene of interest and the housekeeping gene is calculated for each experimental sample. Then, the difference in the ΔCt values between the experimental and control samples ΔΔCt is calculated. The fold-change in expression of the gene of interest between the two samples is then equal to $2^{(-\Delta\Delta Ct)}$ of the gene of interest relative to internal control gene. (https://www.qiagen.com/it/service-and-support/learning-hub/molecular-biology-methods/pcr/)

7.3.4 Genomic DNA extraction from cultured cells

Genomic DNA was extracted using QIAamp® DNA Blood Mini Kit (QIAGEN®).

The protocol is:

- Detach cells, grown in a monolayer, and collect them in a microcentrifuge tube.
- Centrifuge at 200 rcf for 5 minutes and resuspend pellet in 200 µL of PBS 1X.
- Pipet 20 µL of QIAGEN® protease (QIAGEN®).
- Add 200 µL of Buffer AL (QIAGEN®) in order to ensure efficient lysis and mix them by vortexing for 15 seconds.
- Incubate at 56°C for 10 minutes.
- Briefly centrifuge the 1.5 mL microcentrifuge tube to remove drops from the

inside of the lid. Add 200 µL 96-100% ethanol to the sample and vortex for 15 seconds.

- Transfer the solution to the QIAamp® Mini Spin column (QIAGEN®) in a 2 mL collection tube without wetting the rim. Close the cap and centrifuge at 6.000 rcf for 1 minute and place QIAamp® Mini Spin column (QIAGEN®) in a clean 2 mL collection tube. Discard the tube containing the filtrate.
- Add 500 µL of Buffer AW1 (QIAGEN®) without wetting the rim. Close the cap and centrifuge at 6.000 rcf for 1 minute and place QIAamp® Mini Spin column (QIAGEN®) in a clean 2 mL collection tube. Discard the tube containing the filtrate.
- Add 500 µL of Buffer AW2 (QIAGEN®) without wetting the rim. Close the cap and centrifuge at full speed for 3 minutes.
- Place the QIAamp® Mini Spin column (QIAGEN®) in a clean 2 mL collection tube and discard the old collection tube containing the filtrate. Centrifuge at full speed for 1 minute to eliminate the chance of possible Buffer AW2 carryover.
- Place QIAamp® Mini Spin column (QIAGEN®) in a clean 1.5 mL microcentrifuge tube and elute DNA with 200 µL of Buffer AE (QIAGEN®) or distilled water. Incubate at room temperature for 5 minute and then centrifuge at 6.000 rcf for 1 minute.
- DNA was collected in microcentrifuge tube can be stored at -20°C.

7.3.5 Polymerase Chain Reaction (PCR)

DNA was amplified using Phire™ Green Hot Start II PCR Master Mix (Thermo Fisher Scientific™).

Phire™ Green Hot start II PCR Master Mix consists of all the necessary reaction components providing 1.5 $MgCl_2$, 200 µM of each dNTP in final reaction concentration and DNA polymerase. The amplification reactions were performed in

20 µL reaction mix (Table 7.5) following the PCR conditions reported in Table 7.6. In Table 7.7 are gathered primers sequences and product sizes. Primers were designed by using the 'Primer3 input' software and the specificity of each primer was confirmed using the BLAST software (NCBI).

Table 7.5 Amount of PCR reagents for genomic DNA amplification

Components	**Volume**
Phire Green Hot Start II Master Mix (2X)	10 µL
Primer Forward (10 µM)	1 µL
Primer Reverse (10 µM)	1 µL
DNA or cDNA	200-300 ng or 2 µL
H_2O	Add to 20 µL
Final Volume	**20 µL**

Table 7.6 Thermal cycler conditions to perform PCR

Cycle Step	**Temperature**	**Time**	**Number of Cycles**
Initial Denaturation	98°C	30 seconds	1
Denaturation	98°C	5 seconds	30-35
Annealing	56°C	5 seconds	
Extension	72°C	30 seconds	
Final Extension	72°C	60 seconds	1

Table 7.7 Primer sequences and product sizes

Type	Target	Sequence (5' – 3')	PCR Product Length (bp)	Project
Pluripotency marker	OCT4	fw- gtactcctcggtccctttcc	168	1 and 2
		rev- caaaaaccctggcacaaact		
	SOX2	fw- acaccaatcccatccacact	273	1 and 2
		rev- tttttcgtcgcttggagact		
	NANOG	fw- ttccttcctccatggatctg	213	1 and 2
		rev- tctgctggaggctgaggtat		
	REX1	fw- cagatcctaaacagctcgcagaat	306	1 and 2
		rev- gcgtacgcaaattaaagtccaga		
	GDF3	fw- cttatgctacgtaaaggagctggg	631	1 and 2
		rev- gtgccaacccaggtcccggaagtt		
	ESG1	fw- atatcccgccgtgggtgaaagttc	243	1 and 2
		rev- actcagccatggactggagcatcc		
	NODAL	fw- gggcaagaggcaccgtcgacatca	234	1 and 2
		rev- gggactcggtggggctggtaacgtttc		
	DPPA2	fw- ccgtccccgcaatctccttccatc	606	1 and 2
		rev- atgatgccaacatggctcccggtg		

	DPPA4	fw- ggagccgcctgccctggaaaattc rev- tttttcctgatattctattcccat	408	1 and 2
Housekeeping gene	GAPDH	fw- catgttccaatatgattccaccc rev- gggatctcgctcctggaagat	142	1 and 2
Retroviral transgenes	Oct4 cDNA on pMXs-hOCT3/4	fw - ccccagggccccattttggtacc rev - ccctttttctggagactaaataaa	339	1
	Sox2 cDNA on pMXs-hSOX-2	fw - ggcacccctggcatggctcttggctc rev - ccctttttctggagactaaataaa	496	1
	Myc cDNA on pMXs-hcMYC	fw - caacaaccgaaaatgcaccagccccag rev - ccctttttctggagactaaataaa	542	1
	Klf4 cDNA on pMXs-hKLF4	fw - acgatcgtggccccggaaaaggacc rev - ccctttttctggagactaaataaa	518	1
SeV transgenes	SeV	fw - ggatcactaggtgatatcgagc rev- accgacaagagtttaagagatatgtatc	181	1
	SeV-KOS	fw - atgcaccgctacgacgtgagcgc rev -accttgacaatcctgatgtgg	528	1
	SeV-Klf4	fw - ttcctgcatgccagaggagccc rev - aatgtatcgaaggtgctcaa	410	1

	SeV-cMyc	fw - taactgactagcaggcttgtcg	532	1
		rev - tccacatacagtcctggatgatgatg		
Target mutation analysis and sequencing	KCNQ1 exon 3	fw - gttcaaacaggttgcagggtctga	250	1
		rev - ccaggtttccagaccaggaag		
	CALM3 exon	fw- tggaccttgtgacctctgac	322	1
		rev- ctccctgcagtcactcgg		
	KCNH2 exon 7b*	fw - cgtgctgttcttgctcatgt	377	2
		rev - agcagcctcagtttcctcc		

* The exon 7 of KCNH2 is 388 bp length, so two primer pairs were designed to amplify the entire exon in overlapping PCR fragments.

7.3.6 Agarose gel electrophoresis

In this work horizontal electrophoresis was performed on 2% agarose gel prepared with agarose powder dissolved in 100 mL of TAE 1X buffer (Euroclone), the solution was heated in the micro-waves to ensure agarose melting and poured into a casting tray at room temperature to solidify. An intercalating agent of DNA, SYBR™ Safe DNA Gel Stain (Invitrogen®), was added to the gel before solidification at a 1:10000 dilution, in order to stain DNA and make it visible to UV light after the run. Once the gel is solid, DNA samples were loaded at the top of the gel and, an electrical voltage of 100 V was applied for 50-60 minutes. When the run was terminated, different DNA fragments were visualized under ultraviolet rays. DNA fragment size was determined by comparison to commercially available DNA weight molecular markers of known length (ladder).

7.3.7 Mycoplasma test

For the detection of mycoplasma in cell culture the EZ-PCR Mycoplasma Test Kit (Biological Industries) was used.

The protocol is:

- Transfer 1 mL cell culture supernatant into a 1.5 mL centrifuge tube.
- Centrifuge at 15000-20000 rcf for 10 minutes to sediment mycoplasma.
- Discard the supernatant and resuspend the pellet with 50 µL of the Buffer Solution supplied by the kit.
- Heat to 95°C for 3 minutes.
- Prepare the reaction mixture in a PCR tube by combining the reagents as reported in table 7.8 for each sample and the negative control.

Table 7.8 Amount of Mycoplasma PCR reagents for samples and negative control

Components	**Volume**
Nuclease Free Water	29 µL
Reaction Mix	10 µL
Test sample/water (for negative control)	5 µL
Internal control DNA template	1 µL
Internal control primer mix	5 µL
Final Volume	**50 µL**

- Prepare the reaction mixture in a PCR tube by combining the reagents as reported in table 7.9 for positive control.

Table 7.9 Amount of Mycoplasma PCR reagents for positive control

Components	**Volume**
Nuclease Free Water	33 µL
Reaction Mix	10 µL
Positive control DNA	1 µL
Internal control DNA template	1 µL
Internal control primer mix	5 µL
Final Volume	**50 µL**

- Place all tubes in a thermal cycler setting the parameters reported in table 7.10.

Table 7.10 Thermal cycler conditions to perform Mycoplasma PCR

Cycle Step	Temperature	Time	Number of Cycles
Initial Denaturation	94°C	30 seconds	1
Denaturation	94°C	30 seconds	35
Annealing	60°C	2 minutes	
Extension	72°C	60 seconds	
Final Extension	72°C	5 minutes	1

- Carefully load 20 µL of the PCR product into 2% agarose gel for electrophoresis.

The size of DNA fragment amplified using the mycoplasma specific primers in the kit is 270 bp, while the size of the PCR product obtained using the internal control template is 375 bp.

7.3.8 DNA purification and sample preparation for sequencing

Wizard® SV Gel and PCR Clean-Up System (Promega) was used to purify PCR products.

- The DNA bands are excised from gel using a cutter and placed in 1.5 mL microcentrifuge tube with the addition of 10 µL of Membrane Binding Solution (Promega) per 10 mg of gel slice.
- Vortex the sample and incubate at 60°C until gel slice is completely dissolved.
- Prepare a SV Mini Column (Promega) into a collection tube, then transfer the dissolved gel mixture to the SV Mini Column (Promega) and incubate for 1 minutes at room temperature to allow the binding of DNA to the membrane of the column.
- Centrifuge at 16.000 rcf for 1 minute, discard flow-through and reinsert SV Mini Column (Promega) into collection tube.
- Add 700 µL of Membrane Wash Solution (ethanol added, Promega). Centrifuge at 16.000 rcf for 1 minute, discard flow-through and reinsert SV Mini Column (Promega) into collection tube.
- Add 500 µL of Membrane Wash Solution (Promega) to the SV Mini Column

(Promega) and centrifuge at 16.000 rcf for 5 minutes.

- Empty the collection tube and re-centrifuge the SV Mini Column (Promega) for 1 minute with the microcentrifuge lid open (or off) to allow evaporation of any residual ethanol.
- Carefully transfer the SV Mini Column (Promega) to a clean 1.5 mL microcentrifuge tube.
- Add 50 µL of nuclease free water (NFW) to elute DNA.
- Incubate at room temperature for 1 minute and centrifuge at 16.000 rcf for 1 minute.
- The flow-through is the DNA of interest.

7.5 µL of the purified amplicon was collected in a 1.5 mL minicentrifuge tube with 2.5 µL of primer forward or reverse. For each sample 2 tubes were prepared, one with the forward primer and one with the reverse. Samples were sent to Lightrun service, GATC Biotech AG in Germany for sequencing. The analysis was carried out using a 96-capillary 3730XL and 3130XL Analyzer systems, in accordance with Sanger's method. The sequencing reaction used the BigDye™ Terminator v3.1 Cycle Sequencing Kit (Thermo Fisher Scientific™) with standard dideoxy sequencing.

7.3.9 Protein extraction and quantification

Proteins were extracted from cell culture in order to evaluate the expression of proteins listed in table 7.10.

The steps of the protocol are:

- Wash cells twice with PBS 1X.
- Lysate cells with RIPA buffer (Sigma Aldrich) supplemented with a Protease Inhibitor Cocktail (Thermo Fisher Scientific™) for 5 minutes at room temperature.
- By means of a scraper, collect cell lysate and transfer it in 1.5 mL microcentrifuge tube.
- Incubate cell lysate for 30 minutes at 4°C with agitation.

- Centrifuge at 9.000 rcf for 30 minutes at 4°C.
- Collect the supernatant and store at -30°C or quantify it.

Proteins concentration was measured by bicinchoninic acid method (BCA, Sigma-Aldrich®), which consists of Protein Reagent Assay A and Protein Reagent Assay B that were mixed with a ratio of 50:1. The mixture, with a characteristic green color, is added to protein sample and incubated at 60°C for 30 minutes. At the end of incubation period, absorbance at 562 nm was measured with a spectrophotometer. The absorbance value of the samples is compared to absorbance value of proteins standard and concentration was extrapolated through a titration curve.

7.3.10 SDS-PolyAcrylamide Gel Electrophoresis (SDS-PAGE) and Western Blot (WB)

To perform SDS-PAGE, Mini-PROTEAN® TGX™ Precast gel was used (Bio-Rad) following this protocol:

- Combine in a tube 20 - 40 µg protein sample, 2.5 µL DTT 2M, 12.5 µL Laemmli Sample Buffer 4X (Bio-Rad), and nuclease-free water to a final volume of 50 µL.
- Heat sample at 95°C for 5 minutes.
- Insert the 7.5% or 12% Mini-PROTEAN® TGX™ Precast Protein Gel (Bio-Rad) in the cassette, remove the comb and the tape at the bottom.
- Put the cassette inside the Mini-PROTEAN® Tetra system (Bio-Rad) and add Tris Glicine-SDS running buffer to inner and outer chambers and load the samples into the wells. Precision Plus Protein™ Kaleidoscope™ Prestained (Bio-Rad) was used as protein standard.
- Run the gel at 200 V, until the dye front reaches the reference line.
- Open the cassette and gently remove the gel.
- Open a Trans-Blot Turbo Mini (or Mini) Nitrocellulose Transfer Pack (Bio-Rad) and place the pad with the membrane on the base of the transfer cassette.

- Place the gel on top of the membrane, place the top pad on the gel, and roll out bubbles.
- Insert the cassette into either instrument bay.
- When the transfer is over, disassemble the blotting sandwich and place the blot in a container with PBS 1X, and then keep in agitation for 10 minutes at room temperature.
- For immunoblotting, block the membrane by adding OBB (Li-COR®), diluted 1:1 with PBS 1X, for 1 hour with agitation (50 rpm) at room temperature.
- Dilute primary antibody in OBB (Li-COR®) diluted 1:1 with PBS 1X supplemented with 0.2% Tween®20. Dilutions of primary antibodies used in this thesis work are indicated in table 7.8.
- Incubate for 1 hours with agitation (50 rpm) at room temperature. For greatest sensitivity continue incubation overnight at 4°C.
- Wash five times with PBST for 5 minutes with agitation.
- Dilute IRDye 680 or IRDye 800-conjugated secondary antibodies (Li-COR®) 1:10.000 in OBB (Li-COR®) 1:1 with PBS 1X and 0.2% Tween®20. Incubate for 1 hour with gentle shaking at room temperature, protecting membrane from light during incubation.
- Wash five times with PBST for 5 minutes with agitation.
- Maintain the membrane in PBS 1X.
- Scan the membrane with detection in 700 nm and/or 800 nm channels, for IRDye 680 or IRDye 800 secondary (Li-COR®) antibodies respectively, using the Odyssey® Infrared Imaging System (Li-COR®).

Table 7.10 Antibodies dilution for WB

Type	Antibody	Specie	Dilution	Project
Differentiation markers (CMs)	anti-cTnT	Rabbit	1:1000	2 and 3
Hormone receptors	anti-GPER	Rabbit	1:1000	2
SARS-CoV-2 target	anti-ACE2	Rabbit	1:1000	3 and 4
	anti-TMPRSS2	Rabbit	1:1000	4

Loading Control	anti-Tubulin	Mouse	1:1000	3
	anti-Actin	Mouse	1:400	4
ICW secondary antibodies	IRDye® 800 anti-rabbit	Goat	1:10000	2, 3 and 4
	IRDye® 680 anti-mouse	Goat	1:10000	2, 3 and 4

7.3.11 Enzyme-Linked Immunosorbent Assay (ELISA)

ACE2 levels in conditioned media generated by 1 x 10^5 MSCs [project 4] were quantified using the RayBio® Human ACE-2 ELISA kit (ELH-ACE2, RayBiotech).

The standard curve is prepared by making serial dilutions of one known concentration of ACE2 Standard. The concentration of unknown samples is determined by interpolation that relies on a properly generated standard curve.

The protocol is:

- Add 100 µL of each standard and sample into appropriate wells.
- Cover wells and incubate for 2.5 hours at room temperature with gentle shaking.
- Discard the solution and wash 4 times with 300 µL/well of 1X Wash Solution (RayBiotech), previously diluted in deionized water.
- Prepare 1X biotinylated antibody. Add 100 µL of 1X Assay Diluent (RayBiotech) into the vial to prepare a detection antibody concentrate. The detection antibody concentrate should be diluted 80-fold with 1X Assay Diluent (RayBiotech).
- Add 100 µL/well of 1X biotinylated antibody. Incubate for 1 hour at room temperature with gentle shaking.
- Discard the solution. Repeat 4 times the wash with Wash Solution (RayBiotech).
- Prepare Streptavidin solution. Dilute HRP-Streptavidin solution (RayBiotech) 150-fold with 1X Assay Diluent (RayBiotech).

- Add 100 µL of Streptavidin solution to each well. Incubate 45minutes at room temperature with gentle shaking.
- Discard the solution. Repeat 4 times the wash with Wash Solution (RayBiotech).
- Add 100 µL of TMB One-Step Substrate Reagent (RayBiotech) to each well.
- Incubate for 30 minutes at room temperature in the dark with gentle shaking.
- Add 50 µL Stop Solution (RayBiotech). Read at 450 nm immediately with Infinite® 200 Pro (Tecan).

7.4 Electrophysiology

These experiments were carried out at the Department of Biotechnology and Bioscience of the University of Milano-Bicocca.

The baseline solution for all patch-clamp recordings was standard Tyrode's solution containing (nM): 154 NaCl, 4 KCl, 2 $CaCl_2$, 1$MgCl_2$, 5 HEPES-NaOH, 5.5 D-glucose, adjusted to pH 7.35 with NaOH. Membrane capacitance and series resistance were measured and automatically compensated in every cell. Signal were acquired with a MultiClamp™ 700B Microelectrode Amplifier (Axon Instrument®), connected to a Digidata® 1440A (Axon Instrument®) and filtered with an appropriate Bessel filter via pClamp™ 10 (Molecular Devices). All measurements were performed at 36.5°C.

7.4.1 I-Clamp and dynamic clamp recordings

Membrane potential was recorded during steady-state pacing at a cycle length of 1 Hz. "Synthetic" I_{K1} was injected by the dynamic clamp (DC) technique to correct for low endogenous I_{K1} expression of hiPSC-CMs. I_{K1} conductance required to achieve a diastolic potential (Ediast) around -80 mV was 1.9 nS/µF (kept constant in all cells); this abolished automatic activity and resulted in physiological AP contours. hiPSC-CMs with ventricular-like APs were selected based on an ADP90/ADP50 ration lower than 2 (under DC condition). The following parameters were considered: AP duration 90% repolarization

(ADP90, measured beat by beat an automated routine); incidence and time of occurrence of afterdepolarizations (EADs and DADs), defined as transient membrane depolarizations > 0.5 mV occurring before and after AP repolarization respectively. “Triggered activity” was defined as APs arising from afterdepolarization; it was distinguished from “automaticity” because of the absence of a proper diastolic depolarization phase. Only cells in which DC successfully polarized diastolic potential were used. Synthetic I_{K1} was generated by a human numerical current model derived from Rudy-O’Hara one and injected in the cell using the Real-Time eXperiment Interface (RTXI). I_{K1} conductance was the same in all cells.

hiPSC-CMs in project 2 were subjected to 10 nM E2 exposure and difference in AP was recorded.

References

1. Takahashi, K. & Yamanaka, S. Induction of Pluripotent Stem Cells from Mouse Embryonic and Adult Fibroblast Cultures by Defined Factors. *Cell* **126**, 663–676 (2006).

2. Wang, Z., Zheng, J., Pan, R. & Chen, Y. Current status and future prospects of patient-derived induced pluripotent stem cells. *Hum Cell* **34**, 1601–1616 (2021).

3. Kanherkar, R. R., Bhatia-Dey, N., Makarev, E. & Csoka, A. B. Cellular reprogramming for understanding and treating human disease. *Front Cell Dev Biol* **2**, (2014).

4. Gurdon, J. B. The developmental capacity of nuclei taken from intestinal epithelium cells of feeding tadpoles. *J Embryol Exp Morphol* **10**, 622–640 (1962).

5. Yu, J. *et al.* Induced Pluripotent Stem Cell Lines Derived from Human Somatic Cells. *Science* **318**, 1917–1920 (2007).

6. Yu, J. *et al.* Induced pluripotent stem cell lines derived from human somatic cells. *Science (1979)* (2007) doi:10.1126/science.1151526.

7. Zhang, J., Chou, O. H.-I., Tse, Y.-L., Ng, K.-M. & Tse, H.-F. Application of Patient-Specific iPSCs for Modelling and Treatment of X-Linked Cardiomyopathies. *Int J Mol Sci* **22**, 8132 (2021).

8. Maherali, N. & Hochedlinger, K. Guidelines and Techniques for the Generation of Induced Pluripotent Stem Cells. *Cell Stem Cell* **3**, 595–605 (2008).

9. Hockemeyer, D. & Jaenisch, R. Induced pluripotent stem cells meet genome editing. *Cell Stem Cell* **18**, 573–586 (2016).

10. Gähwiler, E. K. N. *et al.* Human iPSCs and Genome Editing Technologies for Precision Cardiovascular Tissue Engineering. *Front Cell Dev Biol* **9**, 1–21 (2021).

11. Guha, P., Morgan, J. W., Mostoslavsky, G., Rodrigues, N. P. & Boyd, A. S. Lack of immune response to differentiated cells derived from syngeneic induced pluripotent stem cells. *Cell Stem Cell* **12**, 407–412 (2013).

12. McKernan, R. & Watt, F. M. What is the point of large-scale collections of human induced pluripotent stem cells? *Nat Biotechnol* **31**, 875–877 (2013).

13. Ntai, A. *et al.* A review of research-grade human induced pluripotent stem cells qualification and biobanking processes. *Biopreserv Biobank* **15**, 384–392 (2017).

14. Morrison, M. *et al.* The European General Data Protection Regulation: Challenges and considerations for iPSC researchers and biobanks. *Regenerative Med* **12**, 693–703 (2017).

15. Fishman, M. C. & Chien, K. R. Fashioning the vertebrate heart: Earliest embryonic decisions. *Development* **124**, 2099–2117 (1997).

16. Kehat, I. *et al.* Human embryonic stem cells can differentiate into myocytes with structural and functional properties of cardiomyocytes. *Journal of Clinical Investigation* **108**, 407–414 (2001).

17. James, E. C., Tomaskovic-Crook, E. & Crook, J. M. Bioengineering clinically relevant cardiomyocytes and cardiac tissues from pluripotent stem cells. *Int J Mol Sci* **22**, 1–34 (2021).

18. Zhao, M. T., Shao, N. Y. & Garg, V. Subtype-specific cardiomyocytes for precision medicine: Where are we now? *Stem Cells* **38**, 822–833 (2020).

19. Schweizer, P. A. *et al.* Subtype-specific differentiation of cardiac pacemaker cell clusters from human induced pluripotent stem cells. *Stem Cell Res Ther* **8**, 229 (2017).

20. Gharanei, M. *et al.* Atrial-specific hiPSC-derived cardiomyocytes in drug discovery and disease modeling. *Methods* **203**, 364–377 (2021).

21. Sharma, A. *et al.* Derivation of highly purified cardiomyocytes from human induced pluripotent stem cells using small molecule-modulated differentiation and subsequent glucose starvation. *Journal of Visualized Experiments* **2015**, 3–10 (2015).

22. Zhang, J. *et al.* Functional cardiomyocytes derived from human induced pluripotent stem cells. *Circ Res* **104**, 30–41 (2009).

23. Verkerk, A. O. *et al.* Patch-Clamp Recording from Human Induced Pluripotent Stem Cell-Derived Cardiomyocytes: Improving Action Potential Characteristics through Dynamic Clamp. *Int J Mol Sci* **18**, 1873 (2017).

24. Veerman, C. C. *et al.* Immaturity of Human Stem-Cell-Derived Cardiomyocytes in Culture: Fatal Flaw or Soluble Problem? *Stem Cells Dev* **24**, 1035–1052 (2015).

25. Wilders, R. Dynamic clamp: A powerful tool in cardiac electrophysiology. *Journal of Physiology* **576**, 349–359 (2006).

26. Spira, M. E. & Hai, A. Multi-electrode array technologies for neuroscience and cardiology. *Nat Nanotechnol* **8**, 83–94 (2013).

27. Mahmoodzadeh, S. & Dworatzek, E. The role of 17β-estradiol and estrogen receptors in regulation of Ca2+ channels and mitochondrial function in Cardio myocytes. *Front Endocrinol (Lausanne)* **10**, 1–15 (2019).

28. Lin, B. *et al.* Modeling and study of the mechanism of dilated cardiomyopathy using induced pluripotent stem cells derived from

individuals with duchenne muscular dystrophy. *DMM Disease Models and Mechanisms* **8**, 457–466 (2015).

29. Pan, Z., Ebert, A. & Liang, P. Human-induced pluripotent stem cells as models for rare cardiovascular diseases: from evidence-based medicine to precision medicine. *Pflugers Arch* **473**, 1151–1165 (2021).

30. Abriel, H., Rougier, J. S. & Jalife, J. Ion Channel Macromolecular Complexes in Cardiomyocytes: Roles in Sudden Cardiac Death. *Circ Res* **116**, 1971–1988 (2015).

31. Sharma, A. *et al.* Human iPSC-Derived Cardiomyocytes Are Susceptible to SARS-CoV-2 Infection. *Cell Rep Med* **1**, 100052 (2020).

32. Bermejo, J. A. P. *et al.* SARS-CoV-2 infection of human iPSC derived cardiac cells reflects cytopathic features in hearts of patients with COVID-19. *Sci Transl Med* **13**, 1–15 (2021).

33. Bojkova, D. *et al.* SARS-CoV-2 infects and induces cytotoxic effects in human cardiomyocytes. *Cardiovasc Res* **116**, 2207–2215 (2020).

34. Fermini, B. & Fossa, A. A. The impact of drug-induced QT interval prolongation on drug discovery and development. *Nat Rev Drug Discov* **2**, 439–447 (2003).

35. James, A. F., Choisy, S. C. M. & Hancox, J. C. Recent advances in understanding sex differences in cardiac repolarization. *Prog Biophys Mol Biol* **94**, 265–319 (2007).

36. Vink, A. S., Clur, S. A. B., Wilde, A. A. M. & Blom, N. A. Effect of age and gender on the QTc-interval in healthy individuals and patients with long-QT syndrome. *Trends Cardiovasc Med* **28**, 64–75 (2018).

37. Schwartz, P. J., Woosley, R. L. & Woosley, R. L. Predicting the Unpredictable: Drug-Induced QT Prolongation and Torsades de Pointes. *J Am Coll Cardiol* **67**, 1639–1650 (2016).

38. Roden, D. M. Predicting drug-induced QT prolongation and torsades de pointes. *Journal of Physiology* **594**, 2459–2468 (2016).

39. Waddell-Smith, K. E., Skinner, J. R. & Bos, J. M. Pre-Test Probability and Genes and Variants of Uncertain Significance in Familial Long QT Syndrome. *Heart Lung Circ* **29**, 512–519 (2020).

40. Schwartz, P. J., Crotti, L. & Insolia, R. Long-QT Syndrome. *Circ Arrhythm Electrophysiol* **5**, 868–877 (2012).

41. Giudicessi, J. R. & Ackerman, M. J. Genotype- and Phenotype-Guided Management of Congenital Long QT Syndrome. *Curr Probl Cardiol* **38**, 417–455 (2013).

42. Sanguinetti, M. C. & Tristani-Firouzi, M. hERG potassium channels and cardiac arrhythmia. *Nature* **440**, 463–469 (2006).

43. Smith, J. L. *et al.* Molecular pathogenesis of long QT syndrome type 2. *J Arrhythm* **32**, 373–380 (2016).

44. Bauer, C. K. & Schwarz, J. R. Ether-à-go-go K + channels: effective modulators of neuronal excitability. *Journal of Physiology* **596**, 769–783 (2018).

45. Warmke, J. W. & Ganetzky, B. A family of potassium channel genes related to eag in Drosophila and mammals. *Proc Natl Acad Sci U S A* **91**, 3438–3442 (1994).

46. Farrelly, A. M. *et al.* Expression and function of KCNH2 (HERG) in the human jejunum. *Am J Physiol Gastrointest Liver Physiol* **284**, 883–895 (2003).

47. Bianchi, L. *et al.* herg encodes a K+ current highly conserved in tumors of different histogenesis: A selective advantage for cancer cells? *Cancer Res* **58**, 815–822 (1998).

48. Regitz-Zagrosek, V. & Kararigas, G. Mechanistic Pathways of Sex Differences in Cardiovascular Disease. *Physiol Rev* **97**, 1–37 (2017).

49. Salama, G. & Bett, G. C. L. Sex differences in the mechanisms underlying long QT syndrome. *Am J Physiol Heart Circ Physiol* **307**, 640–648 (2014).

50. Migdalovich, D. *et al.* Mutation and gender-specific risk in type 2 long QT syndrome: Implications for risk stratification for life-threatening cardiac events in patients with long QT syndrome. *Heart Rhythm* **8**, 1537–1543 (2011).

51. Zareba, W. *et al.* Modulating effects of age and gender on the clinical course of long QT syndrome by genotype. *J Am Coll Cardiol* **42**, 103–109 (2003).

52. Escobar-Morreale, H. F. Polycystic ovary syndrome: Definition, aetiology, diagnosis and treatment. *Nat Rev Endocrinol* **14**, 270–284 (2018).

53. Azziz, R. *et al.* Polycystic ovary syndrome. *Nat Rev Dis Primers* **2**, 16057 (2016).

54. Carmina, E. & Lobo, R. A. Polycystic Ovary Syndrome (PCOS): Arguably the most common endocrinopathy is associated with significant morbidity in women. *Journal of Clinical Endocrinology and Metabolism* **84**, 1897–1899 (1999).

55. Azziz, R. *et al.* The prevalence and features of the polycystic ovary syndrome in an unselected population. *Journal of Clinical Endocrinology and Metabolism* **89**, 2745–2749 (2004).

56. Zore, T., Joshi, N., Lizneva, D. & Azziz, R. Polycystic Ovarian Syndrome: Long-Term Health Consequences. *Semin Reprod Med* **35**, 271–281 (2017).

57. Lizneva, D. *et al.* Criteria, prevalence, and phenotypes of polycystic ovary syndrome. *Fertil Steril* **106**, 6–15 (2016).

58. Dapas, M. *et al.* Family-Based Quantitative Trait Meta-Analysis Implicates Rare Noncoding Variants in DENND1A in Polycystic Ovary Syndrome. *J Clin Endocrinol Metab* **104**, 3835–3850 (2019).

59. Goodarzi, M. O., Dumesic, D. A., Chazenbalk, G. & Azziz, R. Polycystic ovary syndrome: etiology, pathogenesis and diagnosis. *Nat Rev Endocrinol* **7**, 219–231 (2011).

60. Grange, J. M., Gandy, M., Farmer, P. & Zumla, A. Historical declines in tuberculosis: nature, nurture and the biosocial model. *Int J Tuberc Lung Dis* **5**, 208–12 (2001).

61. Fauser, B. C. J. M. Revised 2003 consensus on diagnostic criteria and long-term health risks related to polycystic ovary syndrome. *Fertil Steril* **81**, 19–25 (2004).

62. Fauser, B. C. J. M. *et al.* Revised 2003 consensus on diagnostic criteria and long-term health risks related to polycystic ovary syndrome. *Human Reproduction* **19**, 41–47 (2004).

63. Azziz, R. *et al.* Position statement: Criteria for defining polycystic ovary syndrome as a predominantly hyperandrogenic syndrome: An androgen excess society guideline. *Journal of Clinical Endocrinology and Metabolism* **91**, 4237–4245 (2006).

64. Azziz, R. *et al.* The Androgen Excess and PCOS Society criteria for the polycystic ovary syndrome: the complete task force report. *Fertil Steril* **91**, 456–488 (2009).

65. Stepto, N. K. *et al.* Women with polycystic ovary syndrome have intrinsic insulin resistance on euglycaemic-hyperinsulaemic clamp. *Human Reproduction* **28**, 777–784 (2013).

66. de Groot, P. C. M., Dekkers, O. M., Romijn, J. A., Dieben, S. W. M. & Helmerhorst, F. M. PCOS, coronary heart disease, stroke and the influence of obesity: A systematic review and meta-analysis. *Hum Reprod Update* **17**, 495–500 (2011).

67. El-Battrawy, I. *et al.* Estradiol protection against toxic effects of catecholamine on electrical properties in human-induced pluripotent stem cell derived cardiomyocytes. *Int J Cardiol* **254**, 195–202 (2018).

68. Glintborg, D., Rubin, K. H., Nybo, M., Abrahamsen, B. & Andersen, M. Cardiovascular disease in a nationwide population of Danish women with polycystic ovary syndrome. *Cardiovasc Diabetol* **17**, 1–12 (2018).

69. Alpaslan, M., Onrat, E., Yilmazer, M. & Fenkci, V. QT dispersion in patients with polycystic ovary syndrome. *Jpn Heart J* **43**, 487–493 (2002).

70. Gazi, E. *et al.* Relationship between QT dispersion with sex hormones and insulin in young women with polycystic ovary syndrome: an observational study. *Anadolu Kardiyoloji Dergisi/The Anatolian Journal of Cardiology* **13**, 772–777 (2013).

71. Meden-Vrtovec, H., Vrtovec, B. & Osredkar, J. Metabolic and cardiovascular changes in women with polycystic ovary syndrome. *International Journal of Gynecology & Obstetrics* **99**, 87–90 (2007).

72. Morselli, E. *et al.* The effects of oestrogens and their receptors on cardiometabolic health. *Nat Rev Endocrinol* **13**, 352–364 (2017).

73. Nilsson, S. *et al.* Mechanisms of estrogen action. *Physiol Rev* **81**, 1535–1565 (2001).

74. Grohé, C. *et al.* Cardiac myocytes and fibroblasts contain functional estrogen receptors. *FEBS Lett* **416**, 107–112 (1997).

75. Bell, J. R. *et al.* Aromatase deficiency confers paradoxical postischemic cardioprotection. *Endocrinology* **152**, 4937–4947 (2011).

76. Jazbutyte, V. *et al.* Aromatase inhibition attenuates desflurane-induced preconditioning against acute myocardial infarction in male mouse heart in vivo. *PLoS One* **7**, 1–9 (2012).

77. Iorga, A. *et al.* Rescue of pressure overload-induced heart failure by estrogen therapy. *J Am Heart Assoc* **5**, 1–12 (2016).

78. Huang, C. K., Lee, S. O., Chang, E., Pang, H. & Chang, C. Androgen receptor (AR) in cardiovascular diseases. *Journal of Endocrinology* **229**, R1–R16 (2016).

79. Burris, T. P. *et al.* Nuclear Receptors and Their Selective Pharmacologic Modulators. *Pharmacol Rev* **65**, 710–778 (2013).

80. Prossnitz, E. R. & Arterburn, J. B. International union of basic and clinical pharmacology. XCVII. G protein–coupled estrogen receptor and its pharmacologic modulators. *Pharmacol Rev* **67**, 505–540 (2015).

81. Prossnitz, E. R. & Arterburn, J. B. International union of basic and clinical pharmacology. XCVII. G protein–coupled estrogen receptor and its pharmacologic modulators. *Pharmacol Rev* **67**, 505–540 (2015).

82. Thomas, P., Pang, Y., Filardo, E. J. & Dong, J. Identity of an estrogen membrane receptor coupled to a G protein in human breast cancer cells. *Endocrinology* **146**, 624–632 (2005).

83. Revankar, C. M., Cimino, D. F., Sklar, L. A., Arterburn, J. B. & Prossnitz, E. R. A Transmembrane Intracellular Estrogen Receptor Mediates Rapid Cell Signaling. *Science (1979)* **307**, 1625–1630 (2005).

84. Haas, E. *et al.* NIH Public Access. **104**, 288–291 (2010).

85. Yu, X. *et al.* Activation of G protein-coupled estrogen receptor induces endotheliumindependent relaxation of coronary artery smooth muscle. *Am J Physiol Endocrinol Metab* **301**, 882–888 (2011).

86. Dong, W. H., Chen, J. C., He, Y. L., Xu, J. J. & Mei, Y. A. Resveratrol inhibits Kv2.2 currents through the estrogen receptor GPR30-mediated PKC pathway. *Am J Physiol Cell Physiol* **305**, 547–557 (2013).

87. Patel Vanlata H. *et al.* G-protein coupled estrogen receptor 1 expression in rat and human heart: Protective role during ischaemic stress. *Int J Mol Med* **26**, 193–199 (2010).

88. Groban, L. *et al.* Female Heart Health: Is GPER the Missing Link? *Front Endocrinol (Lausanne)* **10**, 1–16 (2020).

89. Jessup, J. A. *et al.* Estrogen therapy, independent of timing, improves cardiac structure and function in oophorectomized mRen2.Lewis rats. *Menopause* **20**, 860–868 (2013).

90. Pedram, A. *et al.* ERβ selective agonist inhibits angiotensin-induced cardiovascular pathology in female mice. *Endocrinology* **154**, 4352–4364 (2013).

91. Skavdahl, M. *et al.* Estrogen receptor-β mediates male-female differences in the development of pressure overload hypertrophy. *Am J Physiol Heart Circ Physiol* **288**, 469–476 (2005).

92. Arias-Loza, P. A. *et al.* Both estrogen receptor subtypes, α and β, attenuate cardiovascular remodeling in aldosterone salt-treated rats. *Hypertension* **50**, 432–438 (2007).

93. Babiker, F. A. *et al.* Estrogen receptor β protects the murine heart against left ventricular hypertrophy. *Arterioscler Thromb Vasc Biol* **26**, 1524–1530 (2006).

94. Luo, T., Liu, H. & Kim, J. K. Estrogen protects the female heart from ischemia/reperfusion injury through manganese superoxide dismutase phosphorylation by mitochondrial p38β at threonine 79 and serine 106. *PLoS One* **11**, 1–20 (2016).

95. Machuki, J. O., Zhang, H. Y., Harding, S. E. & Sun, H. Molecular pathways of oestrogen receptors and β-adrenergic receptors in cardiac cells: Recognition of their similarities, interactions and therapeutic value. *Acta Physiologica* **222**, 1–19 (2018).

96. Broselid, S. *et al.* G protein-coupled receptor 30 (GPR30) forms a plasma membrane complex with membrane-associated guanylate kinases (MAGUKs) and protein kinase a-anchoring protein 5 (AKAP5) that constitutively inhibits cAMP production. *Journal of Biological Chemistry* **289**, 22117–22127 (2014).

97. Guo, X., Razandi, M., Pedram, A., Kassab, G. & Levin, E. R. Estrogen induces vascular wall dilation: Mediation through kinase signaling to nitric oxide and estrogen receptors α and β. *Journal of Biological Chemistry* **280**, 19704–19710 (2005).

98. Pedram, A., Razandi, M. & Levin, E. R. Nature of functional estrogen receptors at the plasma membrane. *Molecular Endocrinology* **20**, 1996–2009 (2006).

99. Lizotte, E., Grandy, S. A., Tremblay, A., Allen, B. G. & Fiset, C. Cellular Physiology Biochemistry and Biochemistr y Expression , Distribution and Regulation of Sex Steroid Hormone Receptors in Mouse Heart. *Cellular Physiology and Biochemistry* **8**, 75–86 (2009).

100. Chambliss, K. L. *et al.* Estrogen receptor alpha and endothelial nitric oxide synthase are organized into a functional signaling module in caveolae. *Circ Res* **87**, 1–9 (2000).

101. Li, L., Haynes, M. P. & Bender, J. R. Plasma membrane localization and function of the estrogen receptor α variant (ER46) in human endothelial cells. *Proc Natl Acad Sci U S A* **100**, 4807–4812 (2003).

102. Chambliss, K. L., Yuhanna, I. S., Anderson, R. G. W., Mendelsohn, M. E. & Shaul, P. W. Erβ has nongenomic action in caveolae. *Molecular Endocrinology* **16**, 938–946 (2002).

103. Ding, Q., Gros, R., Limbird, L. E., Chorazyczewski, J. & Feldman, R. D. Estradiol-mediated ERK phosphorylation and apoptosis in vascular smooth muscle cells requires GPR 30. *Am J Physiol Cell Physiol* **297**, 1178–1187 (2009).

104. Simoncini, T., Rabkin, E. & Liao, J. K. Molecular basis of cell membrane estrogen receptor interaction with phosphatidylinositol 3-kinase in endothelial cells. *Arterioscler Thromb Vasc Biol* **23**, 198–203 (2003).

105. Chen, Z. *et al.* Estrogen receptor mediates the nongenomic activation of endothelial nitric oxide synthase by estrogen. *Journal of Clinical Investigation* **103**, 401–406 (1999).

106. Liu, M. M. *et al.* Opposing action of estrogen receptors α and β on cyclin D1 gene expression. *Journal of Biological Chemistry* **277**, 24353–24360 (2002).

107. Gao, X., Liang, Q., Chen, Y. & Wang, H. S. Molecular mechanisms underlying the rapid arrhythmogenic action of bisphenol A in female rat hearts. *Endocrinology* **154**, 4607–4617 (2013).

108. Wang, C., Liu, Y. & Cao, J. M. G protein-coupled receptors: Extranuclear mediators for the non-genomic actions of steroids. *Int J Mol Sci* **15**, 15412–15425 (2014).

109. Holm, A. *et al.* The G protein-coupled estrogen receptor 1 (GPER1/GPR30) agonist G-1 regulates vascular smooth muscle cell Ca handling. *J Vasc Res* **50**, 421–429 (2013).

110. Kabir, M. E. *et al.* G protein-coupled estrogen receptor 1 mediates acute estrogen-induced cardioprotection via MEK/ERK/GSK-3β Pathway after Ischemia/Reperfusion. *PLoS One* **10**, 1–23 (2015).

111. Hill, B. J. F. & Muldrew, E. Oestrogen upregulates the sarcoplasmic reticulum Ca2+ ATPase pump in coronary arteries. *Clin Exp Pharmacol Physiol* **41**, 430–436 (2014).

112. Grohé, C. *et al.* Cardiac myocytes and fibroblasts contain functional estrogen receptors. *FEBS Lett* **416**, 107–112 (1997).

113. Pugach, E. K., Blenck, C. L., Dragavon, J. M., Langer, S. J. & Leinwand, L. A. Estrogen receptor profiling and activity in cardiac myocytes. *Mol Cell Endocrinol* **431**, 62–70 (2016).

114. Ren, J. & Kelley, R. O. Cardiac health in women with metabolic syndrome: Clinical aspects and pathophysiology. *Obesity* **17**, 1114–1123 (2009).

115. Yang, X. P. & Reckelhoff, J. F. Estrogen, hormonal replacement therapy and cardiovascular disease. *Curr Opin Nephrol Hypertens* **20**, 133–138 (2011).

116. Mosca, L. *et al.* Effectiveness-based guidelines for the prevention of cardiovascular disease in women-2011 update: A Guideline from the American Heart Association. *Circulation* **123**, 1243–1262 (2011).

117. Li, S. & Gupte, A. A. The role of estrogen in cardiac metabolism and diastolic function. *Methodist Debakey Cardiovasc J* **13**, 4–8 (2017).

118. Benatar, A. & Feenstra, A. QT correction methods in infants and children: Effects of age and gender. *Annals of Noninvasive Electrocardiology* **20**, 119–125 (2015).

119. Vicente, J., Johannesen, L., Galeotti, L. & Strauss, D. G. Mechanisms of sex and age differences in ventricular repolarization in humans. *Am Heart J* **168**, 749-756.e3 (2014).

120. Lehmann, M. H. *et al.* Age-gender influence on the rate-corrected QT interval and the QT-heart rate relation in families with genotypically characterized long QT syndrome. *J Am Coll Cardiol* **29**, 93–99 (1997).

121. Ozawa, J. *et al.* Pediatric cohort with long QT syndrome – KCNH2 mutation carriers present late onset but severe symptoms. *Circulation Journal* **80**, 696–702 (2016).

122. Vink, A. S. *et al.* Effect of Age and Sex on the QTc Interval in Children and Adolescents with Type 1 and 2 Long-QT Syndrome. *Circ Arrhythm Electrophysiol* **10**, 1–8 (2017).

123. Anneken, L. *et al.* Estradiol regulates human QT-interval: Acceleration of cardiac repolarization by enhanced KCNH2 membrane trafficking. *Eur Heart J* **37**, 640–650 (2016).

124. Harrison, A. G., Lin, T. & Wang, P. Mechanisms of SARS-CoV-2 Transmission and Pathogenesis. *Trends Immunol* **41**, 1100–1115 (2020).

125. Lu, R. *et al.* Genomic characterisation and epidemiology of 2019 novel coronavirus: implications for virus origins and receptor binding. *The Lancet* **395**, 565–574 (2020).

126. Hoffmann, M. *et al.* SARS-CoV-2 Cell Entry Depends on ACE2 and TMPRSS2 and Is Blocked by a Clinically Proven Protease Inhibitor. *Cell* **181**, 271-280.e8 (2020).

127. Chu, H. *et al.* Comparative tropism, replication kinetics, and cell damage profiling of SARS-CoV-2 and SARS-CoV with implications for clinical manifestations, transmissibility, and laboratory studies of COVID-19: an observational study. *Lancet Microbe* **1**, e14–e23 (2020).

128. Liao, Y. *et al.* Distinct infection process of SARS-CoV-2 in human bronchial epithelial cell lines. *J Med Virol* **92**, 2830–2838 (2020).

129. Takayama, K. In Vitro and Animal Models for SARS-CoV-2 research. *Trends Pharmacol Sci* **41**, 513–517 (2020).

130. Wahid, M., Jawed, A., Mandal, R. K., Dailah, H. G. & Janahi, E. M. Variants of SARS-CoV-2, their effects on infection, transmission and neutralization by vaccine induced antibodies. *Eur Rev Med Pharmacol Sci* **25**, 5857–5864 (2021).

131. Gómez, C. E., Perdiguero, B. & Esteban, M. Emerging sars-cov-2 variants and impact in global vaccination programs against sars-cov-2/covid-19. *Vaccines (Basel)* **9**, 1–13 (2021).

132. Korber, B. *et al.* Tracking Changes in SARS-CoV-2 Spike: Evidence that D614G Increases Infectivity of the COVID-19 Virus. *Cell* **182**, 812-827.e19 (2020).

133. Hou, Y. J. *et al.* SARS-CoV-2 D614G variant exhibits efficient replication ex vivo and transmission in vivo. *Science (1979)* **370**, 1464–1468 (2020).

134. Davies, N. G. *et al.* Estimated transmissibility and impact of SARS-CoV-2 lineage B.1.1.7 in England. *Science (1979)* **372**, 0–10 (2021).

135. Tegally, H. *et al.* Detection of a SARS-CoV-2 variant of concern in South Africa. *Nature* **592**, 438–443 (2021).

136. Sabino, E. C. *et al.* Resurgence of COVID-19 in Manaus, Brazil, despite high seroprevalence. *The Lancet* **397**, 452–455 (2021).

137. Hendaus, M. A. & Jomha, F. A. Delta variant of COVID-19: A simple explanation. *Qatar Med J* **2021**, 1–5 (2021).

138. Araf, Y. *et al.* Omicron variant of SARS-CoV-2: Genomics, transmissibility, and responses to current COVID-19 vaccines. *J Med Virol* **94**, 1825–1832 (2022).

139. Gavriatopoulou, M. *et al.* Organ-specific manifestations of COVID-19 infection. *Clin Exp Med* **20**, 493–506 (2020).

140. Elrobaa, I. H. & New, K. J. COVID-19: Pulmonary and Extra Pulmonary Manifestations. *Front Public Health* **9**, 1–26 (2021).

141. Wu, Z. & McGoogan, J. M. Characteristics of and Important Lessons from the Coronavirus Disease 2019 (COVID-19) Outbreak in China: Summary of a Report of 72314 Cases from the Chinese Center for Disease Control and Prevention. *JAMA - Journal of the American Medical Association* **323**, 1239–1242 (2020).

142. Yang, J. *et al.* Prevalence of comorbidities and its effects in coronavirus disease 2019 patients: A systematic review and meta-analysis. *International Journal of Infectious Diseases* **94**, 91–95 (2020).

143. Tian, S. *et al.* Pathological study of the 2019 novel coronavirus disease (COVID-19) through postmortem core biopsies. *Modern Pathology* **33**, 1007–1014 (2020).

144. Zheng, Y. Y., Ma, Y. T., Zhang, J. Y. & Xie, X. COVID-19 and the cardiovascular system. *Nat Rev Cardiol* **17**, 259–260 (2020).

145. Wang, D. *et al.* Clinical Characteristics of 138 Hospitalized Patients with 2019 Novel Coronavirus-Infected Pneumonia in Wuhan, China. *JAMA - Journal of the American Medical Association* **323**, 1061–1069 (2020).

146. Nuzzi, V. *et al.* The prognostic value of serial troponin measurements in patients admitted for COVID-19. *ESC Heart Fail* **8**, 3504–3511 (2021).

147. Ghio, S. *et al.* Cardiac involvement at presentation in patients hospitalized with COVID-19 and their outcome in a tertiary referral hospital in Northern Italy. *Intern Emerg Med* **15**, 1457–1465 (2020).

148. Iorio, A. *et al.* Combined Role of Troponin and Natriuretic Peptides Measurements in Patients With Covid-19 (from the Cardio-COVID-Italy Multicenter Study). *American Journal of Cardiology* **167**, 125–132 (2022).

149. Aleksova, A. *et al.* Effects of sars-cov-2 on cardiovascular system: The dual role of angiotensin-converting enzyme 2 (ace2) as the virus receptor and homeostasis regulator-review. *Int J Mol Sci* **22**, 1–14 (2021).

150. Fried, J. A. *et al.* The Variety of Cardiovascular Presentations of COVID-19. *Circulation* **141**, 1930–1936 (2020).

151. Gnecchi, M. *et al.* Myocarditis in a 16-year-old boy positive for SARS-CoV-2. *The Lancet* **395**, e116 (2020).

152. Gnecchi, M. Self-perception of acute symptoms in adolescents with COVID-19. *The Lancet Regional Health - Europe* **16**, 100383 (2022).

153. Tavazzi, G. *et al.* Myocardial localization of coronavirus in COVID-19 cardiogenic shock. *Eur J Heart Fail* **22**, 911–915 (2020).

154. An, J. *et al.* Angiotensin-converting enzyme inhibitors or angiotensin receptor blockers use and covid-19 infection among 824 650 patients with hypertension from a us integrated healthcare system. *J Am Heart Assoc* **10**, 1–7 (2021).

155. Sriram, K. & Insel, P. A. Risks of ACE Inhibitor and ARB Usage in COVID-19: Evaluating the Evidence. *Clin Pharmacol Ther* **108**, 236–241 (2020).

156. di Castelnuovo, A. *et al.* RAAS inhibitors are not associated with mortality in COVID-19 patients: Findings from an observational multicenter study in Italy and a meta-analysis of 19 studies. *Vascul Pharmacol* **135**, 106805 (2020).

157. Malek, R. J., Bill, C. A. & Vines, C. M. Clinical drug therapies and biologicals currently used or in clinical trial to treat COVID-19. *Biomedicine & Pharmacotherapy* **144**, 112276 (2021).

158. Yin, W. *et al.* Structural basis for inhibition of the RNA-dependent RNA polymerase from SARS-CoV-2 by remdesivir. *Science (1979)* **368**, (2020).

159. Furuta, Y. *et al.* Mechanism of action of T-705 against influenza virus. *Antimicrob Agents Chemother* **49**, 981–986 (2005).

160. Driouich, J. S. *et al.* Favipiravir antiviral efficacy against SARS-CoV-2 in a hamster model. *Nat Commun* **12**, 1–13 (2021).

161. Lipsitch, M., Perlman, S. & Waldor, M. K. Testing COVID-19 therapies to prevent progression of mild disease. *Lancet Infect Dis* **20**, 1367 (2020).

162. Li, Y. *et al.* Efficacy and Safety of Lopinavir/Ritonavir or Arbidol in Adult Patients with Mild/Moderate COVID-19: An Exploratory Randomized Controlled Trial. *Med* **1**, 105-113.e4 (2020).

163. Hung, I. F. N. *et al.* Triple combination of interferon beta-1b, lopinavir–ritonavir, and ribavirin in the treatment of patients admitted to hospital with COVID-19: an open-label, randomised, phase 2 trial. *The Lancet* **395**, 1695–1704 (2020).

164. Urakova, N. *et al.* β-d-N 4-Hydroxycytidine Is a Potent Anti-alphavirus Compound That Induces a High Level of Mutations in the Viral Genome. *J Virol* **92**, 1–22 (2018).

165. Mahase, E. Covid-19: Molnupiravir reduces risk of hospital admission or death by 50% in patients at risk, MSD reports. *BMJ* **375**, n2422 (2021).

166. Singh, A. K., Singh, A., Singh, R. & Misra, A. Molnupiravir in COVID-19: A systematic review of literature. *Diabetes & Metabolic Syndrome: Clinical Research & Reviews* **15**, 102329 (2021).

167. Mahase, E. Covid-19: UK becomes first country to authorise antiviral molnupiravi. *BMJ* **375**, n2602 (2021).

168. Mahase, E. Covid-19: UK becomes first country to authorise antiviral molnupiravir. *BMJ* **375**, n2697 (2021).

169. Puskarich, M. A. *et al.* A multi-center phase II randomized clinical trial of losartan on symptomatic outpatients with COVID-19. *EClinicalMedicine* **37**, 100957 (2021).

170. Villar, J. *et al.* Dexamethasone treatment for the acute respiratory distress syndrome: a multicentre, randomised controlled trial. *Lancet Respir Med* **8**, 267–276 (2020).

171. Ni, Y. N., Chen, G., Sun, J., Liang, B. M. & Liang, Z. A. The effect of corticosteroids on mortality of patients with influenza pneumonia: A systematic review and meta-analysis. *Crit Care* **23**, 1–9 (2019).

172. Horby, P. *et al.* Dexamethasone in Hospitalized Patients with Covid-19. *New England Journal of Medicine* **384**, 693–704 (2021).

173. Qin, C. *et al.* Dysregulation of Immune Response in Patients with COVID-19 in Wuhan, China. *SSRN Electronic Journal* (2020) doi:10.2139/ssrn.3541136.

174. Rosas, I. O. *et al.* Tocilizumab in Hospitalized Patients with Severe Covid-19 Pneumonia. *New England Journal of Medicine* **384**, 1503–1516 (2021).

175. Serisier, D. J. *et al.* Inhaled heparin in cystic fibrosis. *European Respiratory Journal* **27**, 354–358 (2006).

176. van Griensven, J. *et al.* Evaluation of Convalescent Plasma for Ebola Virus Disease in Guinea. *New England Journal of Medicine* **374**, 33–42 (2016).

177. Hung, I. F. N. *et al.* Convalescent plasma treatment reduced mortality in patients with severe pandemic influenza A (H1N1) 2009 virus infection. *Clinical Infectious Diseases* **52**, 447–456 (2011).

178. Salazar, E. *et al.* Convalescent plasma anti–SARS-CoV-2 spike protein ectodomain and receptor-binding domain IgG correlate with virus neutralization. *Journal of Clinical Investigation* **130**, 6728–6738 (2020).

179. Simonovich, V. A. *et al.* A Randomized Trial of Convalescent Plasma in Covid-19 Severe Pneumonia. *New England Journal of Medicine* **384**, 619–629 (2021).

180. Li, L. *et al.* Effect of Convalescent Plasma Therapy on Time to Clinical Improvement in Patients with Severe and Life-threatening COVID-19: A Randomized Clinical Trial. *JAMA - Journal of the American Medical Association* **324**, 460–470 (2020).

181. Dougan, M. *et al.* Bamlanivimab plus Etesevimab in Mild or Moderate Covid-19. *New England Journal of Medicine* **385**, 1382–1392 (2021).

182. Krogstad, D. J., Schlesinger, P. H. & Gluzman, I. Y. Antimalarials increase vesicle pH in Plasmodium falciparum. *Journal of Cell Biology* **101**, 2302–2309 (1985).

183. Liu, J. *et al.* Hydroxychloroquine, a less toxic derivative of chloroquine, is effective in inhibiting SARS-CoV-2 infection in vitro. *Cell Discov* **6**, 6–9 (2020).

184. Self, W. H. *et al.* Effect of Hydroxychloroquine on Clinical Status at 14 Days in Hospitalized Patients with COVID-19: A Randomized Clinical Trial. *JAMA - Journal of the American Medical Association* **324**, 2165–2176 (2020).

185. Gnecchi, M., Danieli, P. & Cervio, E. Mesenchymal stem cell therapy for heart disease. *Vascul Pharmacol* **57**, 48–55 (2012).

186. Hoogduijn, M. J. & Lombardo, E. Mesenchymal Stromal Cells Anno 2019: Dawn of the Therapeutic Era? Concise Review. *Stem Cells Transl Med* **8**, 1126–1134 (2019).

187. Khoury, M. *et al.* Current status of cell-based therapies for respiratory virus infections: applicability to COVID-19. *European Respiratory Journal* **55**, 2000858 (2020).

188. Miteva, K., van Linthout, S., Volk, H.-D. & Tschöpe, C. Immunomodulatory Effects of Mesenchymal Stromal Cells Revisited in the Context of Inflammatory Cardiomyopathy. *Stem Cells Int* **2013**, 1–16 (2013).

189. Gnecchi, M., Zhang, Z., Ni, A. & Dzau, V. J. Paracrine mechanisms in adult stem cell signaling and therapy. *Circ Res* **103**, 1204–1219 (2008).

190. Wu, X. *et al.* Intrinsic Immunity Shapes Viral Resistance of Stem Cells. *Cell* **172**, 423–438 (2018).

191. Leng, Z. *et al.* Transplantation of ACE2- Mesenchymal stem cells improves the outcome of patients with covid-19 pneumonia. *Aging Dis* **11**, 216–228 (2020).

192. Thanunchai, M. *et al.* Tropism of Avian Influenza A (H5N1) Virus to Mesenchymal Stem Cells and CD34+ Hematopoietic Stem Cells. *PLoS One* **8**, e81805 (2013).

193. Sundin, M. *et al.* Mesenchymal stem cells are susceptible to human herpesviruses, but viral DNA cannot be detected in the healthy seropositive individual. *Bone Marrow Transplant* **37**, 1051–1059 (2006).

194. Premkumar, L. *et al.* The receptor-binding domain of the viral spike protein is an immunodominant and highly specific target of antibodies in SARS-CoV-2 patients. *Sci Immunol* **5**, 1–10 (2020).

195. Tregoning, J. S., Flight, K. E., Higham, S. L., Wang, Z. & Pierce, B. F. Progress of the COVID-19 vaccine effort: viruses, vaccines and variants versus efficacy, effectiveness and escape. *Nat Rev Immunol* **21**, 626–636 (2021).

196. Mura, M. *et al.* Generation of the human induced pluripotent stem cell (hiPSC) line PSMi006-A from a patient affected by an autosomal recessive form of long QT syndrome type 1. *Stem Cell Res* **42**, 101658 (2020).

197. Mura, M. *et al.* Generation of the human induced pluripotent stem cell (hiPSC) line PSMi002-A from a patient affected by the Jervell and Lange-Nielsen syndrome and carrier of two compound heterozygous mutations on the KCNQ1 gene. *Stem Cell Res* **29**, 157–161 (2018).

198. Mura, M. *et al.* Generation of the human induced pluripotent stem cell (hiPSC) line PSMi003-A from a patient affected by an autosomal recessive form of Long QT Syndrome type 1. *Stem Cell Res* **29**, 170–173 (2018).

199. Mura, M. *et al.* Generation of the human induced pluripotent stem cell (hiPSC) line PSMi004-A from a carrier of the KCNQ1-R594Q mutation. *Stem Cell Res* **37**, 101431 (2019).

200. Mura, M. *et al.* Generation of the human induced pluripotent stem cell (hiPSC) line PSMi005-A from a patient carrying the KCNQ1-R190W mutation. *Stem Cell Res* **37**, 101437 (2019).

201. Mura, M. *et al.* Generation of the human induced pluripotent stem cell (hiPSC) line PSMi007-A from a Long QT Syndrome type 1 patient carrier of two common variants in the NOS1AP gene. *Stem Cell Res* **36**, 101416 (2019).

202. Mura, M. *et al.* Generation of two human induced pluripotent stem cell (hiPSC) lines from a long QT syndrome South African founder population. *Stem Cell Res* **39**, 101510 (2019).

203. Mehta, A. *et al.* Identification of a targeted and testable antiarrhythmic therapy for long-QT syndrome type 2 using a patient-specific cellular model. *Eur Heart J* **39**, 1446–1455 (2018).

204. Ronchi, C. *et al.* NOS1AP polymorphisms reduce NOS1 activity and interact with prolonged repolarization in arrhythmogenesis. *Cardiovasc Res* **117**, 472–483 (2021).

205. Lee, Y. K. *et al.* MTMR4 SNVs modulate ion channel degradation and clinical severity in congenital long QT syndrome: Insights in the mechanism of action of protective modifier genes. *Cardiovasc Res* **117**, 767–779 (2021).

206. Huo, J., Wei, F., Cai, C., Lyn-Cook, B. & Pang, L. Sex-Related Differences in Drug-Induced QT Prolongation and Torsades de Pointes: A New Model System with Human iPSC-CMs. *Toxicological Sciences* **167**, 360–374 (2019).

207. Thomas, P., Pang, Y., Filardo, E. J. & Dong, J. Identity of an estrogen membrane receptor coupled to a G protein in human breast cancer cells. *Endocrinology* **146**, 624–632 (2005).

208. Curran, M. E. *et al.* A molecular basis for cardiac arrhythmia: HERG mutations cause long QT syndrome. *Cell* **80**, 795–803 (1995).

209. Kurokawa, J. *et al.* Acute effects of oestrogen on the guinea pig and human IKr channels and drug-induced prolongation of cardiac repolarization. *Journal of Physiology* **586**, 2961–2973 (2008).

210. Drici, M. D., Burklow, T. R., Haridasse, V., Glazer, R. I. & Woosley, R. L. Sex hormones prolong the QT interval and downregulate potassium channel expression in the rabbit heart. *Circulation* **94**, 1471–1474 (1996).

211. Song, M. *et al.* Remodeling of Kv4.3 Potassium Channel Gene Expression under the Control of Sex Hormones. *Journal of Biological Chemistry* **276**, 31883–31890 (2001).

212. Sammartino, J. C. *et al.* Evaluation of the Neutralizing Antibodies Response against 14 SARS-CoV-2 Variants in BNT162b2 Vaccinated Naïve and COVID-19 Positive Healthcare Workers from a Northern Italian Hospital. *Vaccines (Basel)* **10**, 703 (2022).

213. Ng, M. L., Tan, S. H., See, E. E., Ooi, E. E. & Ling, A. E. Proliferative growth of SARS coronavirus in Vero E6 cells. *Journal of General Virology* **84**, 3291–3303 (2003).

214. Alnajjar, R., Mostafa, A., Kandeil, A. & Al-Karmalawy, A. A. Molecular docking, molecular dynamics, and in vitro studies reveal the potential of angiotensin II receptor blockers to inhibit the COVID-19 main protease. *Heliyon* **6**, e05641 (2020).

215. Cohen, J. B. *et al.* Continuation versus discontinuation of renin–angiotensin system inhibitors in patients admitted to hospital with COVID-19: a prospective, randomised, open-label trial. *Lancet Respir Med* **9**, 275–284 (2021).

216. Lopes, R. D. *et al.* Effect of Discontinuing vs Continuing Angiotensin-Converting Enzyme Inhibitors and Angiotensin II Receptor Blockers on Days Alive and out of the Hospital in Patients Admitted with COVID-19: A Randomized Clinical Trial. *JAMA - Journal of the American Medical Association* **325**, 254–264 (2021).

217. Derington, C. G. *et al.* Angiotensin II receptor blocker or angiotensin-converting enzyme inhibitor use and COVID-19-related outcomes among US Veterans. *PLoS One* **16**, 1–15 (2021).

218. Dominici, M. *et al.* Minimal criteria for defining multipotent mesenchymal stromal cells. The International Society for Cellular Therapy position statement. *Cytotherapy* **8**, 315–317 (2006).

219. Chu, H. *et al.* Comparative tropism, replication kinetics, and cell damage profiling of SARS-CoV-2 and SARS-CoV with implications for clinical manifestations, transmissibility, and laboratory studies of COVID-19: an observational study. *Lancet Microbe* **1**, e14–e23 (2020).

220. Avanzini, M. A. *et al.* Human mesenchymal stromal cells do not express ACE2 and TMPRSS2 and are not permissive to SARS-CoV-2 infection. *Stem Cells Transl Med* **10**, 636–642 (2021).

221. Avanzini, M. A. *et al.* Generation of mesenchymal stromal cells in the presence of platelet lysate: A phenotypic and functional comparison of umbilical cord blood- and bone marrow-derived progenitors. *Haematologica* **94**, 1649–1660 (2009).

222. Borghesi, A. *et al.* Genomic alterations in human umbilical cord-derived mesenchymal stromal cells call for stringent quality control before any possible therapeutic approach. *Cytotherapy* **15**, 1362–1373 (2013).

223. Bernardo, M. E. *et al.* Optimization of in vitro expansion of human multipotent mesenchymal stromal cells for cell-therapy approaches: Further insights in the search for a fetal calf serum substitute. *J Cell Physiol* **211**, 121–130 (2007).

224. Lisini, D. *et al.* Adipose tissue-derived mesenchymal stromal cells for clinical application: An efficient isolation approach. *Curr Res Transl Med* **67**, 20–27 (2019).

225. Reed, L. J. & Muench, H. A simple method of estimating fifty per cent endpoints. *Am J Epidemiol* **27**, 493–497 (1938).

List of publications

- Mura M, Bastaroli F, Corli M, Ginevrino M, Calabrò F, Boni M, Crott i L, Valente EM, Schwartz PJ, Gnecchi M. Generation of the human induced pluripotent stem cell (hiPSC) line PSMi006-A from a patient affected by an autosomal recessive form of long QT syndrome type 1. *Stem Cell Res* **42**, 101658 (2020). PMID: 31785541. [Collection and assembly of data, data analysis and interpretation]

- Bastaroli F, Mura M, Nykjaer G, Gnecchi M. Human Mesenchymal Stem Cells of Adult and Fetal Origin Do Not Express ACE2 and are Immune to SARS-CoV-2 Spike Pseudotyped Virus. *Circulation* **142**, Issue Suppl_3.16446 (2020). [Collection and assembly of data, data analysis and interpretation, abstract writing and oral communication]

- *Avanzini MA, *Mura M, *Percivalle E, Bastaroli F, Croce S, Valsecchi C, Lenta E, Nykjaer G, Cassaniti I, Bagnarino J, Baldanti F, Zecca M, Comoli P, Gnecchi M. Human mesenchymal stromal cells do not express ACE2 and TMPRSS2 and are not permissive to SARS-CoV-2 infection. *Stem Cells Transl Med* **10**, 636–642 (2021). PMID: 33188579. [Collection and assembly of data, data analysis and interpretation]

- Bastaroli F, Mura M, Sammartino JC, Ferrari A, Corli M, Guarona C, Percivalle E, Gnecchi M. Valsartan Protects Both Cardiac and Lung Cells From SARS-CoV-2 Infection. *Circulation* **144**, Issue Suppl_1.12174 (2021). [Conception and design, collection and assembly of data, data analysis and interpretation, abstract writing and poster presentation]

- Bastaroli F, Mura M, Sammartino JC, Ferrari A, Deidda G, Corli M, Guarona C, Crespan E, Percivalle E, Gnecchi M. Valsartan limits SARS-CoV-2 infection in pulmonary and cardiac experimental models by reducing the expression of ACE2. *Cardiovasc Res* (*under revision*). [Conception and design, collection and assembly of data, data analysis and interpretation, manuscript writing]

Stem Cell Research 42 (2020) 101658

Contents lists available at ScienceDirect

Stem Cell Research

journal homepage: www.elsevier.com/locate/scr

Lab resource: Stem Cell Line

Generation of the human induced pluripotent stem cell (hiPSC) line PSMi006-A from a patient affected by an autosomal recessive form of long QT syndrome type 1

Manuela Mura[a], Francesca Bastaroli[b], Marzia Corli[b], Monia Ginevrino[c,d], Federica Calabrò[a], Marina Boni[e], Lia Crotti[f,g,h], Enza Maria Valente[c,d], Peter J. Schwartz[f], Massimiliano Gnecchi[a,b,i,*]

[a] Coronary Care Unit and Laboratory of Experimental Cardiology for Cell and Molecular Therapy, Fondazione IRCCS Policlinico San Matteo, Pavia, Italy
[b] Department of Molecular Medicine, Unit of Cardiology, Università degli studi di Pavia, Pavia, Italy
[c] Department of Molecular Medicine, Unit of Genetics, Università degli studi di Pavia, Pavia, Italy
[d] Neurogenetics Unit, Fondazione IRCCS Santa Lucia, Rome, Italy
[e] Laboratory of Oncohaematological Cytogenetic and Molecular Diagnostics, Division of Haematology, Fondazione IRCCS Policlinico San Matteo, Pavia, Italy
[f] Istituto Auxologico Italiano, IRCCS, Center for Cardiac Arrhythmias of Genetic Origin and Laboratory of Cardiovascular Genetics, Milan, Italy
[g] Istituto Auxologico Italiano, IRCCS, Department of Cardiovascular, Neural and Metabolic Sciences, San Luca Hospital, Milan, Italy
[h] Department of Medicine and Surgery, Università Milano-Bicocca, Milan, Italy
[i] Department of Medicine, University of Cape Town, Cape Town, South Africa

ARTICLE INFO

Keywords:
Endoderm
Mesoderm
Ectoderm

ABSTRACT

We generated human induced pluripotent stem cells (hiPSCs) from dermal fibroblasts of a 40 years old female patient homozygous for the mutation c.535 *G* > *A* p.G179S on the KCNQ1 gene, causing a severe form of autosomal recessive Long QT Syndrome type 1 (AR-LQT1). The hiPSCs, generated using classical approach of the four retroviruses enconding the reprogramming factors OCT4, SOX2, cMYC and KLF4, display pluripotent stem cell characteristics, and differentiate into cell lineages of all three germ layers: endoderm, mesoderm and ectoderm.

Resource Table

Unique stem cell line identifier	PSMi006-A
Alternative name of stem cell line	HDF39-ARLQT-iPS
Institution	Fondazione IRCCS Policlinico San Matteo, Pavia, Italy
Contact information of distributor	Massimiliano Gnecchi, m.gnecchi@unipv.it
Type of cell line	hiPSC
Origin	human
Additional origin info	Age: 40 Gender: female Ethnicity: Caucasian
Cell source	Dermal fibroblasts
Clonality	Clonal
Method of reprogramming	Retroviruses encoding for the human cDNA of OCT4, SOX2, cMYC, KLF4
Genetic modification	No
Type of modification	None
Associated disease	Long QT Syndrome type 1 (OMIM #192,500)
Gene/locus	c.535 *G* > *A* mutation on KCNQ1, chromosomal locus 11p15.5-p15.4, (NM_000218.2)
Method of modification	N/A
Name of transgene or resistance	N/A
Inducible/Constitutive system	N/A
Date archived/stock date	March 15, 2014
Cell line repository/bank	https://hpscreg.eu/cell-line/PSMi006-A
Ethical approval	The study has been approved by the Ethics Committee of our Institution, Fondazione IRCCS Policlinico San Matteo, on the 29th of October 2010, protocol number 20,100,004,354, proceeding P-20,100,003,369. We obtained patient written informed consent for both skin biopsy procedure and conservation of biological samples.

1. Resource utility

It is now well accepted that the iPSC technology can be efficiently

* Corresponding author at: University of Pavia and Fondazione IRCCS Policlinico S. Matteo, Pavia, Italy.
E-mail address: m.gnecchi@unipv.it (M. Gnecchi).

https://doi.org/10.1016/j.scr.2019.101658
Received 29 January 2019; Received in revised form 7 November 2019; Accepted 13 November 2019
Available online 20 November 2019

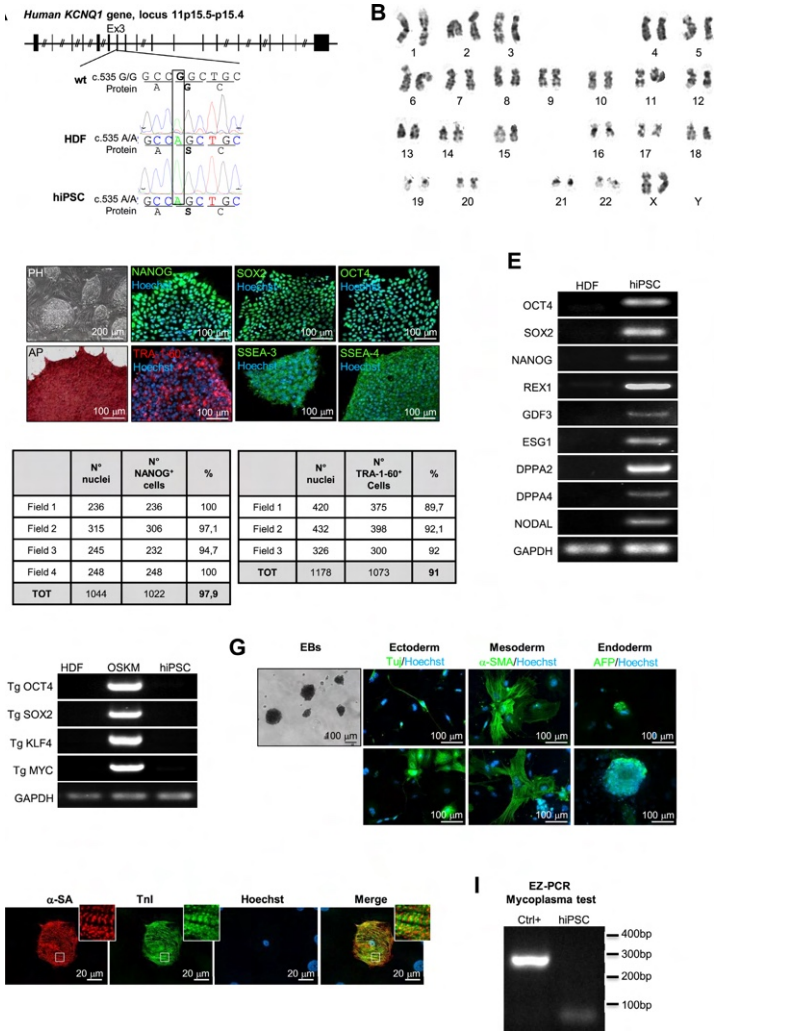

	N° nuclei	N° NANOG+ cells	%
Field 1	236	236	100
Field 2	315	306	97,1
Field 3	245	232	94,7
Field 4	248	248	100
TOT	1044	1022	**97,9**

	N° nuclei	N° TRA-1-60+ Cells	%
Field 1	420	375	89,7
Field 2	432	398	92,1
Field 3	326	300	92
TOT	1178	1073	**91**

(caption on next page)

used to model LQTS and test targeted therapies (Mehta et al., 2018; Gnecchi et al., 2017; Mura et al., 2017). Accordingly, PSMi006-A will be useful for modeling LQTS type 1 and to test novel targeted drug or molecular approaches.

2. Resource details

PSMi006-A line was generated by reprogramming dermal fibroblasts of 40 years old woman affected by an autosomal recessive form of Long QT Syndrome (LQTS) type 1 (AR-LQT1). LQTS is an inherited

Fig. 1. Characterization of the PSMi006-A cell line. A. On top schematic representation of the *KCNQ1* gene with introns (horizontal lines) and exons (vertical lines/boxes). Bottom, DNA sequencing results showing the presence of the mutation 535 G>A in homozygosis on the Exon 3 of *KCNQ1* gene of patient-derived dermal fibroblasts (HDF) and PSMi006-A cell line (hiPSC). The *KCNQ1* coding sequence (CDS) used as a reference is the NCBI sequence NM_000218.2. **B.** Karyotype analysis of PSMi006-A (300 G-bandings) showing normal female karyotype (46, XX). **C.** PH: phase contrast image showing PSMi006-A morphology. AP: alkaline phosphatase colorimetric staining. The other panels on the right: immunofluorescence stainings showing uniform expression of pluripotency markers in the PSMi006-A. Nuclei were counterstained with Hoechst 33258 (Hoechst, blue). **D.** Immunocytochemistry counting of anti Nanog-positive ($Nanog^+$) and anti TRA-1-60-positive ($TRA\text{-}1\text{-}60^+$) cells. The total number of cells in each of the fields analyzed was quantified by counting the nuclei stained with Hoechst 33258. **E.** RT-PCR analysis showing expression of the indicated markers of pluripotency in PSMi006-A (hiPSC), compared with their parental fibroblasts (HDF). **F.** RT-PCR analysis showing no expression of the four viral transgenes (Tg) in naïve fibroblasts (HDF), expression of Tg OCT4, SOX2, KLF4 and cMYC five days after transduction (OSKM) and silencing of the four Tg in PSMi006-A. **G.** Far left panel: floating embryoid bodies (EBs) formed after 7 days of PSMi006-A culture in suspension. Panels on the right: Immunofluorescence staining for markers of the 3 germ layers in iPSC-derived EBs: neuronal class tubulin beta III (Tuj) for ectoderm, smooth muscle actin (SMA) for mesoderm, and Alpha Fetoprotein (AFP) for endoderm. **H.** Co-immunofluorescence staining for the cardiac sarcomeric proteins alpha-sarcomeric actinin (α-SA, red) and troponin I (TnI, green) in cardiomyocytes differentiated from the PSMi006-A. Nuclei were counterstained with Hoechst. The insets show areas of cross-striations. **I.** EZ-PCR test showing the absence of mycoplasma contamination in PSMi006-A. $Ctrl^+$ is the positive PCR control provided by the kit.

Table 1
Characterization and validation of PSMi006-A cell line.

Classification	Test	Result	Data
Morphology	Photography	Normal	Fig. 1 panel C
Phenotype	Qualitative analysis	Positive immunostaining for the pluripotency markers Oct4, Nanog, Sox2, TRA-1-60, SSEA-3, SSEA-4	Fig. 1 panel C
		Positive staining for the alkaline phosphatase	Fig. 1 panel C
		Expression of the pluripotency markers OCT3/4, SOX2, NANOG, REX1, GDF3, ESG1, DPPA2, DPPA4, NODAL, analyzed by RT-PCR	Fig. 1 panel E
	Quantitative analysis	97,9% $NANOG^+$ cells	Fig. 1 panel D
		91% $TRA\text{-}1\text{-}60^+$ cells	
Genotype	Karyotype (300 G-banding) and resolution	46XX, Resolution 450–500	Fig. 1 panel B
Identity	Microsatellite PCR (mPCR)	Not performed	Not available
	STR analysis	7 sites tested for iPSC, all sites matched with donor HDF STR profile	Available with the authors
Mutation analysis	Sequencing	Homozygous for the mutation c.535 *G > A* p.G179S on the KCNQ1 gene	Fig. 1 panel A
Microbiology and virology	Mycoplasma	Mycoplasma testing by RT-PCR. Negative	Fig. 1 panel I
Differentiation potential	Embryoid body formation	The EBs expressed neuronal class tubulin beta III (Tuj) (ectoderm), smooth muscle actin (SMA) (mesoderm), and Alpha Fetoprotein (AFP) (endoderm).	Fig. 1 panel G
	Differentiation into cardiomyocytes	The iPSC-derived cardiomyocytes expressed the cardiac sarcomeric proteins alpha-sarcomeric actinin (α-SA) and troponin I (TnI)	Fig. 1 panel H
Donor screening	HIV 1 + 2 Hepatitis B, Hepatitis C	Not performed	Not available
Genotype additional info	Blood group genotyping	Not performed	Not available
	HLA tissue typing	Not performed	Not available

disease characterized by the prolongation of cardiac repolarization, which is quantified as the duration of the QT interval on the surface electrocardiogram (ECG). This prolonged repolarization time predisposes the patient to develop ventricular arrhythmias that can cause, syncope or sudden cardiac death (SCD) (Schwartz et al., 2012). LQT1 is the commonest LQTS sub-type, accounting for ~40–50% of all cases (Schwartz et al., 2012). It is caused by mutations in the KCNQ1 gene, encoding for the α-subunit of the voltage-dependent potassium channel mediating the I_{Ks} current, which is an important contributor of the action potential (AP) repolarization (Schwartz et al., 2012).

When enrolled, the patient had a markedly prolonged QTc (QT corrected for heart rate) of 576 ms, and she already experienced several episodes of syncope and a documented episode of ventricular fibrillation triggered by emotional stress. Genetic screening revealed the presence of a homozygous c.535 G/A mutation on the KCNQ1 gene, leading to the substitution of the glycine in position 179 with serine. Both her two older sisters carry the same mutation in homozygosis; the firstborn died at age 19 after an intense emotional stress, the second born is still alive but experienced several cardiac episodes (Schwartz, 2012). Finally, her son is heterozygous for the mutation and asymptomatic.

Fibroblasts were reprogrammed by retroviral infection of OCT4, SOX2, KLF4 and c-MYC. The obtained hiPSCs were maintained on feeders, retaining embryonic stem cell (ES)-like morphology (*Fig. 1**C***) and pluripotent features up to passage 50. DNA sequencing proved that both patient's fibroblasts and the derived hiPSCs carry the disease causing mutation on the KCNQ1 gene (*Fig. 1**A**. The KCNQ1 coding sequence -CDS- used as a reference is the NCBI sequence NM_000218.2*), and an identical DNA profile at seven polymorphic loci, as shown by Short tandem Repeat (STR) analysis (available with the authors). Moreover the DNA karyotyping revealed normal female chromosome asset (46, XX) (*Fig. 1**B***). PSMi006-A uniformly expresses the human ES surface antigens Tumor Related Antigen-1-60 (TRA-1-60), Stage Specific Embryonic Antigen-3 and −4 (SSEA-3, SSEA-4) (*Fig. 1**C–E***), and the pluripotent markers NANOG, OCT4, SOX2 (*Fig. 1**C–E***), REX1, GDF3, ESG1, DPPA2, DPPA4 and NODAL (*Fig. 1**E***). Likewise, it shows alkaline phosphatase (AP) activity (*Fig. 1**C***). RT-PCR in *Fig. 1**F*** shows no expression of the four viral transgenes (Tg) in naïve fibroblasts (HDF), clear expression of Tg OCT4, SOX2, KLF4 and cMYC in fibroblasts five days after transduction (OSKM) and silencing of the four Tg in PSMi006-A at passage 5.

PSMi006-A spontaneously forms embryoid bodies (EBs) able to differentiate into cells belonging to the three germ layers: endoderm, mesoderm and ectoderm (*Fig. 1**G***). In addition we successfully differentiated this AR-LQT1 cell line into spontaneously beating cardiac-like cells expressing typical cardiac markers such as the sarcomeric proteins alpha-actinin (α-SA) and troponin I (TnI) (*Fig. 1**H, the insets show areas of cross-striation***). We also excluded the presence of mycoplasma contamination (*Fig. 1**I***).

3. Materials and methods

Expanded protocols are provided as Supplemental Methods.

Table 2
Reagents details.

Antibodies used for immunocytochemistry			
	Antibody	Dilution	Company Cat # and RRID
Pluripotency Markers	Rabbit anti Nanog	1:200	Stemgent *Cat#* 09-0020, *RRID:* AB_2,298,294
	Mouse anti Oct3/4 (C-10)	1:500	SCBT *Cat#* sc-5279, *RRID:* AB_628,051
	Mouse anti Sox2	1:500	R&D Systems *Cat#* MAB2018, *RRID:* AB_358,009
	Mouse anti TRA-1-60	1:100	Stemgent *Cat#* 09-0010, *RRID:* AB_1,512,170
	Rat anti SSEA-3	1:100	Millipore *Cat#* MAB4303, *RRID:* AB_177,628
	Mouse anti SSEA-4	1:100	Stemgent *Cat#* 09-0006, *RRID:* AB_1,512,169
Differentiation Markers (EBs)	Mouse anti neuronal class tubulin beta III (Tuj)	1:500	Covance *Cat#* MMS-435P, *RRID:* AB_2,313,773
	Mouse anti smooth muscle actin	1:1000	Millipore *Cat#* CBL171, *RRID:* AB_2,223,166
	Mouse anti alpha-fetoprotein	1:500	Millipore *Cat#* SCR030, *RRID:* AB_597,591
Cardiac Markers	Rabbit anti Troponin I	1:250	Abcam *Cat#* ab52862, *RRID:* AB_869,983
	Mouse anti alpha actinin	1:800	Sigma Aldrich *Cat#* A7811, *RRID:* AB_476,766
Secondary antibodies	Alexa-Fluor® 488 Goat anti-rabbit IgG	1:500	ThermoFisher Cat# A11008, *RRID:*AB_143,165
	Alexa-Fluor® 488 Goat anti-rat IgM	1:500	ThermoFisher Cat# A21212, *RRID:*AB_11,180,047
	Alexa-Fluor® 488 Goat anti-mouse IgG	1:500	ThermoFisher Cat# A11001, *RRID:* AB_2,534,069
	Alexa-Fluor® 546 Goat anti-mouse IgG	1:500	ThermoFisher Cat# A11003, *RRID:* AB_141,370

Primers		
	Target	Forward/Reverse primer (5′ − 3′)
Targeted mutation analysis/sequencing	KCNQ1 Exon 3	Fw: 5′- gttcaaacaggttgcagggtctga −3′ Rev: 5′- ccaggtttccagaccaggaag-3′
Pluripotency Markers (RT-PCR)	Oct4	Fw: 5′-gtactcctcggtcccttttcc-3′ Rev: 5′-caaaaaccctggcacaaact-3′
	Sox2	Fw: 5′-acaccaatcccatccacact-3′ Rev: 5′-tttttcgtcgcttggagact-3′
	Nanog	Fw: 5′-ttccttcctccatggatctg-3′ Rev: 5′-tctgctggaggctgaggtat-3′
	Rex1	Fw: 5′-cagatcctaaacagctcgcagaat-3′ Rev: 5′-gcgtacgcaaattaaagtccaga-3′
	GDF3	Fw: 5′-cttatgctacgtaaaggagctggg-3′ Rev: 5′-gtgccaacccaggtcccggaagtt-3′
	ESG1	Fw: 5′-atatcccgccgtgggtgaaagttc-3′ Rev: 5′-actcagccatggactggagcatcc-3′
	DPPA4	Fw: 5′-ggagccgcctgccctggaaaattc-3′ Rev: 5′-tttttcctgatattctattcccat-3′
	DPPA2	Fw: 5′-ccgtcccccgcaatctccttccatc-3′ Rev: 5′-atgatgccaacatggctcccggtg-3′
	Nodal	Fw: 5′-gggcaagaggcaccgtcgacatca-3′ Rev:5′-gggactcggtgggcgtggtaacgtttc-3′
House-Keeping Genes (RT-PCR)	GAPDH	Fw 5′-catgttccaatatgattccacce-3′ Rev 5′-gggatctcgctcctggaagat-3′
Retroviral transgenes	Oct4 cDNA on pMXs-hOCT3/4	Fw: 5′-ccccagggccccattttggtacc-3′
	Sox2 cDNA on pMXs-hSOX-2	Fw: 5′-ggcacccctggcatggctctttggctc-3′
	cMyc cDNA on pMXs-hcMYC	Fw: 5′-caacaaccgaaaatgcaccagccccag-3′
	Klf4 cDNA on pMXs-hKLF4	Fw: 5′-acgatcgtggccccggaaaaggacc-3′
	pMX viral vector	Rev: 5′-ccctttttctggagactaaataaa-3′

3.1. Generation of hiPSCs

Skin fibroblasts were reprogrammed using four retroviruses encoding OCT4, SOX2, KLF4 and c-MYC. Emerging iPSC clones were manually picked, individually placed into a separate cell culture well and expanded on a feeder-layer of mitotically-inactivated mouse embryonic fibroblasts (iMEF), in DMEM/F12, 20% Knockout Serum Replacement (KO-SR), 2 mM L-glutamine, 50 U/ml penicillin, 50 U/ml streptomycin, 1% Non-Essential Amino Acids (NEAA), 0.1 mM beta-mercaptoethanol, 10 ng/ml basic Fibroblast Growth Factor (bFGF) (*Table 1*).

3.2. Mutation analysis

Genomic DNA from hiPSCs and their parental fibroblasts was amplified with the GoTaq G2 DNA polymerase (Promega) and primers in *Table 2*. The resulting amplicons were purified and sequenced (Lightrun service - GATC Biotech AG – Germany).

3.3. STR analysis

The PowerPlex® CS7 human identification kit (Promega) was used to co-amplify a set of seven variable short tandem repeat loci (LPL, F13B, FESFPS, F13A01, Penta_D, Penta_C, Penta_E) on genomic DNA from fibroblasts and hiPSCs in order to compare the genetic profile of the two cell lines. After PCR-amplification, fragments were run on a 3130xl capillary sequencer (Applied Biosystems) and then analyzed using GeneMarker software (SoftGenetics).

3.4. Karyotyping

hiPSCs were blocked at metaphase by exposure to 10 μg/ml demecolcine solution for 3 h (Sigma Aldrich). Karyotyping was performed using 300 G-banding chromosome analysis.

3.5. Immunocytochemistry

hiPSCs grown on glass coverslips were fixed for 15 min in 4% paraformaldehyde (Affymetrix USB), permeabilized in PBS containing 0.1% Triton X-100 (Sigma Aldrich) for 5 min, and blocked in 1% bovine

serum albumin (BSA, Sigma Aldrich) for 1 h at room temperature (RT). Then they were incubated for 1 h at RT with the primary antibody (*Table 2*) diluted in blocking solution, washed three times, and incubated for 1 h at RT with an appropriate secondary antibody (*Table 2*). Finally, the cells were stained with 1 μg/ml of Hoechst 33,258 (Sigma Aldrich). Images were acquired using the Carl Zeiss fluorescence microscope Observer.Z1 equipped with the Apotome system and AxioVision 6.0 software (Zeiss GmbH, Gottingen, Germany).

3.6. Immunocytochemistry counting

Nanog$^+$ and TRA-1-60$^+$ cells were counted using the AxioVision 6.0 software (Zeiss GmbH, Gottingen, Germany). A total of 1000 cells were counted in 3-4 fields.

3.7. AP colorimetric assay

AP was detected by using the Alkaline Phosphatase Staining kit (00-0009 Stemgent).

3.8. RT-PCR

Total RNA was purified using TRIzol (ThermoFisher Scientific). cDNA was synthesized using the Superscript II Reverse Transcriptase (ThermoFisher). RT-PCR was performed with the GoTaq G2 DNA polymerase (Promega) and primers in *Table 2*.

3.9. EB formation

hiPSCs were enzimatically detached and grown for 7 days in non-adherent conditions in a modified iPS medium deprived of bFGF and containing 20% FBS instead of KO-SR. Forming EBs were then transferred to gelatin-coated dishes to allow differentiation in adhesion in the same medium for additional 7 days. Finally, the cells were processed for immunostaining of the three germ layers as described above.

3.10. Cardiac differentiation

Cardiac differentiation was induced using the PSC Cardiomyocyte Differentiation Kit (ThermoFisher).

3.11. Mycoplasma test

For the detection of mycoplasma in cell culture we used the EZ-PCR Mycoplasma Test Kit (Biological Industries).

Declaration of Competing Interest

None.

Acknowledgements

This work was supported by the Leducq Foundation for Cardiovascular Research [18CVD05] 'Towards Precision Medicine with Human iPSCs for Cardiac Channelopathies', by the Italian Ministry of Health, "Ricerca Corrente" projects numbers 08064017 and 08064018, and by a grant to the Department of Molecular Medicine of the University of Pavia under the initiative "Dipartimenti di Eccellenza" (2018–2022).

Supplementary materials

Supplementary material associated with this article can be found, in the online version, at doi:10.1016/j.scr.2019.101658.

References

Mehta, A., Ramachandra, C.J.A., Singh, P., Chitre, A., Lua, C.H., Mura, M., Crotti, L., Wong, P., Schwartz, P.J., Gnecchi, M., Shim, W., 2018. Identification of a targeted and testable antiarrhythmic therapy for long-QT syndrome type 2 using a patient-specific cellular model. Eur. Heart J. 39, 1446–1455.

Gnecchi, M., Stefanello, M., Mura, M., 2017. Induced pluripotent stem cell technology: toward the future of cardiac arrhythmias. Int. J. Cardiol. 237, 49–52.

Mura, M., Mehta, A., Ramachandra, C.J., Zappatore, R., Pisano, F., Ciuffreda, M.C., Barbaccia, V., Crotti, L., Schwartz, P.J., Shim, W., Gnecchi, M., 2017. The KCNH2-IVS9-28A/G mutation causes aberrant isoform expression and hERG trafficking defect in cardiomyocytes derived from patients affected by long QT syndrome type 2. Int. J. Cardiol. 240, 367–371.

Schwartz, P.J., Crotti, L., Insolia, R., 2012. Long-QT syndrome: from genetics to management. Circ. Arrhythm Electrophysiol. 5, 868–877.

Schwartz, P.J., 2012. The role of the sympathetic nervous system in the long qt syndrome: the long road from pathophysiology to therapy. Card Electrophysiol. Clin. 4, 75–85.

COVID-19
SESSION TITLE: MECHANISMS OF SARS-COV-2 INFECTION

Abstract 16446: Human Mesenchymal Stem Cells of Adult and Fetal Origin Do Not Express ACE2 and are Immune to SARS-CoV-2 Spike Pseudotyped Virus

Francesca Bastaroli, **Manuela Mura**, **Giulia Nykjaer** and **Massimiliano Gnecchi**

Originally published 12 Nov 2020 | https://doi.org/10.1161/circ.142.suppl_3.16446 | Circulation. 2020;142:A16446

Abstract

Background: Angiotensin-converting enzyme 2 (ACE2) expression in the lung has a protective role against injury. However, ACE2 is the main host cell receptor for the Severe Acute Respiratory Syndrome-Coronavirus 2 (SARS-CoV-2) entry. Human mesenchymal stem cells (hMSCs) are currently under investigation for the treatment of pulmonary and cardiac complications of the SARS-CoV-2 disease (COVID-19). However, it is unclear if hMSCs express ACE2 and if they possibly can secrete ACE2. Also, their predisposition to be infected by SARS-CoV-2 is unknown.

Aim: To assess if hMSCs of fetal and adult origin constitutively express and secrete ACE2 and if they can be infected by SARS-CoV-2.

Methods: We studied 8 hMSC lines: 4 of fetal origin isolated from human placentas (hA-MSC) and 4 of adult origin isolated from bone marrow aspirates (hBM-MSCs). The lung epithelial cancer cell line CALU-3, which expresses high levels of ACE2, was used as positive control. ACE2 expression was evaluated in both standard culture conditions and after 48 hrs of hypoxia exposure (1% O_2). We quantified the mRNA levels by RT-qPCR and verified protein content by western blot on both cell lysates and serum-free 48 hrs-conditioned media (MSC-CM). ACE2 levels in MSC-CM were quantified by ELISA assay. Finally, to test MSC viral susceptibility, we produced replication-defective, GFP-tagged retroviral particles bearing the SARS-CoV-2 Spike protein; the pantropic VSV glycoprotein (VSV-G) was used as positive control.

Results: ACE2 mRNA level in both fetal and adult MSC was 200-fold lower than in CALU-3. ACE2 protein expression was undetectable in MSC lysates and CM, both by western blot and ELISA. Hypoxia slightly increased ACE2 mRNA level, but not protein level, which still was undetectable. Finally, CALU-3 but not MSC were infected by SARS-CoV-2 Spike pseudovirus, whereas both cell types were susceptible to VSV-G pseudovirus infection.

Conclusions: Both fetal and adult MSC do not express significant levels of ACE2 both under normoxia and hypoxia, and therefore the putative therapeutic mechanism of hMSCs in COVID-19 cannot go through the release of ACE2. Importantly, MSCs are immune to SARS-CoV-2 infection and therefore their use appears safe.

Received: 16 August 2020 | Accepted: 25 October 2020

DOI: 10.1002/sctm.20-0385

TISSUE-SPECIFIC PROGENITOR AND STEM CELLS

STEM CELLS TRANSLATIONAL MEDICINE

Human mesenchymal stromal cells do not express ACE2 and TMPRSS2 and are not permissive to SARS-CoV-2 infection

Maria A. Avanzini[1,2] | Manuela Mura[3] | Elena Percivalle[4] | Francesca Bastaroli[5] | Stefania Croce[1,6] | Chiara Valsecchi[1,2] | Elisa Lenta[1] | Giulia Nykjaer[5] | Irene Cassaniti[4] | Jessica Bagnarino[1,2] | Fausto Baldanti[4] | Marco Zecca[2] | Patrizia Comoli[1,2] | Massimiliano Gnecchi[3,5,7]

[1]Cell Factory, Fondazione IRCCS Policlinico San Matteo, Pavia, Italy

[2]Pediatric Hematology Oncology, Fondazione IRCCS Policlinico San Matteo, Pavia, Italy

[3]Intensive Cardiac Care Unit and Laboratory of Experimental Cardiology for Cell and Molecular Therapy, Fondazione IRCCS Policlinico San Matteo, Pavia, Italy

[4]Molecular Virology Unit, Microbiology and Virology Department, Fondazione IRCCS Policlinico San Matteo, Pavia, Italy

[5]Department of Molecular Medicine, Unit of Cardiology, University of Pavia, Pavia, Italy

[6]General Surgery I, Fondazione IRCCS Policlinico San Matteo, Pavia, Italy

[7]Department of Medicine, University of Cape Town, Cape Town, South Africa

Correspondence
Massimiliano Gnecchi, MD, PhD, University of Pavia and Fondazione IRCCS Policlinico San Matteo, Pavia, Italy.
Email: m.gnecchi@unipv.it

Maria A. Avanzini, PhD, Cell Factory/Pediatric Hematology Oncology, Fondazione IRCCS Policlinico San Matteo, Pavia, Italy.
Email: ma.avanzini@smatteo.pv.it

Funding information
Department of Molecular Medicine of the University of Pavia; Italian Ministry of Health and Fondazione IRCCS Policlinico San Matteo, Grant/Award Numbers: 80380, 08064009

Abstract

Anti-inflammatory and immune-modulatory therapies have been proposed for the treatment of COVID-19 and its most serious complications. Among others, the use of mesenchymal stromal cells (MSCs) is under investigation given their well-documented anti-inflammatory and immunomodulatory properties. However, some critical issues regarding the possibility that MSCs could be infected by the virus have been raised. Angiotensin-converting enzyme 2 (ACE2) and type II transmembrane serine protease (TMPRSS2) are the main host cell factors for the severe acute respiratory syndrome-coronavirus 2 (SARS-CoV-2), entry, but so far it is unclear if human MSCs do or do not express these two proteins. To elucidate these important aspects, we evaluated if human MSCs from both fetal and adult tissues constitutively express ACE2 and TMPRSS2 and, most importantly, if they can be infected by SARS-CoV-2. We evaluated human MSCs derived from amnios, cord blood, cord tissue, adipose tissue, and bone marrow. ACE2 and TMPRSS2 were expressed by the SARS-CoV-2-permissive human pulmonary Calu-3 cell line but not by all the MSCs tested. MSCs were then exposed to SARS-CoV-2 wild strain without evidence of cytopathic effect. Moreover, we also excluded that the MSCs could be infected without showing lytic effects since their conditioned medium after SARS-CoV-2 exposure did not contain viral particles. Our data, demonstrating that MSCs derived from different human tissues are not permissive to SARS-CoV-2 infection, support the safety of MSCs as potential therapy for COVID-19.

KEYWORDS

adult stem cells, angiotensin, cellular therapy, fetal stem cells, mesenchymal stromal cells (MSCs)

Maria A. Avanzini, Manuela Mura, and Elena Percivalle contributed equally to this study.

1 | INTRODUCTION

In December 2019, an outbreak caused by a novel coronavirus, later named SARS-CoV-2, occurred in China and rapidly spread throughout several other countries, becoming pandemic.[1] COVID-19, the disease caused by SARS-CoV-2, mainly affects the respiratory system and can progress to respiratory distress syndrome (ARDS), a fatal condition in more than 50% of the cases.[1] Up to 30% of COVID-19 patients may develop cardiac damage due to acute coronary syndrome, septic heart, or acute myocarditis.[2-4] As there are no specific therapeutics for treating COVID-19, in particular for the most severe cases complicated by ARDS or acute fulminant myocarditis, new innovative therapeutic approaches are urgently needed. Anti-inflammatory drugs have been proposed as possible approaches and it has been suggested that immunosuppressive therapy may mitigate the manifestations of COVID-19.[5,6] Mesenchymal stem cells (MSCs) possess immunomodulatory

Significance statement

Human mesenchymal stromal cells (hMSCs) are currently under investigation for the treatment of COVID-19. However, the potential safety profile of hMSCs in this context has never been defined since none has described if they express ACE2 and TMPRSS2, the main host cell factors for SARS-CoV-2 entry, and if they can be infected by SARS-CoV-2. This study provides the first evidence that ACE2 and TMPRSS2 are not expressed in hMSCs derived from both adult and fetal human tissues and, most importantly, that hMSCs are not permissive to SARS-CoV-2 infection. These results support the safety of MSCs as potential therapy for COVID-19.

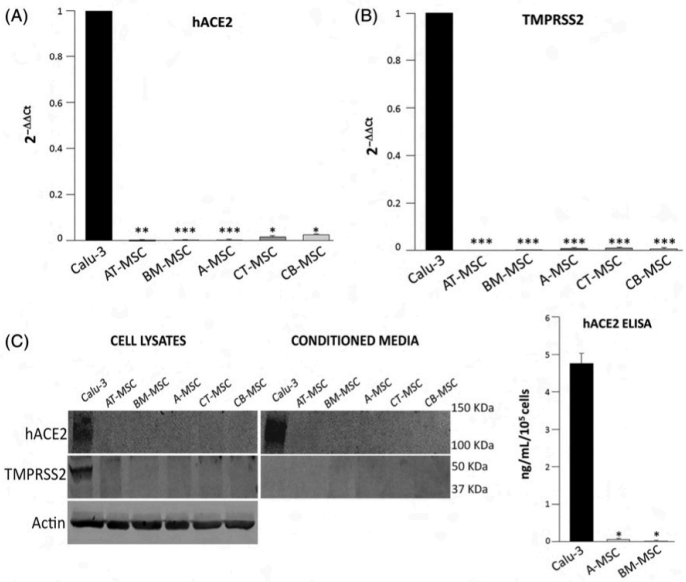

FIGURE 1 hACE2 and TMPRSS2 expression in human MSCs from fetal and adult tissues. A, Relative quantification by quantitative reverse transcription PCR (RT-qPCR) and the $2^{-\Delta\Delta Ct}$ method of ACE2 (left) and TMPRSS2 (right) mRNA levels in MSCs from cord blood (CB-MSC, n = 2 lines), cord tissue (CT-MSC, n = 2 lines), amnios (A-MSC, n = 4 lines), bone marrow (BM-MSC, n = 4 lines), and adipose tissue (AT-MSC, n = 2 RNA samples from the same line), compared with the Calu-3 cell line. Each sample was loaded in triplicate. Columns represent mean $2^{-\Delta\Delta Ct}$ values and SD. The glyceraldehyde 3-phosphate dehydrogenase (GAPDH) was used as a reference gene. *P < .05, **P < .01, ***P < .001 vs Calu-3. B, Representative Western blot of hACE2 and TMPRSS2 in cell lysates (left) and serum free 48 hours-conditioned media (right) of the different MSC types, and the positive control cell line Calu-3. Actin was used as loading control for cell lysates. The amount of conditioned media loaded for each sample was obtained from 1×10^5 cells. C, ACE2 protein quantification by enzyme-linked immunoadsorbent assay (ELISA) in serum-free 48 hours-conditioned media generated by 1×10^5 MSCs. The bars represent the mean and SD of triplicates obtained from a single line of Calu-3 and 4 distinct lines of both A-MSCs and BM-MSCs. *P < .001 vs Calu-3. MSCs, mesenchymal stromal cells

properties as demonstrated by numerous in vitro and animal model studies. These effects are mediated by cytokines and soluble factors able to modulate the systemic but also the tissue inflammatory response.[7] In particular, when administered intravenously, most MSCs lodge in the pulmonary vascular bed where they survive for at least a few days.[8] Importantly, several clinical studies, including phase III trials, documented their efficacy in the control of graft-vs-host disease in recipients of allogeneic hematopoietic stem cell transplantation, and there are evidences also in other immune-mediated disorders.[7] In addition, there are existing preclinical and a few preliminary feasibility and safety clinical studies supporting further investigation of cell-based therapies, particularly with MSC, or the MSC-derived secretome, for potential treatment of ARDS and acute myocarditis.[7-9] For all these reasons, it has been hypothesized that the administration of MSCs may be useful in the treatment of severe cases of COVID-19. A pilot study conducted in China on seven patients affected by SARS-CoV-2 pneumonia has reported feasibility and safety of MSC therapy,[10] and a total of 39 phase I/II trials testing MSC-therapy for COVID-19 are currently registered in ClinicalTrials.gov. However, infusion of MSCs in the presence of active viraemia has raised some critical issues regarding the possibility that the virus may infect MSCs, causing not only lack of efficacy but also possible deleterious effects.

Angiotensin-converting enzyme 2 (ACE2) is the main host cell receptor for SARS-CoV-2 entry, and the virus uses the host cell transmembrane serine protease II (TMPRSS2) for Spike envelope protein priming.[11] It is known that ACE2 and TMPRSS2 are present on the surface of several human cells, such as alveolar cells and capillary endothelium, while immune cells, such as T and B lymphocytes, and macrophage are negative for ACE2.[12] Whether human MSCs of any origin constitutively express ACE2 and/or TMPRSS2 is so far unclear. Leng et al[10] claimed the absence of ACE2 and TMPRSS2 expression on the umbilical cord-derived MSC infused in their study, even though a clear demonstration was not reported. In addition, SARS-CoV-2 could also use other, possibly unknown, receptors for cellular entry.

Accordingly, the aim of the present work was to evaluate whether human MSCs from various sources express ACE2 and TMPRSS2 and, most importantly, if they are permissive to SARS-CoV-2 infection.

2 | MATERIALS AND METHODS

An expanded method section is available as Supporting Information.

2.1 | Cell culture

The MSC lines were previously isolated from amniotic membrane of human placenta, cord blood, cord tissue, bone marrow, and adipose tissue, expanded and characterized.[13-17] All the MSCs fulfill the criteria set by the International Society for Cell & Molecular Therapy (ISCT).[18] To perform the experiments, we used passage 3 to 5 MSCs. Conditioned media were generated as described[13,19] with some minor modification described in the Supporting Information Methods, in order to evaluate the soluble amount of ACE2. The human lung Calu-3 (ATCC HTB-52) and the African green monkey kidney VERO E6 (VERO C1008; ATCC CRL-1586) cell lines were purchased and maintained as indicated by ATCC (www.lgcstandards-atcc.org).

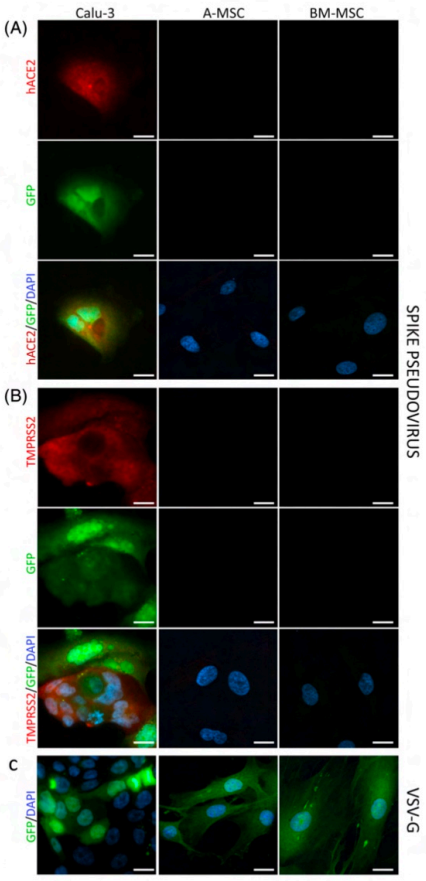

FIGURE 2 MSC infection with a SARS-CoV-2 Spike pseudovirus. A-MSCs, BM-MSCs, and Calu-3 were transduced with a replication-defective, green fluorescent protein (GFP)-tagged, pseudotyped retrovirus bearing the SARS-CoV-2 spike envelope protein (Spike pseudovirus; A, B), or the pantropic vesicular stomatitis virus glicoprotein (VSV-G; C). The green signal is present if cells are infected. Costaining for ACE2 (A) or TMPRSS2 (B) is shown in red. Nuclei were counterstained with the nuclear dye 4′,6-diamidino-2-phenylindole (DAPI Blue). Scale bar = 20 μm

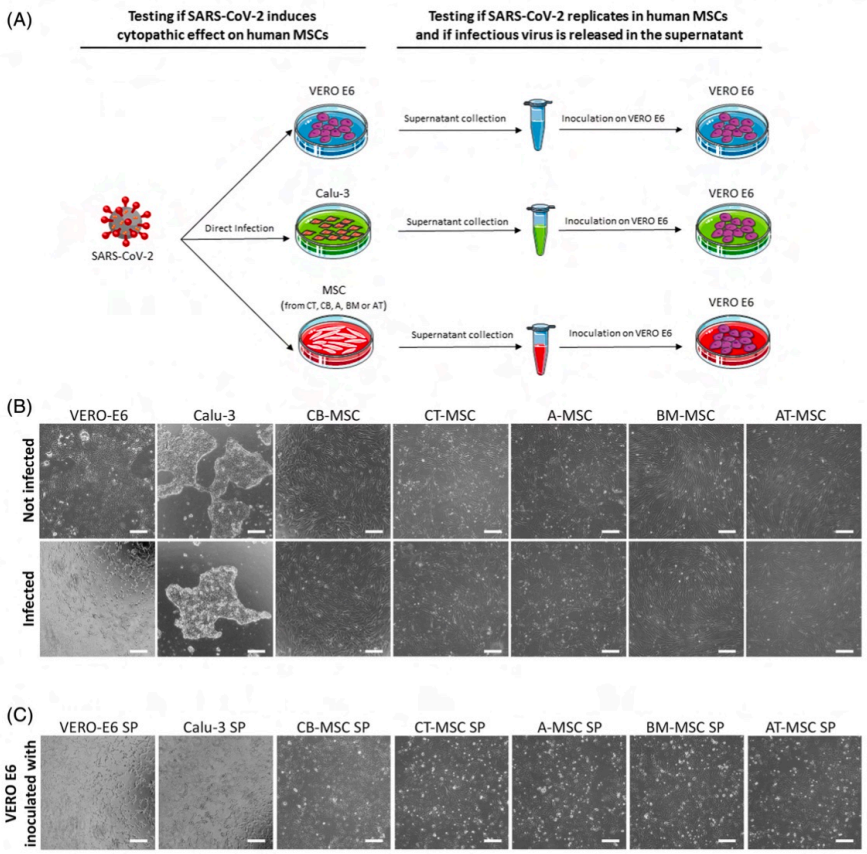

FIGURE 3 MSC infection with SARS-CoV-2. A, Experimental design. First, MSCs from CB, CT, A, BM and AT, and the permissive cell lines VERO E6 and Calu-3 were incubated with SARS-CoV-2 wild-type strain. CPE defined as cell rounding, detachment, degeneration, and/or syncytium formation was assessed by microscopic analysis, and the cells maintained in culture for 7 days, changing the medium every three 3 days. Then, supernatants were collected and tested in a reinoculation experiment on VERO E6. B, Representative phase contrast images of VERO-E6, Calu-3, and hMSCs before (not infected—upper panels) and after exposure to SARS-CoV-2 (infected—lower panels). Scale bar = 200 μm. hMSCs and Calu-3 showed no signs of CPE and maintained their typical spindle-shaped and epithelial morphology, respectively, whereas VERO E6 displayed clear signs of CPE, since almost all the cells were round or fused into syncytia or detached. C, Representative phase contrast images of VERO E6 cells after exposure to supernatant generated by the infected cell lines respectively indicated on top of each frame. Scale bar = 200 μm. CPE, cytopathic effect; hMSCs, human mesenchymal stromal cells; MSCs, mesenchymal stromal cells

2.2 | SARS-CoV-2 spike pseudotyped retrovirus production and MSC infection

SARS-CoV-2 spike pseudotyped retroviral particles were produced by cotransfection of 293T cells (ThermoFisher) with these following three plasmids: a replication-deficient retroviral vector FCQ pMM2-eGFP expressing the green fluorescent protein (GFP)[20]; a packaging vector pUMVC (#8449 Addgene), and an envelope vector 2019-nCoV Spike ORF mammalian expression plasmid (VG40589-UT Sino Biologicals), or pCMV-VSV-G (#8454 Addgene) expressing the vesicular stomatitis virus

glycoprotein (VSV-G) as a positive control. MSCs were incubated with Spike or VSV-G pseudotyped viral particles for 24 hours.

2.3 | Infection with SARS-CoV-2 wild strain

MSCs, Calu-3, and VERO E6 were infected with 100 μL (100 $TCID_{50}$/mL) of a previously titrated SARS-CoV-2 wild strain, isolated from an infected patient. The virus was incubated for 1 hour and then removed; the medium was changed every 3 days. Cells were scored every other day and for 1 week using a light microscope to detect the appearance of cell rounding, detachment, degeneration, and/or syncytium formation, called hereafter cytopathic effect (CPE). To verify if the cells tested can be infected and allow SARS-CoV-2 replication even in the absence of CPE, at day 7 from infection, supernatants from each MSC, Calu-3, and VERO E6 culture were collected and inoculated into VERO E6. CPE occurrence was monitored for 1 week.

2.4 | Statistical analysis

All results are reported as mean ± SD and the data were analyzed with a one-way or two-way analysis of variance followed by Bonferroni all pair-wise multiple comparison test using the InStat software (GraphPad Software, Inc., San Diego, California; http://www.graphpad.com). *P* values less than .05 were considered statistically significant.

3 | RESULTS

We assessed ACE2 and TMPRSS2 expression on human fetal MSCs derived from amniotic membrane of placenta (A, n = 4), cord blood (CB, n = 2) or cord tissue (CT, n = 2), and human adult MSCs derived from bone marrow (BM, n = 4) or adipose tissue (AT, n = 1). The lung epithelial cell line Calu-3, which expresses high levels of both ACE2 and TMPRSS2 and is permissive to SARS-CoV-2 infection and nonlytic replication,[21] was used as positive control. Compared with Calu-3, the levels of ACE2 and TMPRSS2 mRNAs in all MSC lines considered were around 100-fold and 200-fold lower, respectively (Figure 1A). ACE2 and TMPRSS2 protein expression in MSC lysates was undetectable by Western blot (Figure 1B). Finally, we were unable to detect any soluble amount of ACE2 in MSC-derived conditioned media by both Western blot and enzyme-linked immunoadsorbent assay (ELISA) (Figure 1B,C).

To substantiate the absence of ACE2 and TMPRSS2 in fetal and adult MSCs, we transduced both A-MSCs and BM-MSCs, as representative cell populations, with a replication-defective, GFP-tagged, pseudotyped retrovirus bearing the SARS-CoV-2 spike envelope protein. This pseudovirus does not go through a lytic replication and does not induce CPE, but it shares the same host cell factors for viral entry with the authentic SARS-CoV-2. As expected, Calu-3 were infected by the spike-pseudotyped virus and turned green, confirming that the assay properly worked (Figure 2). On the contrary, neither A-MSCs nor BM-MSCs were infected by the pseudovirus (Figure 2). A-MSCs, BM-MSCs, and Calu-3 were all susceptible to entry driven by the pantropic VSV-G, confirming the specificity of the assay (Figure 2). Finally, immunofluorescent analysis confirmed the expression of ACE2 and TMPRSS2 only in the permissive cell line Calu-3, whereas no expression was documented in fetal and adult human MSCs (Figure 2).

To exclude that SARS-CoV-2 can infect MSCs through other host factors/receptors, we infected fetal and adult human MSCs of different origin with a SARS-CoV-2 wild strain under two different conditions: as adherent monolayer or cellular suspension (Figure 3A). All MSCs infected in adhesion showed the typical spindle shape morphology with no signs of CPE (Figure 3B and Table 1). Also, MSCs infected in suspension and seeded in 24 well plates were found adherent to plastic and showed no CPE starting from the day postinoculum up to 7 days (data not shown). Conversely, a 100% CPE was detected in the control VERO E6 cell line (Figure 3B and Table 1). As expected,[21] we did not observe CPE in Calu-3 cells for the entire observation period (Figure 3B and Table 1). At 7 days after infection, supernatants from all experiments were collected and tested in a reinoculation

TABLE 1 Cytopathic effect in human MSCs, Calu-3, and VERO E6 cell lines

		CPE after 1 wk of SARS-CoV-2 exposure			CPE detected in VERO E6 inoculated with supernatants		
Cell line	n	1×10^5	5×10^4	2.5×10^4	1×10^5	5×10^4	2.5×10^4
CB-MSC	2	N	N	N	N	N	N
CT-MSC	2	N	N	N	N	N	N
A-MSC	1	N	N	N	N	N	N
AT-MSC	1	N	N	N	N	N	N
BM-MSC	4	N	N	N	N	N	N
Calu-3	2	N	N	N	P	P	P
VERO E6	2	P	P	P	P	P	P

Note: The presence or absence of virus-induced CPE is reported in the table. Cytopathic effect was defined as cell rounding, detachment, degeneration, and/or syncytium formation after 1 week of direct virus infection or after inoculation with supernatant collected from previously infected cells.
Abbreviations: CPE, cytopathic effect; MSCs, mesenchymal stromal cells; N, negative CPE; P, positive CPE.

experiment in VERO E6 cells (Figure 3A). As expected, a typical CPE was evident in all the wells inoculated with supernatants collected from infected VERO-E6 and Calu-3 cultures (Figure 3C and Table 1). On the contrary, none of the supernatant collected from the different MSC cell lines induced CPE, demonstrating the absence of viral replication inside the MSC lines and, consequently, the absence of SARS-CoV-2 infection (Figure 3C and Table 1).

4 | DISCUSSION

The recent emergence of the COVID-19 pandemic and the absence of specific and validated therapeutic agents against this disease, prompted the search for new therapies able to hamper the strong immune reaction and the life-threatening complications occurring in the most severe cases. The inflammatory nature of COVID-19 points toward a solid rationale for the use of MSCs. Indeed, current understanding of MSC mechanisms of action is that most of their beneficial effects in repair from injury occur through secretion of cytoprotective, repair-promoting, and immunoregulatory factors.[22] Some examples include the induction of M2 macrophages, inhibition of natural killer cell proliferation and their cytotoxic function, anti-inflammatory cytokine production, and promotion of T regulatory cell generation.[8] Overall, these immunomodulatory effects can facilitate the resolution of inflammatory processes, including those characterizing ARDS and acute myocarditis. Furthermore, MSCs have constitutively low immunogenicity allowing off-the-shelf allogeneic use and there is a strong track record of safety for use in a range of diseases. In particular, MSCs from different sources including bone marrow, adipose, cord blood, and placental tissues, have shown promising results in experimental models of lung diseases, following either systemic or direct endobronchial administration.[8] Phase I and II trials have demonstrated feasibility and safety of systemic administration of MSCs in non-COVID ARDS patients and inflammatory cardiomyopathy.[8,9] As alveolar epithelium and capillary endothelium are major sites of viral replication during COVID-19 disease, it was hypothesized that MSCs retained within the lungs and the capillaries, for instance after intravenous infusion, may rapidly undergo infection and relative virus-mediated lysis, with significant decrease in therapeutic efficiency. For this reason, determining if human MSCs can be infected by SARS-CoV-2 is of crucial importance.

Stem cells are generally resistant to viral agents[23] but infection of MSCs by avian influenza or herpesviruses has been reported,[24,25] and a similar concern has been raised for the SARS-CoV-2. So far, evaluation of MSC infectiveness by coronaviruses, in particular by SARS-CoV-2, has not yet been investigated and described. There is only one study in which absence of the viral host cell factors ACE2 and TMPRSS2 expression on human umbilical cord blood-derived MSCs is claimed, but this cannot be considered a surrogate indicating a condition of refractoriness to infection.[10] Indeed, the presence on MSCs of a different receptor able to mediate viral entry cannot be ruled out. Moreover, if all human MSC types express or not ACE2 is still a matter of debate and solid data are missing.

Using a variety of assays, we unequivocally demonstrated that human MSCs do express neither ACE2 nor TMPRSS2. Most importantly, using a direct infection assay, our study provides the first evidence that human MSCs derived from fetal and adult tissues are not permissive to SARS-CoV-2 infection.

5 | CONCLUSION

Our data demonstrating that MSCs derived from different human tissues are resistant to SARS-CoV-2 infection are important to support the use of MSCs as a possible useful tool to down-modulate the immune hyper-activation in COVID-19 patients, and to contrast the pro-fibrotic mechanisms that lead to the severe long-term pulmonary sequelae increasingly observed in patients recovering from acute infection.

ACKNOWLEDGMENTS

This work was supported by the Italian Ministry of Health and Fondazione IRCCS Policlinico San Matteo, "Ricerca Corrente" projects numbers 08064009 (to M.G.), 80380 (to M.A.A.), and by a grant to the Department of Molecular Medicine of the University of Pavia under the initiative "Dipartimenti di Eccellenza" (2018-2022) (to M.G.).

CONFLICT OF INTEREST

F.B. declared consultant/advisory role with Humabs, Biotest, Shire, DiaSorin, MSD Qiagen; research funding from AB Analitica, NTP, Qiagen, Elitechgroup, and DiaSorin. The other authors declared no potential conflicts of interest.

AUTHOR CONTRIBUTIONS

M.A.A.: conception and design, collection and assembly of data, data analysis and interpretation, manuscript writing, financial support, final approval of manuscript; M.M., E.P.: conception and design, collection and assembly of data, data analysis and interpretation, manuscript writing; F. Bastaroli, S.C., C.V., E.L., G.N.: collection and assembly of data, data analysis and interpretation; I.C., J.B., F. Baldanti, M.Z., P.C.: financial support and final approval of manuscript; M.G.: conception and design, financial support, data analysis and interpretation, manuscript writing, final approval of manuscript.

DATA AVAILABILITY STATEMENT

The data that support the findings of this study are available on request from the corresponding author.

ORCID

Massimiliano Gnecchi https://orcid.org/0000-0001-7435-4328

REFERENCES

1. Wiersinga WJ, Rhodes A, Cheng AC, Peacock SJ, Prescott HC. Pathophysiology, transmission, diagnosis, and treatment of coronavirus disease 2019 (COVID-19): a review. *JAMA*. 2020;324(8):782-793.

2. Lombardi CM, Carubelli V, Iorio A, et al. Association of troponin levels with mortality in Italian patients hospitalized with coronavirus disease 2019: results of a multicenter study. *JAMA Cardiol*. 2020;e203538.
3. De Rosa S, Spaccarotella C, Basso C, et al. Reduction of hospitalizations for myocardial infarction in Italy in the COVID-19 era. *Eur Heart J*. 2020;41:2083-2088.
4. Gnecchi M, Moretti F, Bassi EM, et al. Myocarditis in a 16-year-old boy positive for SARS-CoV-2. *Lancet*. 2020;395:e116.
5. Cavagna L, Seminari E, Zanframundo G, et al. Calcineurin inhibitor-based immunosuppression and COVID-19: results from a multidisciplinary cohort of patients in northern Italy. *Microorganisms*. 2020; 8(7):977. https://doi.org/10.3390/microorganisms8070977.
6. Lisi L, Lacal PM, Barbaccia ML, Graziani G. Approaching coronavirus disease 2019: mechanisms of action of repurposed drugs with potential activity against SARS-CoV-2. *Biochem Pharmacol*. 2020;180: 114169.
7. Hoogduijn MJ, Lombardo E. Mesenchymal stromal cells anno 2019: dawn of the therapeutic era? Concise review. *Stem Cells Translational Medicine*. 2019;8:1126-1134.
8. Khoury M, Cuenca J, Cruz FF, et al. Current status of cell-based therapies for respiratory virus infections: applicability to COVID-19. *Eur Respir J*. 2020;55(6):2000858. https://doi.org/10.1183/13993003.00858-2020.
9. Miteva K, Van Linthout S, Volk HD, et al. Immunomodulatory effects of mesenchymal stromal cells revisited in the context of inflammatory cardiomyopathy. *Stem Cells Int*. 2013;2013:353097.
10. Leng Z, Zhu R, Hou W, et al. Transplantation of ACE2(−) mesenchymal stem cells improves the outcome of patients with COVID-19 pneumonia. *Aging Dis*. 2020;11:216-228.
11. Hoffmann M, Kleine-Weber H, Schroeder S, et al. SARS-CoV-2 cell entry depends on ACE2 and TMPRSS2 and is blocked by a clinically proven protease inhibitor. *Cell*. 2020;181:271-280.
12. Sungnak W, Huang N, Becavin C, et al. SARS-CoV-2 entry factors are highly expressed in nasal epithelial cells together with innate immune genes. *Nat Med*. 2020;26:681-687.
13. Danieli P, Malpasso G, Ciuffreda MC, et al. Conditioned medium from human amniotic mesenchymal stromal cells limits infarct size and enhances angiogenesis. *Stem Cells Translational Medicine*. 2015;4: 448-458.
14. Avanzini MA, Bernardo ME, Cometa AM, et al. Generation of mesenchymal stromal cells in the presence of platelet lysate: a phenotypic and functional comparison of umbilical cord blood- and bone marrow-derived progenitors. *Haematologica*. 2009;94:1649-1660.
15. Borghesi A, Avanzini MA, Novara F, et al. Genomic alterations in human umbilical cord-derived mesenchymal stromal cells call for stringent quality control before any possible therapeutic approach. *Cytotherapy*. 2013;15:1362-1373.
16. Bernardo ME, Avanzini MA, Perotti C, et al. Optimization of in vitro expansion of human multipotent mesenchymal stromal cells for cell-therapy approaches: further insights in the search for a fetal calf serum substitute. *J Cell Physiol*. 2007;211:121-130.
17. Lisini D, Nava S, Pogliani S, et al. Adipose tissue-derived mesenchymal stromal cells for clinical application: an efficient isolation approach. *Curr Res Transl Med*. 2019;67:20-27.
18. Dominici M, Le Blanc K, Mueller I, et al. Minimal criteria for defining multipotent mesenchymal stromal cells. The International Society for Cellular Therapy position statement. *Cytotherapy*. 2006;8:315-317.
19. Danieli P, Malpasso G, Ciuffreda MC, et al. Testing the paracrine properties of human mesenchymal stem cells using conditioned medium. *Methods Mol Biol*. 2016;1416:445-456.
20. Lee YK, Sala L, Mura M, et al. MTMR4 SNVs modulate ion channel degradation and clinical severity in congenital long QT syndrome: insights in the mechanism of action of protective modifier genes. *Cardiovasc Res*. 2020.
21. Chu H, Chan H, Yuen TT, et al. Comparative tropism, replication kinetics, and cell damage profiling of SARS-CoV-2 and SARS-CoV with implications for clinical manifestations, transmissibility, and laboratory studies of COVID-19: an observational study. *Lancet Microbe*. 2020;1:e14-e23.
22. Gnecchi M, Zhang Z, Ni A, Dzau VJ. Paracrine mechanisms in adult stem cell signaling and therapy. *Circ Res*. 2008;103:1204-1219.
23. Wu X, Dao Thi VL, Huang Y, et al. Intrinsic immunity shapes viral resistance of stem cells. *Cell*. 2018;172:423-438.
24. Thanunchai M, Kanrai P, Wiboon-Ut S, et al. Tropism of avian influenza A (H5N1) virus to mesenchymal stem cells and CD34+ hematopoietic stem cells. *PLoS One*. 2013;8:e81805.
25. Sundin M, Orvell C, Rasmusson I, et al. Mesenchymal stem cells are susceptible to human herpesviruses, but viral DNA cannot be detected in the healthy seropositive individual. *Bone Marrow Transplant*. 2006;37:1051-1059.

SUPPORTING INFORMATION

Additional supporting information may be found online in the Supporting Information section at the end of this article.

How to cite this article: Avanzini MA, Mura M, Percivalle E, et al. Human mesenchymal stromal cells do not express ACE2 and TMPRSS2 and are not permissive to SARS-CoV-2 infection. *STEM CELLS Transl Med*. 2021;10:636–642. https://doi.org/10.1002/sctm.20-0385

COVID-19
SESSION TITLE: COVID-19 AND CARDIOVASCULAR DISEASE

Abstract 12174: Valsartan Protects Both Cardiac and Lung Cells From SARS-CoV-2 Infection

Francesca Bastaroli, Manuela Mura, JOSE' CAMILLA SAMMARTINO, alessandro ferrari, MARZIA CORLI, Chiara Guarona, Elena Percivalle and **Massimiliano Gnecchi**

Originally published 8 Nov 2021 | https://doi.org/10.1161/circ.144.suppl_1.12174 | Circulation. 2021;144:A12174

Abstract

Background: Severe Acute Respiratory Syndrome-Coronavirus 2 (SARS-CoV-2) disease (COVID-19) mainly affects the respiratory system, but cardiac complications occur very often. SARS-CoV-2 entry in host cells is mediated by the interaction between the viral Spike (S) glycoprotein and the host angiotensin-converting enzyme 2 (ACE2). The use of angiotensin-converting enzyme inhibitors (ACEIs) and angiotensin II type 1 receptor blockers (ARBs) might influence the expression of ACE2 and viral infection, but not much is known about these interactions.

Aim: To evaluate the effects of ACEIs and ARBs during active viraemia.

Methods: We tested the ACEI Lisinopril (at 100nM and 500nM) and the ARB Valsartan (at 10uM and 50uM) for one week on two cell types: cardiomyocytes derived from hiPSC (hiPSC-CMs) as heart model and a lung epithelial cancer cell line (16HBE) as pulmonary model. The SARS-CoV-2 wild strain was inoculated in the two treated cell types for one hour. Cell viability was measured 72 hours after infection. Supernatants were collected and titrated to verify the presence of infectious virus using a micro-neutralization assay on VERO-E6 cells. Levels of ACE2 mRNA and protein content on cell lysates were quantified after each treatment by RT-qPCR and western blot, respectively.

Results: ACEI and ARB at both concentrations affected the viability of neither hiPSC-CMs nor 16HBE cells in the absence of virus. Vice versa, viral infection significantly decreased viability of both hiPSC-CMs (-46%; $p<0,01$) and 16HBE (-19%; $p<0,05$). Viral titration revealed that SARS-CoV-2 replicated in both cell lines and was actively released in supernatants. Importantly, pre-treatment with Valsartan 50uM increased the viability of both hiPSC-CMs and 16HBE after infection, while Lisinopril and the lower dose of Valsartan had neutral effect. Of note, Valsartan 50uM treatment decrease ACE2 mRNA level in both hiPSC-CMs (-47%, $p<0,01$) and 16HBE (-37%, $p<0,01$). Also ACE2 protein levels were reduced in cell lysates of hiPSC-CMs and 16HBE treated with Valsartan 50uM.

Conclusion: These data suggest that ACEIs and ARBs do not worsen the SARS-CoV-2 infection. On the contrary, Valsartan seems to be protective against SARS-CoV-2 infection, possibly by reducing ACE2 expression.